

**ADVANCED CROSSLINKABLE POLYIMIDE MEMBRANES FOR
AGGRESSIVE SOUR GAS SEPARATIONS**

A Dissertation
Presented to
The Academic Faculty

by

Brian E. Kraftschik

In Partial Fulfillment
Of the Requirements for the Degree
Doctor of Philosophy in
Chemical & Biomolecular Engineering

Georgia Institute of Technology
December, 2013

COPYRIGHT © 2013 BRIAN E. KRAFTSCHIK

ADVANCED CROSSLINKABLE POLYIMIDE MEMBRANES FOR AGGRESSIVE SOUR GAS SEPARATIONS

Approved by:

Dr. William J. Koros, Advisor
School of Chemical &
Biomolecular Engineering
Georgia Institute of Technology

Dr. Krista S. Walton
School of Chemical &
Biomolecular Engineering
Georgia Institute of Technology

Dr. Christopher W. Jones
School of Chemical &
Biomolecular Engineering
Georgia Institute of Technology

Dr. Haskell W. Beckham
School of Materials
Science & Engineering
Georgia Institute of Technology

Dr. J. Carson Meredith
School of Chemical &
Biomolecular Engineering
Georgia Institute of Technology

Date Approved: November 13, 2013

ACKNOWLEDGEMENTS

I would like to express my most sincere gratitude to my advisor, Dr. Bill Koros, for his unyielding support and guidance during my time at Georgia Tech. His unrivaled dedication to not only the research conducted by his group but also the professional and personal development of his group members is truly an inspiration. It has been a privilege to learn from such an outstanding mentor for the past several years. I am sure I will continue to carry with me many of the lessons I have learned from him.

My committee members must also be recognized for their insights and participation in the work I've done while at Georgia Tech. I'd like to thank Dr. Christopher Jones, Dr. Carson Meredith, Dr. Krista Walton, and Dr. Haskell Beckham for their support.

All of my colleagues in the Koros group, past and present, have been a pleasure to work with. In particular, I'd like to recognize Dr. J.R. Johnson and Dr. Oguz Karvan, without whom my work would not have been possible. My fellow group members working on sour gas separations projects, Dr. Justin Vaughn and Dr. Carine Achoundong, have shared many of the unique struggles that I encountered during the past few years, and I appreciate their camaraderie. Also, it was a pleasure to have shared an office with Dr. Jong Suk Lee, Steven Burgess, and Danny Kim during the majority of my stay at Georgia Tech; our conversations, both scientific and personal, made for a great place to come to work.

I would also like to recognize Michelle Martin, who is instrumental to the smooth operation of our large research group. Her assistance with an innumerable array of procedures was always much appreciated.

Apart from the residents of our relatively secluded Bunger-Henry laboratory location, there are many people in the ChBE department that have contributed greatly to my experience at Georgia Tech and made it an overwhelmingly positive one. While I won't list them individually here, I would like to recognize my friends, especially those who entered the program at the same time as me, for all of the great and memorable times in Atlanta.

Most importantly, I want to express my supreme gratitude to my parents, Diane and Jim. They have wholeheartedly supported me throughout my time at Georgia Tech. I cannot thank them enough for all they have done and continue to do to encourage my growth. They are the best role models I could ask for.

Last but certainly not least, I want to acknowledge my significant other, Karly Donovan, who I consider my best friend and a trusted companion through thick and thin. She has made immeasurable sacrifices in order to spend the last three years in Atlanta with me. Karly is an uncommonly caring and generous individual, and she has been instrumental in helping me through the tough times over the past few years. She has been a constant source of happiness during this often stressful period. I cannot possibly thank her enough for her support.

TABLE OF CONTENTS

	Page
ACKNOWLEDGEMENTS	iii
LIST OF TABLES	xiii
LIST OF FIGURES.....	xvi
SUMMARY	xxiv
<u>CHAPTER</u>	
1. INTRODUCTION AND MOTIVATION	1
1.1. Natural Gas Processing.....	1
1.2. Membranes for Natural Gas Purification	6
1.3. Membrane Technology Overview	11
1.4. Sour Gas Separation Overview	14
1.5. Research Objectives	19
1.6. Dissertation Overview.....	21
1.7. References	21
2. BACKGROUND AND THEORY	24
2.1. Polymer Membranes for Gas Separations.....	24
2.2. Gas Transport in Membranes	27
2.2.1. Solution-Diffusion Transport Theory	31
2.2.2. Characterizing Solution-Diffusion Membranes	34
2.2.3. Transport in Rubbery Polymer Membranes	41
2.2.4. Transport in Glassy Polymer Membranes	43
2.2.4.1. Dual-mode Sorption Model in Glassy Polymers	43
2.2.4.2. Physical Aging in Glassy Polymers.....	46

2.3. Permeation Modeling in Glassy Polymer Membranes.....	48
2.3.1. Partial Immobilization Model and Competitive Sorption	48
2.3.2. Bulk Flow and the Frame of Reference Model	50
2.4. Penetrant-Polymer Interactions and their Effect of Transport.....	54
2.4.1. Plasticization of Polymers.....	54
2.4.1.1. Plasticization Overview	54
2.4.1.2. Strategies for Polymer Stabilizing Against Plasticization	59
2.4.2. Antiplasticization	61
2.4.3. Conditioning.....	64
2.5. Non-Ideal Gas Thermodynamics.....	64
2.6. Challenges Associated with the Simultaneous Removal of CO ₂ and H ₂ S from Sour Gas	65
2.7. Asymmetric Hollow Fiber Membranes	70
2.7.1. Mechanism of Formation of Asymmetric Hollow Fiber Membranes...	70
2.7.2. Property Requirements for Aggressive Feed Applications	73
2.7.2.1. Skin Integrity	73
2.7.2.2. Substructure Porosity.....	73
2.7.2.3. Morphological Properties	74
2.7.2.4. Additional Challenges Associated with Asymmetric Hollow Fibers	77
2.8. References	78
3. MATERIALS AND EXPERIMENTAL METHODS.....	85
3.1. Materials	85
3.1.1. Polymer Synthesis	85
3.1.2. Crosslinking	88
3.1.2.1. Monoesterification.....	89
3.1.2.2. Transesterification.....	90

3.1.3. Gases	92
3.2. Membrane Formation	92
3.2.1. Formation of Dense Film Membranes	92
3.2.2. Membrane Masking	93
3.2.3. Formation of Asymmetric Hollow Fiber Membranes	95
3.2.3.1. Dope Formulation	95
3.2.3.2. Hollow Fiber Spinning	97
3.2.3.3. Hollow Fiber Module-Making	99
3.2.4. Dense Film and Hollow Fiber Crosslinking	100
3.3. Membrane Characterization Techniques.....	102
3.3.1. Permeation Analysis.....	102
3.3.1.1. Permeation Equipment	102
3.3.1.2. Safety and Design of Sour Gas_	107
3.3.1.3. Pure Gas Dense Film Permeation	108
3.3.1.4. Pure Gas Hollow Fiber Permeation	112
3.3.1.5. Mixed Gas Dense Film Permeation	114
3.3.1.6. Mixed Gas Hollow Fiber Permeation	116
3.3.2. Pressure Decay Sorption Analysis	117
3.3.3. Thermal Analysis	120
3.3.3.1. Thermogravimetric Analysis (TGA).....	120
3.3.3.2. Differential Scanning Calorimetry (DSC)	121
3.3.4. Fourier Transform Infrared – Attenuated Total Reflectance Spectroscopy (FTIR-ATR)	121
3.3.5. Dense Film Bulk Density Measurement.....	121
3.3.6. Gel Permeation Chromatography (GPC).....	122
3.3.7. Scanning Electron Microscopy (SEM)	122
3.3.8. Nuclear Magnetic Resonance Imaging (NMR)	123

3.3.9. Dissolution and Gel Fraction Experiments.....	123
3.4. References	124
4. SOUR GAS TRANSPORT CHARACTERIZATION OF POLYIMIDE DENSE FILMS	127
4.1. Overview.....	172
4.2. Application of Glassy Polymer Membranes to Sour Gas Separations.....	127
4.3. Polymer Physical Property Analysis	130
4.3.1. Thermogravimetric Analysis	131
4.3.2. Glass Transition Temperature, Density, and Fractional Free Volume.....	133
4.4. Pure Gas Transport Analysis.....	133
4.4.1. Pure Gas Permeation	133
4.4.2. Pure Gas Sorption	136
4.4.3. Pure Gas Diffusion Analysis	139
4.5. Mixed Gas Transport.....	142
4.5.1. Binary (5% H ₂ S / 95% CH ₄) Sour Gas Mixture Permeation	142
4.5.2. Ternary (10% H ₂ S / 20% CO ₂ / 70% CH ₄) Sour Gas Mixture (A) Permeation	143
4.5.3. Ternary (20% H ₂ S / 20% CO ₂ / 60% CH ₄) Sour Gas Mixture (B) Permeation	146
4.5.4. Binary (20% CO ₂ / 80% CH ₄) Acid Gas Mixture Permeation.....	150
4.5.5. Mixed Gas Sorption Calculations.....	152
4.5.6. Pure and Mixed Gas Permeation Modeling	155
4.6. Assessment of Sour Gas Separation Performance	161
4.6.1. Upper Bound Comparison	161
4.6.2. Combined Acid Gas Analysis	163
4.7. Path Forward for 6FDA-DAM:DABA Polyimide Backbone	165
4.8. Conclusions	168

4.9. References	169
5. CROSSLINKABLE POLYIMIDE MATERIALS FOR AGGRESSIVE SOUR GAS SEPARATIONS	172
5.1. Overview.....	172
5.2. Sorption-Selective Materials for H ₂ S/CH ₄ Separations	172
5.3. PEGMC Polymer Synthesis for Additional Plasticization Resistance and Augmented H ₂ S/CH ₄ Selectivity	176
5.3.1. Monoesterification of 6FDA-DAM:DABA (3:2).....	176
5.3.2. Crosslinking PEGMC Dense Films	179
5.4. PEGMC Polymer Properties	180
5.4.1. PEGMC Synthesis Results	180
5.4.2. Crosslinking Efficacy.....	185
5.4.3. Physical Property Analysis	189
5.5. PEGMC Pure Gas Transport Properties in Dense Films.....	190
5.5.1. Pure Gas Permeation	190
5.5.2. Pure Gas Sorption	194
5.5.3. Pure Gas Diffusion Analysis	196
5.6. Mixed Gas Transport.....	199
5.6.1. Ternary (20% H ₂ S / 20% CO ₂ / 60% CH ₄) Sour Gas Mixture Permeation	199
5.6.2. Non-Zero Downstream Pressure Ternary Sour Gas Mixture Permeation	203
5.6.3. Binary (20% CO ₂ / 80% CH ₄) Acid Gas Mixture (A) Permeation....	203
5.6.4. Binary (50% CO ₂ / 50% CH ₄) Acid Gas Mixture (B) Permeation....	206
5.6.5. Mixed Gas Sorption	207
5.6.6. Mixed Gas Permeation Modeling.....	210
5.7. Conclusions	215
5.8. References	218

6. FORMATION AND CROSSLINKING OF DEFECT-FREE ASYMMETRIC HOLLOW FIBER MEMBRANES FROM PEGMC POLYIMIDE.....	221
6.1. Overview.....	221
6.2. Spinning PEGMC Hollow Fibers.....	222
6.2.1. Polymer Properties	222
6.2.2. Dope Formulation	223
6.2.2.1. Dope Composition Selection Theory	223
6.2.2.2. Initial Dope Formula for TEGMC Spinning.....	227
6.2.3. TEGMC Spinning: Initial	230
6.2.4. Characterization of Fibers from Initial Spinning	232
6.3. Spinning Defect-free PEGMC Fibers.....	236
6.3.1. Reformulation of PEGMC Dope.....	236
6.3.2. Results of Second Spinning	238
6.3.3. Characterization of PEGMC Fibers	239
6.4. Optimizing PEGMC Spinning for High Performance Fibers	243
6.4.1. Spin Optimization.....	243
6.4.2. Results of Third Spinning Study	244
6.4.3. PEGMC Fiber Characterization	245
6.5. Crosslinking PEGMC Fibers.....	248
6.5.1. Optimization of Thermal Treatment Conditions	248
6.5.2. Effect of Crosslinking and Crosslinking Conditions on Fiber Performance	251
6.6. Module-Making Considerations for Sour Gas Experimentation.....	255
6.6.1. Epoxy Selection for Potting Fibers.....	255
6.6.2. Fiber Post-treatment.....	258
6.7. Conclusions	260
6.8. References	261

7. SOUR GAS SEPARATIONS WITH CROSSLINKABLE PEGMC ASYMMETRIC HOLLOW FIBER MEMBRANES	263
7.1. Overview.....	263
7.2. Pure Gas Permeation	264
7.2.1. Pure CH ₄ Permeance Measurements.....	265
7.2.2. Plasticization Resistance Measurement of Crosslinked and Uncrosslinked Fibers	267
7.2.3. Physical Aging Study on TEGMC Fibers	273
7.2.3.1. Physical Aging Under Ambient Storage Conditions.....	274
7.2.3.2. Suppression of Aging Effects with Active CO ₂ Feed Storage	276
7.3. Mixed Gas Permeation	278
7.3.1. Binary (50% CO ₂ / 50% CH ₄) Acid Gas Mixture Permeation.....	279
7.3.2. Mixed Gas Permeation with Higher Hydrocarbon Contaminant	281
7.3.3. Ternary (5% H ₂ S / 45% CO ₂ / 50% CH ₄) Sour Gas Mixture (A) Permeation	284
7.3.4. Ternary (20% H ₂ S / 20% CO ₂ / 50% CH ₄) Sour Gas Mixture (B) Permeation	287
7.4. Conclusions	290
7.5. References	293
8. SUMMARY AND RECOMMENDATIONS	294
8.1. Conclusions	294
8.1.1. Benchmarking an Advanced Polyimide for Sour Gas Separations..	294
8.1.2. Development of a Novel Crosslinkable Polyimide for Sour Gas Feeds.....	295
8.1.3. Formation of Defect-free Crosslinkable Asymmetric Hollow Fiber Membranes.....	296
8.1.4. Permeation Characterization of Asymmetric Hollow Fibers Under Realistic, Aggressive Sour Gas Feed Conditions	297
8.1.5. Comparison of PEGMC to Alternative Sour Gas Separation Membrane Materials	299

8.2. Recommendations for Future Work.....	302
8.2.1. Investigation of PEGMC Materials with Alternative Monomer Ratios and Longer PEG Crosslinking Agents	302
8.2.2. Study of the Possible Diffusion-Limiting Effect of H ₂ S	303
8.2.3. Development of Improved Model for H ₂ S Permeation	304
8.2.4. Optimization of Dry-Jet/Wet-Quench PEGMC Spinning For Reduced Skin Thickness.....	305
8.2.5. Dual-layer Asymmetric Hollow Fiber Spinning With PEGMC as a Sheath	306
8.2.6. Optimization of Crosslinking Protocol for Higher Fiber Permeance.	307
8.2.7. Study of PDMS Post-treatment Effect on TEGMC Hollow Fiber Membrane Skin Layer.....	308
8.2.8. Pyrolysis of PEGMC and PDMS Post-treated PEGMC to Form Carbon Molecular Sieve (CMS) Membranes	309
APPENDIX A: NON-IDEAL GAS PROPERTY CALCULATIONS	312
APPENDIX B: SYNTHESIS OF 6FDA-DAM:DABA COPOLYIMIDE	317
APPENDIX C: MONOESTERIFICATION OF DABA-CONTAINING POLYIMIDES	321
APPENDIX D: HOLLOW FIBER MEMBRANE POST-TREATMENT [1, 2].....	324
VITA	326

LIST OF TABLES

	Page
Table 1.1: Typical US natural gas pipeline specifications [2].	3
Table 2.1: Physical properties of sour gas components and other common feed gases [8, 20, 21].	33
Table 2.2: Permeability and selectivity properties of PPO dense films with various diluent species measured at 35°C and 10 atm, except where noted otherwise [61].	62
Table 2.3: Permeability and selectivity values for H ₂ S/CH ₄ and CO ₂ /CH ₄ separations in "typical" rubbery and glassy polymer membranes [9, 69-73].	67
Table 2.4: Some key adjustable variables in the dry-jet/wet-quench spinning process. .	71
Table 2.5: Effect of hollow fiber outside diameter on membrane area and membrane area to module volume ratio in a 20 cm diameter and 1 m long module. A fiber packing density of 25% is assumed [52, 84].	75
Table 3.1: List of major system components and vendors for sour gas hollow fiber permeation system.	107
Table 4.1: Properties of 6FDA-DAM:DABA (3:2) dense films	133
Table 4.2: Ideal selectivity of 6FDA-DAM:DABA (3:2) films	136
Table 4.3: Sorption and mobility selectivity in 6FDA-DAM:DABA (3:2) dense films at 35°C.	138
Table 4.4: Dual-mode sorption model best-fit parameters for 6FDA-DAM:DABA (3:2) dense films.	139
Table 4.5: Dual-mobility permeation model parameters for sour gas components at 35°C. Values were calculated from pure gas permeation and sorption data.	141
Table 5.1: GPC results for synthesized PEGMC polymers powders in an uncrosslinked state.	179
Table 5.2: Extent of monoesterification of the 6FDA-DAM:DABA (3:2) carboxylic acid sites to form the PEGMC polymers.	184
Table 5.3: Swelling and solubility of PEGMC and unmodified 6FDA-DAM:DABA (3:2) films in NMP solvent.	186
Table 5.4: Gel content of PEGMC films with TEG crosslinking agent.	187

Table 5.5: Gel content values for 280°C crosslinked PEGMC dense films.	188
Table 5.6: Properties of the dense films samples used throughout this study.	189
Table 5.7: Ideal selectivity values for sour gas separations in crosslinked PEGMC and unmodified 6FDA-DAM:DABA (3:2) films at 65 psi feed pressure and 35°C.	193
Table 5.8: Dual-mode sorption model parameters ^a for pure H ₂ S and CH ₄ in crosslinked PEGMC and uncrosslinked 6FDA-DAM:DABA (3:2) [N/A] films.	194
Table 5.9: Dual-mode sorption parameters ^a for pure CO ₂ sorption in TEG crosslinked PEGMC and uncrosslinked 6FDA-DAM:DABA (3:2) [N/A] at 35°C.	196
Table 5.10: Dual-mobility model parameters for 280°C crosslinked PEGMC at 35°C. Values were calculated using pure gas permeation and sorption data.	198
Table 6.1: Molecular weight and PDI properties of the polymer batches used for each spinning attempt described in this chapter as measured by GPC.	223
Table 6.2: Boiling point temperature and vapor pressure values for volatile and non-volatile dope components.	227
Table 6.3: Potential dope composition for first TEGMC fiber spinning attempt based on results of cloud point experiments.	229
Table 6.4: Spinning conditions used during the first attempt at spinning TEGMC hollow fibers.	231
Table 6.5: Spinning conditions used for select fiber states from Spin # 1.	231
Table 6.6: Pure gas permeation characterization of uncrosslinked Spin #1 TEGMC fibers at 35°C.	234
Table 6.7: Dense film permeability and permselectivity values for uncrosslinked TEGMC at 35°C and 100 psi.	234
Table 6.8: Effective skin layer thickness and skin integrity values (ideal selectivity as a percentage of the intrinsic value) for uncrosslinked TEGMC fibers from Spin #1.	235
Table 6.9: Pure CO ₂ and CH ₄ permeation properties for Spin #1 uncrosslinked TEGMC fibers.	236
Table 6.10: Second generation dope composition for TEGMC asymmetric hollow fiber spinning.	237
Table 6.11: Spinning conditions used for select fiber states during Spin #2.	239
Table 6.12: Spin #2 pure gas permeation results at 35°C and 100 psig feed pressure.	241

Table 6.13: Skin thickness and skin integrity measurements for uncrosslinked Spin #2 TEGMC fibers.	241
Table 6.14: Pure CO ₂ and CH ₄ permeation values for uncrosslinked TEGMC fibers from Spin #2 at 35°C and 100 psig feed pressure.	242
Table 6.15: Spinning parameters for select states from Spin #3 with the TEGMC polymer.	244
Table 6.16: Pure O ₂ , N ₂ , and He permeation results for Spin #3 fibers at 35°C and 100 psig feed pressure.....	246
Table 6.17: Skin thickness and substructure resistance characteristics of uncrosslinked Spin #3 TEGMC fibers.	246
Table 6.18: Uncrosslinked Spin #3 TEGMC fiber permeation properties for CO ₂ and CH ₄ at 35°C and 100 psig.	247
Table 6.19: Various crosslinking conditions for the TEGMC fibers.	250
Table 6.20: Pure gas CO ₂ and CH ₄ permeation results for '2 - 9' TEGMC fibers with different crosslinking procedures at 35°C and 100 psig feed pressure using bore-side feeds.	253
Table 6.21: Comparison of '2 - 9' TEGMC fiber permeation properties for modules made with various epoxies. Measured at 100 psig and 35°C using bore-side feed.....	258
Table 6.22: Pure gas N ₂ , O ₂ , and He permeation results for '2 - 9' TEGMC fibers before and after PDMS post-treatment. Measured at 35°C with 100 psig feed pressure and bore-side feed.	260
Table 6.23: Pure gas CO ₂ and CH ₄ permeation results for '2 - 9' TEGMC fibers before and after PDMS post-treating. Bore-side feeds of 100 psig used at 35°C.	260
Table 7.1: Ideal selectivity values for crosslinked TEGMC fibers under shell-side feed at 35°C.	269
Table A.1: Critical properties and acentric factors for common sour gas components [2, 3].....	314
Table A.2: Binary interaction parameters for sour gas [3, 4].....	314

LIST OF FIGURES

	Page
Figure 1.1: Global energy-related CO ₂ emissions (in billion metric tons) by energy source between 1990 and 2035 [1].	2
Figure 1.2: Worldwide energy consumption (in quadrillion BTU) by fuel source from 1990 to 2035 [1].	2
Figure 1.3: Breakdown of market for membrane-based separations in the years 2000 and 2020 [2, 7].	6
Figure 1.4: A skid-mounted membrane unit (in foreground) was installed to replace a bulky amine absorption process (in background) [8].	7
Figure 1.5: Upper bound relation for CO ₂ /CH ₄ separations using polymeric gas separation membranes [12].	9
Figure 1.6: Membrane surface area achievable per unit of module volume for different membrane morphologies [17, 18].	12
Figure 1.7: Illustration of an asymmetric hollow fiber membrane module for a sour gas separation application. Adapted from [19].	13
Figure 1.8: Schematic of a hybrid membrane-absorption process for the removal of CO ₂ and H ₂ S from sour gas [9].	16
Figure 2.1: Graphical representation of specific volume in a hypothetical polymer sample versus temperature with the glassy and rubbery regimes indicated.	25
Figure 2.2: Depiction of various transport mechanisms through membranes [7, 8].	28
Figure 2.3: Illustration of the diffusion process for a polymeric solution-diffusion membrane. Thermally activated motions of the polymer chains allow for diffusion jumps of sorbed penetrants [6, 9].	28
Figure 2.4: Depiction of a penetrant molecule making a "jump" through a transient gap between densely packed polymer chains.	31
Figure 2.5: Comparison of the relative size and condensability of common sour gas feed components [20, 21].	33
Figure 2.6: Depiction of sour gas separations through a dense film membrane. CO ₂ and H ₂ S selectively permeate through the material due to size and condensability advantages over CH ₄ . Adapted from [8].	34

Figure 2.7: The concentration isotherm for a typical rubbery polymer is linear with a slope given by the Henry's law constant, as shown.	42
Figure 2.8: Sorption in glassy polymers occurs in two distinct modes. These sorption modes are shown individually in the plot on the left and contribute to the overall sorption level shown in the dual-mode plot on the right.	45
Figure 2.9: Physical aging of 6FDA-IPDA polyimide dense films with varying thickness is shown for a He/N ₂ separation application. Permeability decreases and selectivity increases over time. The film thicknesses are as follows: (●) thick, 28.45 μm; (○) intermediate, 2.54 μm; (Δ) thin, 5000 Å; (▲) thin, air dried at room temperature [31]. ...	47
Figure 2.10: Graphical depiction of the effects of plasticization on the productivity and efficiency of a membrane for the CO ₂ /CH ₄ separation.	56
Figure 2.11: A comparison of permselectivity calculated using pure and mixed gas feeds of CO ₂ and CH ₄ gases. Plasticization leads to the overestimation of CO ₂ /CH ₄ permselectivity under pure gas feed conditions [20, 40].	58
Figure 2.12: Illustration of an esterification crosslinking treatment used on polymers containing a carboxylic acid group. The diol crosslinking agent shown is 1,3-propane diol. Adapted from [9].	60
Figure 2.13: Selectivity for He/N ₂ (A) and CO ₂ /CH ₄ (B) with various diluents in PPO dense films.	62
Figure 2.14: Depiction of specific volume of a pure polymer sample and an antiplasticized polymer-diluent mixture (red dashed line). Excess free volume of the pure polymer is greater than that of the antiplasticized mixture.	63
Figure 2.15: Size and condensability differences for CO ₂ /CH ₄ and H ₂ S/CH ₄ gas pairs in sour gas separations. Adapted from [9].	66
Figure 2.16: Schematic of the dry-jet/wet-quench spinning setup used for producing asymmetric hollow fibers in this work [52].	70
Figure 2.17: Hypothetical ternary phase diagram, as well as predicted trajectories for different regions of the dope during the asymmetric hollow fiber membrane spinning process [52].	72
Figure 2.18: SEM images of asymmetric hollow fibers with non-optimal morphologies [52]: (a) non-concentric bore, (b) irregular/non-circular bore [85], (c) oval/partially flattened fiber [86], (d) tear-shaped macrovoids [87].	76
Figure 2.19: SEM images of failed asymmetric hollow fibers [52, 85]: (a) collapse due to high pressure feed (500 psia) on shell-side, (b) fiber wall burst due to high pressure (550 psia) on bore side	76

Figure 3.1: Stoichiometric reaction of dianhydride and diamines to form the polyamic acid precursor of the 6FDA-DAM:DABA (3:2) backbone.	86
Figure 3.2: Schematic showing the imidization of the polyamic acid precursor to form 6FDA-DAM:DABA (3:2).	88
Figure 3.3: Monoesterification reaction with 6FDA-DAM:DABA (3:2). The crosslinking agent shown in this example is 1,3-propane diol, and the resulting material is referred to as PDMC.	90
Figure 3.4: The transesterification crosslinking reaction, which is performed after membrane formation, is shown for the PDMC material.	91
Figure 3.5: Schematic of the dense film permeation cells used for pure and mixed gas experiments. Adapted from [11].	94
Figure 3.6: Schematic of a laboratory-scale asymmetric hollow fiber membrane module for sour gas testing. All components are stainless steel to prevent corrosion by the acid gas components.	100
Figure 3.7: Schematic of isochoric dense film permeation system for pure and mixed gas experiments. System components: (1) upstream volume, (2) upstream pressure transducer, (3) pneumatically-activated feed gas valve, (4) permeation cell, (5) downstream pressure (6) pneumatically-activated GC sampling valve, (7) insulated permeation box, (8) heater/fan.	103
Figure 3.8: Schematic of isobaric hollow fiber permeation system for pure gas experiments. System components: (1) upstream pressure transducer, (2) hollow fiber modules, (3) insulated permeation box, (4) heater/fan.	104
Figure 3.9: Schematic of isobaric hollow fiber permeation system for mixed gas experiments. System components: (1) upstream pressure transducer, (2) hollow fiber module, (3) insulated permeation box, (4) heater/fan, (5) syringe pump, (6) feed reservoir volume.	105
Figure 3.10: Reactions of aqueous NaOH with CO ₂ and H ₂ S in roof-mounted scrubbing unit used to neutralize vented gases from the sour gas testing laboratory.	108
Figure 3.11: Graphical depiction of the early portion of a dense film permeation experiment. Time lag (Θ) is used to quantify the transient portion of the experiment before steady-state operation is attained.	111
Figure 3.12: Schematic of pressure decay sorption system. System components: (1) reservoir volume pressure transducer, (2) sample cell pressure transducer, (3) reservoir volume, (4) sample cell volume, (5) pneumatically-activated valve, (6) oil bath, (7) heater/circulator.	118

Figure 4.1: Productivity-efficiency tradeoff for CO ₂ /CH ₄ separations [10, 11]. Data are for various candidate materials for aggressive sour gas separations [2, 12-14]. Pure gas data measured at 150 psi feed pressure and 35°C. Sour gas data are for various ternary mixtures measured at 22°C or 35°C.	129
Figure 4.2: TGA result for 6FDA-DAM:DABA (3:2) dense film dried at 100°C.....	132
Figure 4.3: Pure H ₂ S permeability at 35°C in 6FDA-DAM:DABA (3:2) films.	134
Figure 4.4: Pure gas CO ₂ and CH ₄ permeability of 6FDA-DAM:DABA (3:2) films measured at 35°C.	135
Figure 4.5: Pure gas H ₂ S, CO ₂ , and CH ₄ sorption in 6FDA-DAM:DABA (3:2) films at 35°C.	137
Figure 4.6: Pure gas diffusion coefficient isotherms at 35°C for annealed 6FDA-DAM:DABA (3:2) dense films.	140
Figure 4.7: Permeation results at 35°C for 6FDA-DAM:DABA (3:2) dense films using a binary mixture of 5% H ₂ S and 95% CH ₄	142
Figure 4.8: Permeation and selectivity results using a 10% H ₂ S, 20% CO ₂ , 70% CH ₄ mixed gas feed for 6FDA-DAM:DABA (3:2) films at 35°C.....	145
Figure 4.9: Permeation results for 6FDA-DAM:DABA (3:2) dense film annealed at 180°C with a 20% H ₂ S, 20% CO ₂ , 60% CH ₄ mixture.	147
Figure 4.10: Non-vacuum downstream pressure permeation for 6FDA-DAM:DABA (3:2) at 35°C with a 20% H ₂ S, 20% CO ₂ , 60% CH ₄ mixed gas feed.	149
Figure 4.11: 6FDA-DAM:DABA (3:2) dense film permeation results at 35°C for a 20% CO ₂ , 80% CH ₄ mixture.....	151
Figure 4.12: Dual-mode sorption model calculations for pure and mixed gas (20% CO ₂ , 80% CH ₄) feeds at 35°C.....	153
Figure 4.13: Pure and mixed gas (10% H ₂ S, 20% CO ₂ , 70% CH ₄) sorption predictions based on the dual-mode sorption model at 35°C.....	154
Figure 4.14: Partial immobilization model projections for pure gas permeability at 35°C in the 180°C annealed 6FDA-DAM:DABA (3:2) dense films.....	155
Figure 4.15: Permeation model predictions for 20% CO ₂ , 80% CH ₄ mixed gas feed at 35°C in 6FDA-DAM:DABA (3:2) dense films.....	157
Figure 4.16: Permeation model calculations for 5% H ₂ S, 95% CH ₄ mixed gas feed at 35°C.	158

Figure 4.17: Model predictions for H ₂ S, CO ₂ , and CH ₄ permeability of a 10% H ₂ S, 20% CO ₂ , 70% CH ₄ mixture at 35°C.....	159
Figure 4.18: Permselectivity projections for 10% H ₂ S, 20% CO ₂ , 70% CH ₄ mixed gas feed at 35°C.	160
Figure 4.19: Productivity-efficiency tradeoff for CO ₂ /CH ₄ separations [10, 11]. Data are for various candidate materials for aggressive sour gas separations [2, 12-14]. 6FDA-DAM:DABA (3:2) pure gas data measured at 150 psi feed pressure and 35°C, and sour gas data are for the 10% H ₂ S, 20% CO ₂ , 70% CH ₄ mixture at 35°C and 600 psi.	162
Figure 4.20: Productivity-efficiency tradeoff for H ₂ S/CH ₄ separations. Data are for various candidate materials for aggressive sour gas separations [2, 12-14]. 6FDA-DAM:DABA (3:2) pure gas data measured at 30 psi feed pressure and 35°C, and sour gas data are for the 10% H ₂ S, 20% CO ₂ , 70% CH ₄ mixture at 35°C and 600 psi.	162
Figure 4.21: Productivity-efficiency tradeoff for combined acid gas separations. Ternary gas data are shown for rubbers (black symbols) as well as the glassy polymers, CA and 6FDA-DAM:DABA (3:2). The data points used for 6FDA-DAM:DABA (3:2) films are for 600 psi feed pressure and 35°C using the 10% H ₂ S, 20% CO ₂ , 70% CH ₄ mixture. ...	164
Figure 4.22: H ₂ S/CH ₄ selectivity as a function of ether content in a series of Pebax® rubbers. The value for Selexol™ selectivity is the RK for H ₂ S and CH ₄ [13, 22]......	168
Figure 5.1: Chemical structure of a polyamide-polyether copolymer, where PA is a polyamide block and PE is a polyether block.....	174
Figure 5.2: Chemical structure of the SELEXOL™ physical solvent used for acid gas separations.....	174
Figure 5.3: PEGMC synthesis reaction via monoesterification of 6FDA-DAM:DABA (3:2) with a short-chain PEG.	177
Figure 5.4: Reaction scheme for transesterification crosslinking of PEGMC polymers.	179
Figure 5.5: ¹ H-NMR spectra for neat 6FDA-DAM:DABA (3:2) powder (Top) and monoesterified PEGMC powder using TEG crosslinking agent (Bottom).	181
Figure 5.6: ¹ H-NMR spectrum of monoesterified (uncrosslinked) PEGMC powers with DEG (Top) and TetraEG (Bottom) crosslinking agents.....	182
Figure 5.7: The structure of PEGMC is shown and the protons used for calculating monoesterification yield are indicated.	183
Figure 5.8: Pure gas CO ₂ and H ₂ S permeation at 35°C for PEGMC dense films with a TEG crosslinking agent using several crosslinking temperatures.	186
Figure 5.9: Pure H ₂ S permeation for uncrosslinked PEGMC films and the 6FDA-DAM:DABA (3:2) starting material at 35°C	190

Figure 5.10: Pure H ₂ S permeation after crosslinking the PEGMC films at 280°C. Experiments performed at 35°C.....	190
Figure 5.11: Pure CO ₂ and CH ₄ permeation isotherms at 35°C for PEGMC dense films and 6FDA-DAM:DABA (3:2).....	193
Figure 5.12: Pure gas H ₂ S and CH ₄ sorption isotherms at 35°C for crosslinked PEGMC dense films. The 6FDA-DAM:DABA (3:2) dual-mode model fit is shown for comparison.....	194
Figure 5.13: Pure CO ₂ sorption isotherm for TEG crosslinked PEGMC at 35°C.....	196
Figure 5.14: Pure gas diffusion coefficients at 35°C for TEG crosslinked PEGMC.....	197
Figure 5.15: Mixed gas H ₂ S/CH ₄ permselectivity of crosslinked PEGMC dense films at 35°C.	200
Figure 5.16: Mixed gas CO ₂ /CH ₄ permselectivity of crosslinked PEGMC dense films at 35°C.	200
Figure 5.17: Crosslinked PEGMC sour gas permeability at 35°C for a 20% H ₂ S, 20% CO ₂ , 60% CH ₄ mixed gas feed.	202
Figure 5.18: Non-vacuum-downstream pressure permeation results for TEG crosslinked PEGMC with a 20% H ₂ S, 20% CO ₂ , 60% CH ₄ feed.....	204
Figure 5.19: Permeation results for 20% CO ₂ , 80% CH ₄ mixture with TEG crosslinked PEGMC, crosslinked at 280°C.	205
Figure 5.20: Mixed gas (50% CO ₂ , 50% CH ₄) permeation at 35°C for PEGMC with TEG crosslinking agent.	206
Figure 5.21: Dual-mode sorption model calculations for pure and mixed gas (20% CO ₂ , 80% CH ₄) feeds at 35°C.....	207
Figure 5.22: Pure and mixed gas (20% H ₂ S, 20% CO ₂ , 60% CH ₄) sorption isotherms at 35°C for 6FDA-DAM:DABA (3:2) and TEG crosslinked PEGMC.....	209
Figure 5.23: Pure gas permeation showing agreement between experimental data and partial immobilization model predictions at 35°C.	210
Figure 5.24: Permeation model predictions for 20% CO ₂ , 80% CH ₄ mixed gas feed in TEG crosslinked PEGMC crosslinked at 280°C.....	211
Figure 5.25: Partial immobilization and frame of reference model predictions for 50% CO ₂ , 50% CH ₄ mixed gas feed permeation at 35°C.	212
Figure 5.26: Permeability calculations for 20% H ₂ S, 20% CO ₂ , 60% CH ₄ mixed gas feed with TEG crosslinked PEGMC treated at 280°C.....	213

Figure 5.27: H ₂ S/CH ₄ and CO ₂ /CH ₄ permselectivity projections for 20% H ₂ S, 20% CO ₂ , 60% CH ₄ mixed gas feed at 35°C.	214
Figure 6.1: Ternary phase diagram from a Gibbs free energy of mixing calculation for a spinning dope (polymer/solvent/non-solvent) system, with the binodal line in bold [3, 9].....	225
Figure 6.2: Ternary phase diagram showing the cloud point technique. Red circles and red semi-circles represent experimental dope compositions in the one- and two-phase regions, respectively, with the binodal located at the composition where the transition occurs [3].....	226
Figure 6.3: Ternary phase diagram constructed based on cloud point experiments using TEGMC polymer at approximately 50°C. The binodal is located where experimental dopes transition from one to two-phase (cloudy).	228
Figure 6.4: SEM images of fiber cross sections from syringe tests using the initial dope formulation.	230
Figure 6.5: Cross section SEM images of several TEGMC fibers from Spin #1. (A) is State #2, (B) is State #3, (C) is State #6, and (D) is State #7. All fibers samples are uncrosslinked.	232
Figure 6.6: Ternary phase diagram for TEGMC-containing dope showing the location of the Spin #2 dope. The apparent binodal location for the system is located where the dopes transition from one to two-phase (cloudy).	238
Figure 6.7: SEM images of TEGMC Spin #2 cross sections. (A) is State 3, (B) is State 4, (C) is State 6, (D) is State 9. All samples shown are uncrosslinked.	240
Figure 6.8: Uncrosslinked TEGMC fiber cross sections from Spin #3. (A) is State 1, (B) is State 2, (C) is State 4, (D) is State 5.	245
Figure 6.9: SEM images showing the skin and transition layer morphology of TEGMC fibers (ID '2 - 9'). (A) is uncrosslinked, (B) is crosslinked at 255°C with protocol C and (C) is crosslinked at 280°C with protocol E.	251
Figure 6.10: Pure CO ₂ permeance in uncrosslinked (left) and crosslinked (right) TEGMC fibers (Fiber ID '2 - 9') at 35°C with shell-side feed.	254
Figure 7.1: Pure CH ₄ permeation in crosslinked TEGMC hollow fibers at 35°C using a shell-side feed.	266
Figure 7.2: CO ₂ permeation of '2 - 9' TEGMC fibers with various treatments. Measured using shell-side feed at 35°C.	268
Figure 7.3: H ₂ S permeation in '2 - 9' TEGMC fibers with various treatments. Measured using shell-side feed at 35°C.	271

Figure 7.4: Normalized pure gas CO ₂ and CO ₄ permeation at 35°C in TEGMC fibers stored under ambient conditions for several months.	274
Figure 7.5: Permeation properties at 35°C of TEGMC fibers stored under ambient conditions for several months.	275
Figure 7.6: Normalized pure gas CO ₂ and CH ₄ permeation in TEGMC fibers stored under active CO ₂ feed for several months.	277
Figure 7.7: Permeation properties of TEGMC fibers stored under active CO ₂ feed for several months.	277
Figure 7.8: Mixed gas (50% CO ₂ , 50% CH ₄) permeation results for crosslinked TEGMC fibers. Measured using shell-side feed at 35°C.	280
Figure 7.9: Mixed gas permeation of 50% CO ₂ mixtures with and without 500 ppm toluene contaminant through crosslinked TEGMC fibers using shell-side feed at 35°C.	282
Figure 7.10: Sour gas (5% H ₂ S, 45% CO ₂ , 50% CH ₄) permeance measurements in crosslinked TEGMC fibers at 35°C.	285
Figure 7.11: Permselectivity of crosslinked TEGMC fibers using a 5% H ₂ S, 45% CO ₂ , 50% CH ₄ sour gas mixture.	286
Figure 7.12: Permeance measurements for a sour gas mixture (20% H ₂ S, 20% CO ₂ , 60% CH ₄) in crosslinked TEGMC fibers at 35°C.	288
Figure 7.13: Sour gas permselectivity of crosslinked TEGMC fibers at 35°C.	289
Figure 8.1: Productivity-efficiency tradeoff for combined acid gas separations. Ternary gas data are shown for rubbers (black symbols) as well as for several glassy polymers. The data points for crosslinked TEGMC, 6FDA-DAM:DABA (3:2), and GCV-Modified CA correspond to ternary sour gas mixtures with total feed pressure greater than 500 psi (5% H ₂ S, 45% CO ₂ , 50% CH ₄ for TEGMC – Fiber (A); 10% H ₂ S, 20% CO ₂ , 70% CH ₄ for 6FDA-DAM:DABA (3:2); and 20% H ₂ S, 20% CO ₂ , 60% CH ₄ for the others).....	300
Figure B.1: A schematic of the assembled reaction setup for the 6FDA-DAM:DABA synthesis and monoesterification reactions [1, 2].....	320
Figure C.1: Monoesterification of 6FDA-DAM:DABA (3:2) with a PEG crosslinking agent.	321

SUMMARY

The use of natural gas as a primary energy source has expanded rapidly over the past decade and this trend is expected to continue into the foreseeable future. By the year 2035, the worldwide consumption of natural gas is predicted to increase to more than 152% of its 2008 level. Unfortunately, the overwhelming majority of natural gas reserves require some degree of upgrading before the product can be transported through pipeline networks.

The acid gases carbon dioxide (CO_2) and hydrogen sulfide (H_2S) are two of the most commonly found impurities in natural gas. They are especially problematic contaminants, since they can rapidly corrode processing and transportation equipment. Also, the extremely toxic nature of the H_2S gas means it must be reduced to very low levels. At present, roughly 30% of proven natural gas resources in the US require treatment due to excessive CO_2 and H_2S concentrations. It has been estimated that as much as 40% of remaining worldwide natural gas resources are contaminated with high concentrations of H_2S .

Typical pipeline specifications for these components in the US are $< 2\%$ for CO_2 and $< 4\text{ppm}$ for H_2S . Absorption processes account for about 70% of current natural gas treatment operations. While absorption-based purification has been successful in the past, it is highly energy intensive and has a number of other drawbacks. As a result, membrane processes have garnered attention as a means of supplementing or replacing absorption units in certain situations. Membranes offer greater energy efficiency, operational flexibility, ease of process scale-up, and are more environmentally benign. However, membranes are not without their own problems. The most notable of

these are high methane (CH_4) loss due to low separation efficiency, poor membrane stability under aggressive feed conditions, and difficulty in fabricating high-quality membrane morphologies and modules.

Few studies so far have focused on the simultaneous removal of CO_2 *and* H_2S from sour natural gas feeds. Additionally, the sour gas feeds used in these studies typically contain very low partial pressures of H_2S . In actual field operations, wellhead pressures can exceed 1000 psi and H_2S concentrations may be greater than 5%. Membrane plasticization, which can lead to a loss of separation efficiency, is more likely to occur under these aggressive feed conditions, and this is almost always accompanied by a significant decrease in membrane performance.

The overarching goal of this study was to develop or identify of a glassy polymer membrane material that can be used for aggressive sour gas separations to simultaneously remove CO_2 and H_2S at high feed partial pressures. This material must have excellent stability against the harsh feed conditions in order to maintain acceptable separation performance, in terms of productivity and separation efficiency. Moreover, it should be possible to produce high-quality asymmetric hollow fiber membranes from the selected material.

The well-studied glassy copolyimide 6FDA-DAM:DABA was investigated as a polymer backbone for membranes used in this application. An esterification crosslinking mechanism, which is compatible with 6FDA-DAM:DABA, was employed in order to synthesize materials with augmented $\text{H}_2\text{S}/\text{CH}_4$ selectivity and plasticization resistance. These materials make use of polyethylene glycol (PEG) crosslinking agents and are referred to as PEGMC polymers. Rigorous dense film characterization of the novel crosslinkable materials indicates that excellent $\text{H}_2\text{S}/\text{CH}_4$ selectivity (24) is achievable

while still maintaining high CO₂/CH₄ selectivity (29) under high pressure ternary mixed gas (CO₂/H₂S/CH₄) feeds. Defect-free asymmetric hollow fiber membranes were formed and appropriate crosslinking conditions were determined, allowing for the characterization of these fibers under realistic sour gas feed conditions. Also, a PDMS post-treatment was used to give ultra-high permselectivity for aggressive feeds.

Using several mixed gas feeds containing high concentrations of CO₂ and H₂S at feed pressures up to 700 psig, it is shown that the crosslinked asymmetric hollow fiber membranes developed and manufactured through this work are capable of maintaining excellent separation performance even under exceedingly taxing operating conditions. For example, CO₂/CH₄ and H₂S/CH₄ permselectivity values of 47 and 29, respectively, were obtained for a 5% H₂S, 45% CO₂, 50% CH₄ feed at 35°C with 700 psig feed pressure. An extremely aggressive 20% H₂S, 20% CO₂, 60% CH₄ mixed gas feed with 500 psig feed pressure was also used; the maximum CO₂/CH₄ and H₂S/CH₄ permselectivity values were found to be 38 and 22, respectively.

The main results of this investigation indicate that aggressive, simultaneous sour gas separations of CO₂ and H₂S from natural gas may be accomplished with membrane processes. The crosslinkable material developed in this work, PEGMC, highlights the excellent productivity, separation efficiency, and stability properties of this class of ester-crosslinkable polyimides. Also, these crosslinkable polyimides, and PEGMC in particular, are attractive due to the ability to tune their performance, which allows for specific process requirements to be achieved over a wider range of feed compositions. Furthermore, the concept of selecting a crosslinking agent to attain a targeted permselectivity improvement, in addition to the typical stability improvement due to crosslinking, represents a novel concept in the field of membrane-based gas separations.

CHAPTER 1

INTRODUCTION AND MOTIVATION

1.1. Natural Gas Processing

With the continuing rise in world population and the economic growth of developing nations, the global demand for energy is projected to rapidly expand in the near future. Total worldwide energy consumption is expected to grow by 53%, from 505 quadrillion BTU in the year 2008 to 770 quadrillion BTU by the year 2035, which equates to an annual increase of 1.6% [1]. Based on these numbers and the expansion of governmental regulation focusing on more efficient energy technologies and lower CO₂ emissions, natural gas and the technologies related to natural gas production have garnered much attention. Figure 1.1 shows the projected trends in CO₂ emissions by energy source over the next several decades [1]. Coal is predicted to remain the primary fossil fuel source of atmospheric CO₂ emissions, and natural gas is expected to continue to contribute the least to atmospheric CO₂ despite its increased global use. Natural gas is particularly attractive compared to the alternative fossil fuels because of its lower carbon footprint, increased thermal efficiency, and increased availability due to the development and expansion of non-traditional production processes such as hydraulic fracturing and horizontal drilling. The combination of all these facts has led to the prediction that natural gas consumption will continue to rise steadily over the next several decades, despite the increased reliance upon renewable energy sources (Figure 1.2).

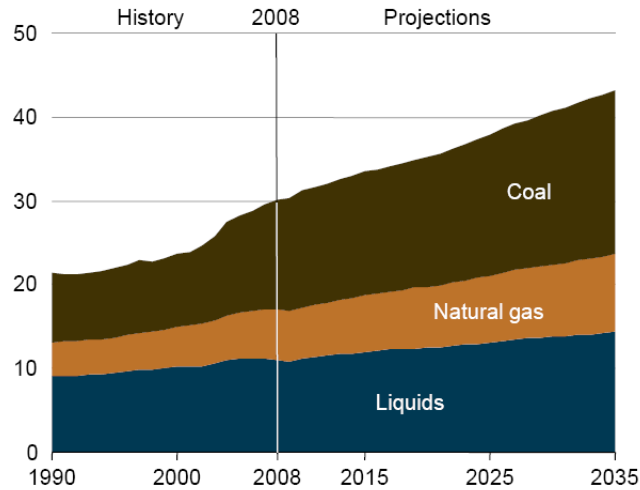


Figure 1.1: Global energy-related CO₂ emissions (in billion metric tons) by energy source between 1990 and 2035 [1].

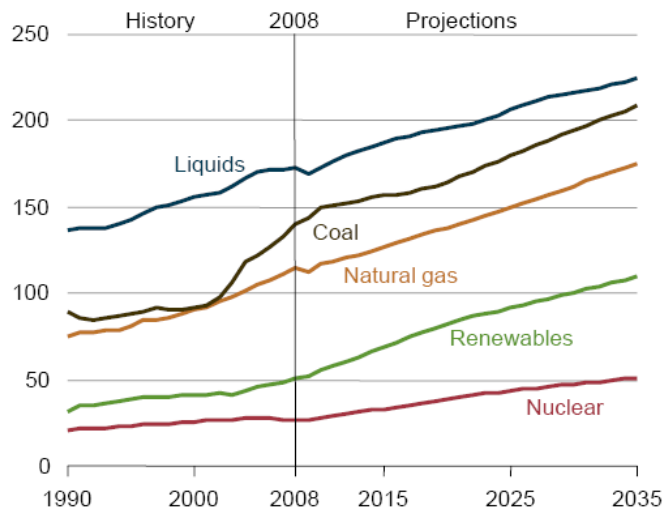


Figure 1.2: Worldwide energy consumption (in quadrillion BTU) by fuel source from 1990 to 2035 [1].

Although the natural gas product that is eventually used by consumers is primarily composed of CH₄, many impurities can be present in natural gas wells. These unwanted impurities include CO₂, H₂S, H₂O, N₂, and C₂₊ hydrocarbons. It should be noted, however, that the specific type and concentration of each component can vary widely depending on geographical location and the origin of each natural gas reserve.

Nevertheless, almost all natural gas requires treatment, or upgrading, before transport of the product gas to the consumer. The natural gas impurities must be reduced to certain levels, referred to as ‘pipeline specifications’, prior to transport and distribution through extensive pipeline networks. Typical natural gas pipeline specifications for the United States are shown in Table 1.1.

Table 1.1: Typical US natural gas pipeline specifications [2].

Natural Gas Component	Pipeline Specification
CO ₂	< 2%
H ₂ S	< 4 ppm
H ₂ O	< 120 ppm
C ₃₊	950-1050 BTU/scf; Dew Point: -20°C
Inert Gases (N ₂ , He, etc.)	< 4%

While the heavier hydrocarbon components (C₂₊) have very significant value in other markets and are typically extracted and sold separately, a greater challenge for the production of an economical natural gas product stream is the removal of the lower-value contaminants. The acid gases CO₂ and H₂S are in many cases the most prevalent of these impurities. In fact, enhanced oil recovery operations – which involve the reinjection of CO₂, H₂S, or N₂ to improve extraction of valuable raw material from fossil fuel reserves – can lead to extremely high levels of these contaminants. For instance, CO₂ concentrations exceeding 50% are not uncommon and, in the most extreme cases, concentrations can be as high as 80% [3]. The two acid gases, along with H₂O, may cause corrosion of natural gas pipelines and processing equipment. As such, their removal is essential to the maintenance of a properly functioning natural gas distribution network. Furthermore, the removal of these non-flammable or lower energy content gases is important for maintaining an acceptable heating value and reducing the compression and transportation costs of a natural gas stream. It is also important to

point out the very serious health and safety issues that go along with high concentrations of H₂S [4]. This is a highly toxic and flammable compound that necessitates the use of rigorous gas handling safety protocols and equipment. Furthermore, the combustion of natural gas containing H₂S can contribute significantly to environmentally harmful SO₂ emissions. Hence, the removal of these so-called acid gases constitutes a critical step in natural gas production and is, in fact, the largest industrial gas separation process [5].

To avoid confusion, the term 'acid gas' is used to refer to any acidic gas component (e.g. CO₂ or H₂S). Conventionally, a feed stream is referred to as a 'sour gas' whenever H₂S is present at high levels. This term is a reflection of the strong unpleasant odor associated with H₂S. Thus, the term sour gas refers to a specific type of acid gas. The process of upgrading a natural gas stream containing H₂S is referred to as 'sweetening', again alluding to the removal of the foul-smelling H₂S contaminant from the feed gas.

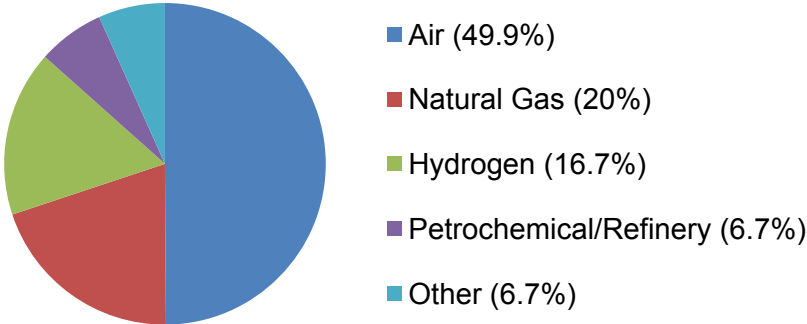
Separation processes as a whole represent 40-70% of industrial capital and operating costs [6]. As such, the search for more efficient separation technologies is a perpetual effort that is critical to the long-term stability and competitiveness of many businesses. The most common separation technologies that are used for natural gas purification include cryogenic distillation, solvent-based absorption (including amines and others), and membranes.

Cryogenic distillation is a highly energy intensive process due to the low temperatures and large feed streams involved. Solvent-based absorption processes, specifically those involving amine solvents, are considered the industry standard for acid gas removal at the present time. While absorption processes are time-tested and offer high-performance under the right operating conditions, they are not without their own

drawbacks. Large energy requirements, resulting from thermally-driven solvent regeneration, and complex processing equipment, including large-scale absorption columns, lead to significant maintenance and capital expenditures. Also, the large footprints of these processing facilities makes them ill-suited for remote, offshore, and low-volume locations where the majority of new natural gas plays are likely to occur as the highest quality reserves providing the easiest production opportunities become depleted. The disposal of large amounts of waste solvent represents a significant challenge, as well, with numerous environmental restrictions that must be adhered to.

Membrane processes represent a growing technology in the field. In recent decades, most membrane processes have been employed for bulk CO₂ removal applications where the process economics are most favorable to membranes compared to absorption. This niche has afforded membrane processes an opportunity to prove themselves as a viable alternative gas separation technology for the future. Figure 1.3 shows the predicted expansion of membrane use for natural gas and petrochemical separations between the years 2000 and 2020 [2, 7].

Membrane Separations Market in 2000 (\$150 million)



Membrane Separations Market in 2020 (\$760 million)

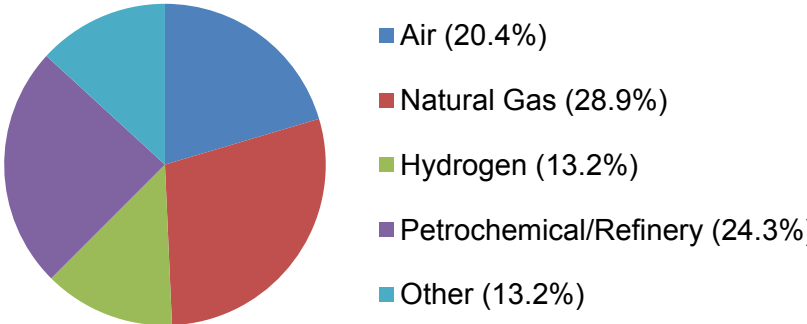


Figure 1.3: Breakdown of market for membrane-based separations in the years 2000 and 2020 [2, 7].

1.2. Membranes for Natural Gas Purification

The expansion of membrane-based gas separations in recent years is the result of the many advantages they hold over absorption processes. These include smaller weight and footprint, reduced adverse environmental impact, higher energy efficiency, ease of operation and maintenance, and excellent separation efficiency and productivity for CO₂ removal. Membrane units are normally skid-mounted and modular, involve few moving parts, and can provide outstanding separation surface area-to-volume ratios. Perhaps most notably, membrane processes take advantage of a so-called ‘free driving

force' to perform the intended separation. Specifically, membranes rely upon a transmembrane partial pressure differential to drive the separation, which arises from the high wellhead pressure normally present in natural gas reserves. Despite these numerous advantages, the choice of a particular separation processes is ultimately determined by factors related to each individual reserve; offshore production facilities, for example, tend to favor membranes due to the premium placed on space and weight. Figure 1.4 highlights the compactness of membranes compared to absorption processes.



Figure 1.4: A skid-mounted membrane unit (in foreground) was installed to replace a bulky amine absorption process (in background) [8].

Hybrid membrane-absorption processes are also a commonly encountered separation process setup. These are of particular utility when the concentration of contaminants like CO_2 and H_2S are very high, making the membrane separation step ideal for bulk contaminant removal and the secondary absorption step well-suited for polishing in order to meet pipeline specifications [5, 9, 10]. On their own, currently

available membranes are often unable to achieve the very high purity levels that are necessary for pipeline transport without relatively high and costly methane loss. This is the result of the moderate separation efficiencies that are realizable under actual operating conditions. In fact, most membrane processes attempt to mitigate these losses by using multiple membrane units operating with a recycle stream. Unfortunately, this requires the extensive use of compressors, which can significantly cut into the overall energy efficiency of the process. The development of materials and morphologies that provide high productivity (flux), high separation efficiency (selectivity), and stable performance under realistic conditions may allow membranes to overcome these challenges.

The past several decades of membrane material research and development has revealed a practical upper limit for the performance of polymeric membranes. Referred to as an 'upper-bound tradeoff', this trend was first documented by Robeson in 1991 for several gas pairs and has since been updated to reflect the gradual performance improvements achieved by more advanced polymers [11-13]. The general trend of increased membrane productivity leading to decreased membrane separation efficiency reflected in this plot characterized performance that membrane scientists endeavor to overcome. The upper bound line for the CO₂/CH₄ separation is shown in Figure 1.5. To date, there has not been sufficient experimental data collected on H₂S/CH₄ separations to allow for the calculation of such an upper bound line.

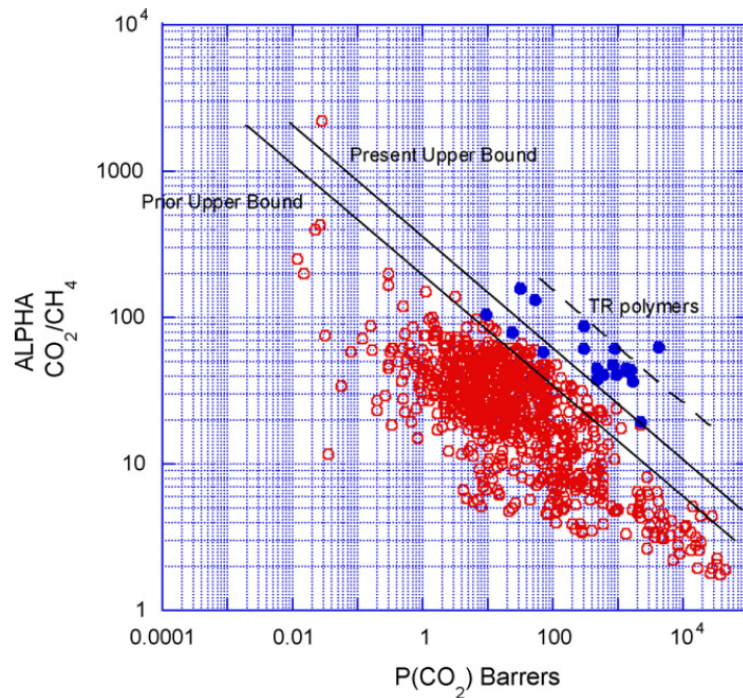


Figure 1.5: Upper bound relation for CO₂/CH₄ separations using polymeric gas separation membranes [12].

Robeson and Freeman have discussed the origin of the polymeric membrane material upper-bound [12, 14]. Essentially, this effect arises from the fact that membrane separations rely primarily on molecular size or solubility differences between a gas pair. As the productivity of a membrane material increases, the difference in the rate of transport of the gases, or separation efficiency, is reduced – primarily due to smaller differences in diffusion coefficients of the components in the less restrictive medium.

For a membrane material to be commercially viable, it is desirable for its productivity-efficiency properties to approach the upper-bound for the gas pair of interest. Major efforts in recent years have led to the development of several advanced polymers that meet these requirements for the CO₂/CH₄ separation. Polyimides are one of the most common classes of high performance materials currently under investigation for this application. Unfortunately, the material performance requirements mentioned

above are not in and of themselves sufficient to justify the use membranes in the field. In reality, membranes almost always suffer significant performance reductions under the harsh conditions encountered in practice, and the ability of a material to resist these performance losses is another key to its success.

Membrane materials that exhibit properties approaching the upper-bound line under fairly benign laboratory testing conditions can experience a phenomenon known as penetrant-induced plasticization when exposed to high concentrations of polar or condensable gases, such as CO₂ and H₂S. Plasticization is the result of high-level gas sorption within the membrane that leads to swelling of the polymer chains, increased polymer chain segmental mobility, and, ultimately, a radical increase in the flux of all gases through the membrane. This is almost always associated with a significant loss of the membrane's size discriminating ability. CHAPTER 2 presents a more complete discussion of this complicated phenomenon.

Plasticization plays an especially important role in natural gas separations involving CO₂ and H₂S. These condensable species comprise a large fraction of many natural gas reserves. In the case of particularly harsh or 'aggressive' natural gas feeds, which contain these two acid gases at high partial pressures, materials that are either specifically designed for or given additional processing steps to stabilize the membrane and reduce the effect of plasticization are a necessity. A number of methods for controlling the extent of membrane plasticization have been used and are also discussed in CHAPTER 2. Because of the high likelihood of plasticization, membranes intended for these sour gas separation applications must be characterized under aggressive conditions that mimic those likely to be encountered in the field.

1.3. Membrane Technology Overview

For a membrane process to be selected for commercial application, several practical requirements must be met. Pioneering researchers in the field of membranes for gas separations have identified four key elements that will enable the advancement of membrane technology: (1) the development of high-efficiency membrane modules with excellent separation surface area-to-volume ratios for large-scale commercial processes, (2) the creation of advanced materials capable of high-efficiency separations, (3) the development of a capability to alter morphologies at multiple levels within the cross-section of a membrane, and (4) the development of production methods that rapidly, economically, and efficiently combine the first three elements into “defect-free” modules [15].

Of course, polymers are not the only materials that are used to form gas separation membranes. Ceramics, zeolites, metal-organic frameworks, and carbons have also been used by membrane researchers and are each attractive due to their own particular strengths [10, 16]. However, polymers remain the dominant membrane material type used for natural gas separations and are the focus of this work. Polymeric membranes can be implemented in several different morphologies, including plate in frame, spiral wound, and hollow fiber modules. In recent years, the asymmetric hollow fiber membrane morphology has emerged as the most promising option for achieving the four elements discussed above.

Asymmetric hollow fibers are tubular with a thin effective membrane layer on the outermost portion of the fiber, a highly porous substructure comprising the majority of the fiber wall and lending mechanical support to the membrane, and an open interior that enables gas flow along the length of the fiber with minimal mass transfer resistance.

Critically, asymmetric hollow fibers can be formed such that the effective separation layer is reduced to an integral “skin” of minimal thickness [17]. This leads to extremely high flux membranes, which are necessary for high productivity modules. Additionally, the asymmetric hollow fiber morphology is preferred industrially because of the outstanding fiber packing densities and surface area-to-volume ratios that are achievable within each module. A comparison of the surface area-to-volume ratios of the different membrane module types is shown in Figure 1.6. This ratio for hollow fiber modules can exceed 10,000 m²/m³ for small diameter fibers, which significantly outperforms the plate in frame and spiral wound module morphologies [17].

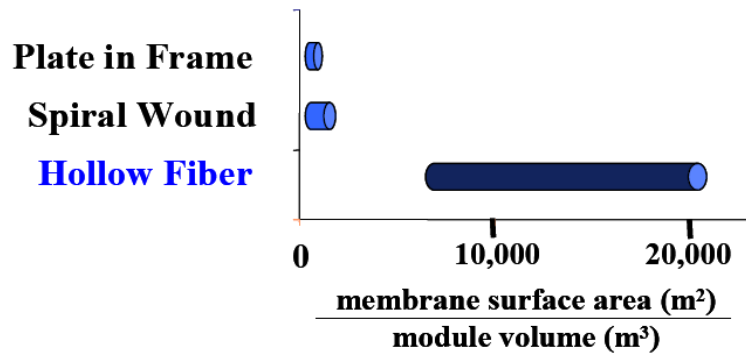


Figure 1.6: Membrane surface area achievable per unit of module volume for different membrane morphologies [17, 18].

Furthermore, asymmetric hollow fiber modules are able to withstand large transmembrane pressure differentials and, thus, take full advantage of the free separation driving force mentioned previously. Figure 1.7 shows a schematic of a typical asymmetric hollow fiber membrane module. The membrane skin layer of an asymmetric hollow fiber can be as low as 100 nm, and the outside diameter of the fiber can be on the order of 200 μm. A greater level of detail on the design of asymmetric hollow fibers is given in CHAPTER 3 and CHAPTER 6.

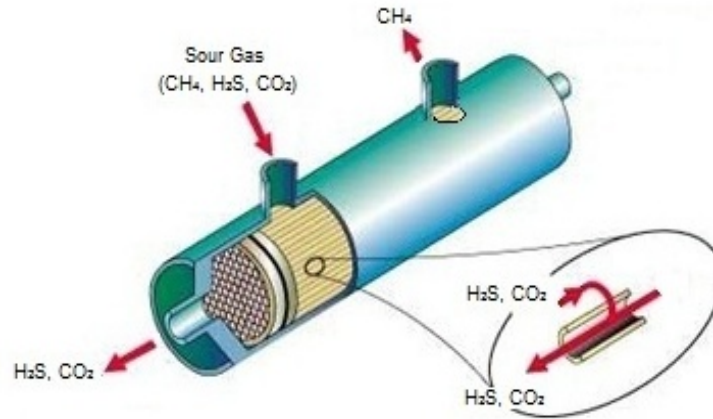


Figure 1.7: Illustration of an asymmetric hollow fiber membrane module for a sour gas separation application. Adapted from [19].

In the context of the four elements of membrane technology advancement described above, all but the second element are addressed within the framework of the selected membrane morphology. For the present study, the preferred morphology is the asymmetric hollow fiber membrane. The second element, creation of advanced membrane materials, plays a more fundamental role across all of membrane technology and for this reason has traditionally been the focus of most membrane separations research. Some of greatest challenges associated with membrane material creation have already been touched upon – namely, productivity-efficiency tradeoff optimization and performance stability under harsh conditions. The research presented here spans all four of the membrane technology elements, with the unique goal of applying membrane technology to the heretofore sparsely studied **aggressive sour gas separation** (i.e. simultaneous removal of high concentration CO₂ and H₂S from high pressure natural gas feeds).

1.4. Sour Gas Separation Overview

Despite the greater emphasis on CO₂/CH₄ separations, the preceding discussion on membrane-based natural gas purification pertains to the removal of both CO₂ and H₂S. The stress that is placed on CO₂ removal through the course of this discussion is a reflection of the far larger body of academic research that has been directed at CO₂/CH₄ separations compared to H₂S/CH₄ separations. Numerous factors have contributed to this trend over the lifetime of membrane gas separations research. These include the greater prevalence of CO₂-contaminated reserves, the relative ease of CO₂ removal and subsequent disposal compared to H₂S, and the stringent safety requirements and additional gas handling equipment that are needed when working with high concentrations of H₂S, to name a few. This lack of sour gas separations research notwithstanding, the simultaneous removal of CO₂ and H₂S from natural gas feeds is already an important commercial separation at the present time and has the potential to become much more commonplace as higher quality natural gas reserves become rapidly depleted. Although sour gas reserves have traditionally been passed over in favor of abundant, easier production opportunities, it is believed that as much as 40% of remaining worldwide natural gas reserves are contaminated with H₂S [20-23].

The limited amount of membrane-related research and development aimed at H₂S removal from sour gas has focused almost exclusively on the use of rubbery polymers and is normally restricted to fairly low H₂S partial pressures. Several researchers have investigated rubbery polyether-block-amide membranes, which tend to have excellent H₂S/CH₄ separation efficiency and productivity [24-26]. However, the performance of these materials for the CO₂/CH₄ separation tends to be much less impressive. Similarly, the few glassy polymer membrane materials that have been tested for sour gas separations, while typically giving excellent CO₂/CH₄ separation

performance, appear to be ill-suited for H₂S/CH₄ separations due to low separation efficiency. Based on these results, it has been suggested that no currently available material is likely to give outstanding separation performance for both CO₂ and H₂S removal. In other words, no material will approach the upper bound tradeoff curve for both CO₂/CH₄ and H₂S/CH₄ separations. In fact, the fundamental explanation for this phenomenon is related to the mechanism by which gas molecules are transported through polymer membranes and the different selectivity mechanisms by which rubbery and glassy materials achieve a separation. These fundamentals will be discussed in CHAPTER 2.

In addition to the challenge of developing a material capable of simultaneous CO₂ and H₂S removal, a major obstacle to the use of membranes for sour gas separations is the tendency of H₂S to cause membrane plasticization at partial pressures lower than that of even CO₂. This arises from the fact that H₂S is a highly polar and even more condensable gas than CO₂, which results in extremely high solubility and rapid membrane swelling. Clearly, the obstacles that exist towards sour gas separations using membranes are significant, and this explains the relatively minimal amount of research in this field to date.

In the simpler cases of natural gas reserves that are contaminated with only CO₂ or only H₂S, membrane material selection would be fairly straightforward. CO₂-selective glassy polymers would be used for CO₂/CH₄ separations and H₂S-selective rubbery polymers would be used for H₂S/CH₄ separations. However, the motivation for this work – the development of a material capable of performing simultaneous CO₂ and H₂S removal under highly aggressive feed conditions – is the fact that many natural gas reserves require the removal of both acid gas species [5].

Several authors have investigated the economics of performing sour gas separations with membrane, absorption, or hybrid membrane/absorption processes using currently available membrane materials and absorption solvents. One set of papers by Hao et al. simulated different configurations of membrane units that involved CO₂-selective materials, H₂S-selective materials, or a combination of the two in series [27, 28]. They found that the appropriate membrane unit configuration depends largely on the feed composition, but the most economical situation generally involves the use of a single membrane type that is selective to the contaminant gas of the highest concentration in the feed. Unfortunately, this study did not account for the possibility of plasticization under the aggressive feed conditions of interest.

Another paper by Bhide et al. focused on the process economics of a hybrid membrane/absorption process configuration (Figure 1.8) for sour gas separations [9].

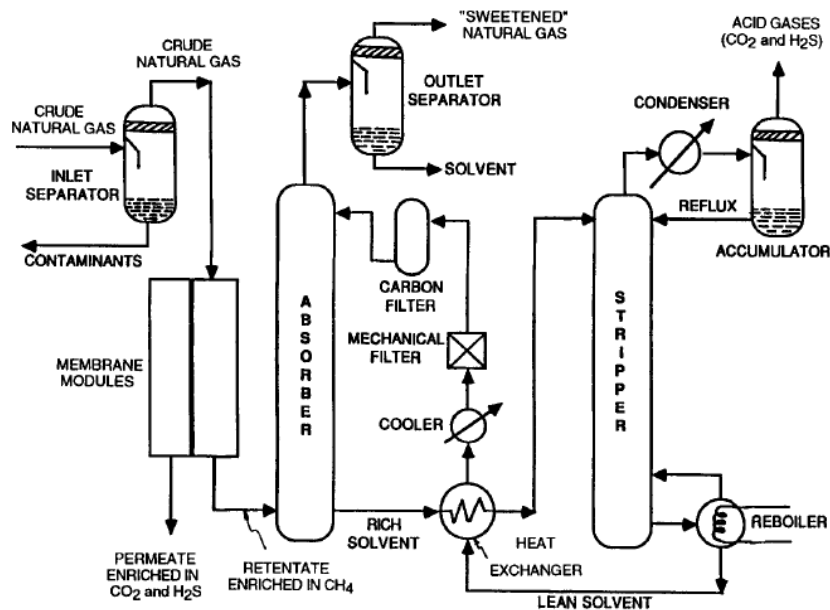


Figure 1.8: Schematic of a hybrid membrane-absorption process for the removal of CO₂ and H₂S from sour gas [9].

The membrane properties assumed in this study were reflective of the current industrial standard glassy polymer membrane material for bulk CO₂ removal, cellulose acetate (CA). The absorption process solvent properties assumed were those of an aqueous diethanolamine (DEA) solution. A membrane unit was placed upstream of the absorber column, and this acted as a bulk removal system for both CO₂ and H₂S with the absorption step acting as a polisher to bring the acid gas concentrations down to pipeline specification. While many variables were considered, these authors concluded that the most favorable process economics for a feed containing 24.5% CO₂ and up to 1.0% H₂S is obtained either with membranes alone or with a hybrid membrane/absorption process design. This is a promising result for the application of membrane technologies to sour gas separations, particularly considering the modest CO₂/CH₄ and H₂S/CH₄ separation properties of CA compared to more advanced membrane materials. On the other hand, this study also did not attempt to account for membrane performance losses due to the plasticization phenomenon. This could potentially have serious ramifications for the findings presented by these authors.

Regardless of the material or process configuration, it is not likely that membranes alone could be used economically to reduce the concentrations of CO₂ and H₂S down to pipeline specifications in cases when a sour gas feed contains a large fraction of acid gases, especially H₂S. This is mostly due to the stringent pipeline specification for H₂S (4ppm), which would require either much higher efficiency materials than are currently available or much more recycling (to avoid overwhelming CH₄ losses) than is economically viable. However, membranes certainly appear to be very well-suited for the bulk removal of CO₂ and H₂S from sour gas. This step would significantly reduce the acid gas content of a sour gas feed stream entering the secondary

absorption polishing step and greatly reduce the size and cost of the absorption process, since cost scales with acid gas concentration.

Following the conclusions of Hao et al., it is likely that a single membrane material would be preferred for simultaneous CO₂ and H₂S removal in a bulk separation application, provided it is more selective to the acid gas component of highest concentration and has reasonable separation efficiency for the second acid gas component.

In the United States and, in fact, in most locations, the majority of sour natural gas reserves contain higher CO₂ concentrations than H₂S [3, 5, 26]. Therefore, it is likely that an appropriate glassy polymer material with high CO₂/CH₄ separation efficiency and moderate H₂S/CH₄ efficiency would be suitable for many sour gas production opportunities. Traditionally, CA has been the industrial standard glassy polymer for bulk CO₂ removal, and the H₂S/CH₄ separation efficiency of CA may be sufficient for simultaneous bulk CO₂ and H₂S removal in certain cases. However, process economics would be further improved by the identification or development of a more advanced glassy polymer material, such as a polyimide, with even more attractive CO₂/CH₄ and H₂S/CH₄ separation properties in terms of productivity, efficiency, and stability.

Based on the above discussion, it is believed that the application of membranes to simultaneous CO₂ and H₂S separations from sour gas may be viable. Also, glassy polymer materials, rather than the rubbery polymers that have so far been the focus of sour gas separations research, appear to be the most promising option. A great deal of room exists for research into the development and characterization of glassy polymer membranes for sour gas separations because of the limited amount of previous academic research and the focus that has so far been placed on rubbery polymers and

feeds containing low H₂S partial pressures. Before membranes can be deployed commercially for this application, it is important that further investigation of these materials under highly aggressive, realistic feed conditions be performed. Furthermore, the development and characterization of asymmetric hollow fiber membrane modules under sour gas feed conditions is also an important next step in the use of membrane technology within this field.

The overarching goals of this work are the identification and/or development of a promising glassy polymer material for use in aggressive sour gas separation application; rigorous characterization of this material to evaluate its productivity, separation efficiency, and stability properties; formation of defect-free asymmetric hollow fiber membranes and modules; and characterization of these modules under sour gas feed conditions.

1.5. Research Objectives

(1) Develop advanced glassy polymer materials with excellent simultaneous CO₂/CH₄ and H₂S/CH₄ separation performance as measured by productivity, separation efficiency, and membrane stability under aggressive feed conditions by using pure and mixed gas transport characterization.

In this objective, we identify existing polymeric materials with promising separation and stability properties for this aggressive feed application. The advanced polyimide 6FDA-DAM:DABA is selected for further study as a result of its proven CO₂/CH₄ separation performance in the literature and its capacity for performance-enhancing crosslinking modifications. Extensive sour gas transport characterization is performed in order to identify any necessary material property improvements as well as

a path forward for development of the 6FDA-DAM:DABA backbone. A novel crosslinkable material, PEGMC, is synthesized and subjected to transport characterization using aggressive sour gas feeds.

(2) Produce defect-free asymmetric hollow fiber membranes using the most attractive polyimide material developed in Research Objective 1.

This objective addresses the feasibility of fabricating, or ‘spinning’, high-quality asymmetric hollow fiber membranes that are free of defects using the novel crosslinkable polyimide material (PEGMC) developed in Objective 1. The separation efficiencies and stability of these fibers should approach the values measured in the analogous dense film membranes, and the fiber dimensions should enable the manufacture of high-productivity modules.

(3) Develop and characterize suitably crosslinked asymmetric hollow fiber membrane modules from the fibers produced in Research Objective 2 using realistic, aggressive sour gas feed conditions.

Objective 3 deals with the development of an appropriate crosslinking procedure for the PEGMC asymmetric hollow fiber membranes, a process for making high-quality modules of these fibers, and the evaluation of the crosslinkable hollow fiber membranes using sour gas feeds. The modules are exposed to aggressive mixed gas feeds and their productivity, separation efficiency, and stability properties are characterized.

1.6. Dissertation Overview

CHAPTER 2 presents background and theory for the concepts alluded to throughout this dissertation. This will include a discussion of challenges associated with the unique sour gas separation of interest, including membrane plasticization and potential means of controlling this phenomenon. CHAPTER 3 contains information on the materials and experimental methods used. This will range from polymer synthesis and dense film casting to transport characterization, asymmetric hollow fiber spinning, and module-making. CHAPTER 4 describes the identification and evaluation of potentially high-performing glassy polymer materials through dense film transport characterization. CHAPTER 5 presents the results of synthesis and crosslinking a novel glassy polyimide, as well as sour gas transport characterization under aggressive feed conditions. CHAPTER 6 is related to the formation of high-quality, defect-free asymmetric hollow fiber membranes, the crosslinking of these fibers, and the manufacture of modules from these fibers. CHAPTER 7 contains results from characterizing the crosslinked and uncrosslinked asymmetric hollow fibers with sour gas feeds. Finally, CHAPTER 8 gives a summary of the major findings contained within this dissertation and presents recommendations for future work.

1.7. References

1. *International Energy Outlook 2011*, 2011, U.S. Energy Information Administration: Washington, D.C.
2. Baker, R.W., *Future Directions of Membrane Gas Separation Technology*. Industrial & Engineering Chemistry Research, 2002. **41**(6): p. 1393-1411.
3. Tabe-Mohammadi, A., *A Review of the Applications of Membrane Separation Technology in Natural Gas Treatment*. Separation Science and Technology, 1999. **34**(10): p. 2095-2111.

4. *Hydrogen Sulfide, MSDS # 001029*. [Material Safety Data Sheet] 2010 26 April 2010 [cited 2010 3 December]; Available from: <http://www.airgas.com/documents/pdf/001029.pdf>.
5. Baker, R.W. and K. Lokhandwala, *Natural Gas Processing with Membranes: An Overview*. Industrial & Engineering Chemistry Research, 2008. **47**(7): p. 2109-2121.
6. Legault, A.R., R., *Mainstreaming Efficient Industrial Separation Systems*. International Energy Agency (IEA) OPEN Energy Technology Bulletin, 2008(55).
7. Chen, C.C., *Thermally Crosslinked Polyimide Hollow Fiber Membranes for Natural Gas Purification*, in *School of Chemical and Biomolecular Engineering*2011, Georgia Institute of Technology: Atlanta, GA.
8. *Gas Sweetening Membranes*. Available from: <http://www.prosep.com/files/GasMembranes.pdf>.
9. Bhide, B.D., A. Voskericyan, and S.A. Stern, *Hybrid processes for the removal of acid gases from natural gas*. Journal of Membrane Science, 1998. **140**(1): p. 27-49.
10. Bernardo, P., E. Drioli, and G. Golemme, *Membrane Gas Separation: A Review/State of the Art*. Industrial & Engineering Chemistry Research, 2009. **48**(10): p. 4638-4663.
11. Robeson, L.M., *Correlation of separation factor versus permeability for polymeric membranes*. Journal of Membrane Science, 1991. **62**(2): p. 165-185.
12. Robeson, L.M., *The upper bound revisited*. Journal of Membrane Science, 2008. **320**(1-2): p. 390-400.
13. Koros, W.J. and R.T. Chern, *Separation of Gaseous Mixtures Using Polymer Membranes*, in *Handbook of Separation Process Technology*, R.W. Rousseau, Editor. 1987, John Wiley & Sons, Ltd.: New York.
14. Freeman, B.D., *Basis of Permeability/Selectivity Tradeoff Relations in Polymeric Gas Separation Membranes*. Macromolecules, 1999. **32**(2): p. 375-380.
15. Koros, W.J., *Evolving beyond the thermal age of separation processes: Membranes can lead the way*. AIChE Journal, 2004. **50**(10): p. 2326-2334.
16. Koros, W.J. and G.K. Fleming, *Membrane-based gas separation*. Journal of Membrane Science, 1993. **83**(1): p. 1-80.
17. Baker, R.W., *Membrane Technology and Applications*. 2 ed. 2004, West Sussex: John Wiley & Sons, Ltd.
18. Omole, I.C., *Crosslinked Polyimide Hollow Fiber Membranes for Aggressive Natural Gas Feed Streams*, in *School of Chemical and Biomolecular Engineering*2008, Georgia Institute of Technology: Atlanta, GA. p. 305.

19. *Nitrogen Membranes - Technology*. 2010 [cited 2010 3 December]; Available from: <http://www.medal.airliquide.com/en/nitrogen-membranes/nitrogen-membranes-technology.html>.
20. Canty, D. *The Middle East Sour Oil & Gas Upstream Profile*. 2012 May 8, 2012 [cited 2013 March 21, 2013]; p. 1-2]. Available from: <http://www.arabianoilandgas.com/article-10245-the-middle-east-sour-oil-gas-upstream-profile/1/#.UUs2ZxyKf-t>.
21. *Sour and Acid Gas*. [cited 2013 March 21, 2013]; Available from: <http://www.total.com/en/our-energies/natural-gas/-exploration-and-production/our-skills-and-expertise/sour-acid-gas-940886.html>.
22. Rojey, A., *Natural Gas: Production, Processing, Transport*. 1997, Paris, France: Enfield Pub & Distribution Company.
23. Gadon, J.L., *Test of distribution of natural gas reserves by gas composition*. Revue De L'Institut Francais Du Petrole, 1987. **42**(6): p. 685-693.
24. Chatterjee, G., A.A. Houde, and S.A. Stern, *Poly(ether urethane) and poly(ether urethane urea) membranes with high H₂S/CH₄ selectivity*. Journal of Membrane Science, 1997. **135**(1): p. 99-106.
25. Mohammadi, T., et al., *Acid Gas Permeation Behavior Through Poly(Ester Urethane Urea) Membrane*. Industrial & Engineering Chemistry Research, 2008. **47**(19): p. 7361-7367.
26. Membrane Technology and Research, I., *Low-Quality Natural Gas Sulfur Removal/Recovery*, 1998, The Department of Energy: Morgantown, WV.
27. Hao, J., P.A. Rice, and S.A. Stern, *Upgrading low-quality natural gas with H₂S- and CO₂-selective polymer membranes: Part I. Process design and economics of membrane stages without recycle streams*. Journal of Membrane Science, 2002. **209**(1): p. 177-206.
28. Hao, J., P.A. Rice, and S.A. Stern, *Upgrading low-quality natural gas with H₂S- and CO₂-selective polymer membranes: Part II. Process design, economics, and sensitivity study of membrane stages with recycle streams*. Journal of Membrane Science, 2008. **320**(1-2): p. 108-122.

CHAPTER 2

BACKGROUND AND THEORY

2.1. Polymer Membranes for Gas Separations

Amorphous polymers are by far the most commonly used material for membrane separations. They offer excellent processability, are relatively inexpensive, and can give high separation efficiency for many applications. In the field of membrane transport, perhaps the most important distinction made between one polymer and the next pertains to its glass transition temperature (T_g). Amorphous polymers with a T_g below the temperature at which it is used are referred to as rubbery polymers, and those with a T_g greater than their operating temperature are known as glassy polymers. Fundamentally, this dichotomy reflects the level of molecular motions and the packing structure of the polymer matrix.

A rubbery polymer sample, which exist above its T_g , is microscopically arranged as densely packed random polymer chains that have a high degree of rotational and vibrational mobility due to relatively long-range, cooperative motions of the many chain segments. The molecular motions of a rubbery polymer are thermally activated and result in transient fluctuations in inter-chain spacing. These short-lived “pockets” of free volume enable gases to sorb into and diffuse through the matrix. Although these free volume pockets are continuously formed and eliminated on a very short timescale, no net change in intersegmental chain spacing throughout the polymer matrix as a whole occurs. The flux of gas molecules through rubbery polymers is typically greater than that through glassy polymers as a result of the high degree of chain mobility. However, rubbery polymers tend to have lower molecular size discriminating ability than glassy

polymers for the same reason. In fact, a rubbery polymer behaves very much like a high viscosity, high molecular weight liquid due to the mobility of its polymeric chains.

In contrast, a glassy polymer sample is comprised of more rigid polymer chains that exist in a non-equilibrium state. At temperatures below their T_g , polymers chains lack sufficient rotational and vibrational mobility to enter their most thermodynamically favorable configuration. The result of this low chain mobility in glassy polymers is the creation of long-lived molecular-scale packing defects, also known as excess free volume or microvoids. These microvoids are, in essence, “frozen” into the glassy polymer matrix. Figure 2.1 shows the specific volume of a polymer sample versus temperature.

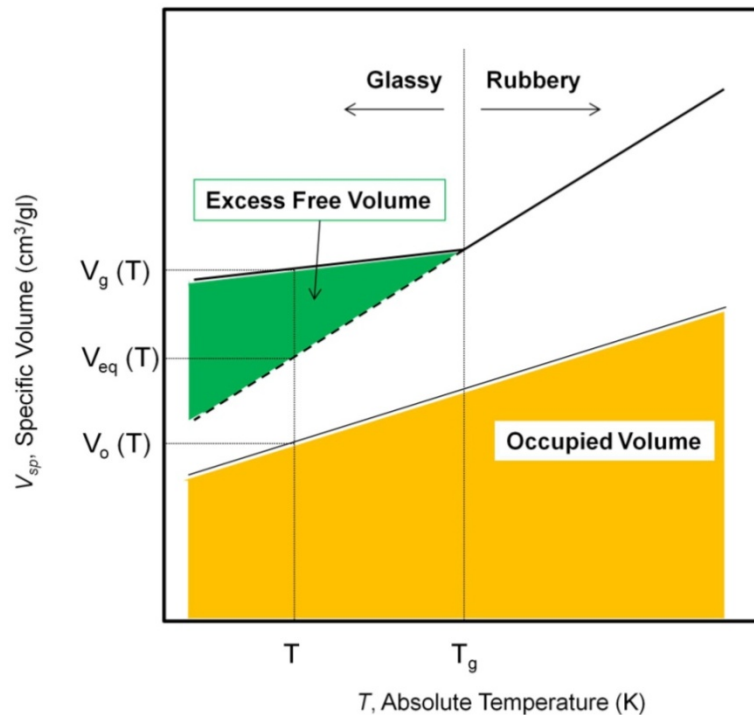


Figure 2.1: Graphical representation of specific volume in a hypothetical polymer sample versus temperature with the glassy and rubbery regimes indicated.

As shown, a glassy polymer has a specific volume, V_g , which is greater than the hypothetical equilibrium specific volume, V_{eq} . In other words, V_{eq} represents the specific volume that the material would have if it still behaved as a rubbery polymer at that temperature. The difference between V_g and V_{eq} ($V_g - V_{eq}$) is the excess free volume of the glassy polymer, which is trapped within the polymer matrix. Excess free volume should not be confused with free volume, which constitutes the difference between the actual specific volume of the sample and the specific volume occupied by its molecules (V_o). Free volume, often calculated as fractional free volume (*FFV*), is present in both rubbery and glassy materials and represents the interstitial space between adjacent polymer molecules; it is the volume included in the mass of a polymer sample that is not occupied by the molecules.

The thermally activated chain motions of glassy polymers are more localized than in rubbery polymers. These restricted chain motions lead to a more defined distribution of intersegmental spacing and free volume, affording glassy polymers greater capacity for separating gas molecules based on their relative size [1]. Reflecting their non-equilibrium nature, the amount of excess free volume in a glassy polymer sample depends on the age of the sample and the rate of quenching below the glass transition [2, 3]. As a sample ages, microvoids undergo a process of essentially diffusing out of the polymer matrix, thus reducing V_g relative to V_{eq} . Similarly, a glassy polymer sample that is cooled more slowly has additional time for its chains to relax into a more thermodynamically favorable conformation. Taking this a step further, in the limit of infinite age or infinite cooling time, respectively, all of the microvoids can diffuse out of the polymer matrix or none will form in the first place. Such a glassy polymer sample would have a V_g equal to V_{eq} , or zero excess free volume [1].

The distinction between rubbery and glassy polymers is critical to membrane separations because a polymer membrane's separation properties are largely determined by chain segmental mobility in the sample, intersegmental chain spacing, free volume, and the distribution between chain spacing and free volume. In addition, thermodynamically-controlled partitioning (sorption) of a penetrant into the polymer matrix and polymer-penetrant physiochemical interactions are also determining factors of the membrane's transport properties. The extent of each factor described above varies from one polymer to the next, but the difference in these factors between a rubbery polymer and a glassy polymer are especially pronounced. As such, membranes composed of rubbery polymers tend to express good properties for some separations (e.g. H₂S/CH₄) whereas glassy polymer membranes are preferable for others (e.g. CO₂/CH₄). This concept will be discussed more thoroughly in the context of sour gas separations in Section 2.6.

2.2. Gas Transport in Membranes

While a number of different membrane types exist, all membranes can be described as a selective barrier between two phases. The different membrane types make use of a variety of mechanisms for the transport of small molecules. Transport through membranes that contain pores is governed by the size of the pores and the mean free path of the penetrant molecules within the pores. On the other hand, the transport of gases in a non-porous membrane is described by a two part solution-diffusion mechanism [4-6]. During this process, penetrant molecules first sorb in the upstream, high chemical potential side of the membrane, then diffuse through the membrane down a chemical potential gradient, and finally desorb from the downstream,

low chemical potential side of the membrane. Figure 2.2 illustrates several different membrane transport mechanisms for both porous and non-porous membranes. The solution diffusion model is shown in greater detail in Figure 2.3.

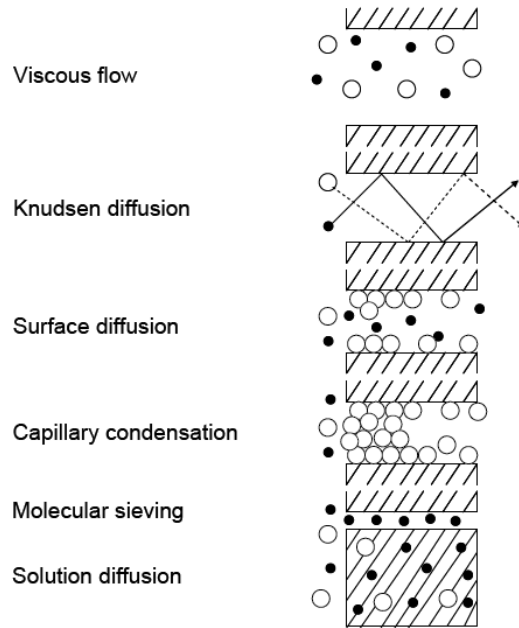


Figure 2.2: Depiction of various transport mechanisms through membranes [7, 8].

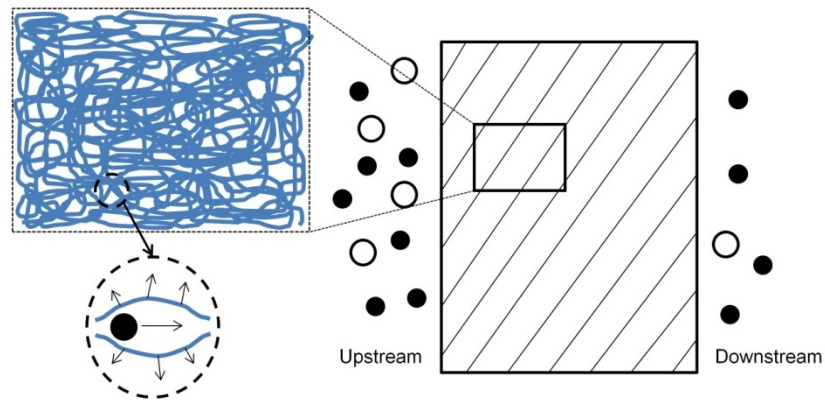


Figure 2.3: Illustration of the diffusion process for a polymeric solution-diffusion membrane. Thermally activated motions of the polymer chains allow for diffusion jumps of sorbed penetrants [6, 9].

Viscous flow through pores occurs when the pore radius is much larger than the mean free path of a penetrant molecule under a particular set of operating conditions. There is no discrimination between penetrant molecules during viscous flow within the actual pore. However, pore configurations that enable viscous flow find utility in hydrodynamic sieving applications, where small penetrant molecules can be separated from much larger molecules based on their ability to enter the pores of such a membrane. As the pore size is reduced relative to the mean free path of a penetrant molecule, the transport mechanism changes. Knudsen diffusion can occur once the pore radius is less than the mean free path of a penetrant. Unlike viscous flow, Knudsen diffusion permits discrimination between penetrant molecules within the pore based on their molecular mass and the temperature of the system. An expression for the diffusion coefficient, $D_{K,i}$, of component i (cm²/s) under Knudsen diffusion conditions with pores that are assumed to be round and straight is given in Eq. (2.1) [10].

$$D_{K,i} = 4850 \cdot d \cdot \left(\frac{T}{M_i} \right)^{0.5} \quad (2.1)$$

In the above equation, d is the pore diameter (cm), T is the absolute temperature of the system (K), and M_i is the penetrant molecule's molecular weight (g/mol).

The other transport mechanisms through porous membranes indicated in Figure 2.2 can occur as the pore size is further reduced compared to the mean free path of the penetrant molecules. As with Knudsen diffusion, these alternative transport modes can separate molecules that enter the pores based on size, shape, or other factors. Although porous membranes are currently being investigated for gas separations, they present a number of key challenges that limit their attractiveness. Namely, as the size of a penetrant molecule is reduced or the size difference between two species becomes less,

pore dimensions must be tailored and controlled with greater precision. Predictably, high performance porous membranes are difficult to manufacture on a large scale and are often expensive to synthesize [11]. Despite these problems, molecular sieving membranes based on carbons, zeolites, and metal-organic frameworks are an area of great interest because of the very high separation efficiencies that are possible with these materials [12-18]. Nevertheless, non-porous membranes that rely upon solution-diffusion transport to effect a separation are the focus of this research.

Membranes that utilize the solution-diffusion mechanism for transport of small penetrant molecules are usually polymeric in nature. Polymers are easy to form into the dense, non-porous configuration that is necessary for this type of membrane. Gas transport through non-porous polymer membranes is governed by kinetic and thermodynamic factors: penetrant gas diffusivity and solubility in the membrane, respectively. The diffusion of a penetrant molecule, i , through an isotropic polymer membrane can be described as a function of the frequency and average length of diffusion “jumps” through transient “gaps” in the polymer matrix, as shown in Eq. (2.2) [6].

$$D_i = \frac{f_i \cdot \lambda_i^2}{6} \quad (2.2)$$

In this equation, D_i is the diffusion coefficient of the penetrant, f_i is the jump frequency, and λ_i is the average jump length. The frequency and length of gap openings depends on numerous factors, some that are intrinsic to the polymer material and include polymer chain stiffness and free volume distribution. Operating conditions can also impact diffusivity through factors such as temperature, penetrant gas type, and penetrant gas concentration. Additionally, gap openings can be affected by nearby penetrant

molecules and high activity penetrants, which in extreme cases can alter polymer chain packing (e.g. antiplasticization or plasticization). Figure 2.4 presents a depiction of a single diffusion jump for a penetrant molecule through a thermally activated transient gap.

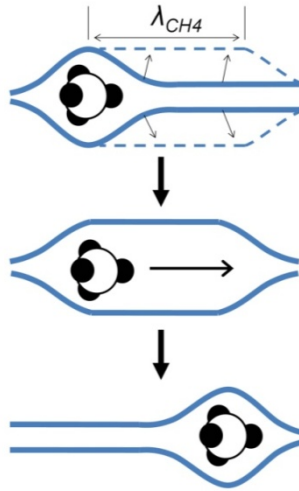


Figure 2.4: Depiction of a penetrant molecule making a "jump" through a transient gap between densely packed polymer chains.

2.2.1. Solution-Diffusion Transport Theory

The first step in the transport, or permeation, of gas molecules through a polymeric solution-diffusion membrane is sorption into the upstream face of the polymer matrix. This thermodynamically-controlled partitioning of the penetrant molecules into the polymer is influenced by the condensability of the penetrant species and polymer-penetrant physiochemical interactions. A commonly used measure of condensability is critical temperature (T_c). Gases with higher T_c usually exhibit higher levels of sorption in a polymer and, therefore, permeate more quickly through solution-diffusion membranes [19]. This is especially true for membranes when sorption is the more dominating mechanism of transport, as is usually the case for *rubbery polymers*.

Diffusion of the penetrant through the polymer matrix is the second step in the solution-diffusion mechanism. A primer on diffusion in polymeric solution-diffusion membranes is given above in Section 2.2. The diffusivity of gas molecules in a dense polymer matrix scales with the size of the molecule, one measure of which is kinetic diameter (d_k). Penetrant molecules with a smaller d_k typically diffuse more quickly through this type of membrane. As a result, the permeation rate of smaller gas molecules is usually greater in membranes with diffusion as the dominant mechanism of selective transport, which tends to be true for *glassy polymers*.

Despite the trends for rubbery and glassy polymers noted above, it is important to recognize that membranes utilizing the solution-diffusion transport mechanism are subject to both portions of the model. Thus, the permeation of a highly condensable gas molecule through a rubbery polymer may actually be very slow if the molecule is large. The easiest separations for solution-diffusion membranes tend to be those for which the faster permeating species holds both a condensability (solubility) and size (diffusivity) advantage over the slower permeating molecule, regardless of the polymer's T_g . In the context of natural gas purification, the CO_2/CH_4 separation is a good example of a system that is well-suited for solution-diffusion membranes. As shown in Figure 2.5 and Table 2.1, CO_2 is both smaller and more condensable than CH_4 .

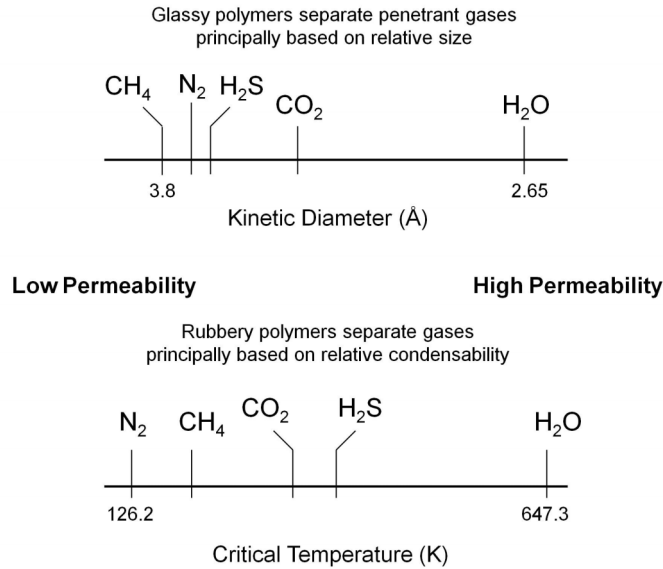


Figure 2.5: Comparison of the relative size and condensability of common sour gas feed components [20, 21]. Slow permeating species are on the left and fast gases are on the right.

Table 2.1: Physical properties of sour gas components and other common feed gases [8, 20, 21].

	CH ₄	CO ₂	H ₂ S	N ₂	O ₂	He	H ₂ O
d_k (Å)	3.8	3.3	3.6	3.64	3.46	2.6	2.65
T_c (K)	190.6	304.2	373.3	126.2	154.4	5.2	647.3

The driving force for mass transport through solution-diffusion membranes is a chemical potential gradient ($\Delta\mu_i$) from the upstream side of the membrane to the downstream side. Diffusion occurs in the direction of decreasing chemical potential. In normal operation, this chemical potential gradient is achieved by maintaining the upstream, or feed, side of the membrane at higher pressure than the downstream, or permeate, side. As the chemical potential gradient is increased through either increased feed pressure or decreased permeate pressure, the rate of mass transport across the membrane is increased. Figure 2.6 shows how a solution-diffusion membrane that selectively allows ‘fast gases’ (CO₂ and H₂S) to permeate more quickly than a ‘slow gas’

(CH₄) can effectively enrich the permeate and retentate streams with the fast and slow gases, respectively.

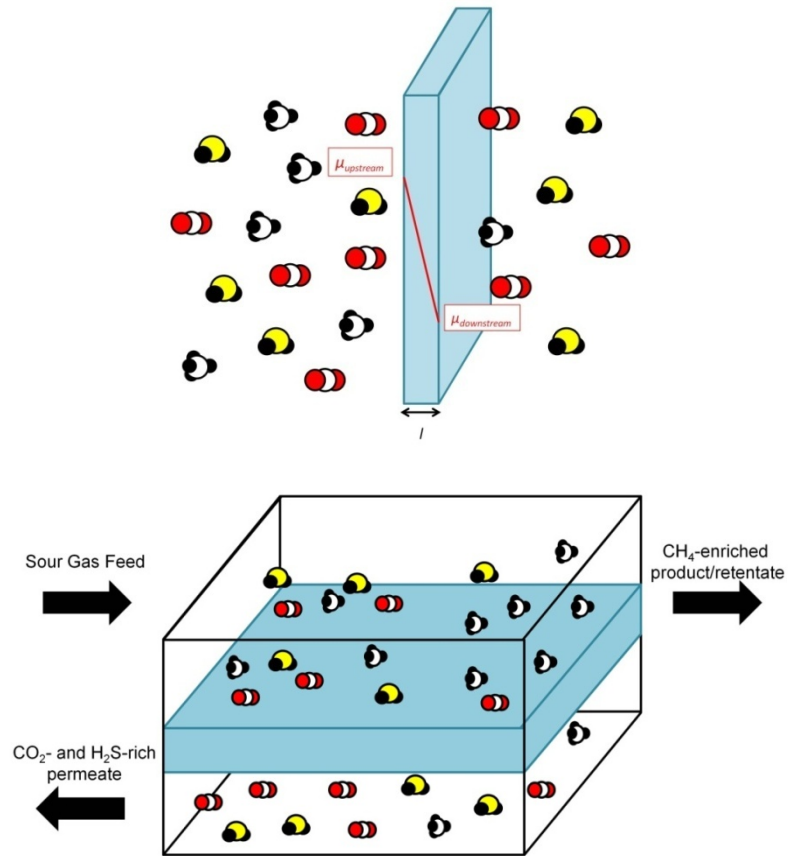


Figure 2.6: Depiction of sour gas separations through a dense film membrane. CO₂ and H₂S selectively permeate through the material due to size and condensability advantages over CH₄. Adapted from [8].

2.2.2. Characterizing Solution-Diffusion Membranes

The performance of membranes is most commonly evaluated using two key intrinsic properties: permeability and selectivity. Permeability is a measure of the membrane's productivity, and it is calculated as the pressure- and thickness-normalized flux as shown in Eq. (2.3) for a penetrant gas, i .

$$P_i = \frac{n_i \cdot l}{\Delta p_i} \quad (2.3)$$

In the above equation, P_i is the permeability of component i through the membrane, n_i is the flux, l is the membrane thickness, and Δp_i is the transmembrane pressure differential. The use of partial pressure in the denominator of Eq. (2.3) assumes ideal gas behavior in the feed gas. A more accurate version of Eq. (2.3) would instead use the transmembrane fugacity difference (Δf_i) to account for non-ideal behavior, which is likely under high-pressure sour gas conditions with the polar CO₂ and H₂S gases in the feed. This topic is addressed more fully in Section 2.5. The most common unit for a membrane's permeability is the Barrer, which is defined as follows.

$$\text{Barrer} = 10^{-10} \frac{\text{cm}_{STP}^3 \cdot \text{cm}}{\text{cm}^2 \cdot \text{s} \cdot \text{cmHg}} \quad (2.4)$$

In asymmetric hollow fiber membranes, the actual membrane thickness is not easily determined. As such, an alternative measure of membrane productivity, permeance, is used in place of permeability. Permeance is simply the flux of a component normalized by the transmembrane pressure (or fugacity), as given by Eq. (2.5).

$$\left(\frac{P}{l} \right)_i = \frac{n_i}{\Delta p_i} \quad (2.5)$$

The unit used for permeance is the "gas permeation unit," or GPU:

$$\text{GPU} = 10^{-6} \frac{\text{cm}_{STP}^3}{\text{cm}^2 \cdot \text{s} \cdot \text{cmHg}} \quad (2.6)$$

Starting from a more fundamental description of mass diffusion, Fick's first law can be used to describe the flux of gas molecules in solution-diffusion membranes [5]. The appropriate form of this equation for one-dimensional diffusion is given below.

$$n_i = -D_i \frac{dC_i}{dx} \quad (2.7)$$

In Eq. (2.7), n_i is the mass flux of component i , D_i is the diffusion of component i through the polymer membrane, C_i is the concentration, and x is the coordinate in the direction of permeation. The definition of flux from Eq. (2.7) can be substituted into the equation for permeability to obtain the following expression.

$$\frac{P_i}{l} = \frac{-D_i \frac{dC_i}{dx}}{\Delta p_i} \quad (2.8)$$

Furthermore, an average diffusion coefficient, \bar{D}_i , for component i in the membrane can be defined as shown in Eq. (2.9). This simplifies the calculation, since the diffusivity of a penetrant in reality depends upon its local concentration.

$$\bar{D}_i = \frac{\int_{C_{i,down}}^{C_{i,up}} D_i(C_i) dC_i}{\int_{C_{i,down}}^{C_{i,up}} dC_i} \quad (2.9)$$

In the formulation given above, $C_{i,up}$ and $C_{i,down}$ are the concentrations of component i in the upstream and downstream faces of the membrane, respectively.

Therefore, substituting Eq. (2.9) into Eq. (2.8) gives an expression for permeability in terms of the average diffusion coefficient.

$$P_i = \frac{\bar{D}_i (C_{i,up} - C_{i,down})}{\Delta p_i} \quad (2.10)$$

If the thermodynamic contribution to the solution-diffusion mechanism, penetrant solubility in the material, is defined as follows,

$$\bar{S}_i = \frac{(C_{i,up} - C_{i,down})}{\Delta p_i} \quad (2.11)$$

where \bar{S}_i is the average sorption coefficient for component i in the membrane, then Eq.

(2.10) can be further simplified.

$$P_i = \bar{D}_i \cdot \bar{S}_i \quad (2.12)$$

Eq. (2.12) expresses the permeability of a solution-diffusion membrane as the product of the kinetic and thermodynamic factors, diffusivity and solubility.

The sorption coefficient of a penetrant gas in a solution-diffusion membrane can be calculated from the concentration of sorbed gas in the material. This relationship is shown more generically in Eq. (2.13).

$$S_i = \frac{C_i}{p_i} \quad (2.13)$$

S_i is the sorption coefficient of component i and C_i is the equilibrium concentration of the gas within the material at a pressure, p_i , in the surrounding gas.

As mentioned previously, operating temperature can affect the permeability of a solution-diffusion membrane. For the kinetic factor, this temperature dependence is captured through an Arrhenius relation. The diffusivity of a gas molecule in a membrane

is related to temperature through the system's activation energy of diffusion, E_d , as shown in Eq. (2.14).

$$D_i = D_{o,i} \exp\left(\frac{-E_d}{R \cdot T}\right) \quad (2.14)$$

Because E_d is always positive, higher operating temperatures will result in greater diffusion coefficients.

The thermodynamic factor, solubility, is related to temperature through a van't Hoff type equation, given in Eq. (2.15).

$$S_i = S_{o,i} \exp\left(\frac{-\Delta H_s}{R \cdot T}\right) \quad (2.15)$$

In this equation, ΔH_s is the enthalpy of sorption for the penetrant gas in the polymer membrane, and the value of this term is normally negative since sorption is almost always exothermic. As a result, gas solubility within a polymer matrix typically decreases with increasing temperature. More specifically, the enthalpy of sorption can be expressed as the summation of two factors, as Eq. (2.16) shows.

$$\Delta H_s = \Delta H_{cond} + \Delta H_{mix} \quad (2.16)$$

The term ΔH_{cond} is the enthalpy of condensation, which is effectively the negative of the enthalpy of vaporization of the penetrant gas at the operating conditions of interest. However, for penetrants above their critical temperature, this is really only a hypothetical parameter. The second term, ΔH_{mix} is the enthalpy of mixing a penetrant gas with the polymer matrix. So, gas sorption into a polymer matrix can be thought of as consisting of two steps: (1) condensation of the gas molecule into the polymer at a liquid-like density

and (2) mixing of the gas molecule with the polymer chains [21]. For most gases, ΔH_{cond} is negative. ΔH_{mix} , however, can be positive or negative depending on the extent of polymer-penetrant interactions and the energy required to “create” space in the polymer matrix in order to accommodate a penetrant molecule.

The D_i and S_i terms in Eqs. (2.14 and 2.15) are the diffusion and sorption coefficients for component i in the membrane, respectively. $D_{o,i}$ and $S_{o,i}$ are the pre-exponential factors, R is the universal gas constant, and T is the absolute temperature.

Based on Eq. (2.12), a similar equation giving the temperature dependence of permeability can be obtained by taking the product of Eqs. (2.14 and 2.15).

$$P_i = (D_{o,i} \cdot S_{o,i}) \exp\left[\frac{-(E_d + \Delta H_s)}{R \cdot T}\right] \quad (2.17)$$

The pre-exponential factor and activation energy of permeation for component i in the membrane, $P_{o,i}$ and E_p , can be written as follows.

$$P_{o,i} = D_{o,i} \cdot S_{o,i} \quad (2.18)$$

$$E_p = E_d + \Delta H_s \quad (2.19)$$

Eq. (2.20) is a simplified version of Eq. (2.17).

$$P_i = P_{o,i} \exp\left(\frac{-E_p}{R \cdot T}\right) \quad (2.20)$$

Since the diffusion coefficient typically has greater temperature dependence than the sorption coefficient, E_p is generally positive, which results in permeability increasing with increasing temperature, usually.

The second key measure of performance for a solution-diffusion membrane is selectivity, which is a measure of separation efficiency. The most basic form of selectivity is the ‘ideal selectivity’. This separation efficiency metric is calculated from pure gas permeation data and is simply the ratio of the fast gas permeation rate to that of the slow gas, as given in Eq. (2.21).

$$\alpha_{i/j}^* = \frac{P_i}{P_j} = \frac{(P/l)_i}{(P/l)_j} = \frac{\bar{D}_i}{\bar{D}_j} \cdot \frac{\bar{S}_i}{\bar{S}_j} \quad (2.21)$$

Using Eq. (2.12), the ideal selectivity can also be deconvoluted into a ‘mobility selectivity’ term and a ‘sorption selectivity’ term, as shown above. These are the ratios of the average diffusion and sorption coefficients of the two components, respectively.

A common measure of separation efficiency for mixed gas feed cases, where more complicated phenomena such as plasticization and competitive sorption may be present, is the ‘separation factor’, SF .

$$SF = \frac{y_i/y_j}{x_i/x_j} \quad (2.22)$$

In Eq. (2.22) above, x and y are the mole fractions of the gases in the upstream and downstream, respectively. As an alternative to separation factor, the ‘permselectivity’ – that is, the ratio of fast gas permeability to slow gas permeability – can be calculated for mixed gas feeds. This is accomplished by using the known or measured upstream and downstream mole fractions of each gas to determine the transmembrane partial pressure (or fugacity) difference for each component to calculate the permeation rate of each species in the mixture, as shown in Eqs. (2.23 - 2.24),

$$P_{i,mix} = \frac{(y_i \cdot n_{total}) \cdot l}{[(x_i \cdot p_{up}) - (y_i \cdot p_{down})]} \quad (2.23)$$

$$\alpha_{i/j} = \frac{P_{i,mix}}{P_{j,mix}} \quad (2.24)$$

where $P_{i,mix}$ is the permeability of component i under mixed gas feed conditions, n_{total} is the flux of all components through the membrane, and p_{up} and p_{down} are the total pressure on the upstream and downstream sides of the membrane, respectively. Permselectivity, α_{ij} , is a preferred method of calculating separation efficiency for mixed gas feeds when the downstream pressure is non-zero or when the fugacity coefficient corrections are necessary to account for non-ideal behavior of the feed gas. Thus, as the downstream pressure approaches zero and the feed gas approaches ideal gas behavior, the permselectivity given by Eq. (2.24) approaches the separation factor given by Eq. (2.22).

2.2.3. Transport in Rubbery Polymer Membranes

Compared to glassy polymers, transport via solution-diffusion through rubbery materials is mechanistically simpler. This results from the difference in how penetrant gases sorb into a rubbery polymer compared to glasses. Essentially, sorption in rubbers is analogous to the dissolution, or absorption, of gases into a liquid. In fact, penetrant molecules that are sorbed into a rubbery polymer are referred to as being in the ‘dissolved’ sorption mode to reflect this similarity. Henry’s law [Eq. (2.25)] can be used to capture the linear relationship between sorbed gas concentration and feed pressure, as shown in Figure 2.7.

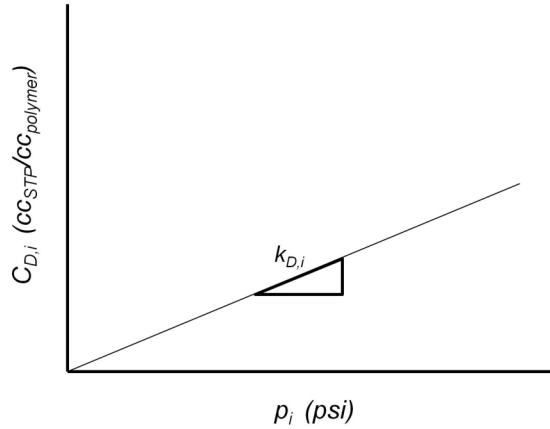


Figure 2.7: The concentration isotherm for a typical rubbery polymer is linear with a slope given by the Henry's law constant, as shown.

$$C_{D,i} = k_{D,i} \cdot p_i \quad (2.25)$$

In the above equation, $C_{D,i}$ refers to the concentration of the sorbed component, i , in the rubbery polymer matrix and $k_{D,i}$ is the Henry's Law constant, which relates dissolved gas concentration to feed pressure. As discussed in Section 2.1, rubbery polymers are equilibrium materials and do not contain microvoids of excess free volume, as is the case with non-equilibrium glassy polymers. Therefore, in the absence of severe polymer chain swelling, the sorption coefficient, S_i , of a rubbery polymer is equal to its Henry's law coefficient.

Mass transport through rubbery solution-diffusion membranes is envisioned to occur as sequential jumps from one dissolved sorption site to the next dissolved sorption site down a chemical potential gradient. Since all sorption environments in a rubbery polymer are the same (i.e. the penetrant gas remains in the dissolved mode), the diffusion coefficient in rubbery polymers also accounts for diffusion through the dissolved mode alone. Therefore, the permeability of rubbery polymer membranes is given as follows,

$$P_i = D_{D,i} \cdot S_i = D_{D,i} \cdot k_{D,i} \quad (2.26)$$

where $D_{D,i}$ is the diffusion coefficient of component i through the dissolved mode. However, when highly sorbing gases or vapors are present in the feed, a significant degree of swelling of the polymer matrix can occur. In this case, it is likely that Henry's law will not adequately describe sorption within the membrane due to greater free volume and added penetrant solubility. The diffusion coefficient of a penetrating gas is also likely to be significantly increased under conditions that lead to swelling of the polymer matrix.

In general, the diffusivity of rubbery polymers to a particular penetrant gas species is much greater than that of glassy polymers. This almost always implies low capacity for molecular discrimination based on size in rubbers. Thus, the primary separation mechanism of rubbery polymers is sorption selectivity rather than mobility selectivity. As shown in Eq. (2.21), sorption selectivity is achieved through a difference in solubility of the components that make up the gas pair of interest. Considering the above discussion, rubbery polymers are favored over glassy polymers when there is a significant difference in the condensability of the components to be separated. In fact, rubbery polymers can be so efficient at separating molecules based on their relative level of condensability that they can allow for the selective permeation of a larger, more condensable gas over a smaller, more permanent gas in some situations [22].

2.2.4. Transport in Glassy Polymer Membranes

2.2.4.1. Dual-mode Sorption Model in Glassy Polymers

The sorption, and thus permeation, of a penetrant gas in glassy polymers is more complex than the corresponding process in rubbery materials. When a polymer crosses

its glass transition point, molecular-scale packing defects in the form of microvoids of excess free volume are created within the polymer matrix. This process results in the formation of two unique environments in the polymer: one which consists of densely packed polymer chains that resemble the microstructure of a rubbery polymer and another which is comprised of the microvoids, or 'holes', that are formed when the material is quenched below its glass transition.

These two distinct chain packing environments give rise to an additional sorption mode in glassy polymers that is not present in the rubbery materials. Namely, the sorption of penetrant gases into the microvoid packing defects resembles Langmuir-type sorption in adsorbents, and is, therefore, referred to as the Langmuir, or 'hole-filling', sorption mode. The concentration of a gas in the Langmuir mode, designated as $C_{H,i}$, is described by Eq. (2.27) below for a pure gas feed.

$$C_{H,i} = \frac{C'_{H,i} \cdot b_i \cdot p_i}{1 + b_i \cdot p_i} \quad (2.27)$$

The $C'_{H,i}$ term is the Langmuir sorption capacity of the polymer for component i and b_i is the Langmuir affinity constant of component i for the hole-filling sorption sites. The Langmuir sorption capacity is the maximum concentration of penetrant gas that can adsorb into the glassy polymer matrix. The Langmuir affinity constant represents the ratio of the adsorption rate constant to the desorption rate constant in the non-equilibrium microvoids.

The total sorption of gases in a glassy polymer is the sum of sorption in the two different sorption modes. This more complex representation of sorption in glassy polymers is also known as the dual-mode sorption model. For a pure gas feed, the dual-mode sorption model is given as follows.

$$C_i = C_{D,i} + C_{H,i} = k_{D,i} \cdot p_i + \frac{C'_{H,i} \cdot b_i \cdot p_i}{1 + b_i \cdot p_i} \quad (2.28)$$

The values of the dual-mode sorption parameters are typically determined by calculating a best-fit curve of the model to concentration versus feed pressure data. The concentration of gases in the Langmuir sorption mode and in a glassy polymer as a whole is shown in Figure 2.8.

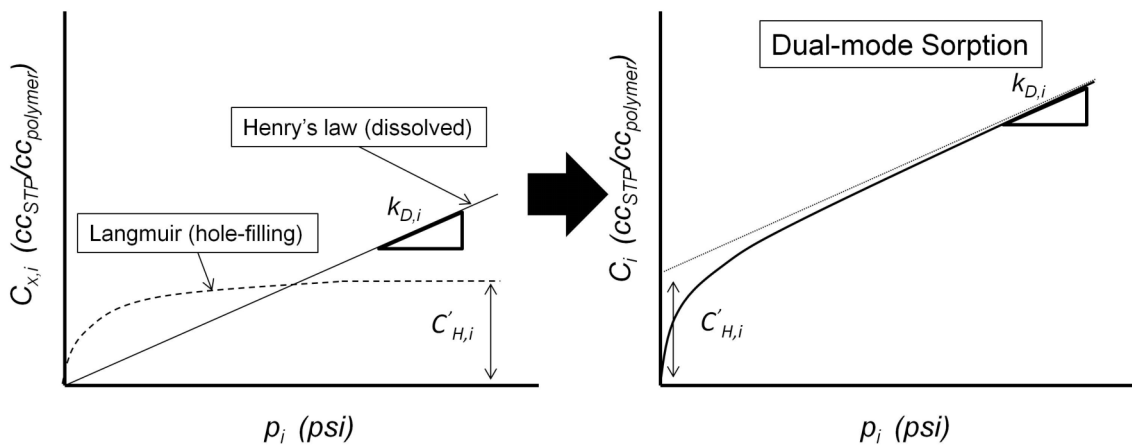


Figure 2.8: Sorption in glassy polymers occurs in two distinct modes. These sorption modes are shown individually in the plot on the left and contribute to the overall sorption level shown in the dual-mode plot on the right.

The relative importance of the Langmuir sorption mode is related to the amount of excess free volume within the glassy polymer matrix, which is itself related to the proximity of the polymer under operating conditions to its T_g , as well as the age of the sample. Under the same operating temperature, polymers with a higher T_g tend to have greater excess free volume and, as a result, a larger $C'_{H,i}$ for a given penetrant gas species. However, as shown in Figure 2.8, these Langmuir sorption sites become saturated as the feed pressure is increased. As the majority of Langmuir ‘holes’ are

filled, the predominant mode of sorption within a glassy polymer transitions to the Henry's law mode.

Models that have been developed to describe mass transport through glassy polymers have identified that penetrant gases in the two different sorption sites have different diffusion coefficients. Early attempts to describe solution-diffusion transport in glassy polymers postulated that gases in the Langmuir sorption sites were completely immobilized and did not contribute to the total diffusive flux [23, 24]. However, subsequent studies have led to the modification of this hypothesis, with the diffusivity of gases in the Langmuir microvoid sorption sites being non-zero. The partial immobilization, or dual-mobility, model of gas transport through glassy polymer membranes deals with this complicated issue by making the assumption that a fraction of molecules sorbed in the Langmuir mode, the mobile fraction, contribute to the overall diffusive flux through the membrane. This model accounts for diffusion of penetrants through these two distinct modes by extending the application of Fick's first law originally given in Section 2.2.2 [5, 25].

$$n_i = -D_{D,i} \frac{dC_{D,i}}{dx} - D_{H,i} \frac{dC_{H,i}}{dx} \quad (2.29)$$

In Eq. (2.29), $D_{D,i}$ and $D_{H,i}$ are the diffusion coefficients of component i in the diffusive and hole-filling modes, respectively. Further discussion of the partial immobilization model and other models for mass transport through glassy polymer membranes is given in Section 2.3.

2.2.4.2. Physical Aging in Glassy Polymers

As mentioned previously, the non-equilibrium nature of glassy polymers results in a time-dependent relaxation process involving the diffusion of excess free volume out of

the polymer matrix. This process is known as *physical aging* and has been the subject of several investigations by researchers looking at glassy polymer membranes [26-28]. This physical aging process results in decreasing permeability and increasing selectivity over the lifespan of a polymeric solution-diffusion membrane. The level of “unrelaxed volume” in a glassy polymer sample depends upon the polymer itself, processing conditions, thermal history, and gas exposure history [29, 30]. It has been shown that membrane thickness plays a large role in physical aging [31]. Thinner membranes age more quickly than thicker ones. The effect of membrane age on permeability and selectivity for He/N₂ separations for samples of different thicknesses is shown in Figure 2.9 [31].

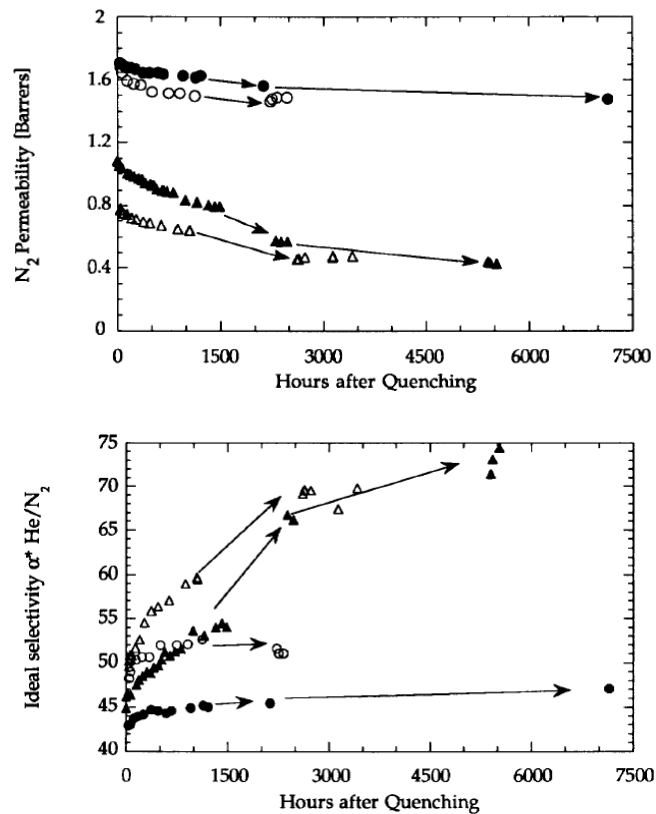


Figure 2.9: Physical aging of 6FDA-IPDA polyimide dense films with varying thickness is shown for a He/N₂ separation application. Permeability decreases and selectivity increases over time. The film thicknesses are as follows: (●) thick, 28.45 μm ; (○) intermediate, 2.54 μm ; (Δ) thin, 5000 Å; (▲) thin, air dried at room temperature [31].

2.3. Permeation Modeling in Glassy Polymer Membranes

2.3.1. Partial Immobilization Model and Competitive Sorption

Permeation data analysis and modeling can be a powerful tool for process design and membrane materials development. As mentioned in Section 2.2.4.1, the dual-mode sorption model for glassy polymers can be extended to describe mass flux through glassy polymer membranes via the so-called partial immobilization model (or dual-mobility model), shown previously in Eq. (2.29) [25].

A more convenient way to express the partial immobilization model for a component, i , is given in Eqs. (2.30-2.32).

$$n_i = -D_{D,i} \frac{dC_{m,i}}{dx} \quad (2.30)$$

$$C_{m,i} \equiv C_{D,i} + F_i \cdot C_{H,i} \quad (2.31)$$

$$F_i \equiv \frac{D_{H,i}}{D_{D,i}} \quad (2.32)$$

In the above expressions, $C_{m,i}$ is the “mobile” concentration of component i and F_i is a convenient dimensionless quantity. The diffusion coefficients through both environments are assumed to be functions of temperature, but not concentration. Additionally, local equilibrium between the two sorption modes (i.e. local equality of chemical potentials for component i in the two sorption modes) is assumed. Following a somewhat lengthy derivation, it can be shown that the permeability of a penetrant gas is given by the following equation,

$$P_i = D_{D,i} \cdot k_{D,i} \left(1 + \frac{F_i \cdot K_i \cdot p_{i,down} (p_{i,down} - p_{i,up})}{1 + b_i \cdot p_{i,down}} - \frac{F_i \cdot K_i \cdot p_{i,up} (p_{i,down} - p_{i,up})}{1 + b_i \cdot p_{i,up}} \right) \quad (2.33)$$

where $K_i \equiv C'_{H,i} b_i / k_{D,i}$. Eq. (2.33) is a generic form of the permeability predicted by the dual-mobility model and it makes no assumptions regarding the downstream pressure. However, in many instances for gas separation membrane characterization, the downstream pressure is negligible. Eq. (2.33) can be simplified to the following form, in such a case.

$$P_i = D_{D,i} \cdot k_{D,i} \left(1 + \frac{F_i \cdot K_i}{1 + b_i \cdot p_{i,up}} \right) \quad (2.34)$$

The above treatment applies to permeation through glassy polymer membranes under pure gas feed conditions. However, the partial immobilization model can be extended to include mixed gas feed situations, as well. In order to do so, it is necessary to first formulate an expression for mixed gas sorption in glassy polymers, again accounting for the two distinct sorption environments that a penetrant species can enter. The primary sorption effect for a mixed gas is competition by the various penetrant species for the fixed amount of Langmuir sorption sites, or unrelaxed free volume, within the polymer matrix. As such, a depression in the sorption of all gases in a mixture is expected, with the degree of this depression depending on the relative ability of each species to 'compete'. In contrast, penetrant sorption in rubbery polymers is essentially independent of other components present in the feed, assuming the absence of swelling or plasticization; mixed gas sorption in rubbery polymers follows the Henry's law trend presented in Eq. (2.25). The solubility of components i and j of a binary mixture in a glassy polymer are shown in Eqs. (2.35 and 2.36).

$$C_i = k_{D,i} \cdot p_i + \left(\frac{C'_{H,i} \cdot b_i \cdot p_i}{1 + b_i \cdot p_i + b_j \cdot p_j} \right) \quad (2.35)$$

$$C_j = k_{D,j} \cdot p_j + \left(\frac{C'_{H,j} \cdot b_j \cdot p_j}{1 + b_i \cdot p_i + b_j \cdot p_j} \right) \quad (2.36)$$

Eqs. (2.37 and 2.38) present the permeability of components i and j in a binary mixture through a glassy polymer with vacuum downstream.

$$P_i = D_{D,i} \cdot k_{D,i} \left(1 + \frac{F_i \cdot K_i}{1 + b_i \cdot p_{i,up} + b_j \cdot p_{j,up}} \right) \quad (2.37)$$

$$P_j = D_{D,j} \cdot k_{D,j} \left(1 + \frac{F_j \cdot K_j}{1 + b_i \cdot p_{i,up} + b_j \cdot p_{j,up}} \right) \quad (2.38)$$

More generically, the dual-mobility model can be applied to ternary or even more complex mixtures using the following equation.

$$P_i = D_{D,i} \cdot k_{D,i} \left(1 + \frac{F_i \cdot K_i}{1 + \sum_k^n b_i \cdot p_i} \right) \quad (2.39)$$

2.3.2. Bulk Flow and the Frame of Reference Model

The permeation models discussed in this chapter so far have their foundation in Fick's first law and are derived under the assumption that diffusive flux is the only contributor to overall flux through the membrane. While this is a reasonable assumption in most solution-diffusion transport cases, some instances of a non-negligible bulk flux contribution have been observed. These situations typically arise when sorbed concentrations of penetrant gases are higher than normal or when diffusive flux through a material is particularly high. In mixed gas permeation, especially, the flux of each component can be dependent upon the concentration of all the species in the mixture

[32]. The so-called frame of reference model has been developed to enable permeation analysis and modeling in these cases.

The flux of each component through a membrane is actually the sum of the diffusive and convective (bulk) flux. This more complete evaluation of penetrant flux is shown in Eqs. (2.40-2.43) for a binary mixture of components i and j in a polymer, p .

$$n_i = n_{i,diffusive} + n_{i,convective} \quad (2.40)$$

$$n_i = -\rho \cdot D_{i,m} \cdot \frac{d\omega_i}{dx} + (n_i + n_j + n_p) \cdot \omega_i \quad (2.41)$$

$$n_j = -\rho \cdot D_{j,m} \cdot \frac{d\omega_j}{dx} + (n_i + n_j + n_p) \cdot \omega_j \quad (2.42)$$

$$n_p = -\rho \cdot D_{p,m} \cdot \frac{d\omega_p}{dx} + (n_i + n_j + n_p) \cdot \omega_p \quad (2.43)$$

In the equations given above, $D_{i,m}$ is the effective binary diffusion coefficient for component i in the polymer, ρ is the density of the polymer membrane, and ω_i is the mass fraction of component i in the polymer. Eq. (2.43) represents the flux of the polymer, n_p , however, this term is set equal to zero since the membrane is stationary.

Based on this more rigorous treatment of penetrant gas flux, it can be shown that a component with very high flux may effectively increase the total flux of other components through the convective flux term. An important requirement for the bulk flux term to be non-negligible, even if other high flux components are present in a mixture, is a relatively high mass fraction of the penetrant gas in the polymer matrix, ω_i (i.e. high levels of sorption). Therefore, highly sorbing species, like CO_2 and H_2S , are more likely to have tangible bulk flux contributions during mixed sour gas permeation. For example,

in the case of a ternary mixture consisting of CO₂, H₂S and CH₄, the two acid gas components tend to be very ‘fast’ gases, as a result of their physical properties (i.e. they are small and condensable). This means that both requirements for a non-negligible bulk flux term, namely high total gas flux through the membrane and high mass fraction, are likely to be satisfied for total CO₂ and H₂S flux.

For the binary mixture case presented in Eqs. (2.40-2.43), the mutually dependent flux of the two penetrant gases can be expressed as follows.

$$n_i = \frac{-\rho \cdot D_{i,m} \cdot \frac{d\omega_i}{dx}}{\left[1 - \left(1 + \frac{1}{r}\right) \cdot \omega_i\right]} \quad (2.44)$$

$$n_j = \frac{-\rho \cdot D_{j,m} \cdot \frac{d\omega_j}{dx}}{\left[1 - (1 + r) \cdot \omega_j\right]} \quad (2.45)$$

$$r = \frac{n_i}{n_j} \quad (2.46)$$

Eqs. (2.44 and 2.45) can be solved with the boundary conditions shown below for the mass fractions of components *i* and *j*. The downstream mass fractions of the penetrants approach zero when the downstream of the membrane is under vacuum, as is often the case in a laboratory setting.

$$x=0; \quad \omega_i = \omega_{i,up}; \quad \omega_j = \omega_{j,up}$$

$$x=l; \quad \omega_i = \omega_{i,down} \approx 0; \quad \omega_j = \omega_{j,down} \approx 0$$

The results of integrating Eqs. (2.44 and 2.45) are given below.

$$n_i \cdot l = \frac{\rho \cdot D_{i,m} \cdot \ln \left[\frac{1 - \left(1 + \frac{1}{r}\right) \cdot \omega_{i,down}}{1 - \left(1 + \frac{1}{r}\right) \cdot \omega_{i,up}} \right]}{\left(1 + \frac{1}{r}\right)} \approx \frac{\rho \cdot D_{i,m} \cdot \ln \left[\frac{1}{1 - \left(1 + \frac{1}{r}\right) \cdot \omega_{i,up}} \right]}{\left(1 + \frac{1}{r}\right)} \quad (2.47)$$

$$n_j \cdot l = \frac{\rho \cdot D_{j,m} \cdot \ln \left[\frac{1 - (1+r) \cdot \omega_{j,down}}{1 - (1+r) \cdot \omega_{j,up}} \right]}{(1+r)} \approx \frac{\rho \cdot D_{j,m} \cdot \ln \left[\frac{1}{1 - (1+r) \cdot \omega_{j,up}} \right]}{(1+r)} \quad (2.48)$$

It is appropriate to use the *mobile* mass fractions of component's i and j when solving Eqs. (2.47 and 2.48). The concept of mobile mass fraction is derived from the mobile concentration treatment developed in the partial-immobilization model. As such, the equations for mobile mass fraction [Eqs. (2.49 and 2.50)] are simply manipulations of the equations used in the development of that model.

$$\omega_i = \omega_{i,mobile} = \frac{M_i}{22,400 \cdot \rho} \left(k_{D,i} \cdot p_i + \frac{c'_{H,i} \cdot b_i \cdot p_i}{1 + b_i \cdot p_i + b_j \cdot p_j} \right) \quad (2.49)$$

$$\omega_j = \omega_{j,mobile} = \frac{M_j}{22,400 \cdot \rho} \left(k_{D,j} \cdot p_j + \frac{c'_{H,j} \cdot b_j \cdot p_j}{1 + b_i \cdot p_i + b_j \cdot p_j} \right) \quad (2.50)$$

The flux for components i and j can be determined iteratively using the preceding equations and the definition of r . An initial value for r is guessed to start the iterative process. Solutions for n_i and n_j are obtained and a new r value is determined. The process continues until r converges upon the value given by Eq. (2.46). After values for the flux of the penetrant gases have been found, the permeability, or permeance, of a glassy polymeric solution-diffusion membrane with the bulk flux contribution taken into account can be predicted using Eq. (2.51).

$$P_i = \frac{22,400 \cdot n_i \cdot l}{M_i \cdot \Delta p_i} \quad (2.51)$$

The frame of reference model can be applied to pure gas permeation, as well. Penetrant gases with high solubility and high diffusive flux through a particular membrane are likely to experience some bulk flux contributions to their overall flux. The derivation of pure gas equations is fairly straightforward. Furthermore, a derivation of the frame of reference model for ternary mixed gas feeds is available in the reference [33].

2.4. Penetrant-Polymer Interactions and their Effect of Transport

2.4.1. Plasticization of Polymers

2.4.1.1. Plasticization Overview

Membrane plasticization is an important phenomenon to separations involving condensable penetrants under high-activity feed conditions, since it can seriously hamper a polymer's ability to efficiently separate species based on their relative size. Plasticization occurs when the concentration of sorbed penetrants in a polymer membrane is high enough to cause physical swelling, or an increase in free volume, of the membrane and increase polymer chain segmental mobility, thereby increasing the diffusivity of all components through the material [34-36]. Typically, the diffusion coefficient of large molecules increases more than that of smaller molecules. Hence, a plasticized membrane is less effective at separating gases based on size than an unplasticized one. Because of the serious implications of plasticization to polymeric gas separation membrane performance, the phenomenon has been studied by numerous researchers.

While the dual-mobility model for gas permeation through glassy polymers does predict an increase in effective gas diffusivity (D_{eff}) with increasing pressure [Eq. (2.52)], this is not associated with membrane swelling.

$$D_{eff,i} = D_{D,i} \cdot \left[\frac{\left(1 + \frac{F_i \cdot K_i}{1 + \left(c_{D,i} \cdot \frac{b_i}{k_{D,i}} \right)^2} \right)}{\left(1 + \frac{K_i}{1 + \left(c_{D,i} \cdot \frac{b_i}{k_{D,i}} \right)^2} \right)} \right] \quad (2.52)$$

An increase in the effective diffusivity of the membrane beyond that predicted by the dual-mobility model is often related to non-idealities in the penetrant transport mechanism, such as swelling or plasticization.

The radical increase in polymer chain segmental mobility, which is induced by plasticization, results in a loss of size discriminating ability by the polymer membrane. In a permeation isotherm for a glassy polymer membrane that has experienced plasticization, an upswing in permeability of the penetrants and a corresponding loss of selectivity are normally observed. The effects of membrane plasticization on permeation properties are depicted in Figure 2.10.

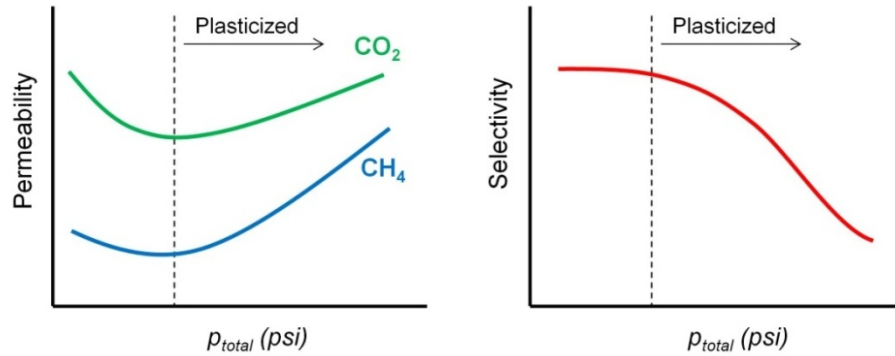


Figure 2.10: Graphical depiction of the effects of plasticization on the productivity and efficiency of a membrane for the CO₂/CH₄ separation.

The pressure at which the permeability passes through a minimum is referred to as the plasticization pressure [35]. The plasticization pressure of a membrane is most often given under conditions of zero downstream pressure. However, the plasticization pressure can be reduced when the downstream pressure is non-zero, sometimes significantly. In Figure 2.10 above, there is an initial decrease in permeability as the pressure is increased for both species, even before the onset of plasticization. This trend is reflective of dual-mode sorption in glassy polymers, and corresponds to the pressure range in which Langmuir sorption sites are being saturated. As the feed pressure is increased further, sorption into the Henry's law mode becomes the dominant thermodynamically-driven component of transport. Eventually, excess sorption in the dissolved mode leads to swelling of the densely packed polymer chains. When the level of swelling becomes sufficient to drastically reduce the polymer chain inter- and intra-segmental interactions, plasticization can occur. Based on these observations, it is believed that the key to controlling plasticization is to prevent excessive swelling [34, 37, 38]. Methods for suppressing plasticization will be discussed in the follow section.

In terms of membrane material physical property changes associated with plasticization, this phenomenon is evidenced by a decrease in the glass transition temperature and a softening, or decrease in modulus, of the membrane [35, 36]. Glassy polymer membranes tend to be far more susceptible to the deleterious effects of plasticization than rubbery polymers. Since glasses rely primarily on mobility selectivity, or differences in the diffusivity of penetrants, plasticization can severely limit the separation efficiency of this class of polymer. On the other hand, rubbery polymers normally have low mobility selectivity and derive the majority of their separation ability from sorption selectivity. Therefore, rubbery polymers are not affected by plasticization to the same extent as glassy polymers, and may, in fact, actually benefit from plasticization in extreme cases. This may be observed since the increase in free volume caused by plasticization increases gas sorption in the membrane. It is possible under these conditions that the sorption coefficient of the fast gas will increase to a greater extent than that of the slow gas [39]. Also, if a non-plasticized rubbery polymer membrane has reverse mobility selectivity (i.e. $D_{fast\ gas} < D_{slow\ gas}$), plasticization may reduce this unfavorable relationship and result in greater overall selectivity.

In any case, plasticization represents a continuous deterioration of a polymer membrane resulting from excessive swelling stresses and it is inherently undesirable. Thinner membranes have been found to plasticize more easily [31]. This can have important consequences for commercial membrane configurations such as the asymmetric hollow fiber membrane morphology, where the effective membrane thickness is on the order of 100 nm, or so. In these membranes, it has been observed that plasticization sets in almost immediately when condensable penetrant gases are used. Another factor that may add to the susceptibility of asymmetric hollow fibers to plasticization is their production process, which involves a rapid quenching step that

traps large amounts of excess free volume in the polymer matrix. The suppression of plasticization is critical for membrane stability and the prediction of membrane performance, particularly in thin membrane morphologies that are used in the field.

The acid gas components of sour gas, CO_2 and H_2S , are highly condensable and polar/polarizable, meaning they tend to have very high solubility in polymer membranes. Thus, these components have the capacity to plasticize membranes at relatively low partial pressure. As a result, plasticization and its suppression are especially important to the field of natural gas separations. It is important to test membranes with aggressive mixed gas feeds when their intended application involves plasticizing species, like CO_2 and H_2S . Pure gas permeation results alone are not sufficient for predicting the performance of these membranes under realistic feed conditions. In fact, the use of pure gas permeation results on their own can lead to seriously erroneous predictions of membrane performance, as shown in Figure 2.11.

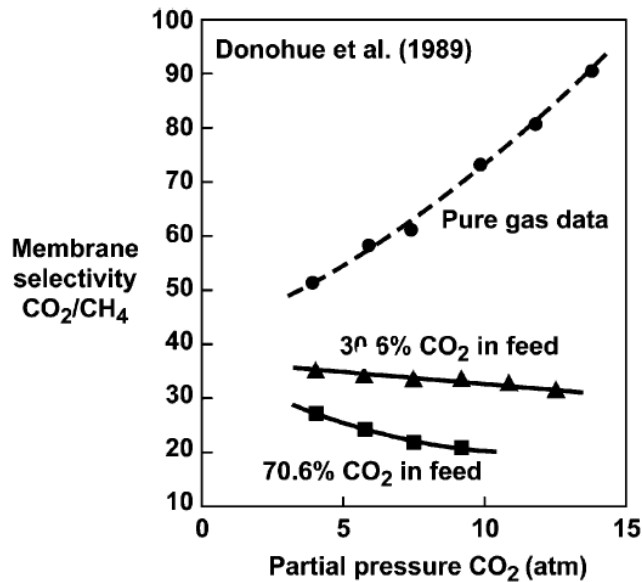


Figure 2.11: A comparison of permselectivity calculated using pure and mixed gas feeds of CO_2 and CH_4 gases. Plasticization leads to the overestimation of CO_2/CH_4 permselectivity under pure gas feed conditions [20, 40].

2.4.1.2. Strategies for Polymer Stabilizing Against Plasticization

Several methods have been employed to impart greater stability into polymeric gas separation membranes. These include thermal treatment [41-43], polymer blending [44, 45], semi-interpenetrating polymer networks [46], and crosslinking [8, 38, 47-52]. The simplest method involves selecting more chemically stable polymers, such as fluorinated polymers, polyimides or polyamides. Typically, glassy polymers with higher T_g are preferred for aggressive separations since they exhibit greater resistance to penetrant-induced plasticization. Unfortunately, this straightforward method for suppressing plasticization is not sufficient in many natural gas separation applications.

Crosslinking is a widely used method of increasing polymer membrane resistance to swelling and plasticization. By introducing strong chemical or physical crosslinking interactions into a polymer matrix, segmental mobility can be effectively restricted and the degree to which a polymer sample can “open up” due to swelling can be limited.

Of particular interest to natural gas separations involving plasticizing penetrant gases are a class of crosslinkable polyimides based on the 4,4'-(hexafluoroisopropylidene)diphthalic anhydride (6FDA) monomer. The method of crosslinking used by this class of polymer was developed by Staudt-Bickel and Koros for high pressure CO_2/CH_4 separation applications [48]. These materials include a carboxylic acid containing monomer, diaminobenzoic acid (DABA), which is used as a crosslinking site. A diol crosslinking agent, such as ethylene glycol or 1,3-propane diol, is first attached on one end to a DABA group through a pre-treatment esterification reaction. Then, after polymer processing and membrane formation, a post-treatment transesterification crosslinking reaction is performed by heating the membrane under

vacuum conditions. During this secondary reaction, the pendant hydroxyl group of the diol crosslinking agent reacts with a nearby DABA monomer to form a covalent crosslink. A schematic of the resultant crosslinked polymer network for this class of material is presented in Figure 2.12.

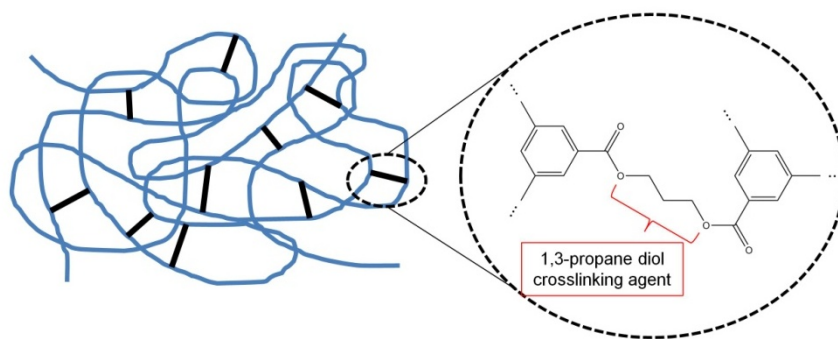


Figure 2.12: Illustration of an esterification crosslinking treatment used on polymers containing a carboxylic acid group. The diol crosslinking agent shown is 1,3-propane diol. Adapted from [9].

The particular diol crosslinking agent selected depends upon its reactivity and the separation properties of the resulting membranes. A few studies have investigated the effects of crosslinking agent on membrane performance [38, 49]. Recent work using 1,3-propane diol as the crosslinking agent with the copolyimide 6FDA-DAM:DABA (3:2) as the base polymer, have shown promise for highly plasticizing CO₂/CH₄ separation environments [49, 53-55].

The crosslinked polyimides discussed above have been shown to give plasticization pressures upwards of 500 psi under pure CO₂ feed conditions. Compared to a typical pure CO₂ plasticization pressure of 200 psi or less for a glassy polymer membrane, this level of stability is quite impressive [38, 47]. As mentioned, mitigating polymer matrix dilation and swelling due to excessive penetrant sorption was the key to enabling the plasticization suppression observed in these crosslinked polyimide

membranes. This was achieved by reducing chain mobility in the Henry's law regime through a fairly high crosslinking density along the polymer backbone [34, 35].

2.4.2. Antiplasticization

Low molecular weight compounds inside a polymer matrix at *low concentration* (10-20 wt%) have been shown to limit the segmental mobility of the polymer chains [56-61]. These compounds can be purposefully added diluents or penetrant molecules from a feed stream. Certain characteristics of polymer samples with these low molecular weight components indicate that a phenomenon opposite to plasticization can occur in these samples. These characteristics include increased modulus under short term testing and decreased elongation at break, which are contrary to what is observed for a plasticized polymer sample. Accordingly, this phenomenon is termed 'antiplasticization' and the low molecular weight component capable of inducing such a state is referred to as an 'antiplasticizer'.

Investigations of antiplasticization have been performed by several researchers [56-64]. When this phenomenon occurs in polymeric gas separation membranes, it has been found, not surprisingly, to cause a reduction in permeation rates through membranes. However, the effect of antiplasticization on membrane selectivity is less clear. Maeda and Paul found that certain aromatic compounds acting as antiplasticizers at low concentration can cause an increase in membrane selectivity. Yet, by continuing to increase the concentration of the low molecular weight compound, a decline in selectivity was observed. Some of these results for membranes of poly(phenylene oxide) are shown in Table 2.2 and Figure 2.13 [61]. These trends seem to indicate that a delicate balance exists between antiplasticization and plasticization in terms of the effect of low molecular weight penetrants on membrane selectivity. A transition from the

antiplasticized regime to the plasticized regime can potentially occur with minimal change in the level of low molecular weight component inside the polymer matrix.

Table 2.2: Permeability and selectivity properties of PPO dense films with various diluent species measured at 35°C and 10 atm, except where noted otherwise [61].

Material	P_{He}	P_{CO_2}	P_{CH_4}	$P_{\text{He}}/P_{\text{CH}_4}$	$P_{\text{He}}/P_{\text{CO}_2}$	$P_{\text{CO}_2}/P_{\text{CH}_4}$
PPO	78.5	60.4	3.78	20.8	1.30	15.6
TCP 10%	39.3	19.6	1.28	30.7	2.01	15.3
TCP 20%	19.7	8.75	0.56	35.5	2.25	15.8
TCP 30% ^a	12.4	5.71	0.37	33.5	2.17	15.5
K-50 10%	39.5	22.20	1.45	27.3	1.78	15.3
K-50 20%	20.4	9.24	0.55	37.0	2.21	16.8
K-50 30% ^a	13.3	7.10	0.52	25.2	1.87	14.8
DOS 10%	36.5	22.8	1.84	19.8	1.60	12.4
DOS 20%	27.1	16.5	0.54	3.0	1.64	5.0
DMS 5%	52.7	36.0	2.54	20.8	1.46	14.2
DMS 10%	39.5	31.5	2.45	16.2	1.25	12.9
DBS 5%	51.9	35.1	2.49	20.9	1.48	14.1
DBS 10%	37.4	25.7	2.11	17.7	1.46	12.2
DOP 10%	35.3	16.7	1.20	29.7	2.11	14.0
DOP 20%	22.5	10.4	1.19	18.9	2.16	8.7
DDS 20%	23.2	8.2	0.50	46.1	2.84	16.3

^aDriving pressure = 5 atm. Abbreviations PPO, poly(phenylene oxide); TCP, tricresyl phosphate; K-50, Kronitex 50; DOS, dioctyl sebacate; DMS, dimethyl sebacate; DBS, dibutyl sebacate; DOP, di-2-ethylhexyl phthalate.

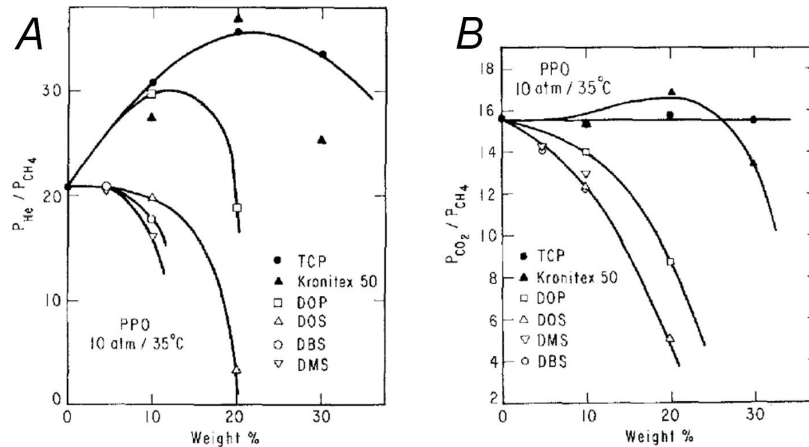


Figure 2.13: Selectivity for He/N₂ (A) and CO₂/CH₄ (B) with various diluents in PPO dense films.

The antiplasticization phenomenon can be better understood by examining the effect of low molecular weight additives on the fractional free volume of a polymer. It has been postulated that the fractional free volume (*FFV*) of a glassy polymer can be reduced and its stiffness increased by the presence of an antiplasticizer, as shown in Figure 2.14 [6, 65].

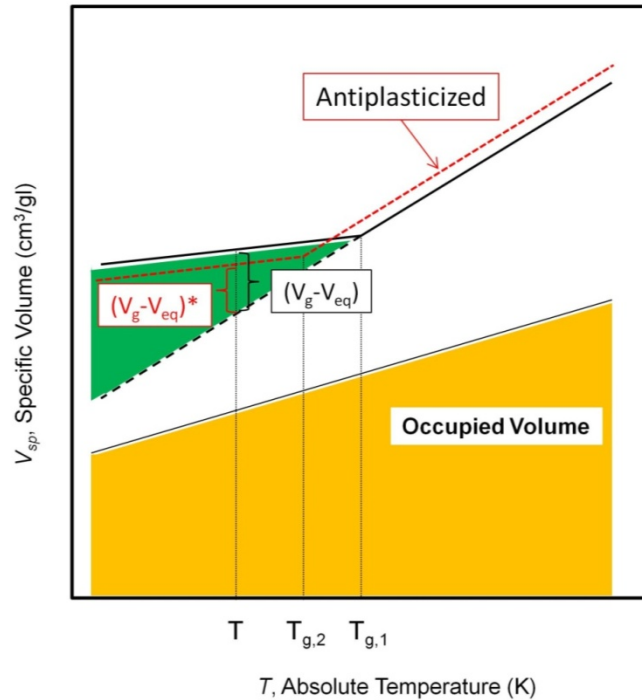


Figure 2.14: Depiction of specific volume of a pure polymer sample and an antiplasticized polymer-diluent mixture (red dashed line). Excess free volume of the pure polymer is greater than that of the antiplasticized mixture.

The excess free volume of the neat polymer and the polymer sample containing a low molecular weight antiplasticizer are given by $(V_g - V_{eq})$ and $(V_g - V_{eq})^*$, respectively. The reduction of excess free volume due to the presence of the antiplasticizer hinders diffusion and reduces gas permeability across the membrane.

2.4.3. Conditioning

The conditioning of a polymer sample is the hysteretic change in physical properties following initial exposure to high activities of penetrants [66-68]. Essentially, the configuration of polymer chains becomes altered in order to accommodate additional penetrant molecules when the concentration of a highly sorbing penetrant reaches the point that physical swelling occurs. After the penetrant has been removed, there is likely to be a residual effect on the polymer chain configuration and the polymer may not return to its original state. The conditioned polymer sample will have increased free volume compared to an unconditioned polymer. This extra free volume causes a greater sorption capacity and hysteresis in the sorption and permeation isotherms [66-68]. Over time, the conditioning effect may diminish as the polymer chains relax back towards their original unconditioned configuration.

2.5. Non-Ideal Gas Thermodynamics

The equations presented in Sections 2.2-2.4 use the transmembrane partial pressure difference as the driving force for calculating permeability or permeance. However, the fugacity of a penetrant species can be used instead of partial pressure in order to obtain more accurate results when dealing with highly non-ideal feeds. Since the true driving force for permeation is a chemical potential gradient across the membrane, the transmembrane fugacity difference (Δf_i) is a more accurate representation of that driving force than the unadjusted pressure difference (Δp_i). The effect of non-ideal behavior on permeability calculations is especially pronounced for systems with highly interacting components, like H₂S and CO₂, at high pressures. As

such, all material property calculations performed in this work use fugacity in place of partial pressure, except when otherwise noted.

The fugacity coefficients for pure or mixed gas feeds may be calculated using the thermophysical property calculation software, SUPERTRAPP, developed by NIST. This program allows for the use of an extended corresponding states model or the Peng-Robinson equation of state to calculate thermophysical properties. The Peng-Robinson equation of state is well-suited to natural gas feeds, since it was expressly developed for this application. Alternatively, process simulators that take advantage of other equations of state are widely available, and these may be more appropriate depending on the feed gas composition of interest. APPENDIX A presents a property calculator based on the Peng-Robinson equation of state that was developed specifically for the present work. This model was found to give excellent agreement with the SUPERTRAPP software using the Peng-Robinson equation and, as a result, was used extensively throughout the research presented in this dissertation.

2.6. Challenges Associated with the Simultaneous Removal of CO₂ and H₂S from Sour Gas

The differences between rubbery and glassy polymers have been discussed extensively in the preceding sections. In brief, rubbery polymer membranes achieve the separation of a gas pair primarily based on differences in solubility of the two species – rubbery polymer membranes are primarily sorption selective. On the other hand, glassy polymers usually take advantage of differences in the molecular size of two species to effect a separation – glassy polymer membranes are mainly mobility selective.

Most polymeric solution-diffusion membranes are expected to separate a single gas pair. As such, choosing between a rubbery polymer and a glassy polymer is typically straightforward and determined by the physical properties of the gases of interest. This choice can be more ambiguous for situations where a fast gas holds both a size and condensability advantage over a slow gas. However, these are normally the easiest separations for a solution-diffusion membrane, and material selection is ultimately determined by process requirements. A far more difficult material selection scenario arises for polymeric solution-diffusion membranes when *multiple* gas pairs are to be separated *simultaneously* by a *single membrane* type. The simultaneous removal of CO₂ and H₂S from sour gas presents such a case. Figure 2.15 gives some of the physical properties, namely kinetic diameter and critical temperature, of gases that are commonly found in sour gas reserves.

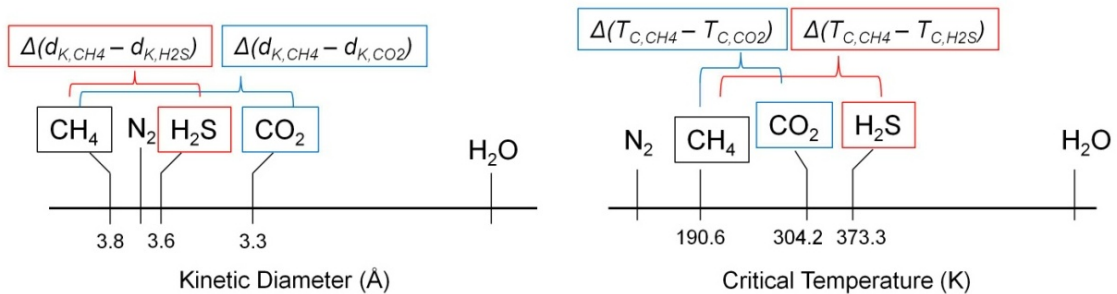


Figure 2.15: Size and condensability differences for CO₂/CH₄ and H₂S/CH₄ gas pairs in sour gas separations. Adapted from [9].

In terms of molecular sizes, CH₄ is the largest of the three gases. The kinetic diameter difference between CO₂ and CH₄ is 0.5 Å, but the difference between H₂S and CH₄ is only 0.2 Å. Similarly, CH₄ has the lowest critical temperature and is again the least favored species for permeation based on its expected solubility in polymers. The critical temperature of H₂S is 184 K greater than that of CH₄, and CO₂ has a critical

temperature that is just 114 K greater than CH₄. Based on these numbers, CO₂ and H₂S are ideally suited as fast gases for solution-diffusion membranes; both of these molecules are smaller and more condensable than CH₄. This is promising for the application of membrane technology to sour gas separations and it indicates that a single membrane material may be capable of removing both of the acid gas species from sour gas.

The numbers discussed above indicate that either a rubbery or glassy polymer should be able to perform the two separations simultaneously. Unfortunately, the more favored mechanism of selectivity – and, therefore, the more favored type of polymer – is expected to differ between the CO₂/CH₄ and H₂S/CH₄ separations. Because of the large size difference between CO₂ and CH₄, glassy polymers normally give the best selectivity for this gas pair. On the other hand, the greater condensability difference between H₂S and CH₄ has resulted in the best H₂S/CH₄ selectivities being observed in rubbery polymer membranes. Table 2.3 gives a rough estimate of the sour gas separation properties that have been observed in rubbery and glassy polymer membranes, to date.

Table 2.3: Permeability and selectivity values for H₂S/CH₄ and CO₂/CH₄ separations in "typical" rubbery and glassy polymer membranes [9, 69-73].

	P_{H₂S} (Barrer)	P_{CO₂} (Barrer)	H₂S/CH₄	CO₂/CH₄
"Typical" Rubbery Polymer	250-650	11-15	35-50	8-10
"Typical" Glassy Polymer	3-20	20-350	10-15	30-60

A surprising observation that has been made regarding H₂S/CH₄ selectivity in glassy polymers is that despite the smaller size of H₂S compared to CH₄, the mobility selectivity of these materials is usually very low (approximately 1.0), or even reversed (< 1.0). This severely limits the overall permselectivity of these materials, especially in the case of reversed mobility selectivity. Almost all the glassy polymer membranes that have

been tested so far have $\text{H}_2\text{S}/\text{CH}_4$ ideal selectivities less than 20, and most are closer to 10. It is likely that the unexpectedly low diffusivity of H_2S through glassy polymers is caused by strong polymer-penetrant physiochemical interactions. The H_2S molecule is highly polar and capable of hydrogen bonding with many functional groups that are common in the glassy polymers used for gas separation membranes.

Hence, the main mechanism of molecular separation in glassy polymers appears to be hindered for separations involving H_2S , or at least the $\text{H}_2\text{S}/\text{CH}_4$ separation. It is unlikely that this phenomenon of low H_2S diffusivity relative to CH_4 can be easily suppressed for polymeric membranes because of the presence of polar or hydrogen bonding functional groups in high-performance polymers. A more feasible approach to separating H_2S from CH_4 based on molecular size may be to use much more rigid, chemically neutral materials such as carbon molecular sieves (CMS). In fact, sour gas separations using CMS membranes are currently under investigation by other researchers in our research group.

Nevertheless, the above discussion seems to indicate that the best approach to improving the overall $\text{H}_2\text{S}/\text{CH}_4$ separation in glassy polymers is through optimizing the sorption selectivity. This can be achieved through the incorporation of polar functional groups that are known to attract H_2S , and may also favor CO_2 sorption. However, a few difficulties are introduced through this approach: (1) the sorption selectivity-enhancing groups should not interact with H_2S to such an extent that mobility selectivity (and overall selectivity) is further reduced, (2) the glassy polymer character of the membrane (i.e. its excellent CO_2/CH_4 selectivity via mobility selectivity) must not be compromised, and (3) increased sorption in the material should not result in uncontrolled swelling and plasticization of the membrane. As discussed in CHAPTER 1, the $\text{H}_2\text{S}/\text{CH}_4$ selectivity in these materials does not need to be enhanced to the point of being equal to CO_2/CH_4

selectivity (~30 or higher). Rather, H₂S/CH₄ selectivity simply needs to be sufficient to make bulk removal of the acid gases economically feasible by minimizing CH₄ loss during separation. It is our belief that a membrane with H₂S/CH₄ selectivity of around 25, coupled with CO₂/CH₄ selectivity of 30, would be highly attractive for this application. These numbers far exceed any polymeric membrane material that has been studied so far, and at least one economic analysis on sour gas separations using a hybrid membrane/absorption process concluded that currently available membranes with H₂S/CH₄ and CO₂/CH₄ selectivities lower than the numbers cited above would be economical [74].

Because of the inherent differences between rubbery and glassy polymers in terms of the CO₂/CH₄ and H₂S/CH₄ separations, it can be difficult to compare the efficacy of the two types of materials for the overall sour gas separation. Rubbery polymers tend to lie much closer to a hypothetical productivity-efficiency upper-bound tradeoff for the H₂S/CH₄ separation than glassy polymers. On the other hand, glassy polymers look more attractive based on their proximity to the CO₂/CH₄ upper-bound tradeoff. Therefore, it is helpful to introduce a separation efficiency term that takes both of the separations into account. The ‘combined acid gas separation factor’, $SF_{CAG}^{\#}$, is given as follows,

$$SF_{CAG}^{\#} = \frac{(y_{H_2S} + y_{CO_2}) / y_{CH_4}}{(f_{H_2S} + f_{CO_2}) / f_{CH_4}} \quad (2.53)$$

where f_i is the fugacity of component i in the upstream and y_i is the mole fraction in the downstream. Although the specific feed composition largely determines the relative importance of the two separations to the process as a whole, the combined acid gas separation factor allows for rapid comparison of different polymers (glassy and rubbery)

for sour gas separations in general. The combined acid gas separation factor is not intended to replace standard productivity and efficiency metrics for individual gas pairs, but rather to augment these membrane performance metrics and give a rough estimate of overall performance relative to alternative materials.

2.7. Asymmetric Hollow Fiber Membranes

2.7.1. Mechanism of Formation of Asymmetric Hollow Fiber Membranes

Asymmetric hollow fiber membranes have been discussed in CHAPTER 1 and were formed as part of this research. A dry-jet/wet-quench spinning process was used to form these membranes. Figure 2.16 illustrates this process and Table 2.4 gives the more important key spinning parameters that can be controlled during the manufacture of asymmetric hollow fiber membrane.

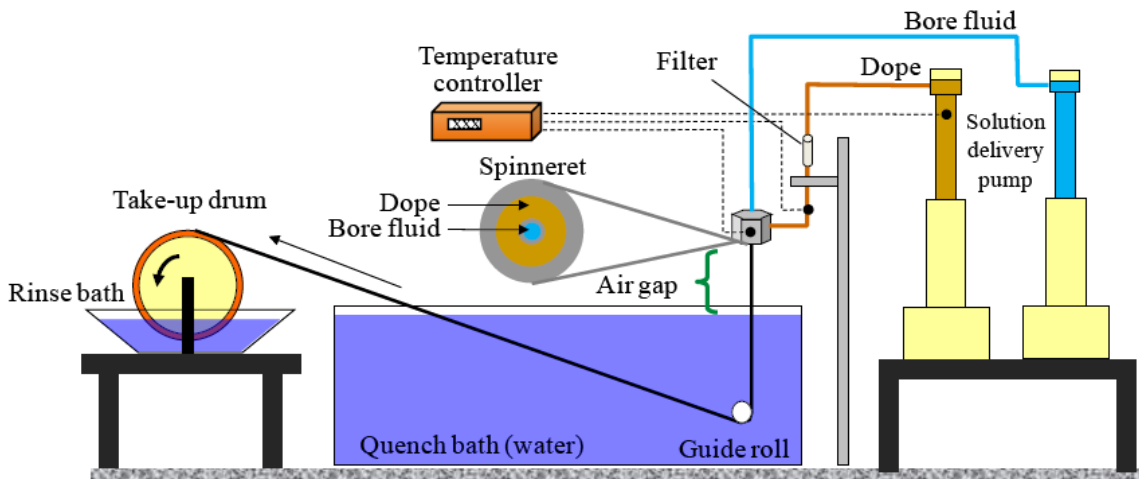


Figure 2.16: Schematic of the dry-jet/wet-quench spinning setup used for producing asymmetric hollow fibers in this work [52].

Table 2.4: Some key adjustable variables in the dry-jet/wet-quench spinning process.

Dope Composition	Spinneret/Dope Temperature	Quench Bath Temperature
Bore Fluid Composition	Dope/Bore Fluid Flow Rates	Quench Bath Composition
Air Gap Height	Take-up Rate	Quench Bath Height

During spinning, a polymer containing solution, also known as a 'dope', and a bore fluid are coextruded through an annular die, called a 'spinneret'. The dope and bore fluid, which comprise the nascent fiber, initially enter an air gap ("dry-jet") and then continue on into an aqueous quench bath ("wet-quench"). In the air gap, the outermost portion of the fiber densifies into an ultra-thin integral selective skin, or membrane. This process is brought about by the rapid evaporation of volatile liquid components of the dope in this region of the fiber. Once in the quench bath, the polymer solution undergoes phase separation, forming the solid walls that comprise the majority of the fiber and the pores that enable rapid mass transfer to and from the membrane layer. After being guided through the quench bath at high speed, the fibers are finally collected on the take-up drum. Qualitative representations of the dope composition trajectories in the air gap and quench bath are shown in Figure 2.17.

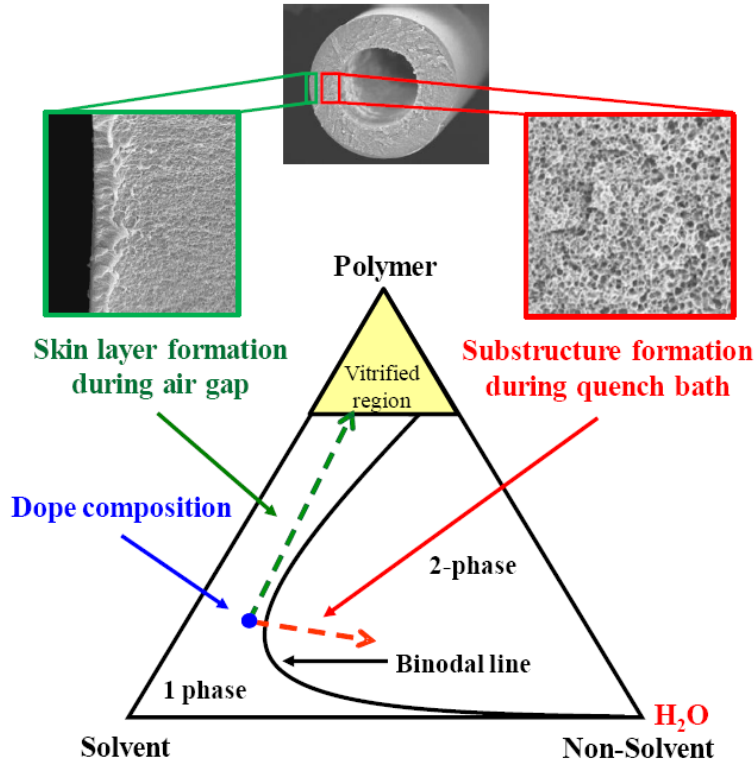


Figure 2.17: Hypothetical ternary phase diagram, as well as predicted trajectories for different regions of the dope during the asymmetric hollow fiber membrane spinning process [52].

Ideally, the initial dope composition is in the one phase region, but close to the binodal line, which separates the one phase and two phase regions. This position facilitates rapid phase separation in the quench bath. The trajectory of the dope composition in the air gap should allow the membrane to enter the vitrified region without passing through the two phase region, as this would compromise the integrity of the selective skin layer [8, 75-77]. Upon entering the quench bath, H_2O diffuses into the fiber and acts as a non-solvent, thus bringing the composition of the fiber walls into the two phase region where the dope undergoes phase separation and forms a porous substructure.

The bore fluid is not shown in Figure 2.17, because it is designed to be thermodynamically neutral to the dope and, ideally, not participate in the spinning process. The bore fluid is coextruded with the dope for the simple purpose of holding the interior of the fiber open and preventing collapse of the fiber as it is guided through the spinning setup.

2.7.2. Property Requirements for Aggressive Feed Applications

2.7.2.1. Skin Integrity

The discussion given above regarding the formation process for asymmetric hollow fiber membranes should clearly indicate that membrane formation is highly complex. As a result, the majority of commercial membranes rely on post-treatments to “caulk” pinhole defects and provide the expected level of membrane performance. Despite the attractive selectivity and productivity properties of post-treated membranes for some non-aggressive applications, defect-free membranes (i.e. membranes that do not require post-treatment) offer significant advantages under aggressive feed conditions. The advantages of defect-free membranes include long-term stability (conditioning resistance) under high pressure or high activity feed conditions [8, 78]. As such, the formation of a *defect-free integral skin layer* is critical for robust separation performance of asymmetric hollow fiber membranes for aggressive feed applications.

2.7.2.2. Substructure Porosity

The porous substructure of asymmetric hollow fibers provides mechanical support for the separating membrane layer and should enable rapid mass transfer of gases from the bore to the membrane surface. To meet these requirements, the substructure should have a highly porous, interconnected pore structure that is able to withstand high pressure drops across the membrane. When the non-selective mass

transfer resistance imparted by the porous substructure cannot be neglected in comparison to the skin layer, both selectivity and permeance can be significantly reduced [79].

Lower selectivity has been observed in essentially defect-free asymmetric membranes, and it is the result of a more pronounced reduction in permeance of the fast gas than the slow gas due to substructure resistance [80-82]. The effect of substructure resistance becomes relatively more important as the membrane layer thickness (and, therefore, resistance due to the selective membrane layer) is decreased. This can be particularly problematic for high-performance asymmetric hollow fiber membranes with ultra-thin skin layers that give high productivity and separation efficiency [79]. The simultaneous formation of a defect-free skin layer and a high-quality substructure is very challenging. However, it represents one of the keys to the expansion of membrane technologies that was presented in CHAPTER 1 and is necessary for practical applications.

2.7.2.3. Morphological Properties

One of the most attractive properties of the asymmetric hollow fiber membrane morphology is the outstanding separation surface area to volume ratios that are attainable. However, small diameter fibers must be produced in order to take advantage of this property. Additionally, smaller diameter fibers tend to have better mechanical strength in terms of their resistance to the compressive forces exerted by high pressure feeds. The optimal dimensions for an asymmetric hollow fiber are often said to be ~200 μm outside diameter and ~100 μm inside diameter [83].

A number of non-ideal morphological defects in asymmetric hollow fibers exist and can significantly reduce the mechanical properties of these membranes. These

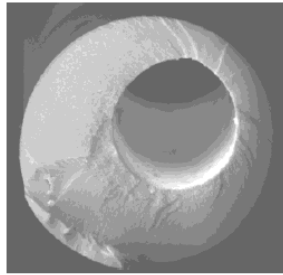
defects must be eliminated in order to maintain reliable performance under high pressure feed conditions. Examples of undesirable fiber characteristics include offset or non-concentric bores, irregular bores, non-circular fibers, and large tear-shaped macrovoids that span the majority of the fiber wall [83]. When any of the above non-ideal morphological phenomena are present, asymmetric hollow fiber membranes can fail at high pressure, leading to potentially expensive product losses and module replacement costs. Fibers capable of withstanding transmembrane pressure differentials of 1000 psi are most desirable for aggressive feed situations.

Table 2.5 gives a few examples of the effect of fiber dimensions on module surface area to volume ratio. Figure 2.18 and Figure 2.19 show scanning electron micrograph images of fiber cross-sections highlighting morphological defects that may be found in asymmetric hollow fibers and fibers that have failed at high pressure as a result of these defects, respectively.

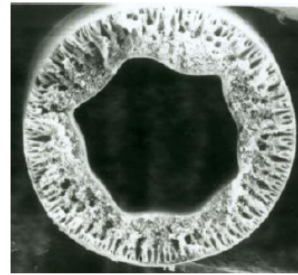
Table 2.5: Effect of hollow fiber outside diameter on membrane area and membrane area to module volume ratio in a 20 cm diameter and 1 m long module. A fiber packing density of 25% is assumed [52, 84].

Fiber diameter (μm)	100	250	500
Number of fibers per module (thousands)	1000	250	40
Membrane area (m^2)	315	155	65
Membrane area to module volume ratio (m^2/m^3)	10000	5000	2000

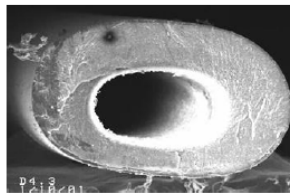
(a) non-concentric bore



(b) irregular bore



(c) oval



(d) macrovoids

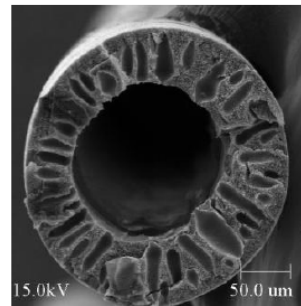
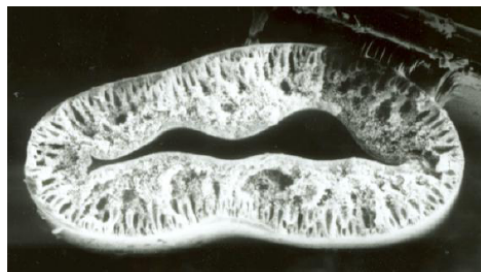


Figure 2.18: SEM images of asymmetric hollow fibers with non-optimal morphologies [52]: (a) non-concentric bore, (b) irregular/non-circular bore [85], (c) oval/partially flattened fiber [86], (d) tear-shaped macrovoids [87].

(a) Fiber collapse



(b) Fiber burst

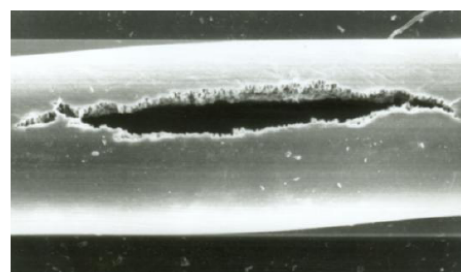


Figure 2.19: SEM images of failed asymmetric hollow fibers [52, 85]: (a) collapse due to high pressure feed (500 psia) on shell-side, (b) fiber wall burst due to high pressure (550 psia) on bore side .

2.7.2.4. Additional Challenges Associated with Asymmetric Hollow Fibers

The majority of approaches to stabilizing membranes against swelling and plasticization, discussed in Section 2.4.1.2, have been studied in dense film form only. Extension of some of these methods to industrially relevant membrane morphologies presents new challenges. It may be particularly difficult to apply these plasticization suppression strategies to asymmetric hollow fibers because of their delicate, ultra-thin membrane layers and tightly controlled substructure morphology. For example, aggressive thermal treatments are often required during crosslinking post-treatment. These harsh conditions can cause substructure compaction and increased substructure resistance [81, 88], as well as a reduction in the integrity of the skin layer [77, 89]. In an industrially viable membrane, these negative effects must be minimized while still allowing for sufficient membrane stabilization through high degrees of crosslinking, for example.

Ultimately, the attractiveness of any process for commercial application comes down to economics. The cost of producing asymmetric hollow fiber membranes, therefore, must be economically feasible and should not prohibit their use. One factor affecting membrane cost is the production speed. Asymmetric hollow fibers that can be collected at 50 m/min or higher are preferred. In addition, simple thermal post-treatment crosslinking is attractive, since it can be easily integrated into the current commercial membrane formation process [11]. Cost of the membrane material, the polymer in this case, also plays a large role in the economic equation. As such, the separation performance benefits of membranes formed with more expensive specialty polymers must justify their higher cost.

2.8. References

1. Kesting, R.E. and A.K. Fritzsche, *Polymeric gas separation membranes*. 1993: Wiley.
2. Hachisuka, H., et al., *Gas transport properties in polycarbonate films with various unrelaxed volumes*. *Polymer*, 1991. **32**(13): p. 2382-2386.
3. Hachisuka, H., et al., *Gas transport properties of annealed polyimide films*. *Journal of Polymer Science Part B: Polymer Physics*, 1991. **29**(1): p. 11-16.
4. Ghosal, K. and B.D. Freeman, *Gas separation using polymer membranes: an overview*. *Polymers for Advanced Technologies*, 1994. **5**(11): p. 673-697.
5. Koros, W.J. and R.T. Chern, *Separation of Gaseous Mixtures Using Polymer Membranes*, in *Handbook of Separation Process Technology*, R.W. Rousseau, Editor. 1987, John Wiley & Sons, Ltd.: New York.
6. Koros, W.J. and G.K. Fleming, *Membrane-based gas separation*. *Journal of Membrane Science*, 1993. **83**(1): p. 1-80.
7. Cussler, E.L., *Diffusion: Mass Transfer in Fluid Systems*. 1997: Cambridge University Press.
8. Omole, I.C., *Crosslinked Polyimide Hollow Fiber Membranes for Aggressive Natural Gas Feed Streams*, in *School of Chemical and Biomolecular Engineering2008*, Georgia Institute of Technology: Atlanta, GA. p. 305.
9. Vaughn, J., *Development and Evaluation of Aromatic Polyamide-imide Membranes for H₂S and CO₂ Separations from Natural Gas*, in *School of Chemical and Biomolecular Engineering2013*, Georgia Institute of Technology: Atlanta, GA.
10. Welty, J.R., C.E. Wicks, and R.E. Wilson, *Fundamentals of momentum, heat, and mass transfer*. 1976: Wiley.
11. Koros, W.J. and R. Mahajan, *Pushing the limits on possibilities for large scale gas separation: which strategies?* *Journal of Membrane Science*, 2000. **175**(2): p. 181-196.
12. Vu, D.Q., W.J. Koros, and S.J. Miller, *Mixed matrix membranes using carbon molecular sieves: I. Preparation and experimental results*. *Journal of Membrane Science*, 2003. **211**(2): p. 311-334.
13. Miller, S.J., et al., *Mixed matrix membrane technology: enhancing gas separations with polymer/molecular sieve composites*, in *Studies in Surface Science and Catalysis*. 2007, Elsevier. p. 1590-1596.
14. Bird, A.J. and D.L. Trimm, *Carbon molecular sieves used in gas separation membranes*. *Carbon*, 1983. **21**(3): p. 177-180.

15. Barton, T.J., et al., *Tailored Porous Materials*. Chemistry of Materials, 1999. **11**(10): p. 2633-2656.
16. Jones, C.W. and W.J. Koros, *Carbon molecular sieve gas separation membranes-I. Preparation and characterization based on polyimide precursors*. Carbon, 1994. **32**(8): p. 1419-1425.
17. Bae, T.-H., et al., *A High-Performance Gas-Separation Membrane Containing Submicrometer-Sized Metal–Organic Framework Crystals*. Angewandte Chemie International Edition, 2010. **49**(51): p. 9863-9866.
18. Mahajan, R. and W.J. Koros, *Factors Controlling Successful Formation of Mixed-Matrix Gas Separation Materials*. Industrial & Engineering Chemistry Research, 2000. **39**(8): p. 2692-2696.
19. Matteucci, S., et al., *Transport of Gases and Vapors in Glassy and Rubbery Polymers*. Materials Science of Membranes for Gas and Vapor Separation. 2006: John Wiley & Sons, Ltd. 1-47.
20. Baker, R.W. and K. Lokhandwala, *Natural Gas Processing with Membranes: An Overview*. Industrial & Engineering Chemistry Research, 2008. **47**(7): p. 2109-2121.
21. Prausnitz, J.M., R.N. Lichtenthaler, and E.G. Azevedo, *Molecular Thermodynamics of Fluid-Phase Equilibria*. 3 ed. Prentice Hall International Series in the Physical and Chemical Engineering Sciences, ed. N.R. Amundson. 1999, Upper Saddle River, NJ: Prentice Hall.
22. W. Baker, R., et al., *Separation of organic vapors from air*. Journal of Membrane Science, 1987. **31**(2–3): p. 259-271.
23. Frisch, H.L., *Sorption and transport in glassy polymers—a review*. Polymer Engineering & Science, 1980. **20**(1): p. 2-13.
24. Stannett, V., *The transport of gases in synthetic polymeric membranes — an historic perspective*. Journal of Membrane Science, 1978. **3**(2): p. 97-115.
25. Koros, W.J., et al., *A model for permeation of mixed gases and vapors in glassy polymers*. Journal of Polymer Science: Polymer Physics Edition, 1981. **19**(10): p. 1513-1530.
26. Kratochvil, A.M., *Thickness Dependent Physical Aging and Supercritical Carbon Dioxide Conditioning Effects on Crosslinkable Polyimide Membranes for Natural Gas Purification*, in *School of Chemical and Biomolecular Engineering 2008*, Georgia Institute of Technology: Atlanta, ga.
27. Kim, J.H., W.J. Koros, and D.R. Paul, *Effects of CO₂ exposure and physical aging on the gas permeability of thin 6FDA-based polyimide membranes: Part 1. Without crosslinking*. Journal of Membrane Science, 2006. **282**(1–2): p. 21-31.

28. Kim, J.H., W.J. Koros, and D.R. Paul, *Effects of CO₂ exposure and physical aging on the gas permeability of thin 6FDA-based polyimide membranes: Part 2. with crosslinking*. Journal of Membrane Science, 2006. **282**(1–2): p. 32-43.
29. Moe, M., et al., *Effects of film history on gas transport in a fluorinated aromatic polyimide*. Journal of Applied Polymer Science, 1988. **36**(8): p. 1833-1846.
30. Pope, D.S., G.K. Fleming, and W.J. Koros, *Effect of various exposure histories on sorption and dilation in a family of polycarbonates*. Macromolecules, 1990. **23**(11): p. 2988-2994.
31. Pfromm, P.H. and W.J. Koros, *Accelerated physical ageing of thin glassy polymer films: evidence from gas transport measurements*. Polymer, 1995. **36**(12): p. 2379-2387.
32. Denny Kamaruddin, H. and W.J. Koros, *Some observations about the application of Fick's first law for membrane separation of multicomponent mixtures*. Journal of Membrane Science, 1997. **135**(2): p. 147-159.
33. Achoundong, C.S.K., *Engineering Economical Membrane Materials for Aggressive Sour Gas Separations*, in *School of Chemical and Biomolecular Engineering 2013*, Georgia Institute of Technology: Atlanta, GA.
34. Wind, J.D., et al., *Carbon Dioxide-Induced Plasticization of Polyimide Membranes: Pseudo-Equilibrium Relationships of Diffusion, Sorption, and Swelling*. Macromolecules, 2003. **36**(17): p. 6433-6441.
35. Bos, A., et al., *CO₂-induced plasticization phenomena in glassy polymers*. Journal of Membrane Science, 1999. **155**(1): p. 67-78.
36. Ismail, A.F. and W. Lorna, *Penetrant-induced plasticization phenomenon in glassy polymers for gas separation membrane*. Separation and Purification Technology, 2002. **27**(3): p. 173-194.
37. Koros, W.J., et al., *Relaxation dynamics of CO₂ diffusion, sorption, and polymer swelling for plasticized polyimide membranes*. Macromolecules, 2003. **36**(17): p. 6442-6448.
38. Wind, J.D., et al., *Solid-State Covalent Cross-Linking of Polyimide Membranes for Carbon Dioxide Plasticization Reduction*. Macromolecules, 2003. **36**(6): p. 1882-1888.
39. Lin, H., et al., *Plasticization-Enhanced Hydrogen Purification Using Polymeric Membranes*. Science, 2006. **311**(5761): p. 639-642.
40. Donohue, M.D., B.S. Minhas, and S.Y. Lee, *Permeation behavior of carbon dioxide-methane mixtures in cellulose acetate membranes*. Journal of Membrane Science, 1989. **42**(3): p. 197-214.
41. Bos, A., et al., *Plasticization-resistant glassy polyimide membranes for CO₂/CO₄ separations*. Separation and Purification Technology, 1998. **14**(1-3): p. 27-39.

42. Duthie, X., et al., *Thermal treatment of dense polyimide membranes*. Journal of Polymer Science Part B: Polymer Physics, 2008. **46**(18): p. 1879-1890.
43. Ismail, A.F. and N. Yaacob, *Performance of treated and untreated asymmetric polysulfone hollow fiber membrane in series and cascade module configurations for CO₂/CH₄ gas separation system*. Journal of Membrane Science, 2006. **275**(1-2): p. 151-165.
44. Bos, A., et al., *Suppression of gas separation membrane plasticization by homogeneous polymer blending*. AIChE Journal, 2001. **47**(5): p. 1088-1093.
45. Duthie, X.J., et al., *Plasticization suppression in grafted polyimide-epoxy network membranes*. Industrial & Engineering Chemistry Research, 2007. **46**(24): p. 8183-8192.
46. Bos, A., et al., *Suppression of CO₂-plasticization by semiinterpenetrating polymer network formation*. Journal of Polymer Science Part B: Polymer Physics, 1998. **36**(9): p. 1547-1556.
47. Wind, J.D., et al., *The Effects of Crosslinking Chemistry on CO₂ Plasticization of Polyimide Gas Separation Membranes*. Industrial & Engineering Chemistry Research, 2002. **41**(24): p. 6139-6148.
48. Staudt-Bickel, C. and W. J. Koros, *Improvement of CO₂/CH₄ separation characteristics of polyimides by chemical crosslinking*. Journal of Membrane Science, 1999. **155**(1): p. 145-154.
49. Hillock, A.M.W. and W.J. Koros, *Cross-Linkable Polyimide Membrane for Natural Gas Purification and Carbon Dioxide Plasticization Reduction*. Macromolecules, 2007. **40**(3): p. 583-587.
50. Kratochvil, A.M. and W.J. Koros, *Decarboxylation-Induced Cross-Linking of a Polyimide for Enhanced CO₂ Plasticization Resistance*. Macromolecules, 2008. **41**(21): p. 7920-7927.
51. Liu, Y., R. Wang, and T.-S. Chung, *Chemical cross-linking modification of polyimide membranes for gas separation*. Journal of Membrane Science, 2001. **189**(2): p. 231-239.
52. Chen, C.C., *Thermally Crosslinked Polyimide Hollow Fiber Membranes for Natural Gas Purification*, in *School of Chemical and Biomolecular Engineering 2011*, Georgia Institute of Technology: Atlanta, GA.
53. Omole, I.C., S.J. Miller, and W.J. Koros, *Increased Molecular Weight of a Cross-Linkable Polyimide for Spinning Plasticization Resistant Hollow Fiber Membranes*. Macromolecules, 2008. **41**(17): p. 6367-6375.
54. Omole, I.C., et al., *Effects of CO₂ on a High Performance Hollow-Fiber Membrane for Natural Gas Purification*. Industrial & Engineering Chemistry Research, 2010. **49**(10): p. 4887-4896.

55. Ma, C. and W.J. Koros, *High-performance ester-crosslinked hollow fiber membranes for natural gas separations*. Journal of Membrane Science, 2013. **428**(0): p. 251-259.
56. Maeda, Y. and D.R. Paul, *Effect of antiplasticization on gas sorption and transport. I. Polysulfone*. Journal of Polymer Science Part B: Polymer Physics, 1987. **25**(5): p. 957-980.
57. Maeda, Y. and D.R. Paul, *Effect of antiplasticization on gas sorption and transport. II. Poly(phenylene oxide)*. Journal of Polymer Science Part B: Polymer Physics, 1987. **25**(5): p. 981-1003.
58. Maeda, Y. and D.R. Paul, *Effect of antiplasticization on gas sorption and transport. III. Free volume interpretation*. Journal of Polymer Science Part B: Polymer Physics, 1987. **25**(5): p. 1005-1016.
59. Lee, J.S., W. Madden, and W.J. Koros, *Antiplasticization and plasticization of Matrimid® asymmetric hollow fiber membranes—Part A. Experimental*. Journal of Membrane Science, 2010. **350**(1-2): p. 232-241.
60. Lee, J.S., W. Madden, and W.J. Koros, *Antiplasticization and plasticization of Matrimid® asymmetric hollow fiber membranes. Part B. Modeling*. Journal of Membrane Science, 2010. **350**(1-2): p. 242-251.
61. Maeda, Y. and D.R. Paul, *Effect of antiplasticization on selectivity and productivity of gas separation membranes*. Journal of Membrane Science, 1987. **30**(1): p. 1-9.
62. Lee, J.S., *Fundamental of Transport in Advanced Barrier Materials Based on Engineered Antiplasticization*, in *School of Chemical and Biomolecular Engineering 2011*, Georgia Institute of Technology: Atlanta, GA.
63. Vrentas, J.S., J.L. Duda, and H.C. Ling, *Antiplasticization and volumetric behavior in glassy polymers*. Macromolecules, 1988. **21**(5): p. 1470-1475.
64. Duda, J.L., I. Hadj Romdhane, and R.P. Danner, *Diffusion in glassy polymers — relaxation and antiplasticization*. Journal of Non-Crystalline Solids, 1994. **172–174, Part 2**(0): p. 715-720.
65. Madden, W., *The Performance of Hollow Fiber Gas Separation Membranes in the Presence of an Aggressive Feed Stream*, in *School of Chemical and Biomolecular Engineering 2005*, Georgia Institute of Technology: Atlanta, GA.
66. Horn, N.R. and D.R. Paul, *Carbon dioxide plasticization and conditioning effects in thick vs. thin glassy polymer films*. Polymer, 2011. **52**(7): p. 1619-1627.
67. Fleming, G.K. and W.J. Koros, *Carbon dioxide conditioning effects on sorption and volume dilation behavior for bisphenol A-polycarbonate*. Macromolecules, 1990. **23**(5): p. 1353-1360.

68. Kratochvil, A.M., S. Damle-Mogri, and W.J. Koros, *Effects of Supercritical CO₂ Conditioning on Un-Cross-Linked Polyimide Membranes for Natural Gas Purification*. *Macromolecules*, 2009. **42**(15): p. 5670-5675.
69. Chatterjee, G., A.A. Houde, and S.A. Stern, *Poly(ether urethane) and poly(ether urethane urea) membranes with high H₂S/CH₄ selectivity*. *Journal of Membrane Science*, 1997. **135**(1): p. 99-106.
70. Mohammadi, T., et al., *Acid Gas Permeation Behavior Through Poly(Ester Urethane Urea) Membrane*. *Industrial & Engineering Chemistry Research*, 2008. **47**(19): p. 7361-7367.
71. Membrane Technology and Research, I., *Low-Quality Natural Gas Sulfur Removal/Recovery*, 1998, The Department of Energy: Morgantown, WV.
72. Hao, J., P.A. Rice, and S.A. Stern, *Upgrading low-quality natural gas with H₂S- and CO₂-selective polymer membranes: Part I. Process design and economics of membrane stages without recycle streams*. *Journal of Membrane Science*, 2002. **209**(1): p. 177-206.
73. Hao, J., P.A. Rice, and S.A. Stern, *Upgrading low-quality natural gas with H₂S- and CO₂-selective polymer membranes: Part II. Process design, economics, and sensitivity study of membrane stages with recycle streams*. *Journal of Membrane Science*, 2008. **320**(1-2): p. 108-122.
74. Bhide, B.D., A. Voskericyan, and S.A. Stern, *Hybrid processes for the removal of acid gases from natural gas*. *Journal of Membrane Science*, 1998. **140**(1): p. 27-49.
75. Clausi, D.T. and W.J. Koros, *Formation of defect-free polyimide hollow fiber membranes for gas separations*. *Journal of Membrane Science*, 2000. **167**(1): p. 79-89.
76. Carruthers, S., *Integral-skin Formation in Hollow Fiber Membranes for Gas Separations*, in *Department of Chemical Engineering* 2001, University of Texas at Austin: Austin, TX.
77. Wallace, D.W., *Crosslinked Hollow Fiber Membranes for Natural Gas Purification and Their Manufacture from Novel Polymers*, in *Department of Chemical Engineering* 2004, University of Texas at Austin: Austin, TX.
78. Wallace, D.W., et al., *Characterization of crosslinked hollow fiber membranes*. *Polymer*, 2006. **47**(4): p. 1207-1216.
79. Pinnau, I. and W.J. Koros, *Relationship between substructure resistance and gas separation properties of defect-free integrally skinned asymmetric membranes*. *Industrial & Engineering Chemistry Research*, 1991. **30**(8): p. 1837-1840.
80. Kosuri, M.R. and W.J. Koros, *Defect-free asymmetric hollow fiber membranes from Torton (R), a polyamide-imide polymer, for high-pressure CO₂ separations*. *Journal of Membrane Science*, 2008. **320**(1-2): p. 65-72.

81. Li, Y., et al., *Fabrication of dual-layer polyethersulfone (PES) hollow fiber membranes with an ultrathin dense-selective layer for gas separation*. Journal of Membrane Science, 2004. **245**(1–2): p. 53-60.
82. Pinnau, I. and W.J. Koros, *Influence of quench medium on the structures and gas permeation properties of polysulfone membranes made by wet and dry/wet phase inversion*. Journal of Membrane Science, 1992. **71**(1–2): p. 81-96.
83. McKelvey, S.A., D.T. Clausi, and W.J. Koros, *A guide to establishing hollow fiber macroscopic properties for membrane applications*. Journal of Membrane Science, 1997. **124**(2): p. 223-232.
84. Baker, R.W., *Membrane Technology and Applications*. 2 ed. 2004, West Sussex: John Wiley & Sons, Ltd.
85. McKelvey, S.A., *Formation and Characterization of Hollow Fiber Membranes for Gas Separations*, in *Department of Chemical Engineering 1997*, University of Texas at Austin: Austin, TX.
86. Wallace, D.W., *Crosslinked Hollow Fiber Membranes for Natural Gas Purification and Their Manufacture from Novel Polymers*, in *Department of Chemical Engineering 2004*, University of Texas: Austin, TX. p. 221.
87. Husain, S., *Formation of Non-crosslinked Asymmetric Hollow Fiber Mixed Matrix Polymer/Molecular Sieve Membranes*, in *School of Chemical and Biomolecular Engineering 2006*, Georgia Institute of Technology: Atlanta, GA.
88. Ren, J., et al., *The effects of chemical modifications on morphology and performance of 6FDA-ODA/NDA hollow fiber membranes for CO₂/CH₄ separation*. Journal of Membrane Science, 2003. **222**(1–2): p. 133-147.
89. Chen, C.-C., et al., *Plasticization-resistant hollow fiber membranes for CO₂/CH₄ separation based on a thermally crosslinkable polyimide*. Journal of Membrane Science, 2011. **382**(1–2): p. 212-221.

CHAPTER 3

MATERIALS AND EXPERIMENTAL METHODS

3.1. Materials

3.1.1. Polymer Synthesis

The polymer backbone that is the primary focus of this work is a glassy copolyimide, 6FDA-DAM:DABA. This polymer is synthesized through a two-reaction polycondensation sequence, described by a number of authors [1, 2]. The monomers used to form the 6FDA-DAM:DABA backbone are 4,4'-(hexafluoroisopropylidene) diphtalic anhydride (6FDA), 2,4-diamino mesitylene (DAM), and 3,5-diaminobenzoic acid (DABA). Using *n*-methylpyrrolidone (NMP) as the solvent, the three monomers are added to the reactor stoichiometrically to produce a copolymer of the desired composition.

The majority of this work deals with 6FDA-DAM:DABA copolymers containing a 3:2 monomer ratio. That is, there are three 6FDA-DAM segments for every two 6FDA-DABA segments; hence, the polymer with this composition is referred to as 6FDA-DAM:DABA (3:2). The choice of monomer ratio within the polymer has a number of effects on the separation properties of membranes formed from this material. The 3:2 monomer ratio used in this work was selected based on its excellent CO₂/CH₄ separation performance and high resistance to CO₂-induced plasticization [1, 3, 4]. Also, this ratio has been found to provide an appropriate concentration of crosslinking sites along the polymer backbone for further stability enhancement; the carboxylic acid group on the 6FDA-DABA monomer can be used in an esterification crosslinking scheme, which will be described shortly. In general, the DAM subunit provides higher permeability

in this material due to the greater level of free volume introduced by the bulky $-\text{CH}_3$ groups. On the other hand, the DABA subunit tends to favor higher selectivity (for CO_2/CH_4 , at least) because of the polar carboxylic acid group, which can lend additional inter- and intra-molecular polymer chain segmental interactions that may increase the rigidity of the polymer matrix.

This first step in the reaction sequence results in the formation of a polyamic acid, as shown in Figure 3.1.

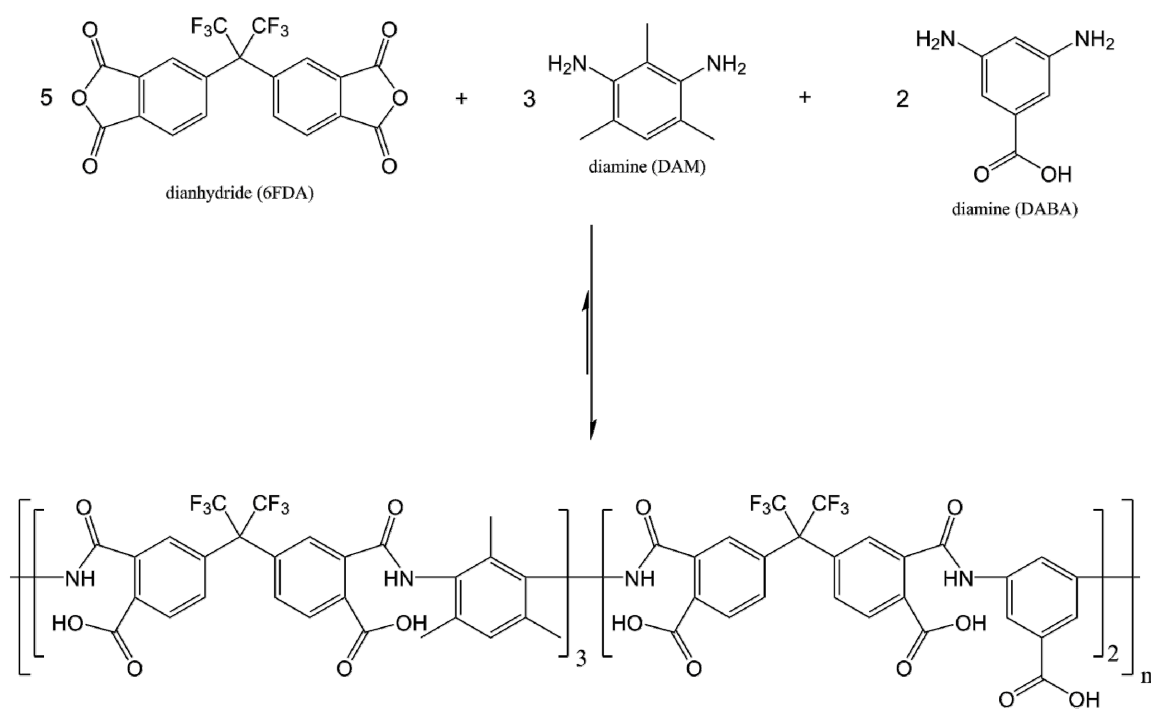


Figure 3.1: Stoichiometric reaction of dianhydride and diamines to form the polyamic acid precursor of the 6FDA-DAM:DABA (3:2) backbone.

This reaction step is highly water-sensitive, and great care is taken to removal all traces of residual humidity from the reactor setup and NMP solvent. All liquid reagents used in the production of 6FDA-DAM:DABA are dried over molecular sieve (4Å) beads and the

reaction is maintained under constant UHP N₂ purge to minimize exposure of the reaction to moisture.

After formation of the polyamic acid precursor, a secondary imidization reaction is performed in order to obtain the desired copolyimide. The imidization reaction involves dehydration to form a cyclic polyimide. Imidization reactions are most commonly carried out either chemically or thermally. Chemical imidization can be performed at lower temperatures and relies upon the use of an imidization catalyst and chemical dehydrating agent, since the reaction temperatures are usually not high enough to efficiently remove water thermally. The most common imidization catalysts for this reaction are pyridine, triethyl amine (TEA), and β -picoline. Acetic anhydride is often used as a chemical dehydrating agent. The dehydrating agent reduces the possibility of hydrolytic degradation that can decrease reactivity of the anhydride or even cause chain scissioning and, therefore, lower molecular weight of the final copolyimide. Thermal imidization occurs by heating the reaction solution at high temperature, around 180-200°C in this case. An azeotropic drying agent such as toluene or *o*-dichlorobenzene (ODCB) is used to aid in the removal of water formed during the reaction. This drives the reaction forward and reduces the unwanted side effects of H₂O on the reaction.

In this work, a combination of chemical and thermal imidization was used to ensure complete conversion of the polyamic acid. A detailed synthesis protocol is presented in APPENDIX B. The resulting copolyimide is normally precipitated in methanol (MeOH) and dried at 75-100°C under vacuum prior to further processing steps. The imidization reaction step is represented in Figure 3.2.

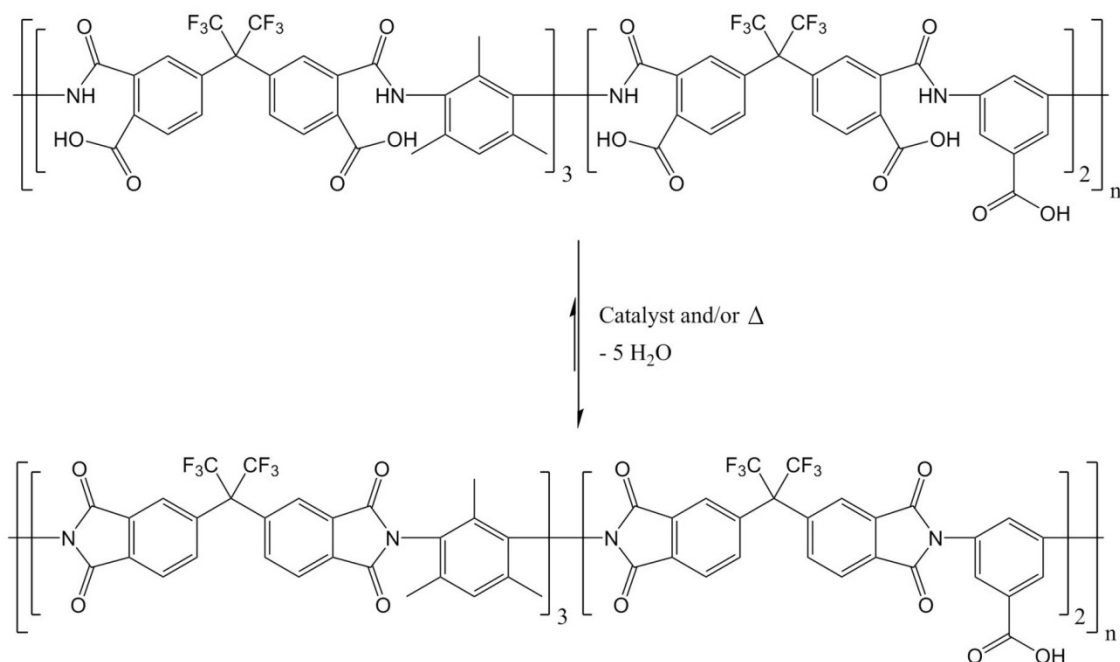


Figure 3.2: Schematic showing the imidization of the polyamic acid precursor to form 6FDA-DAM:DABA (3:2).

3.1.2. Crosslinking

One of the most attractive qualities of the 6FDA-DAM:DABA polymer backbone is the potential for covalent crosslinking through an esterification reaction scheme. This crosslinking method occurs in two steps: (1) the formation of a ‘monoesterified’ crosslinkable polyimide, which can be processed in solution to form a membrane, and (2) crosslinking, or ‘transesterification’, which takes place in the solid state of the formed membrane. This method eliminates the need to expose the formed membrane to a liquid crosslinking agent during the reaction, which could potentially introduce defects and alter the membrane morphology. For the highly aggressive feed steams that are typical for sour gas separations, crosslinking is particularly attractive. As such, a major focus of this research was the development of a crosslinkable polymer based on the 6FDA-DAM:DABA backbone that would give appropriate separation performance for CO₂/CH₄

and H₂S/CH₄ separations in terms of plasticization resistance, selectivity, and productivity.

3.1.2.1. Monoesterification

It has been shown that different diols (e.g. ethylene glycol, 1,3-propane diol) can react with the carboxylic acid moiety of the DABA subunit to form covalent ester bonds [5, 6]. Several authors have used 1,3-propane diol for this reaction to form the crosslinkable material known as PDMC, which stands for 1,3-**P**ropane **D**iol **M**onoesterified **C**rosslinkable [1, 4, 7, 8].

PDMC is initially formed by ‘monoesterification’, or attaching one end of 1,3-propane diol crosslinking agents to the DABA subunit, as shown in Figure 3.3. The resulting material is still soluble in solvents like NMP since it has not been crosslinked after the first reaction. As mentioned, the actual crosslinking, or transesterification reaction, is performed *after processing the polymer* into the desired membrane morphology, by simply heating under vacuum conditions. The monoesterification reaction can be performed in-line with polymer synthesis or it can be performed as a standalone reaction using previously synthesized and precipitated 6FDA-DAM:DABA polymer.

Monoesterification is a condensation reaction that involves heating a solution of 6FDA-DAM:DABA in the presence of excess diol crosslinking agent and carefully removing water as it is produced. An acid catalyst is typically used to promote esterification. More details on this reaction are given in APPENDIX C.

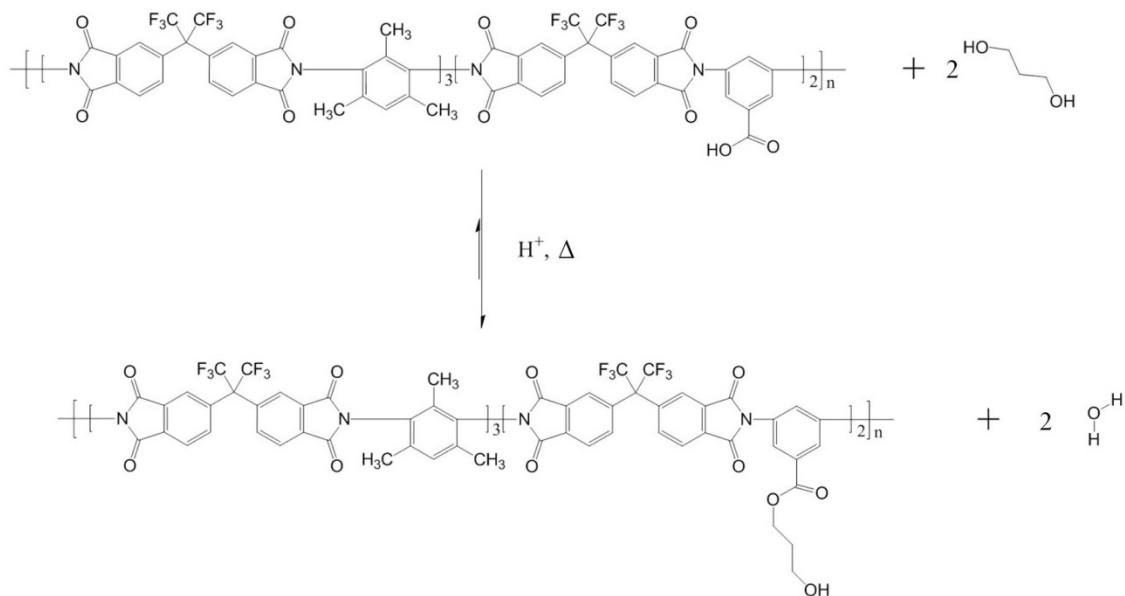


Figure 3.3: Monoesterification reaction with 6FDA-DAM:DABA (3:2). The crosslinking agent shown in this example is 1,3-propane diol, and the resulting material is referred to as PDMC.

3.1.2.2. Transesterification

After the formation of a crosslinkable polymer such as PDMC into the desired membrane morphology, transesterification crosslinking is carried out by heating the material under vacuum or inert sweep gas conditions. The pendant alcohol on one ester reacts with the ester of another converted 6FDA-DABA monomer to form a covalent crosslink. This reaction is depicted in Figure 3.4, below.

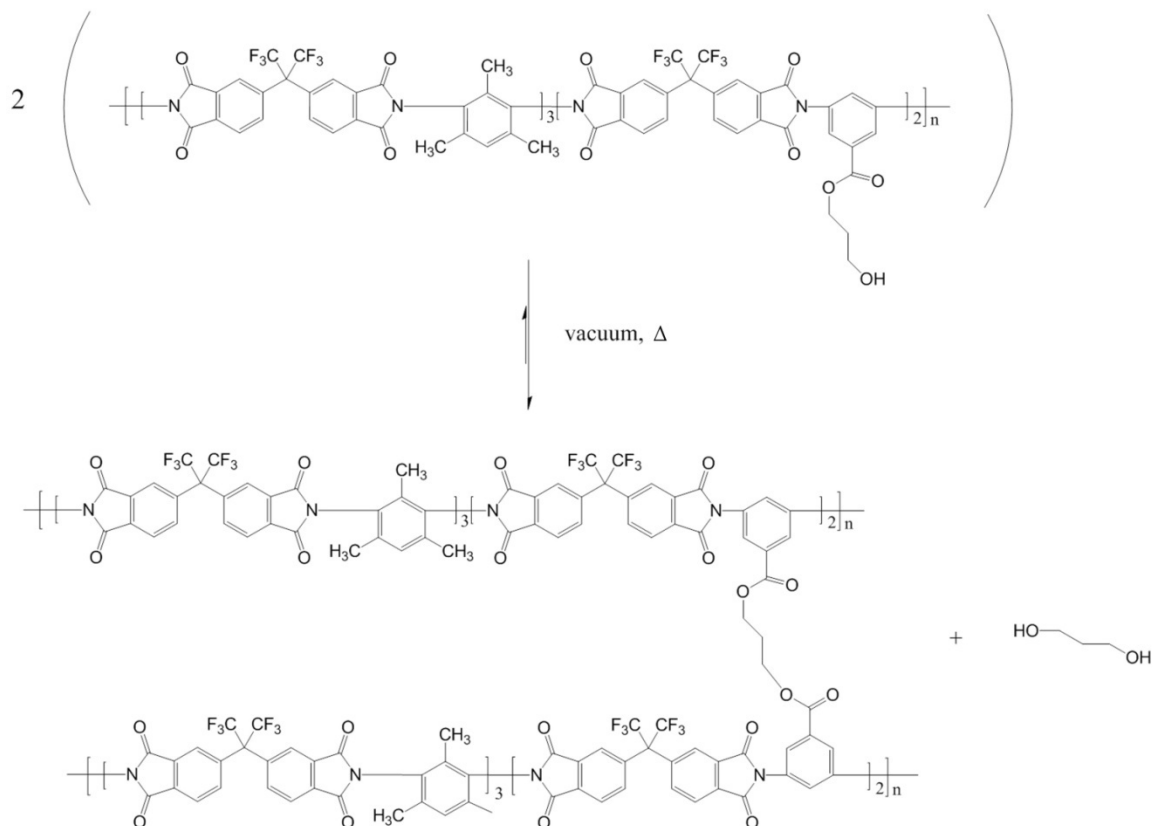


Figure 3.4: The transesterification crosslinking reaction, which is performed after membrane formation, is shown for the PDMAc material.

Assuming the monoesterification reaction has gone to completion and all of the carboxylic acid groups are monoesterified, one diol crosslinking agent is evolved per crosslink that is formed. However, in the more realistic case of incomplete monoesterification, the unconverted carboxylic acid groups may still react with the pendant alcohol of a monoesterified DABA subunit. Instead of a diol crosslinking group, a water molecule is evolved. Thus, a high degree of crosslinking is achievable as long as monoester yield is reasonably high (> 60%, or so) and sufficient activation energy for crosslinking is supplied to the sample. Nevertheless, a monoester yield of ~90% or higher is preferred. Esterification reactions are reversible, and can be pushed toward the

formation of ester crosslinks by pulling vacuum or using an inert sweep gas to remove the transesterification by-products. Following crosslinking, the membrane becomes insoluble and more resistant to swelling and plasticization.

3.1.3. Gases

Pure gases (He, N₂, O₂, CO₂, CH₄), with the exception of H₂S, were of purity greater than 99.999% and were supplied by Airgas. The pure H₂S that was used had a purity of 99.6% and was supplied by Praxair. Mixed gases were supplied by Airgas and Praxair.

3.2. Membrane Formation

3.2.1. Formation of Dense Film Membranes

Dense films are the preferred membrane geometry for studying the intrinsic gas transport properties of new materials. The dense film membranes used throughout this work were fabricated with a knife-casting technique. Dried polymer powder was weighed out and then combined with tetrahydrofuran (THF) (>99.9%, anhydrous, Sigma-Aldrich) solvent to form a homogenous solution, referred to as a casting 'dope'. In this work, the casting dopes contained 15-25 wt% polymer, depending on the M_w of the polymer and the viscosity of the dope. Once completely dissolved, the dope was placed in a Glove Bag™ (Glas-col, LLC) and carefully spread across a clean glass plate using a steel doctor blade, or casting knife, with a gap of approximately 500 μm. Prior to casting, the glove bag had been purged with N₂ several times to remove any humidity; the dry N₂ inside the glove bag was then saturated with THF vapor by opening several containers of THF inside the glove bag and waiting for 4-6 hrs before casting. By saturating the glove bag atmosphere with THF, the rate of evaporation of THF out of the casting dope

was reduced. This allows the polymer chains within the dense film to relax as the sample vitrifies, which decreases the effect of physical aging on the dense film's transport properties. After knife-casting, the dope was left in the Glove Bag™ overnight to allow the majority of the volatile THF solvent to evaporate, forming a solid dense film. Next, the dense film was removed from the Glove Bag™ and transferred from the glass plate onto a piece of aluminum foil. Paper clips were used on the edges of the film to prevent curling. The sample was then dried at 100°C in a vacuum oven for 24 hrs to removal all remaining traces of THF and H₂O. Once dry, the dense films were ready for transport testing, further thermal treatment, or storage. The glass plates used for knife-casting in this work were treated with Glassclad® 18 (Gelest, Inc.), an organosilane concentrate which provides a more hydrophobic surface, to make removal of the vitrified polymer films easier.

3.2.2. Membrane Masking

Dense film permeation testing requires the preparation of a small sample that is free of any visible defects. This process, known as masking, involves “clamping” the dense film sample between two annular pieces of impermeable aluminum tape. The dense film masking procedure is described in detail elsewhere [9, 10]. The inside and outside diameters of the aluminum tape pieces used in this work were approximately 2.0 cm and 4.5 cm, respectively; the size of the dense film sample was selected so that the entire opening on the inside of the aluminum tape pieces was filled, with enough excess to ensure that the sample was securely held in place on all sides by the adhesive on the aluminum tape. The membrane thickness was measured with a digital micrometer before loading the masked sample into the permeation cell. A typical dense film membrane thickness was 50-100 μm.

In order to perform gas permeation tests on the masked sample, it was loaded into a stainless steel permeation cell. A cross-section of the dense film permeation cells that were used in this work is shown in Figure 3.5. The masked sample was placed on a sintered stainless steel platform with a single piece of filter paper between the film and the sintered metal to provide support and prevent damage to the film. Another piece of annular aluminum tape was used to secure the masked sample to the permeation cell and help create a seal between the upstream and downstream sides of the membrane.

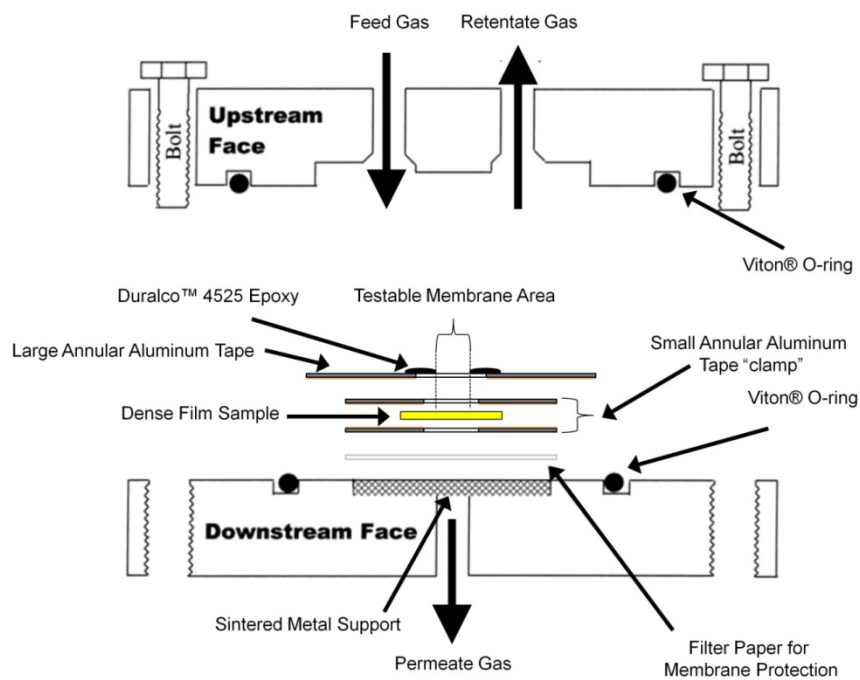


Figure 3.5: Schematic of the dense film permeation cells used for pure and mixed gas experiments. Adapted from [11].

When the gases used for permeation testing are highly condensable or if high pressures are going to be used, an additional step must be taken to prevent bypass of gas penetrants through the adhesive and around the masked film sample. If the amount of gas bypassing the membrane is significant, permeation measurements can be seriously affected and sensitive equipment on the downstream side of the permeation

system may be compromised. To avoid such a scenario, the interface between the film sample and the aluminum tape was sealed with a two-part, high-temperature epoxy, Duralco™ 4525 (Cotronics Corp.). After application of the epoxy to the masked sample, it was allowed to cure at 35°C for 24 hrs while pulling vacuum on the downstream side of the sample to help with adhesion between the film and the epoxy (only the bottom half of the permeation cell was loaded into the system during this step). Once the epoxy was cured, the permeation cell was removed from the permeation system and a high-resolution scan was taken of the upstream side of dense film sample. This allowed for accurate calculation of the effective film surface area with a digital image processing program, ImageJ (National Institutes of Health). At this point, the sample was ready for permeation testing and the permeation cell was assembled and loaded into the system.

3.2.3. Formation of Asymmetric Hollow Fiber Membranes

3.2.3.1. Dope Formulation

The mechanism of forming asymmetric hollow fiber membranes and some of the most important qualities of this membrane type are discussed in Section 2.7.1. Also tabulated in that section are key spinning parameters that can impact the quality of the fibers. Perhaps the most important of these parameters is the composition of the polymer-containing dope itself. For the dry-jet/wet-quench spinning process in general, a dope normally consists of volatile and non-volatile solvents, volatile and non-volatile non-solvents, polymer, and, in some cases, small amounts of other additives.

In this work, the polymer-containing dopes used for spinning were comprised of NMP and THF solvents, EtOH non-solvent, either 6FDA-DAM:DABA or a crosslinkable polymer derived from the 6FDA-DAM:DABA backbone, and lithium nitrate (LiNO₃) as a minor additive component. NMP is chosen as the non-volatile solvent because it is

soluble in many polyimides like 6FDA-DAM:DABA, is a water soluble organic, and it is relatively environmentally benign. THF is also a good solvent for polyimides derived from the 6FDA-DAM:DABA backbone and is highly volatile (boiling point temp. = 66°C). The only non-solvent used in the dope is EtOH, which is also relatively volatile (boiling point temp. = 78°C). EtOH is, in many cases, preferred over H₂O as a non-solvent since it provides a greater window for dope formulation than H₂O, due to the very strong non-solvent nature of H₂O to these polymers [3, 12]. However, the non-solvent used in the quench bath to cause phase separation of the dope is H₂O. LiNO₃ is used as a viscosity and phase separation enhancer [3].

One of the most powerful tools for selecting a specific dope composition is so-called 'cloud point experimentation' [13]. This technique allows for the creation of a rough ternary phase diagram for the dope system of interest. Most importantly, it enables the identification of the binodal line, which separates the one-phase and two-phase regions. Essentially, a series of dope samples of fixed polymer content are mixed with varying EtOH (non-solvent) content. Dopes with a composition that lies within the one-phase region are transparent when completely mixed (although they may be colored), whereas those with a composition that lies near the binodal appear cloudy. An approximation of the binodal line is obtained by performing these tests at a few polymer concentrations and observing the solvent/non-solvent ratios that cause phase separation. Even with this powerful tool, the complex nature of polymer solutions and the multitude of requirements that must be met for successful fiber formation suggest that dope formulation involves considerable trial and error before an optimum dope composition is developed.

Syringe tests are another tool that can be used for identifying potentially viable dope compositions by simulating the fiber spinning process without having to make a

full-sized dope [14]. Experimental dopes of around 25 mL that were based on the results of cloud point experimentation were loaded into disposable syringes and then heated to the anticipated spinning temperature. The dopes were then manually extruded through an air gap and into a small water quench bath to cause phase separation. Obviously, the fibers obtained through this method were not hollow, since there was no bore fluid. Nevertheless, after solvent exchange and drying, the morphology of the fibers was examined by scanning electron microscopy (SEM). Significant morphological problems are indicative of a non-viable dope for the full spinning process.

3.2.3.2. Hollow Fiber Spinning

The dry-jet/wet-quench spinning technique used for hollow fiber spinning is described in Section 2.7.1. After settling upon a dope composition, the full-sized spinning dope was mixed in a 500 mL Qorpak® glass jar and sealed with a Teflon® cap liner. The jars were placed on rollers and simple low-shear mixing, resulting from the intrinsic viscosity of the dope, was used to homogenize the mixture. This is the preferred method of mixing a spinning dope, since it does not require exposure of the dope to air, which could result in evaporation of the volatile components and a significant deviation from the desired composition. A heat lamp was positioned above the dope in order to bring the dope temperature up to approximately 50°C to facilitate mixing and dissolution of the polymer. Once the dope mixture was homogenized (usually after 1-2 weeks on the rollers), it was cooled down to room temperature and then transferred into a 500 mL high-precision, high-pressure syringe pump (Teledyne Isco) and allowed to settle/degas for 24 hrs at 35°C. This step is important because the presence of even a small bubble in the dope can cause major defects in the fiber and even line breakage during spinning. A second syringe pump (100 mL) was used for the bore fluid, which had a composition

of 80% NMP and 20% H₂O. During the spinning process, the dope and bore fluids were filtered in-line between their respective syringe delivery pumps and the spinneret.

A number of variables are controlled during spinning, including spinning temperature, draw ratio (through the dope flow rate and take-up drum speed), air gap, and quench bath temperature. Thermocouples were attached to the dope delivery pump and spinneret, both of which had been wrapped in heat tape, to control the spinning temperature. Spinning was carried out with dope syringe pump and spinneret temperatures in the 50-70°C range. Another thermocouple was submerged in the quench bath and hot water was added as needed to maintain the desired temperature. The quench bath temperature used for this work was 50°C.

The dope and bore fluids were coextruded through the spinneret into the air gap and then guided through the quench bath (height = 1 m). Flow rates for the dope and bore fluid were controlled individually, with the bore fluid flow rate normally kept at 1/3 that of the dope flow rate. The air gap height was varied from 2.5-15 cm by changing the elevation of the spinneret. After passing through the quench bath by way of a series of Teflon® guides, the fibers were collected on a rotating polyethylene take-up drum (diameter = 0.32 m). To ensure complete phase separation and facilitate the removal of solvent from the newly spun fibers, the take-up drum was partially submerged in a separate water bath at room temperature.

The fibers were cut off the take-up drum to form many individual fibers with a length equal to the circumference of the take-up drum (~1 m). Once removed from the spinning setup, the fibers were quickly transferred to a deionized (DI) water bath and soaked for at least 3 - 4 days, with the DI water replaced daily. This promoted the removal of the vast majority of solvent/non-solvent from the fibers. Finally, a 'solvent

exchange' process was performed on the fibers. This consisted of sequential 1 hr soaks in EtOH and hexane, with each solvent soak broken down into three separate 20 minute periods and with fresh solvent added each time. Solvent exchange may be a misnomer here, since the liquids used are actually strong non-solvents for the polymeric fibers. Non-solvents must be used in order to prevent dissolution of the fibers or changes in the fiber morphology. The fibers were next air-dried in a fume hood for 1 hr to remove most of the hexane, and then dried in a vacuum oven at 70 - 80°C for 2 hrs.

3.2.3.3. Hollow Fiber Module-Making

Hollow Fibers were potted into laboratory-scale modules as shown in Figure 3.6. Details on the module-making process have been described elsewhere [15, 16]. For pure gas permeation measurements, a typical module contained between 6-10 fibers with active membrane lengths of ~15-20 cm. Modules for mixed gas permeation, which introduces a number of practical considerations related to gas usage and permeate flow measurement, typically contained only 4-6 fibers with active membrane lengths of 8-15 cm. A reduced membrane surface area is often desired for mixed gas permeation, since less area results in lower permeate flow rate and less gas that must be vented in the retentate stream.

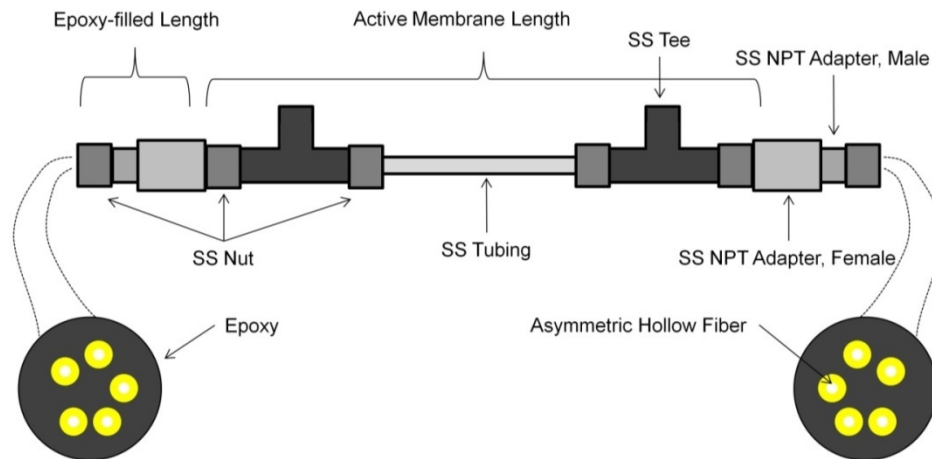


Figure 3.6: Schematic of a laboratory-scale asymmetric hollow fiber membrane module for sour gas testing. All components are stainless steel to prevent corrosion by the acid gas components.

3.2.4. Dense Film and Hollow Fiber Crosslinking

As mentioned previously, the transesterification crosslinking reaction (Figure 3.4) can be performed after membrane formation by simply heating the membrane under vacuum or inert gas purge conditions. This is most easily done in a vacuum oven. However, transesterification crosslinking can also be performed inside the quartz tube of a pyrolysis oven by attaching an appropriate inert gas and purging at a reasonable flow rate. The biggest factors, aside from the extent of monoesterification, that impact transesterification are the crosslinking temperature and crosslinking soak time. For example, it has been shown that PDMC crosslinking may occur at temperatures greater than $\sim 150^{\circ}\text{C}$, and a typical protocol for PDMC hollow fibers calls for a 2 hr soak at around 200°C .

In the case of dense film membranes formed from a crosslinkable polymer, like PDMC or others of this class, there is a much wider window of acceptable crosslinking conditions than for hollow fibers. The crosslinking temperature for a dense film must

remain below the T_g and should, ideally, be as short as possible to avoid excessive physical aging, which is accelerated under high temperature environments. In general, the dense film morphology is not significantly affected by crosslinking. Asymmetric hollow fiber membranes, however, are much more sensitive to crosslinking conditions because of their much greater free volume and their ultra thin selective membrane layers (physical aging is more pronounced in thin membranes). The use of a higher crosslinking temperature tends to form a thicker effective skin layer and reduce gas permeance [4]. Similarly, an excessive crosslinking soak time can result in partial substructure compaction and, therefore, additional mass transfer resistance. In some cases, the effect is worse than simple loss of permeance; non-selective substructure resistance can actually decrease the selectivity of an asymmetric hollow fiber membrane to the gas pair of interest. Furthermore, crosslinking temperatures that approach or exceed the T_g of the material can cause complete loss of the porous substructure morphology, resulting in huge permeance losses. For the reasons described above, shorter crosslinking soak times and lower crosslinking temperatures were investigated for the asymmetric hollow fibers than for dense films used in this work.

As such, selecting an appropriate crosslinking protocol for crosslinkable asymmetric hollow fiber membranes is critical to overall performance. In the past, attempts have been made to use catalysts to reduce the crosslinking temperature and increase permeance [15]. These catalysts, such as *p*-toluenesulfonic acid, are believed to reduce the activation energy of the crosslinking reaction, thus allowing for a high degree of crosslinking under milder crosslinking temperature conditions. Unfortunately, preliminary studies on catalyst-assisted crosslinking of PDMC at 150°C indicated that catalyst treatment can significantly reduce permeance [8]. Therefore, catalysts were not

involved in the crosslinking optimization performed as a part of this study. Further details regarding catalyst-assisted crosslinking of PDMC are available in other sources [8, 15].

3.3. Membrane Characterization Techniques

3.3.1. Permeation Analysis

3.3.1.1. Permeation Equipment

Gas permeability through dense film membrane samples was measured using an isochoric permeation system. This system allows for the calculation of intrinsic permeability values by exposing the upstream side of the membrane to a high feed pressure and monitoring the change in downstream (permeate) pressure with time [17, 18]. The rate of change in the permeate pressure, $\Delta p/\Delta t$, at steady state is proportional to the gas flux through the membrane, which, when normalized by membrane thickness and the transmembrane pressure differential, yields the membrane's permeability.

Figure 3.7 shows a schematic of the isochoric permeation systems used in this work for measuring dense film permeability. Note that the permeation cell depicted in Figure 3.7 is represented as component number '4'. The system was constructed from 0.125" and 0.25" stainless steel tubing (Swagelok®) and all connectors were stainless steel, as well, to prevent corrosion under the aggressive sour gas testing conditions used in this study. The temperature inside the permeation system can be controlled through a temperature controller on the outside of the system. For all measurements performed in this work, the permeation system was maintained at 35°C.

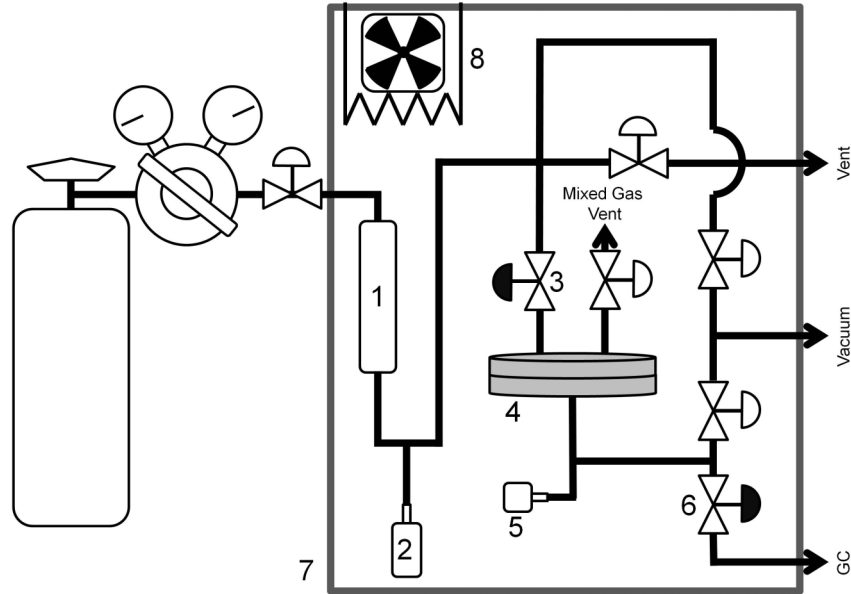


Figure 3.7: Schematic of isochoric dense film permeation system for pure and mixed gas experiments. System components: (1) upstream volume, (2) upstream pressure transducer, (3) pneumatically-activated feed gas valve, (4) permeation cell, (5) downstream pressure (6) pneumatically-activated GC sampling valve, (7) insulated permeation box, (8) heater/fan.

These permeation systems were slightly modified from the typical systems that are used for testing non-toxic gases, since H_2S -containing gases require a more robust design to ensure user safety [11]. The most notable change is the use of pneumatically activated feed and GC sampling valves (shown in Figure 3.7) instead of manual valves. These can be controlled through a LabView (National Instruments Corp.) code running on a computer located outside of the fume hood that contains the system, which also records the upstream and downstream pressure versus time data. This helps reduce the risk of H_2S exposure and can also protect sensitive system elements from over-pressure. More details on the specific equipment used for the construction of these systems are available elsewhere [19].

Asymmetric hollow fiber pure gas permeation was conducted in an isobaric system with a dead-end, counter-current flow configuration, with the feed normally on

the bore side of the fibers. Under high pressure pure gas testing conditions, a shell side feed configuration was sometimes used to prevent fiber blow out. In these pure gas permeation experiments, there is no retentate stream and permeate is collected on the shell side of the modules, except in when shell side feed is used. The permeate flow rate is measured with a simple bubble flowmeter apparatus. This experimental setup is convenient as it allows for testing multiple fiber modules under identical conditions simultaneously by using the same feed. Figure 3.8 depicts the pure gas permeation system setup with multiple fiber modules using bore side feed. The system is insulated and maintained at a constant operating temperature of 35°C.

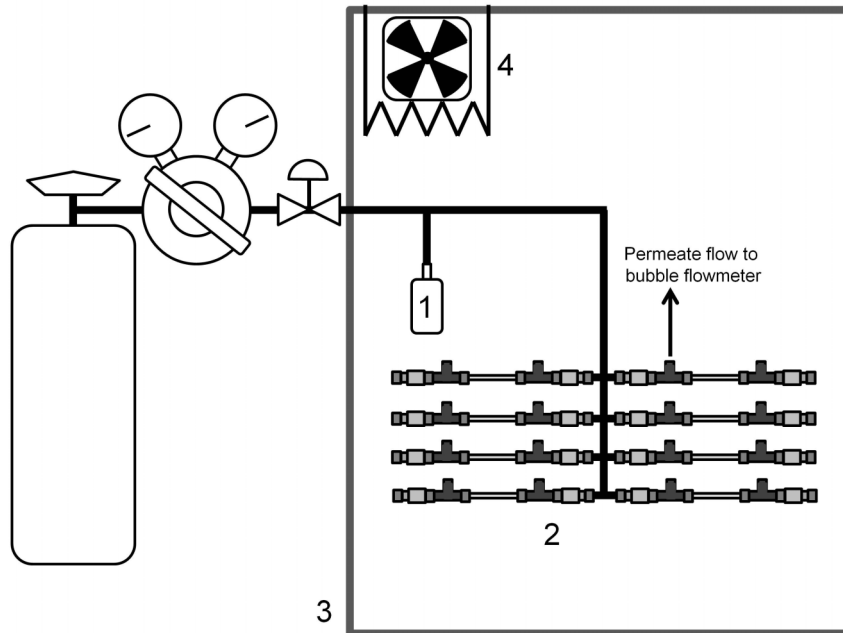


Figure 3.8: Schematic of isobaric hollow fiber permeation system for pure gas experiments. System components: (1) upstream pressure transducer, (2) hollow fiber modules, (3) insulated permeation box, (4) heater/fan. Note that the module outlets not used for the feed or permeate flow are plugged.

The downstream, or permeate, side of the modules are exposed to gas at atmospheric pressure but with a composition that is assumed to be equal to that of the

feed gas. This is a reasonable assumption since the downstream volume within the modules is under constant purge with permeate gas that slowly vents to atmosphere. It should be noted that pure H₂S permeation with asymmetric hollow fiber membranes was performed sparingly in this work, as significant safety concerns necessitated major changes to the system configuration. The mixed sour gas fiber permeation system, described below, was used for pure H₂S fiber permeation measurements.

Mixed gas permeation testing is inherently more complex than pure gas permeation. Since the stage cut of a mixed gas feed must be carefully controlled to prevent concentration polarization, only one module may be tested at a time. A counter-current flow configuration was also used for mixed gas permeation testing, and shell side feed was used in all cases. For mixed gas feeds that did not contain H₂S, a bubble flow meter was used to measure the permeate flow rate and a digital mass flowmeter (FMA Series, Omega Engineering, Inc.) was used to measure the retentate flow rate. Figure 3.9 shows the system used for non-H₂S mixed gas feeds.

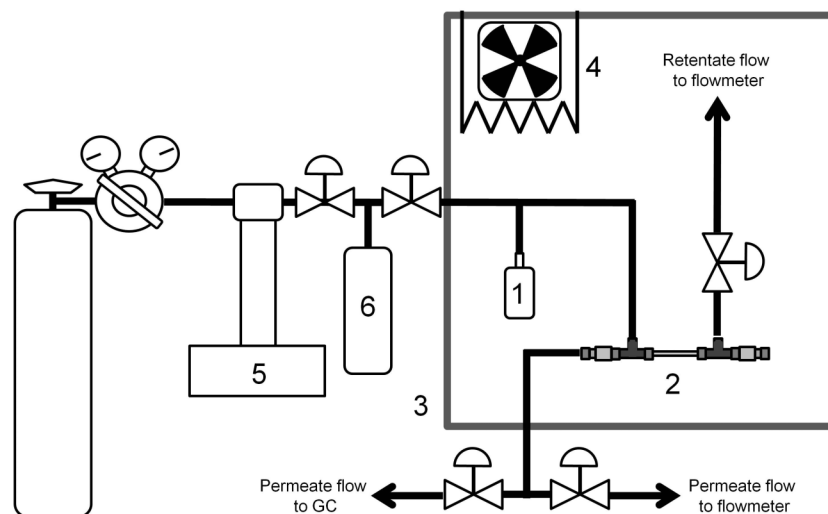


Figure 3.9: Schematic of isobaric hollow fiber permeation system for mixed gas experiments. System components: (1) upstream pressure transducer, (2) hollow fiber module, (3) insulated permeation box, (4) heater/fan, (5) syringe pump, (6) feed reservoir volume.

H₂S-containing mixed gas feeds presented a significant challenge for asymmetric hollow fiber permeation. Bubble flowmeters cannot be used since they may lead to exposure of the user to the permeate gas and they also involve the use of an aqueous surfactant solution, which is not practical for H₂S-containing gases. Instead, a novel system had to be constructed with digital mass flowmeters (mini CORI-FLOW™, Bronkhorst CORI-TECH., B.V.) attached to both the retentate and permeate streams. Unfortunately, digital flowmeters do not provide the sensitivity that is available with bubble flowmeters, so higher permeate flow rates than would normally be used had to be maintained in order to obtain accurate data. This resulted in the undesirable side effect of forcing an increase in the retentate flow rate in order to maintain low stage cuts, a topic that will be discussed in more detail in Section 3.3.1.6. Higher flow rates lead to more rapid use of these fairly expensive specialty gases and a greater load being placed on an H₂S-scrubbing unit used to neutralize the toxic H₂S gas before it is vented to atmosphere.

Table 3.1 lists the major pieces of equipment and their vendors that were used for the construction of the sour gas isobaric asymmetric hollow fiber permeation system.

Table 3.1: List of major system components and vendors for sour gas hollow fiber permeation system.

Major System Components Specs.	Vendor
Double sealed bellows valve	Swagelok
3-way ball valve	Swagelok
Metering valve	Swagelok
Pneumatically-actuated bellows valve, normally closed	Swagelok
High pressure quick connect, male/female	Swagelok
Pressure transducer, 1500psi/1000psi	Honeywell Sensotec
Pressure data acquisition and indicator, SC Series	Honeywell Sensotec
Digital mass flow controller, mini CORI-FLOW	Bronkhorst CORI-TECH
Mass flow controller data acquisition and indicator, E-7000	Bronkhorst CORI-TECH
High pressure syringe pump, 1000D	Teledyne-Isco
Reservoir volume, 2000 mL	Swagelok
SS tubing, 1/8" and 1/4"	Swagelok

3.3.1.2. Safety and Design of Sour Gas Facilities

The highly toxic nature of H₂S led to the implementation of additional safety measures for all experiments involving sour gases. This work was made possible only because of the construction of a dedicated sour gas testing laboratory that was designed with safe H₂S-handling in mind. In addition to the more robust experimentation systems described above, the laboratory includes a large, fully enclosed fume cabinet, which houses all the sour gas testing equipment. Exhaust manifolds from the fume cabinet are directed to a rooftop sour gas scrubber unit. This scrubber was installed exclusively for the sour gas testing laboratory and utilizes a concentrated basic sodium hydroxide (NaOH) solution to neutralize the acidic H₂S and CO₂ gases when they are vented from the experimentation systems, according to the reactions shown in Figure 3.10.

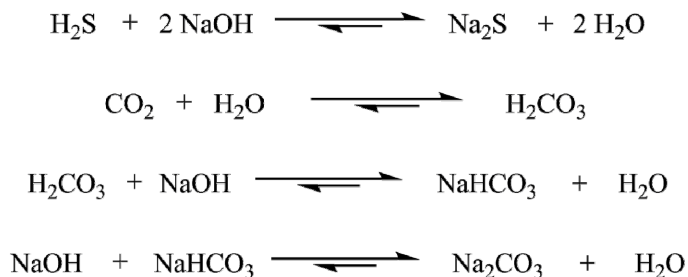


Figure 3.10: Reactions of aqueous NaOH with CO₂ and H₂S in roof-mounted scrubbing unit used to neutralize vented gases from the sour gas testing laboratory.

Several H₂S sensors were placed throughout the lab, both inside and outside the fume cabinet, to ensure user safety and the safety of other building occupants. Additionally, all users of the sour gas testing facility were required to maintain a respirator training certification geared toward H₂S handling and wear a gas purifying respirator at all times when inside the laboratory. Furthermore, individual clip-on H₂S sensors were worn by lab users. Gas cylinders containing H₂S and other flammable gases were stored in a gas cylinder cabinet (Matheson Tri-Gas®) with ventilation to the acid gas scrubber.

3.3.1.3. Pure Gas Dense Film Permeation

To obtain pure gas permeability values for a dense film sample using the system described in Section 3.3.1, the following procedure is performed.

1. After loading the permeation cell, the upstream and downstream faces of the membrane, as well as the upstream gas reservoir, are exposed to vacuum by opening the appropriate valves. Vacuum conditions are maintained for 18-24 hrs to ensure complete degassing of the film and evacuation of the system.

2. All valves are closed and the system is isolated from vacuum. Pressure versus time data is recorded for 1-2 hrs. This allows the measurement of the system's downstream leak rate, which should account for no more than 1% of the total gas flux into the downstream during an active permeation test. Normally, a downstream $\Delta p/\Delta t$ value of $< 1 \times 10^{-6}$ Torr/s is best, but this is dependent upon the downstream volume.
3. The upstream gas reservoir is purged and pressurized with the desired pure feed gas. The pressure should be slightly higher than the desired testing pressure (~5%), since additional upstream volume will be introduced when the actuated feed gas valve is opened.
4. The system is isolated from the vacuum pump and the upstream and downstream volumes are isolated from one another by closing the appropriate valves.
5. The feed gas valve is opened and pressure (p) versus time (t) data recording is started. Simultaneously the upstream pressure and system temperature are noted or recording of these variables is started.
6. The downstream pressure rise is monitored until steady state flux has been achieved. Steady state is assumed to occur after 6-10 time-lag periods (Θ), but can also be checked by comparing the slope of downstream p versus t ($\Delta p/\Delta t$) at several different times.
7. The feed pressure is either increased, to test under different feed conditions, or released and the system exposed to vacuum, to degas the film prior to testing with a new gas.

After completing the protocol listed above, the permeability can be calculated by using the following quantities: rate of change in permeate p versus t ($\Delta p_{i,down}/\Delta t$), in

Torr/sec; the membrane thickness (l), in μm ; effective membrane area (A), in cm^2 ; downstream volume (V_d), in cm^3 ; system operating temperature (T), in K; and transmembrane pressure, or fugacity, difference (Δp or Δf), in psi. These quantities can be plugged into Eq. (3.1) to obtain a value for permeability (P_i), in Barrer.

$$P_i = 6.949 \times 10^4 \frac{\left(\frac{\Delta p_{i,down}}{\Delta t} \right) \cdot l \cdot V_d}{A \cdot T \cdot \Delta p_i} \quad (3.1)$$

In Eq. (3.1), the factor at the front of the expression on the right accounts for several unit conversions needed to express permeability in the preferred unit. It should be noted, the effective value for the rate of pressure rise in the downstream due to permeation through the membrane ($\Delta p_{i,down}/\Delta t$) is the difference between the measured $\Delta p/\Delta t$ value during permeation and the $\Delta p/\Delta t$ from the leak test (step 2 in the above permeation protocol). The use of a fugacity-based driving force is preferred for highly non-ideal gas mixtures, as previously discussed.

The p versus t data for pure gas permeation through a dense film membrane normally follows the trend shown in Figure 3.11, below. The time lag, Θ , is shown and represents the x-axis intercept of a line drawn through the apparent steady state p versus t data. This method for finding Θ is valid only if the starting pressure in the downstream is zero and time zero corresponds to the initial exposure of the upstream side of the dense film to a high pressure feed, with the upstream side of the membrane also under vacuum at $t < 0$. The $\Delta p_{i,down}/\Delta t$ value used for permeability calculations is taken after a permeation time of at least $6-10\Theta$ to ensure steady state permeation has been achieved. After the initial $6-10\Theta$ periods, the downstream may be evacuated by opening the valve to the vacuum pump and, after once again isolating the downstream from the vacuum source, the $\Delta p_{i,down}/\Delta t$ value can be immediately used for permeability

calculations. This is often necessary when the permeation rate through a membrane is very high or when the testing time is very long and the downstream pressure transducer's maximum calibrated pressure is at risk of being exceeded.

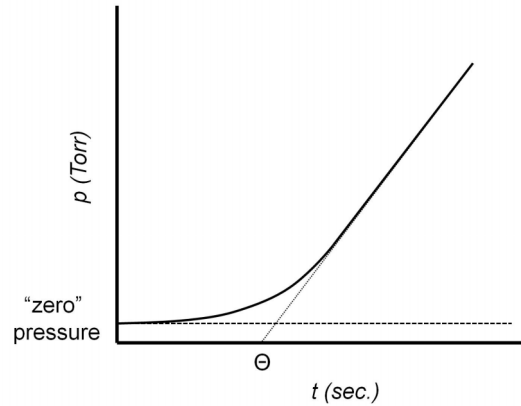


Figure 3.11: Graphical depiction of the early portion of a dense film permeation experiment. Time lag (Θ) is used to quantify the transient portion of the experiment before steady-state operation is attained.

In addition to its use for permeability calculations, the time lag of a pure gas permeation experiment can be used to obtain the apparent diffusion coefficient, as shown in Eq. (3.2) [20].

$$D_{i,apparent} = \frac{l^2}{6 \cdot \Theta} \quad (3.2)$$

Therefore, it is possible using Eqs. (2.12, 3.1 and 3.2) to determine the permeability, sorption coefficient, and diffusion coefficient of a pure gas species through a dense film membrane under a particular set of operating conditions from a single pure gas permeation experiment.

Pure gas permeability values reported in this work are the average of at least two dense film measurements, and the error associated with these measurements is expected to be $\pm 5\%$ or less.

3.3.1.4. Pure Gas Hollow Fiber Permeation

Pure gas hollow fiber permeance values can be obtained by following the procedure given below:

1. After loading the module(s) into the fiber permeation system, the caps on the retentate side of the modules are loosened to allow feed gas to purge through the bores of the fibers.
2. The feed gas is turned on to a pressure of 15-30 psig and the fibers are purged with feed gas for 5-10 min.
3. Once the feed side of the fibers has been purged, the caps on the retentate side of the modules are tightened (with the purge flow still active), so that high pressure feed can be maintained within the modules.
4. The feed pressure is increased to the desired level and an initial 30 min time period is used to allow the modules to reach steady state operation.
5. After the 30 min period, the permeation rate through each of the modules is measured individually by connecting the non-plugged port on the downstream side of the module (the outlet closest to the feed source, such that a counter-current flow is configuration is established) to a bubble flowmeter of appropriate volume. A stopwatch is used to measure the time required for a specific volume of gas to permeate through the module's fibers.

6. An additional 15 min time period is allowed and the permeation rate is again measured using the bubble flowmeter. The results of the second test are compared with those of the initial permeation rate measurement. If the rates differ by more than 5%, the 15 min time period and subsequent measurement is repeated until steady state is obtained.
7. After all measurements have been performed at a given feed pressure, the feed conditions can be changed and the process repeated from Step 4, or the feed can be turned off and the modules depressurized prior to testing with a new gas type.

The permeance of an asymmetric hollow fiber module can be calculated from the following quantities: volumetric flow rate ($\Delta v_p/\Delta t$), in mL/s; temperature of the bubble flowmeter apparatus (T), in K – note that this is not the same as the operating temperature within the permeation system; effective membrane area (A), in cm²; and the transmembrane pressure, or fugacity, difference (Δp or Δf), in psi. Eq. (3.3) is used for pure gas permeance, $(P/l)_i$ calculations, and gives permeance, in GPU, as defined by Eq.(2.6).

$$\left(\frac{P}{l}\right)_i = 5.282 \times 10^7 \frac{\left(\frac{\Delta v_p}{\Delta t}\right)}{Z_{down} \cdot A \cdot T \cdot \Delta p_i} \quad (3.3)$$

The compressibility factor, Z_{down} , is used in Eq. (3.3) to account for non-ideal gas behavior when calculating molar flow rate in the downstream, since the permeate is not at near-vacuum conditions.

Pure gas permeance values reported in this work are the average of at least three measurements, and the error associated with these measurements is generally \pm 5% at most.

3.3.1.5. Mixed Gas Dense Film Permeation

Mixed gas permeation is fairly similar to pure gas permeation. The most notable changes for mixed gas experiments include constant flow past the upstream side of the membrane, monitoring stage-cut, and the use of gas chromatography on the unknown permeate gas to determine its composition after passing through the membrane. Also, time lag measurements are not as meaningful under mixed gas feed conditions as for pure gas feeds, since multiple overlapping time lags are present, due to the different permeating species that have different diffusion coefficients through the membrane.

The use of a constant feed gas flow over the upstream surface of the membrane is necessary for preventing concentration polarization during mixed gas testing. Concentration polarization is a phenomenon that involves depletion (decrease in concentration) of the fast gas in the boundary layer near the membrane, which can alter the permeation driving forces for both components (the slow gas driving force increases and the fast gas driving force decreases) and result in erroneous membrane selectivity and productivity measurements. Hence, by continuously flowing fresh feed gas of known composition across the upstream membrane surface, more accurate measurements of intrinsic membrane properties can be obtained.

The feed gas that flows over the upstream membrane surface without permeating through the membrane is referred to as the 'retentate'. Ideally, the retentate flow rate should be much greater than the permeate flow rate to ensure minimal concentration polarization. In fact, the 'stage cut' is a measure of the relative magnitude

of permeate and feed flow rates, as shown in Eq. (3.3), and should ideally be maintained at or below 1% for mixed gas permeation experiments.

$$\text{Stage Cut \%} = \frac{\dot{n}_{\text{permeate}}}{\dot{n}_{\text{feed}}} \times 100 \quad (3.3)$$

Since time lag cannot be reliably used during mixed gas permeation to check for steady state operation, dense film mixed gas permeation tests are typically allowed to equilibrate for at least 6 hours. After this time period, the permeation rate is checked regularly to make sure it is constant. Ideally, the permeate gas composition would be tested at several different times after this initial equilibration time period, but this is often not feasible.

Once the permeation rate through the membrane has reached steady state, the permeate gas is diverted to a gas chromatograph (GC) (Varian 450-GC, Agilent Technologies) in order to determine its composition. The permeate gas composition is tested a minimum of three times, or until steady state operation is confirmed. The mixed gas permeability, in units of Barrer, of each individual component can be calculated using Eq. (3.4).

$$P_i = 6.949 \times 10^4 \frac{y_i \cdot \left(\frac{\Delta p_{\text{total,down}}}{\Delta t} \right) \cdot l \cdot V_d}{A \cdot T \cdot (x_i \cdot p_{\text{total}} - y_i \cdot p_{\text{total}})} \quad (3.4)$$

In the above equation, y_i is the downstream mole fraction of component i and x_i is the upstream mole fraction, the other variables are the same as in Eq. (3.1). Note that the total permeation rate is used directly, but the effective permeation rate for each individual species is calculated by multiplying the quantity $\Delta p_{\text{total,down}}/\Delta t$ by the downstream mole fraction of the component of interest. As mentioned, a more accurate

result is obtained by substituting fugacity for pressure as the driving force for permeation.

Mixed gas permeation values are based on the average of at least three gas chromatograph (GC) permeate composition measurements, and the typical error associated with these measurements was $\pm 5\%$ or less.

3.3.1.6. Mixed Gas Hollow Fiber Permeation

Like with dense films, mixed gas hollow fiber permeation is quite similar to pure gas hollow fiber permeation. As mentioned in Section 3.3.1.1, the retentate flow and stage cut control that are required for mixed gas permeation mean that only a single module can be tested at a time. Stage cut is ideally maintained at 1%, but, in the case of H₂S-containing gases, may be as high as 3%. While not preferred, this slightly higher stage cut is not expected to significantly impact permeation measurements and, in fact, no measureable difference in permeation results was found. The higher stage cut used in some permeation measurements involving H₂S was a result of the very high retentate flow rates that would have been necessary to achieve a 1% stage cut and safety concerns related to venting such a high volume of H₂S gas to the scrubber unit. The mixed gas permeance, in units of GPU, of each individual component is calculated through Eq. (3.5).

$$\left(\frac{P}{l}\right)_i = 5.282 \times 10^7 \frac{y_i \left(\frac{\Delta v_{p, total}}{\Delta t} \right)}{Z_{mix, down} \cdot A \cdot T \cdot (x_i \cdot p_{total} - y_i \cdot P_{total})} \quad (3.5)$$

In the above equation, y_i is the mole fraction of component i in the permeate, x_i is the mole fraction in the feed, and $Z_{mix, down}$ is the compressibility factor of the mixture in the downstream. Eq. (3.5) applies to the typical mixed gas permeation systems that use a

bubble flowmeter to measure the permeation rate of the modules. However, H₂S-containing mixed gas feeds must be measured in a permeation system where the permeation rate is measured by a digital mass flow meter. As such, Eq. (3.6) may be used to calculate the permeance, in units of GPU, of each component in the binary mixture.

$$\left(\frac{P}{l}\right)_i = 1.204 \cdot \frac{y_i \cdot \left(\frac{dm}{dt}\right) \cdot Z_{mix,down}}{\left[A(M_i \cdot y_i + M_j \cdot y_j)(x_i \cdot p_{total,up} - y_i \cdot p_{total,down})\right]} \quad (3.6)$$

In Eq. (3.6), the quantity dm/dt is the total mass flow rate in the permeate, in g/hr; A is the membrane area, in cm²; M_i is the molar mass of component i , in g/mol; y_i is the mole fraction in the downstream; x_i is the mole fraction in the upstream; p_{total} is the total pressure, in psi; and $Z_{mix,down}$ is the compressibility factor of the mixture in the downstream. The calculation for mixtures containing three or more components is similar to Eq. (3.6), but is omitted here for brevity.

3.3.2. Pressure Decay Sorption Analysis

Pure gas sorption coefficients were determined using a pressure-decay sorption apparatus, depicted in Figure 3.12. In this system, the equilibrium sorbed concentration of a pure gas is calculated through a simple mass balance and the concentration versus pressure isotherm is used to determine the sorption coefficient of a penetrant species in the membrane. The pressure-decay apparatus was originally described by Koros and Paul [21]. As with the permeation systems, the entire sorption system is constructed with stainless steel components to ensure corrosion resistance against acid gas feeds. Again, detailed information on the equipment used in the construction of these systems is available elsewhere [19]. Valve 5 is a pneumatically-activated valve controlled by the

LabView code, which is also used for recording p versus t data for the reservoir and sample cell volumes. The system is maintained at constant temperature by being submerged in an oil bath with a circulation heater. All tests in this work were performed at 35°C.

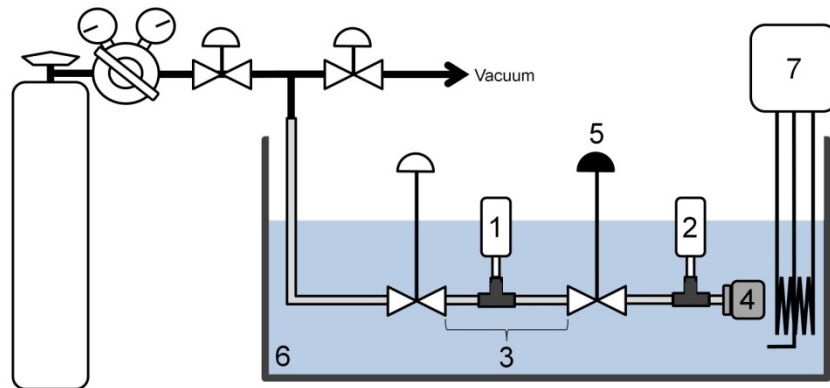


Figure 3.12: Schematic of pressure decay sorption system. System components: (1) reservoir volume pressure transducer, (2) sample cell pressure transducer, (3) reservoir volume, (4) sample cell volume, (5) pneumatically-activated valve, (6) oil bath, (7) heater/circulator.

The procedure for running pressure-decay sorption experiments is as follows:

1. A dried dense film, powder, or hollow fiber sample (> 200 mg, typically) is weighed and then loaded into the sample cell volume. The entire apparatus is then placed in the oil bath.
2. The sorption system is evacuated for 24-48 hrs by opening the vacuum isolation valve and the submerged valves.
3. After the sample has been fully degassed, valve 5, and the vacuum isolation valve are closed. The reservoir volume is then pressurized with the pure feed gas of interest and the reservoir isolation valve is closed.

4. Next, p versus t data recording is initiated and the system is allowed to equilibrate for 1-2 hrs.
5. Valve 5 is then opened very briefly ($\sim 1-3$ s) to introduce a dose of the higher pressure gas in the reservoir volume to the sample cell volume. However, valve 5 should not be left open long enough for a significant quantity of the dosed gas to sorb into the sample, as this would reduce the accuracy of the sorption calculation.
6. With all of the valves closed, the system is again allowed to equilibrate for ~ 24 hrs while recording data from the two pressure transducers. During this second equilibration time, especially within the first minutes, the pressure in the sample cell volume will 'decay' as some of the gas surrounding the sample becomes sorbed.

A mass balance is then used to calculate moles of penetrant gas, i , sorbed into the sample at equilibrium ($\Delta n_{s,i}$). The following quantities are used along with Eq. (3.7): system temperature (T), in K; volume of the sample cell (V_s), in cm^3 ; mass of the sample (m_s), in g; bulk density of the sample (ρ_s), in g/cm^3 ; volume of the reservoir (V_r), in cm^3 ; initial pressure of the sample cell ($p_{s,o}$), in psi; final pressure of the sample cell ($p_{s,f}$), in psi; initial pressure of the reservoir ($p_{r,o}$), in psi; final pressure of the reservoir ($p_{r,f}$), in psi; and the compressibility factors associated with the initial and final conditions of the gas in the sample cell and reservoir (Z).

$$\Delta n_{s,i} = \frac{1}{1205.9 \cdot T} \left[V_r \left(\frac{p_{r,o}}{Z_{r,o}} - \frac{p_{r,f}}{Z_{r,f}} \right) - \left(V_s - \frac{m_s}{\rho_s} \right) \left(\frac{p_{s,f}}{Z_{s,f}} - \frac{p_{s,o}}{Z_{s,o}} \right) \right] \quad (3.7)$$

The concentration of component i sorbed into the sample ($C_{s,i}$), in $\text{cm}^3_{\text{STP}}/\text{cm}^3_{\text{Polymer}}$, can be calculated from $\Delta n_{s,i}$ through Eq. (3.8).

$$C_{s,i} = \frac{22412.7 \cdot n_{s,i}}{\left(\frac{m_s}{\rho_s}\right)} \quad (3.8)$$

The procedure described above is repeated several times, with the number of moles sorbed in each trial added to the cumulative total of moles sorbed into the sample, to determine the sorption isotherm for the system.

As with permeability measurements, pure gas sorption values reported in this work are the average of at least two dense film measurements and the error associated with these measurements is expected to be $\leq 5\%$. Dual-mode sorption model parameters reported for pure gases generally give excellent fit to the measured data. R^2 values from the best fit calculation are in almost all cases > 0.995 .

3.3.3. Thermal Analysis

3.3.3.1. Thermogravimetric Analysis (TGA)

A thermogravimetric analyzer (TGA Q500, TA Instruments) was used to measure residual solvent content, weight losses associated with crosslinking, and polymer degradation temperatures in dense film and powder samples. A heating rate of $10^\circ\text{C}/\text{min}$ was used for all TGA experiments. Initially, the temperature was ramped from room temperature to 110°C followed by a 60 min soak and a second ramp up to 500°C with a final 30 min soak. The initial ramp/soak was designed to measure the weight loss associated with removal of residual H_2O and volatile solvents from the sample. Lower volatility solvents and crosslinking weight losses were measured during the second ramp/soak in the protocol. The sample compartment was purged with N_2 at a flow rate of 20 mL/min for all TGA experiments.

3.3.3.2. Differential Scanning Calorimetry (DSC)

Differential scanning calorimetry (DSC Q200, TA Instruments) was performed on dense film samples to measure the glass transition temperature. A heating rate of 10°C/min and a standard heating-cooling-heating temperature protocol was used for all DSC experiments. Samples were heated to above the expected glass transition temperature, but below the decomposition temperature determined by TGA. N₂ purge gas with a flow rate of 50 mL/min was used in the sample compartment. The T_g of a sample was calculated as the inflection point of the change in heat flow during the second heating cycle.

3.3.4. **Fourier Transform Infrared – Attenuated Total Reflectance Spectroscopy (FTIR-ATR)**

FTIR-ATR spectroscopy was conducted using a Bruker-Tensor 27 spectrometer (Bruker Corp.) with a MVP 2 Series™ ATR attachment (Harrick Scientific Products, Inc.). The system was continuously purged with N₂ and spectra measurements consisted of 128 scans with a resolution of 4 cm⁻¹. Dense films were the preferred sample medium, but powder and liquid samples were also measured by using a liquid sample holder.

3.3.5. **Dense Film Bulk Density Measurement**

Bulk density of dense film polymer samples was measured using a density gradient column (Techne, Inc.) that was filled with aqueous calcium nitrate [Ca(NO₃)₂] (> 99.0%, Sigma Aldrich) solutions of two different densities to create a linear gradient in density within the straight glass column. The solution inside the column was maintained at constant temperature of 25°C to prevent temperature-dependent density changes and natural convection. Once formed, the column was calibrated with small glass beads of precisely known density. Small dense film samples of unknown density were then placed

in the column and given 30 min to settle to the location within the column of the same density as the bulk material.

These measurements were coupled with a group contribution method described by Bondi in order to determine the fractional free volume (*FFV*) of dense film samples [22, 23].

3.3.6. Gel Permeation Chromatography (GPC)

The molecular weight (M_w) and polydispersity index (PDI) of synthesized polymer samples were analyzed by gel permeation chromatography with polystyrene standards used to calibrate the GPC. THF was used to dissolve the samples. These experiments were kindly performed by Doh-Yeon Park of Dr. Haskell Beckham's research group at Georgia Tech.

3.3.7. Scanning Electron Microscopy (SEM)

Asymmetric hollow fiber samples were examined through scanning electron microscopy to determine geometry, dimensions, and morphological characteristics. A high resolution SEM (LEO 1530) was used for the majority of this work, but a lower resolution SEM (Hitachi S-800) was also used for lower magnification imaging. Sample preparation involved soaking the dried fibers in hexane and then quickly transferring them to a liquid N₂ bath. While submerged in the liquid N₂, the fibers were shear-fractured, using two pairs of tweezers, to preserve their morphology. The fiber samples were then mounted vertically on sample mounts (Ted Pella, Inc.) using carbon tape so that the cross section of the fiber could be examined when loaded into the SEM. Samples were sputter coated with a thin gold layer prior to examination.

3.3.8. Nuclear Magnetic Resonance Imaging (NMR)

¹H-NMR experiments were performed in solution by dissolving polymer samples in deuterated dimethyl sulfoxide (DMSO) (99.96 atom %, Sigma Aldrich) at ~2.5 wt%. The solutions were analyzed using a Varian Mercury Vx 300 spectrometer. Dr. Leslie Gelbaum and Dr. Johannes Leisen of the Georgia Tech NMR Center graciously helped run these experiments.

3.3.9. Dissolution and Gel Fraction Experiments

Dissolution tests serve as a rapid method for determining the existence of crosslinking and the relative degree of crosslinking amongst different samples [15, 24]. A highly crosslinked sample has essentially “infinite” molecular weight and is, therefore, rendered insoluble [4]. In these tests, a dense film or hollow fiber sample that has been treated to form crosslinks is placed in a vial with anhydrous NMP at room temperature and sealed with a Teflon® cap. The status of the membrane, including swelling and dissolution of the sample, is observed over several hours. Partially crosslinked samples may be highly swollen in NMP, but will not be completely dissolved. Uncrosslinked, or very poorly crosslinked, samples are completely dissolved by NMP. The temperature of the vial is incrementally increased to 100-110°C while making observations after several hours at each of the temperatures used. If the sample remains undissolved and intact (i.e. still appears to be a film or fiber, even if swollen) in the NMP solvent after soaking at > 100°C, the extent of crosslinking is assumed to be very high and the crosslinks themselves are assumed to be fairly robust. NMP is a strong solvent for uncrosslinked polymers based on the 6FDA-DAM:DABA polymer backbone and its high boiling point (~202°C) allows these dissolution tests to be conducted at elevated temperature. As such, this is a very aggressive test of membrane stability.

Another, more quantitative measure of crosslinking efficacy is so-called gel content experimentation. In these tests, a film or fiber sample is dried to remove all traces of H₂O and precisely weighed (m_1) before being placed in a vial of anhydrous THF at room temperature. The sample is allowed to soak for 48 hrs, and afterwards it is removed from the THF solvent vial. The sample is then carefully dried in a vacuum oven to remove all THF. It is weighed again (m_2), and the gel fraction of the sample is calculated as:

$$Gel\ Fraction = \frac{m_2}{m_1} \quad (3.12)$$

A gel fraction equal to unity is indicative of very effective crosslinking. Obviously, a gel fraction of zero indicates that the sample was completely dissolved and crosslinking was very ineffective, or non-existent. Normally, a gel fraction > 0.95, or so, is desirable to ensure excellent membrane stability.

3.4. References

1. Hillock, A.M.W. and W.J. Koros, *Cross-Linkable Polyimide Membrane for Natural Gas Purification and Carbon Dioxide Plasticization Reduction*. *Macromolecules*, 2007. **40**(3): p. 583-587.
2. Qiu, W.L., et al., *Sub-T(g) Cross-Linking of a Polyimide Membrane for Enhanced CO(2) Plasticization Resistance for Natural Gas Separation*. *Macromolecules*, 2011. **44**(15): p. 6046-6056.
3. Wallace, D.W., C. Staudt-Bickel, and W.J. Koros, *Efficient development of effective hollow fiber membranes for gas separations from novel polymers*. *Journal of Membrane Science*, 2006. **278**(1-2): p. 92-104.
4. Omole, I.C., *Crosslinked Polyimide Hollow Fiber Membranes for Aggressive Natural Gas Feed Streams*, in *School of Chemical and Biomolecular Engineering* 2008, Georgia Institute of Technology: Atlanta, GA. p. 305.

5. Wind, J.D., et al., *The Effects of Crosslinking Chemistry on CO₂ Plasticization of Polyimide Gas Separation Membranes*. Industrial & Engineering Chemistry Research, 2002. **41**(24): p. 6139-6148.
6. Wind, J.D., et al., *Solid-State Covalent Cross-Linking of Polyimide Membranes for Carbon Dioxide Plasticization Reduction*. Macromolecules, 2003. **36**(6): p. 1882-1888.
7. Miller, S.J.S.F., CA, US), Omole, Imona C. (Atlanta, GA, US), Koros, William J. (Atlanta, GA, US), *Method of making a crosslinked fiber membrane from a high molecular weight, monoesterified polyimide polymer*, 2009, Chevron U.S.A. Inc. (San Ramon, CA, US), Georgia Tech Research Corporation (Atlanta, GA, US): United States.
8. Ma, C., *Highly Productive Ester Crosslinkable Composite Hollow Fiber Membranes for Aggressive Natural Gas Separations*, in *School of Chemical and Biomolecular Engineering 2012*, Georgia Institute of Technology: Atlanta, GA.
9. Moore, T.T., *Effects of Materials, Processing, and Operating Conditions on the Morphology and Gas Transport Properties of Mixed Matrix Membranes*, in *Department of Chemical Engineering 2004*, University of Texas at Austin: Austin, TX.
10. Hillock, A.M.W., *Crosslinkable Polyimide Mixed Matrix Membranes for Natural Gas Purification*, in *School of Chemical and Biomolecular Engineering 2005*, Georgia Institute of Technology: Atlanta, GA.
11. Damle, S. and W.J. Koros, *Permeation Equipment for High-Pressure Gas Separation Membranes*. Industrial & Engineering Chemistry Research, 2003. **42**(25): p. 6389-6395.
12. Clausi, D.T. and W.J. Koros, *Formation of defect-free polyimide hollow fiber membranes for gas separations*. Journal of Membrane Science, 2000. **167**(1): p. 79-89.
13. Wallace, D.W., *Crosslinked Hollow Fiber Membranes for Natural Gas Purification and Their Manufacture from Novel Polymers*, in *Department of Chemical Engineering 2004*, University of Texas: Austin, TX. p. 221.
14. Carruthers, S., *Integral-skin Formation in Hollow Fiber Membranes for Gas Separations*, in *Department of Chemical Engineering 2001*, University of Texas at Austin: Austin, TX.
15. Wallace, D.W., *Crosslinked Hollow Fiber Membranes for Natural Gas Purification and Their Manufacture from Novel Polymers*, in *Department of Chemical Engineering 2004*, University of Texas at Austin: Austin, TX.
16. Vu, D.Q., W.J. Koros, and S.J. Miller, *High Pressure CO₂/CH₄ Separation Using Carbon Molecular Sieve Hollow Fiber Membranes*. Industrial & Engineering Chemistry Research, 2001. **41**(3): p. 367-380.

17. O'Brien, K.C., et al., *A new technique for the measurement of multicomponent gas transport through polymeric films*. Journal of Membrane Science, 1986. **29**(3): p. 229-238.
18. Pye, D.G., H.H. Hoehn, and M. Panar, *Measurement of gas permeability of polymers. I. Permeabilities in constant volume/variable pressure apparatus*. Journal of Applied Polymer Science, 1976. **20**(7): p. 1921-1931.
19. Achoundong, C.S.K., *Engineering Economical Membrane Materials for Aggressive Sour Gas Separations*, in *School of Chemical and Biomolecular Engineering 2013*, Georgia Institute of Technology: Atlanta, GA.
20. Paul, D.R. and W.J. Koros, *Effect of partially immobilizing sorption on permeability and the diffusion time lag*. Journal of Polymer Science: Polymer Physics Edition, 1976. **14**(4): p. 675-685.
21. Koros, W.J. and D.R. Paul, *Design considerations for measurement of gas sorption in polymers by pressure decay*. Journal of Polymer Science: Polymer Physics Edition, 1976. **14**(10): p. 1903-1907.
22. Bondi, A., *Physical properties of molecular crystals, liquids, and glasses*. 1968, New York: Wiley.
23. Park, J.Y. and D.R. Paul, *Correlation and prediction of gas permeability in glassy polymer membrane materials via a modified free volume based group contribution method*. Journal of Membrane Science, 1997. **125**(1): p. 23-39.
24. Wallace, D.W., et al., *Characterization of crosslinked hollow fiber membranes*. Polymer, 2006. **47**(4): p. 1207-1216.

CHAPTER 4

SOUR GAS TRANSPORT CHARACTERIZATION OF POLYIMIDE DENSE FILMS

4.1. Overview

This chapter deals with the application of dense film membranes formed using the copolyimide 6FDA-DAM:DABA (3:2) for the simultaneous removal of CO₂ and H₂S from sour natural gas streams. Due to the limited amount of membrane-based sour gas separations data in the literature, and the focus that has been placed on rubbery polymers to date, this work represents a critical benchmarking of one of the first high-performance glassy polymers for this application. The goals of this study include gaining an understanding of the effects of H₂S-induced plasticization on a glassy polymer, the level of H₂S/CH₄ permselectivity of this material and the relative importance of the different mechanisms by which it is achieved, and the effects of mixed sour gas permeation on membrane performance. In short, the work described in this chapter aims to determine whether the 6FDA-DAM:DABA polyimide backbone can be a promising candidate for aggressive sour gas separation applications and, if so, to identify possible areas of improvement in order to guide the optimization of membrane materials based on this precursor.

4.2. Application of Glassy Polymer Membranes to Sour Gas Separations

Glassy polyimides, like 6FDA-DAM:DABA, have been heavily investigated in recent years for use as high-performance membrane materials in CO₂/CH₄ separations.

These high T_g materials derive the majority of their CO_2 removal capacity from size selectivity. For CO_2/CH_4 separations, these materials frequently give superior efficiency, productivity, and resistance to penetrant-induced plasticization compared to cellulose acetate (CA), which is presently the industry standard membrane material for acid gas separations.

6FDA-DAM:DABA and its derivative materials have been studied extensively for CO_2 removal from natural gas. This polyimide exhibits intrinsic CO_2/CH_4 separation performance approaching the theoretical upper bound for polymer membranes (Figure 4.1), its productivity and efficiency can be tuned by altering the monomer ratio, it is crosslinkable through several mechanisms, and it can be formed into high-quality asymmetric hollow fibers [1-9].

Despite the extensive CO_2/CH_4 work, no rigorous examination of an advanced polyimide, such as 6FDA-DAM:DABA, for sour gas separation applications has been reported in the literature. The objective of the current study, therefore, is to gain an understanding of sour gas transport through glassy polymer membranes and, ultimately, to identify methods for engineering high-performance materials for this application. This is achieved through sour gas transport characterization of 6FDA-DAM:DABA (3:2).

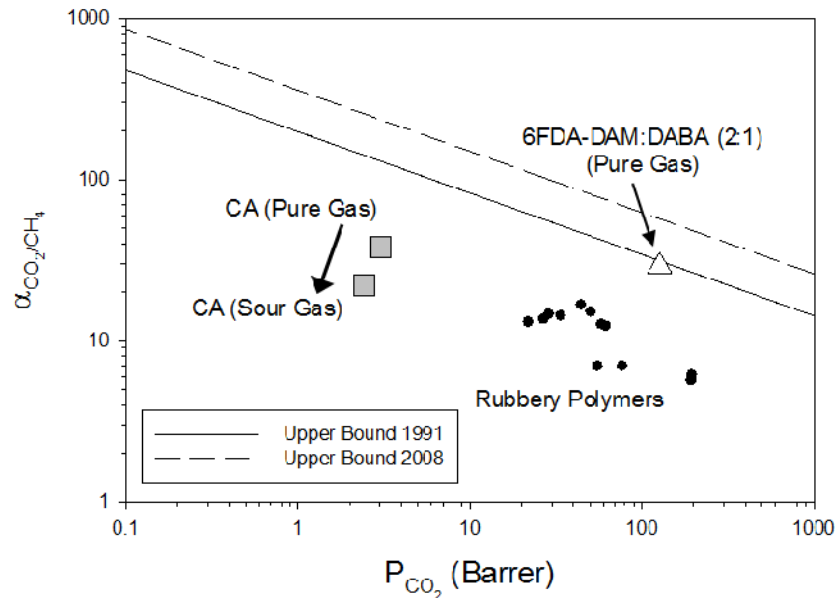


Figure 4.1: Productivity-efficiency tradeoff for CO₂/CH₄ separations [10, 11]. Data are for various candidate materials for aggressive sour gas separations [2, 12-14]. Pure gas data measured at 150 psi feed pressure and 35°C. Sour gas data are for various ternary mixtures measured at 22°C or 35°C.

For the majority of wells, it is likely that CO₂/CH₄ separation performance in the presence of elevated H₂S levels is more important than H₂S/CH₄ separation performance, per se. This is due to the typically higher concentration of CO₂ relative to H₂S and the more stringent H₂S pipeline specification (< 4ppm), which are likely to require H₂S-selective absorption polishing processes in almost all cases. As a result, it is believed that glassy polymers are favorable compared to rubbery polymers for the aggressive sour gas separation being studied.

CA is one of the only glassy polymers for which significant sour gas transport data have been reported. Chatterjee et al. studied CA using a 6% H₂S, 29% CO₂, 65% CH₄ mixture at 150 psi and 35°C. They report a H₂S/CH₄ selectivity of 19 and a CO₂/CH₄ selectivity of only 22 [12]. This value for the CO₂/CH₄ separation efficiency lies significantly below the typically reported ideal selectivity of CA, and it implies some

detrimental effect of H₂S – most likely, either sorptive competition or penetrant-induced plasticization [14]. Figure 4.1 displays the CO₂/CH₄ separation performance for a most of the rubbery polymers that have been studied for sour gas separations, as well as CA and 6FDA-DAM:DABA. The large drop in CA performance from its pure gas level is indicated. It is likely that plasticization and other non-ideal effects in the presence of H₂S will have similar unwanted ramifications for other membrane materials when highly aggressive conditions are employed, and this is a particular concern for other glassy polymers.

As mentioned in previous chapters, the ability of a membrane material to resist penetrant-induced plasticization is one of the most critical material properties to be considered. This is especially true for applications involving natural gas reserves with high concentrations of the acid gases, CO₂ and H₂S, and high wellhead pressures. As such, one of the main goals of this chapter is to determine the intrinsic plasticization resistance of 6FDA-DAM:DABA (3:2) membranes against feeds containing H₂S and CO₂. Furthermore, one of the simplest methods of improving membrane plasticization resistance, sub-T_g thermal annealing, is investigated. Thermal annealing typically results in greater membrane plasticization resistance due to lower free volume, which allows lower levels of penetrant sorption, and greater polymer chain inter- and intramolecular interactions within the polymer matrix.

4.3. Polymer Physical Property Analysis

Dense films were cast as described in CHAPTER 3 using 6FDA-DAM:DABA (3:2) polymer powder. Gel permeation chromatography was used to determine the molecular weight (M_w) and polydispersity index (PDI) of the polymer powder, which were

found to be 200 kDa and 4.7, respectively. In addition to the standard 100°C drying step during membrane casting, a secondary sub- T_g thermal annealing treatment was performed on samples of the 6FDA-DAM:DABA (3:2) dense film as a means of improving plasticization resistance. Annealing temperatures of 180°C and 230°C were used and after an 18 hr thermal soak in a vacuum oven the annealed samples were allowed to cool slowly (20-25°C/hr) back to room temperature. Several physical properties of the annealed and unannealed dense films were then determined using techniques described in CHAPTER 3.

4.3.1. Thermogravimetric Analysis

The unannealed 6FDA-DAM:DABA (3:2) dense films were studied using thermogravimetric analysis to ensure nearly complete removal of the synthesis and casting solvents. When present at high levels, these solvents can lead to erroneous membrane transport properties such as premature onset of membrane plasticization. Since the accurate measurement of CO₂- and H₂S-induced plasticization resistance in 6FDA-DAM:DABA (3:2) membranes was a major goal of this study, these TGA experiments were necessary and the results are displayed in Figure 4.2.

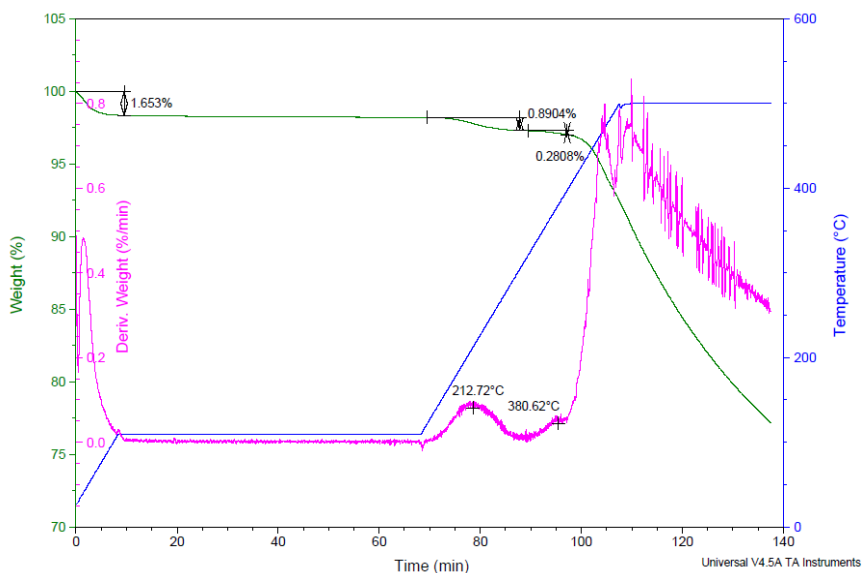


Figure 4.2: TGA result for 6FDA-DAM:DABA (3:2) dense film dried at 100°C.

Small weight losses associated with water and/or THF (~70°C) and NMP (~212°C) are visible. The water/THF weight loss amounts to just 1.7% of the sample mass and the NMP weight loss is only 0.9%. Also, a small weight loss is visible at around 380°C. This is believed to be associated with the thermally-activated decarboxylation crosslinking reaction that has been investigated by previous researchers working with 6FDA-DAM:DABA membranes [6, 15, 16].

The decomposition temperature of the base 6FDA-DAM:DABA (3:2) polymer can be estimated from the TGA result. A large weight loss associated with polymer degradation starts at approximately 400°C. This temperature represents the effective upper limit for thermal treatments of 6FDA-DAM:DABA (3:2) that can be performed without risking significant changes to the polymer chemical structure.

4.3.2. Glass Transition Temperature, Density, and Fractional Free Volume

Density measurements of the 6FDA-DAM:DABA (3:2) films were used to calculate their fractional free volume through a group contribution method described by Bondi [17, 18]. Physical properties of the annealed dense films that were measured by differential scanning calorimetry and density gradient column analysis are listed in Table 4.1. The greater density and T_g values of the 230°C annealed films compared to those treated at 180°C indicate that higher temperature annealing of the dense 6FDA-DAM:DABA (3:2) films results in more efficient chain packing and, presumably, greater intersegmental interactions. It should be pointed out that these annealed samples were *not* crosslinked after thermal treatment; upon placing samples of the films in THF, they completely dissolved almost immediately.

Table 4.1: Properties of 6FDA-DAM:DABA (3:2) dense films

Annealing Temp. (°C)	ρ (g/cm ³)	FFV	T_g (°C)
180	1.402	0.183	385
230	1.403	0.182	394

4.4. Pure Gas Transport Analysis

4.4.1. Pure Gas Permeation

Pure H₂S permeation through unannealed 6FDA-DAM:DABA (3:2) films (i.e. samples dried at 100°C), as well as samples annealed at 180°C and 230°C, was conducted at 35°C (Figure 4.3). The permeation isotherm of the unannealed sample begins to increase immediately, indicating that the onset of H₂S-induced plasticization

occurs at or below 15 psi, which was the minimum feed pressure tested. Samples of the annealed films, however, exhibit non-negligible plasticization pressures. Increasing the annealing temperature from 180°C to 230°C causes an increase in the H₂S plasticization pressure of approximately 25%, from around 28 psi to a value of approximately 35 psi. In addition to increased plasticization resistance in the annealed films, the H₂S permeability of annealed 6FDA-DAM:DABA (3:2) films is reduced with increasing annealing temperature. This is explained by accelerated chain relaxation and reduced free volume in the annealed samples, with greater chain mobility leading to greater free volume reductions and lower permeability under higher annealing temperature conditions.

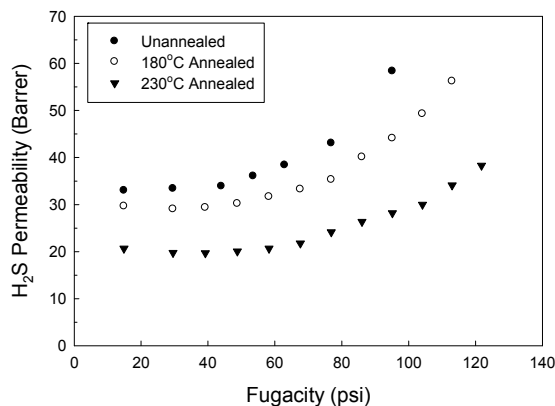


Figure 4.3: Pure H₂S permeability at 35°C in 6FDA-DAM:DABA (3:2) films.

As a result of these findings, annealed samples were used exclusively for the remainder of this study. The low plasticization resistance of unannealed films to pure H₂S feeds indicates that plasticization is likely to occur even at low feed pressures during mixed sour gas permeation. To gain a more fundamental and meaningful understanding of sour gas permeation through the 6FDA-DAM:DABA (3:2) polymer in its native glassy state, it was necessary to focus on the non-plasticized regions of the permeation and

sorption isotherms that were to be collected, and only the annealed samples allowed this option.

Pure gas permeation using CO₂ and CH₄ was also conducted on the annealed films (Figure 4.4). For pure CO₂ feeds, sub-T_g annealing at the temperatures investigated did not result in a measurable increase in plasticization pressure. However, the CO₂ permeability of these films decreases modestly for the sample annealed at higher temperature. In contrast to CO₂, the pure CH₄ feed did not induce plasticization in either sample at any of the pressures investigated (up to 900 psi). As with the acid gases, CH₄ permeability is lower in the 230°C annealed films due to the free volume effects touched upon above.

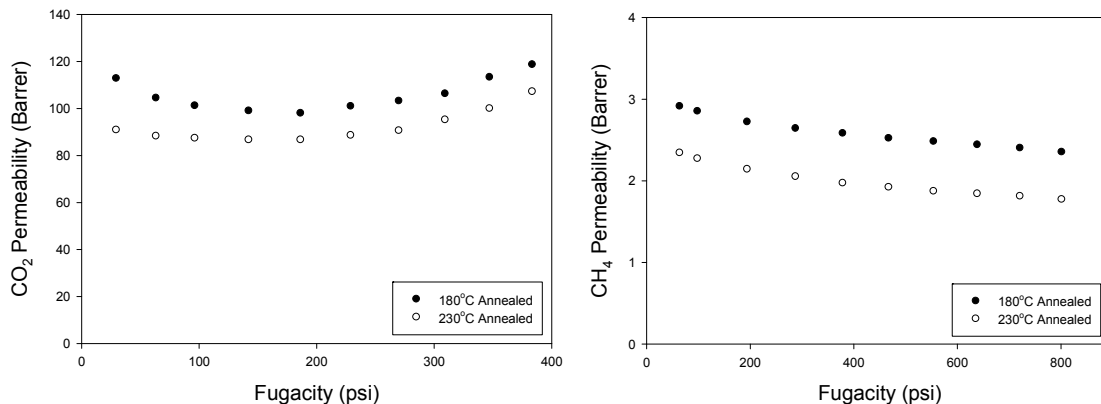


Figure 4.4: Pure gas CO₂ and CH₄ permeability of 6FDA-DAM:DABA (3:2) films measured at 35°C.

Ideal selectivity values for H₂S/CH₄ and CO₂/CH₄ in the 180°C and 230°C annealed films were calculated using the pure gas permeation isotherms, and are provided in Table 4.2. The values for H₂S/CH₄ ideal selectivity are less than or equal to 10 for both films, and fall well below the reported mixed gas value for CA from Figure 4.1 [12]. A somewhat unexpected finding was that the H₂S/CH₄ selectivity in the 230°C

annealed films is actually lower than in the 180°C films. Higher temperature annealing is normally expected to increase the selectivity of glassy polymers through increased size-sieving ability. Since H₂S is, in fact, a smaller molecule than CH₄, it was anticipated that a more size selective material would provide greater H₂S/CH₄ permselectivity. The contributions of diffusivity and solubility to overall selectivity in these annealed films were investigated in order to better understand this effect and are discussed in the following sections.

Table 4.2: Ideal selectivity of 6FDA-DAM:DABA (3:2) films

Annealing Temp. (°C)	$\alpha^*_{\text{H}_2\text{S}/\text{CH}_4}$ (30 psi)	$\alpha^*_{\text{CO}_2/\text{CH}_4}$ (150 psi)
180	10	35
230	8.3	39

4.4.2. Pure Gas Sorption

Sorption isotherms for the three primary sour gas components were measured at 35°C using samples of the annealed dense films. Pure gas sorption data for H₂S, CO₂, and CH₄ in the two films are shown along with the dual-mode model fit in Figure 4.5. The dual-mode sorption behavior – with both Langmuir and Henry’s law sorption contributions – is apparent from the concave nature of the isotherms at low to moderate pressures and the nearly linear behavior at elevated pressures. Also, swelling and plasticization of the films by high-pressure H₂S and, to some extent, CO₂ is evident in the high pressure regime of these sorption isotherms and is indicated by an upward deviation from the dual-mode model fit of these gases.

The sorption capacity of films annealed at 180°C is slightly greater than that of films annealed at 230°C. This minor decrease in sorption capacity for the films annealed at higher temperature is caused by the lower fractional free volume of the 230°C

annealed sample (Table 4.1). It is also interesting to note that H₂S sorption in the fluorine-containing 6FDA-DAM:DABA material is quite high relative to CO₂ sorption. Unfavorable H₂S-fluorine interactions which can cause anomalously low H₂S sorption have been noted previously in very highly-fluorinated polymers [19]. However, the polar imide and carboxylic acid moieties of 6FDA-DAM:DABA (3:2) are believed to interact with the polar H₂S molecule to overcome this effect in the 6FDA-DAM:DABA (3:2) material.

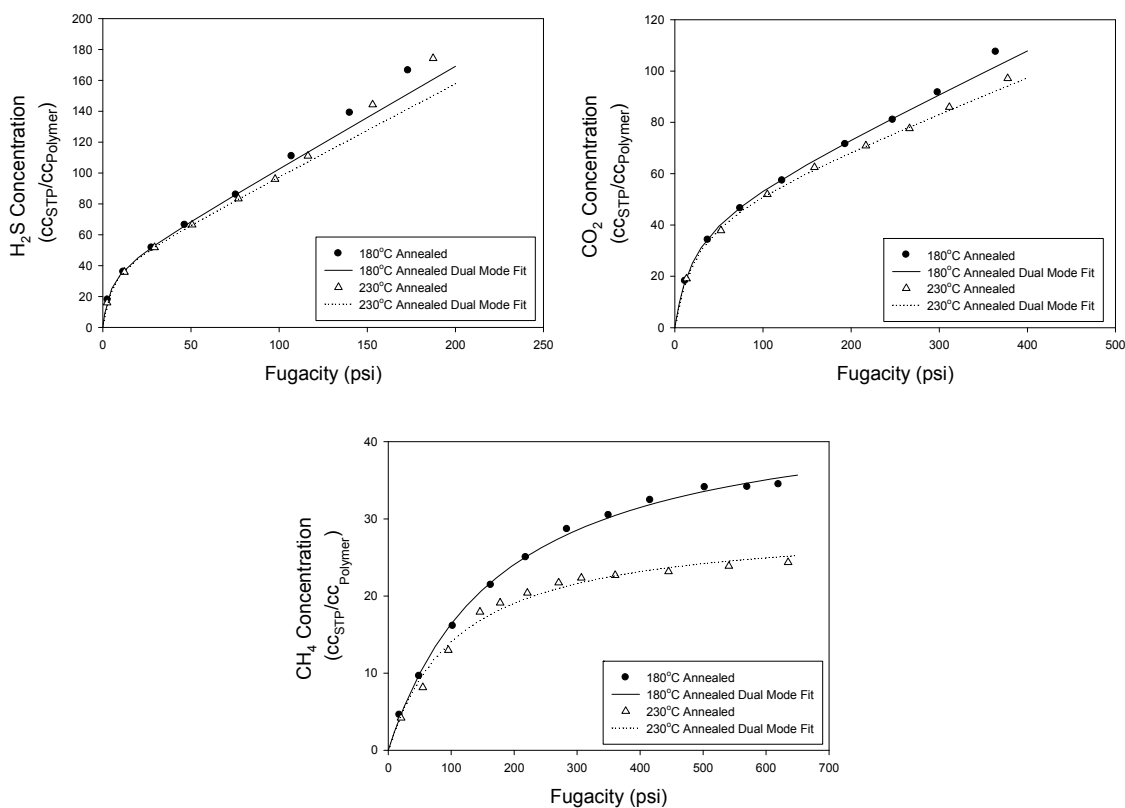


Figure 4.5: Pure gas H₂S, CO₂, and CH₄ sorption in 6FDA-DAM:DABA (3:2) films at 35°C.

Sorption selectivity and mobility selectivity values were calculated using Eq. (2.21) and are provided in Table 4.3. Based on these numbers, the H₂S/CH₄ selectivity of 6FDA-DAM:DABA (3:2) is primarily derived from the sorption selectivity contribution,

despite the fact that it is a glassy material. In fact, the mobility selectivity of 6FDA-DAM:DABA (3:2) is nearly unity in both films and therefore contributes very little to overall permselectivity. Again, the smaller kinetic diameter of H₂S compared to CH₄ suggests that strong polymer-H₂S interactions capable of decreasing the rate of diffusion of H₂S are likely present. On the other hand, the values calculated for CO₂/CH₄ separations are more typical for a glassy polymer, with diffusion selectivity as the major contributor to overall permselectivity.

Table 4.3: Sorption and mobility selectivity in 6FDA-DAM:DABA (3:2) dense films at 35°C. Values are calculated from pure gas permeation and sorption data.

Annealing Temp. (°C)	S _{H₂S} /S _{CH₄} (30 psi)	D _{H₂S} /D _{CH₄} (30 psi)	S _{CO₂} /S _{CH₄} (150 psi)	D _{CO₂} /D _{CH₄} (150 psi)
180	7.2 ± 0.4	1.5 ± 0.1	3.4 ± 0.2	11 ± 1
230	8.0 ± 0.4	1.0 ± 0.1	3.6 ± 0.2	11 ± 1

As shown in Figure 4.5, a best-fit of the dual mode sorption model [Eq. (2.28)] was determined for the measured sorption isotherms at pressures below the onset of plasticization. Good agreement between the model and the sorption data was achieved over the majority of the pressure range tested. Table 4.4 presents the values of the fitted parameters for all three gases in the annealed films. From these values and the sorption isotherms themselves, it appears that varying the annealing temperature of 6FDA-DAM:DABA (3:2) from 180°C to 230°C causes very little change in H₂S and CO₂ sorption and only a slightly more appreciable effect on the solubility of CH₄.

Table 4.4: Dual-mode sorption model best-fit parameters for 6FDA-DAM:DABA (3:2) dense films.

	Annealing Temp. (°C)					
	180			230		
	H ₂ S	CO ₂	CH ₄	H ₂ S	CO ₂	CH ₄
k_D	0.66±0.03	0.16	(4.4±0.8)×10 ⁻³	0.60±0.03	0.13±0.01	(4.7±0.2)×10 ⁻³
C'_H	38±2	44	27±1	39±2	45±2	25±1
b	0.26±0.01	0.050	(1.3±0.1)×10 ⁻²	0.24±0.01	(4.4±0.2)×10 ⁻²	(1.2±0.1)×10 ⁻²

Sorption parameter units: k_D [CC_{STP}/(CC_{Polymer}·psi)], C'_H [CC_{STP}/CC_{Polymer}], b [1/psi]

4.4.3. Pure Gas Diffusion Analysis

Pure gas diffusion coefficient isotherms were calculated from the pure gas permeation isotherms, dual-mode sorption model parameters, and Eq. (2.12). Permeability values below the CO₂ and H₂S plasticization pressures were the only data points that could be used during these calculations. Unfortunately, this limited the extent of the diffusion coefficient isotherms that could be accurately calculated for those gases. The diffusion coefficient isotherms for 180°C and 230°C annealed 6FDA-DAM:DABA (3:2) dense films are given in Figure 4.6.

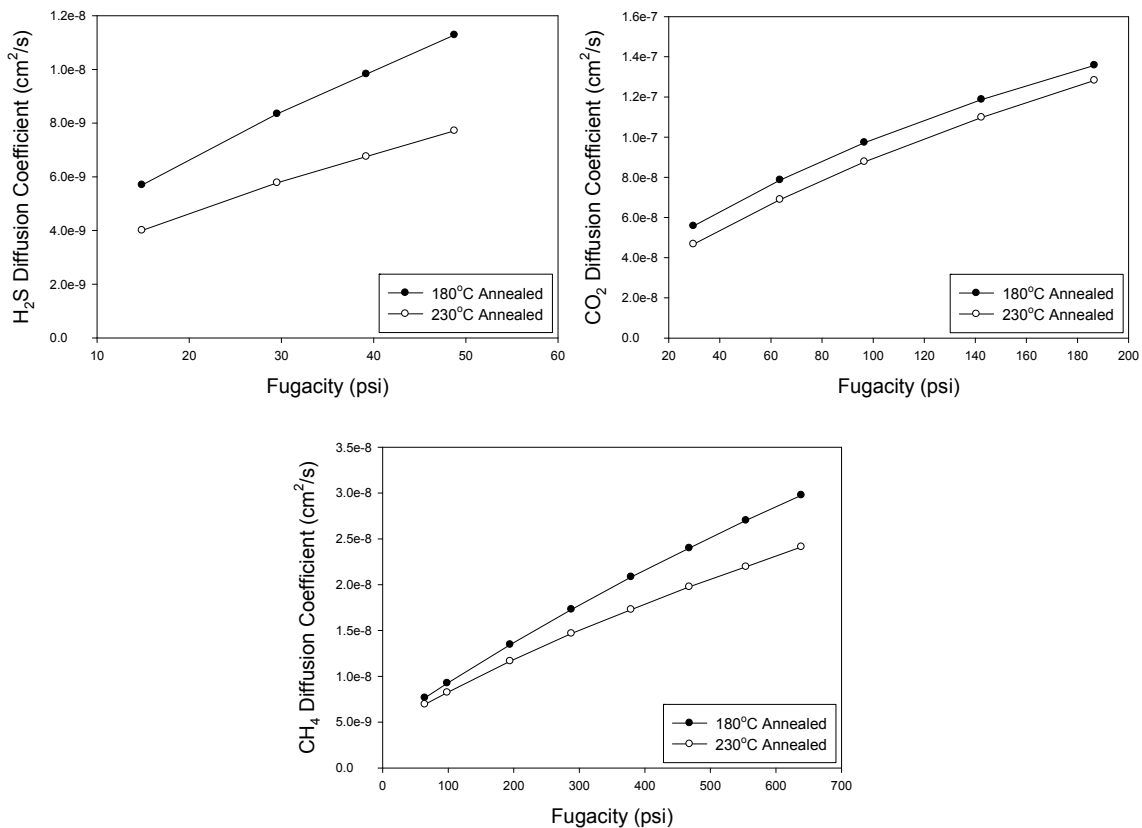


Figure 4.6: Pure gas diffusion coefficient isotherms at 35°C for annealed 6FDA-DAM:DABA (3:2) dense films.

It is not surprising to note that the diffusion coefficients for CO₂ through these membranes are the highest of the three gases. After all, CO₂ is significantly smaller than the other penetrant molecules. However, the relative diffusion coefficient levels calculated for H₂S and CH₄ are notable. Despite the smaller kinetic diameter of H₂S, the diffusion coefficients for these two gases are very close over the pressure range shown in Figure 4.6.

Along with the average diffusion coefficients displayed above, the dual-mobility permeation model (also known as the partial immobilization model) described in Section 2.3.1 can be used to determine the diffusion coefficients for CO₂, H₂S, CH₄ through the

Langmuir and Henry's law sorption modes, D_H and D_D . The dual-mobility model parameters annealed 6FDA-DAM:DABA (3:2) dense films are given in Table 4.5.

Table 4.5: Dual-mobility permeation model parameters for sour gas components at 35°C. Values were calculated from pure gas permeation and sorption data.

	Annealing Temp. (°C)					
	180			230		
	H ₂ S	CO ₂	CH ₄	H ₂ S	CO ₂	CH ₄
K	15	14	80	16	16	64
F	0.024	0.038	0.0062	0.028	0.010	0.011
$D_D \times 10^{-8}$ (cm ² /s)	2.0	30	27	1.6	34	19
$D_H \times 10^{-8}$ (cm ² /s)	0.048	1.2	0.17	0.045	0.34	0.020

Generally, the films annealed at 230°C have lower diffusivity for the sour gas components in both the Langmuir and Henry's law regimes. This result is in good agreement with the average diffusion coefficient isotherms shown in Figure 4.6. Again, free volume reduction, increased polymer chain interactions, and reduced polymer chain segmental mobility in polymer samples annealed at higher temperature account for this trend.

One of the most interesting trends from the data presented above is the very low diffusivity of H₂S in the Henry's law regime (D_D) for both of the samples. Compared to the diffusion coefficients of CO₂ and CH₄ in this regime, H₂S has a diffusivity that is nearly an order of magnitude lower despite the fact that its kinetic diameter falls in between the other two gases. This result may indicate that strong polymer-penetrant interactions exist between H₂S and the 6FDA-DAM:DABA (3:2) polymer backbone in the Henry's law regime. Section 4.5 deals with mixed gas transport through these annealed dense film samples. A number of unexpected transport phenomena are observed under mixed sour gas permeation conditions, and it is possible that these strong H₂S-polymer interactions play a significant role in the observed effects.

4.5. Mixed Gas Transport

4.5.1. Binary (5% H₂S / 95% CH₄) Sour Gas Mixture Permeation

In addition to the pure gas permeation and sorption studies presented in Section 4.4, mixed gas permeation was used to investigate sour gas separations under realistic aggressive sour gas feed conditions with 6FDA-DAM:DABA (3:2) dense films. A binary mixture consisting of 5% H₂S and a balance of CH₄ was used initially to gain an understanding of the effects of H₂S on CH₄ permeability and H₂S/CH₄ permselectivity in the absence of CO₂, which was expected to, and indeed does, result in much more complex transport. Figure 4.7 shows the H₂S permeability and selectivity results for the films annealed at both temperatures.

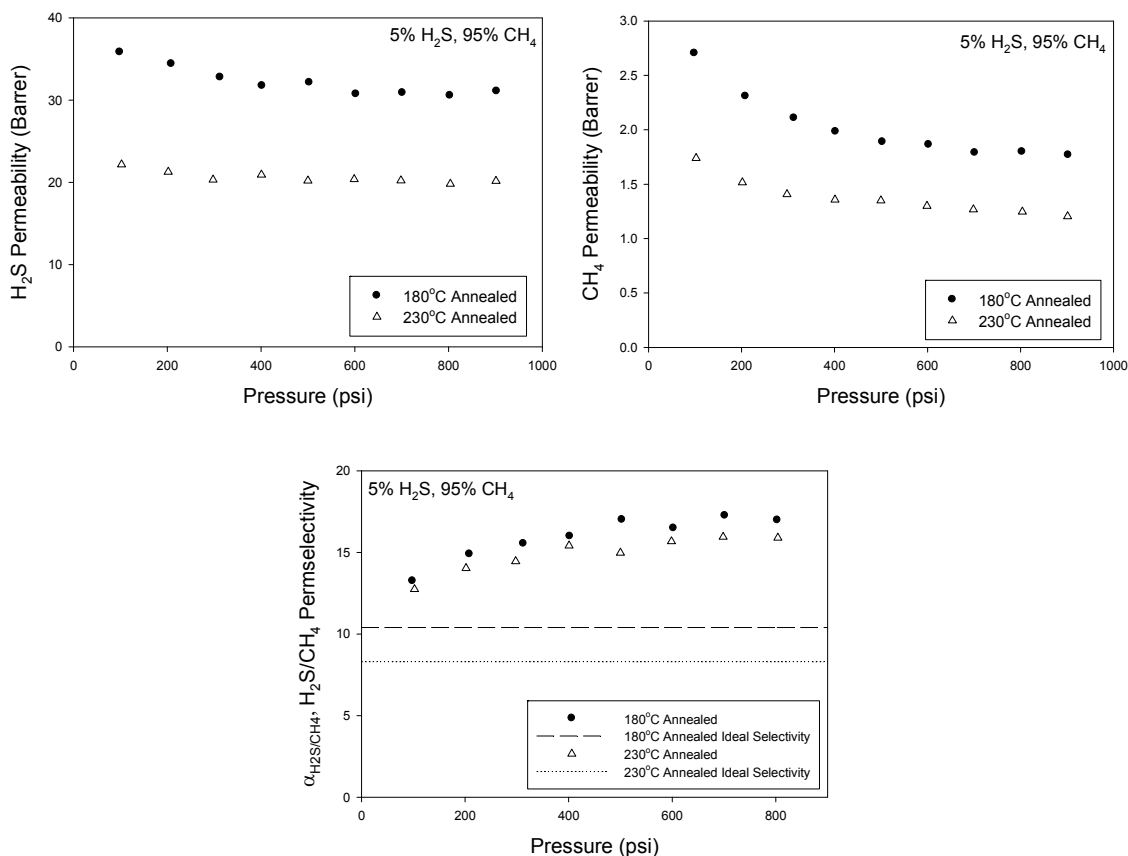


Figure 4.7: Permeation results at 35°C for 6FDA-DAM:DABA (3:2) dense films using a binary mixture of 5% H₂S and 95% CH₄.

Notably, the H₂S/CH₄ separation factor increases rapidly in both samples as the feed pressure is increased and approaches the reported mixed gas H₂S/CH₄ selectivity of CA (reported to be 19 [12]) at the highest feed pressures tested – reaching a value of 18 in the 180°C annealed film. As with the pure gases, the H₂S/CH₄ selectivity of the film annealed at 230°C is slightly lower than that of the 180°C annealed film. The H₂S permeability through these films is close to the pre-plasticization H₂S permeability measured in the pure gas study. Thus, the significant rise in separation efficiency under mixed gas feed conditions is the result of depressed CH₄ permeability relative to the pure gas level. Also, it should be noted that the CH₄ permeation isotherms for the two samples did not pass through a minimum during the course of these mixed gas experiments. This indicates that plasticization of the films did not occur, even though the H₂S fugacity in the feed slightly exceeded the observed pure gas plasticization pressures.

These results indicate that strong competition effects and other polymer-penetrant interaction effects may be present in the case of a multicomponent system containing H₂S. They also suggest that the low H₂S/CH₄ ideal selectivity of 6FDA-DAM:DABA (3:2) may potentially be overcome through modifications to the material which either promote H₂S permeation or further depress CH₄ permeation under mixed gas feed conditions, as will be discussed in a later section.

4.5.2. Ternary (10% H₂S / 20% CO₂ / 70% CH₄) Sour Gas Mixture (A) Permeation

Sour gas feed mixtures – containing H₂S at higher concentration, as well as the third major sour gas component, CO₂ – were also used during this investigation of 6FDA-DAM:DABA (3:2) membranes. The results of mixed gas permeation using a ternary 10% H₂S, 20% CO₂, and 70% CH₄ mixture are presented in Figure 4.8.

As with the permeation measurements using the binary sour gas mixture discussed in Section 4.5.1, H₂S/CH₄ selectivity in both films increases with increasing feed pressure, and eventually rises to levels that are approximately 190% of the ideal selectivity values. Additionally, CO₂/CH₄ selectivity in the 180°C annealed film at low feed pressures was measured to be as high as 49. This value is significantly greater than the measured CO₂/CH₄ ideal selectivity and this phenomenon is believed to result from the three-way competition between CO₂, H₂S, and CH₄ for Langmuir sorption sites. The more condensable CO₂ and H₂S gases effectively block CH₄ molecules from entering the hole-filling sorption regime. However, because CO₂ is present at a higher concentration than H₂S and is much more condensable than CH₄, the sorption of CO₂ is not depressed to the same extent as CH₄. These two effects combine to give an enhanced CO₂/CH₄ selectivity as long as the H₂S partial pressure is below approximately 30 psi, as shown. A H₂S partial pressure of 30 psi corresponds approximately to the saturation point for Langmuir sorption sites in the pure H₂S sorption isotherm (Figure 4.5). Therefore, it is likely that the H₂S molecules occupy the vast majority of Langmuir sorption sites at H₂S partial pressures >30 psi due to the high affinity coefficient for H₂S in 6FDA-DAM:DABA (3:2).

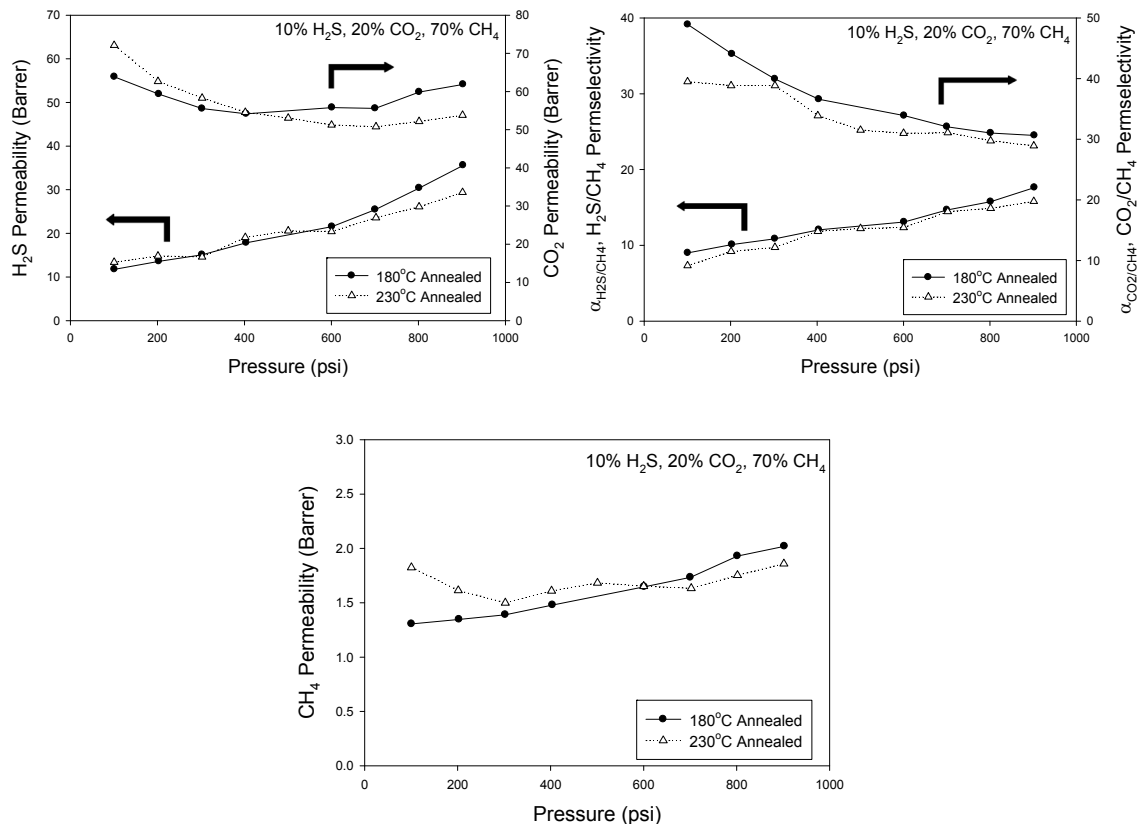


Figure 4.8: Permeation and selectivity results using a 10% H₂S, 20% CO₂, 70% CH₄ mixed gas feed for 6FDA-DAM:DABA (3:2) films at 35°C.

As shown in the Figure 4.8 above, the efficiency of the membranes for the CO₂/CH₄ and H₂S/CH₄ separations is a strong function of feed pressure. Elevated H₂S partial pressure in the feed leads to strong competition between H₂S and CO₂ for sorption sites within the 6FDA-DAM:DABA (3:2) films. The CH₄ permeability depression (compared to the pure gas permeability) that was observed in Section 4.5.1 for the binary sour gas mixture is again present for this ternary mixed gas feed situation; it is this depressed methane flux that leads to the efficiency gains that have been noted. However, unlike the binary 5% H₂S, 95% CH₄ mixture, this more aggressive ternary mixture *does* induce a plasticization response in the annealed films at the higher feed pressures that were tested. This is likely due to the combined effect of the higher H₂S

concentration as well as the presence of CO₂ at fairly high concentration. Nevertheless, the plasticized films do not experience major separation efficiency degradation at the elevated feed pressures (up to 900 psi) that were tested.

It should also be noted that the partial pressures of both CO₂ and H₂S in the feed for the 6FDA-DAM:DABA (3:2) films are significantly greater than those used in most of the sour gas separation studies focusing on rubbery polymer membranes [12, 13, 20]. As such, the reported selectivity values for the materials discussed in the literature studies may not accurately reflect their performance under more realistic aggressive sour gas feed conditions, since some degree of plasticization and selectivity loss is likely to occur. Moreover, the CO₂/CH₄ selectivity of the 6FDA-DAM:DABA (3:2) films does not degrade to anywhere near the same extent as was reported for CA under sour gas feed conditions, even under this much more aggressive sour gas feed [12].

4.5.3. Ternary (20% H₂S / 20% CO₂ / 60% CH₄) Sour Gas Mixture (B) Permeation

A second ternary sour gas mixture consisting of 20% H₂S, 20% CO₂, and 60% CH₄ was also used to make permeation measurements through 6FDA-DAM:DABA (3:2). This mixture represents a significantly more aggressive sour gas feed stream than the mixture used in Section 4.5.2. The H₂S fugacity in the feed is 120 psi at the maximum feed pressure tested (900 psi), compared to just over 60 psi in the first ternary mixture that was used. The CO₂ fugacity is approximately 140 psi in both cases. Dense films annealed at 180°C were the only samples tested with this gas mixture. The results of these permeation experiments are shown in Figure 4.9.

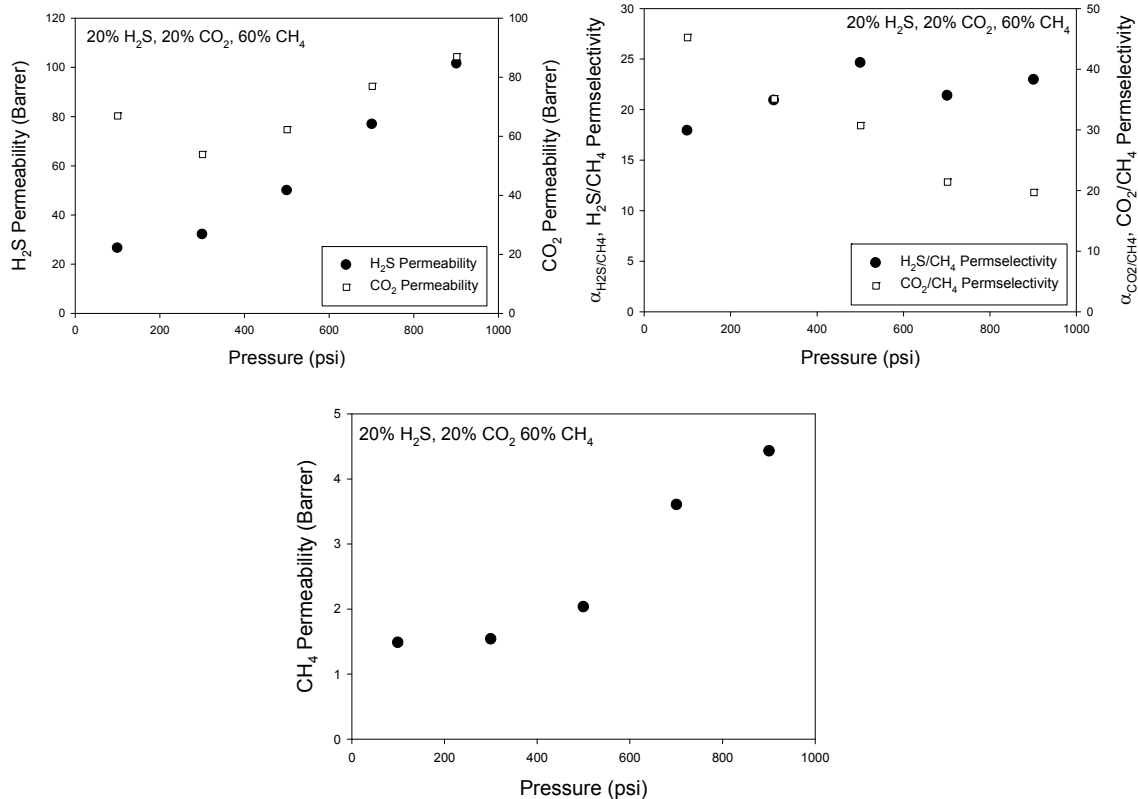


Figure 4.9: Permeation results for 6FDA-DAM:DABA (3:2) dense film annealed at 180°C with a 20% H₂S, 20% CO₂, 60% CH₄ mixture.

Based on the graphs above, it is clear that the more aggressive sour gas feed mixture induces membrane plasticization at a lower total feed pressure than the 10% H₂S, 20% CO₂, 70% CH₄ mixture. The CO₂ permeability isotherm appears to pass through a minimum at around 300 psi and the CH₄ permeability isotherm begins to increase almost immediately, eventually reaching a value almost three times greater than the CH₄ permeability at 100 psi.

In terms of the sour gas separation efficiencies with this mixture, the CO₂/CH₄ permselectivity falls to below 20 at the highest feed pressure tested. This is more than a 50% decrease from the value at 100 psi and well below the material's ideal CO₂/CH₄ selectivity. On the other hand, the H₂S/CH₄ permselectivity of the 6FDA-DAM:DABA

(3:2) membrane is actually somewhat favored under these apparently plasticized conditions. The H₂S/CH₄ separation efficiency reaches a maximum of 25 in at 500 psi, but decreases slightly at higher feed pressures. While these values for the H₂S/CH₄ separation may at first seem attractive, it should be noted that the plasticized condition of the membrane makes it likely that the separation performance and even mechanical integrity are likely to decrease during long-term exposure to these feed conditions. Further discussion of these results is provided in CHAPTER 5.

4.5.4. Non-Zero Downstream Pressure Ternary Mixture (B) Permeation

The results provided for a 20% H₂S, 20% CO₂, 60% CH₄ mixture above were collected using the typical vacuum-downstream isochoric dense film permeation apparatus, described in CHAPTER 3. In addition, a modified isochoric dense film permeation system that enabled non-vacuum-downstream permeation was used to test 6FDA-DAM:DABA (3:2) with the 20% H₂S, 20% CO₂, 60% CH₄ mixture. These experiments were performed on 180°C annealed samples and the results are shown in Figure 4.10.

The permeation system used for these tests was a slightly modified isochoric dense film system, which simply had the downstream pressure transducer (50 Torr) swapped out for a higher pressure transducer (5000 Torr). Permeation data was collected after a permeate pressure of approximately 760 Torr was reached as a result of penetrant gas permeation through the film. This downstream pressure was selected because it is representative of downstream pressure conditions that are often present in constant pressure (isobaric) membrane systems, which are more relevant to industrial applications. A limited number of data points were collected due to the extended experimentation time required to reach 760 Torr downstream pressure.

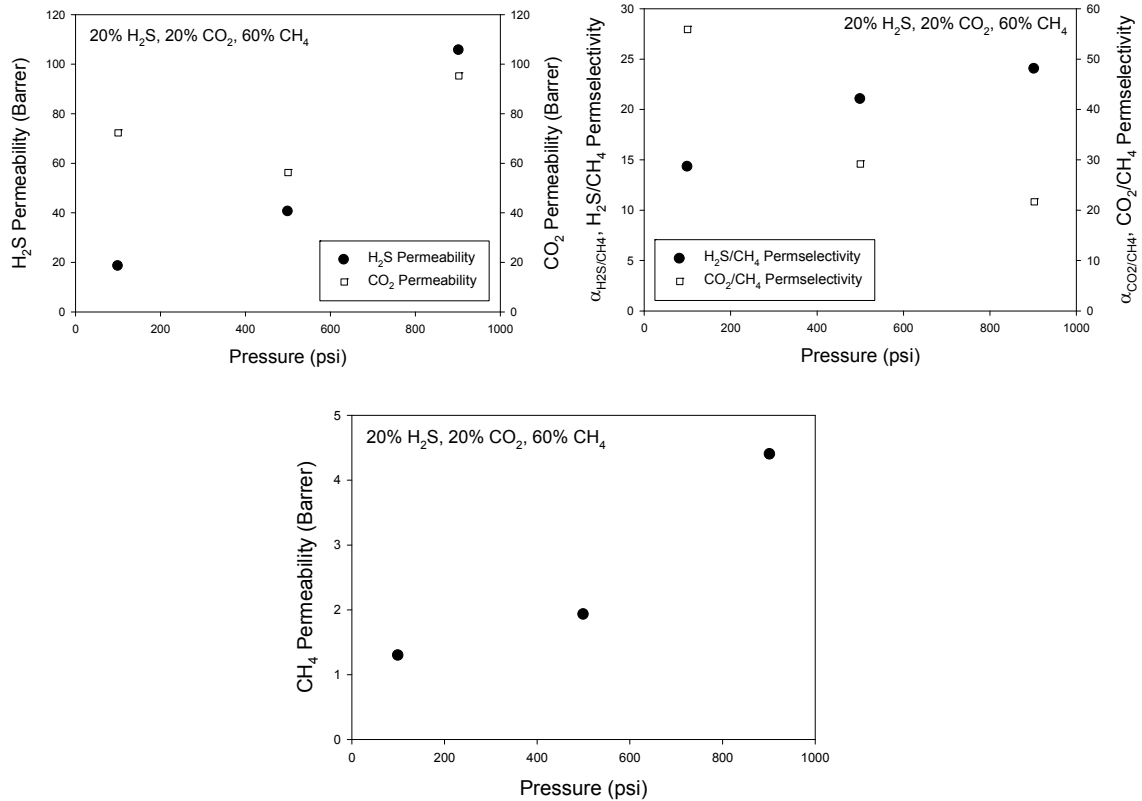


Figure 4.10: Non-vacuum downstream pressure permeation for 6FDA-DAM:DABA (3:2) at 35°C with a 20% H₂S, 20% CO₂, 60% CH₄ mixed gas feed.

It was expected that these non-vacuum conditions in the permeate would favor plasticization of the membrane. Typically, the penetrant gas concentration profile across a polymeric membrane is assumed to be approximately linear. The upstream face of the membrane has a sorbed concentration of a particular penetrant species given by its dual-mode sorption model equilibrium concentration for the feed conditions of interest. For vacuum-downstream conditions, the penetrant gas concentration on the downstream face of the membrane is assumed to be infinitesimal, which is in agreement with the dual-mode sorption model prediction for all gases at zero pressure. However, when the permeate is not under vacuum, the concentration of a penetrant gas sorbed in the

downstream face of a membrane is also non-zero and is, again, given by the dual-mode sorption model prediction for the permeate conditions of interest.

Thus, under non-vacuum-downstream conditions, the average sorbed concentration in the membrane is greater than under vacuum conditions. This problem is exacerbated for sour gas separations – and in fact for any separation where a fast gas is likely to cause plasticization – since CO_2 and H_2S tend to become concentrated in the permeate stream. As such, the average sorbed concentration of the plasticizing components, CO_2 and H_2S , in the membrane may be significantly higher under non-vacuum downstream conditions than under the normal dense film experimental conditions. This can lead to the onset of plasticization at much lower feed pressures.

From the results presented in Figure 4.10, it appears that the permeability and permselectivity trends for the sour gas components are very similar to those observed under vacuum-downstream conditions (Figure 4.9). Based on these observations, it seems that the 180°C annealed 6FDA-DAM:DABA (3:2) membrane possesses sufficient intrinsic stability to avoid plasticization under these conditions. This is a promising result for the 6FDA-DAM:DABA (3:2) polymer backbone, as it indicates that materials based on this polymer template may be robust enough to be used under realistic non-vacuum permeate pressure operating conditions.

4.5.5. Binary (20% CO_2 / 80% CH_4) Acid Gas Mixture Permeation

In addition to the sour gas mixtures that were used to test annealed 6FDA-DAM:DABA (3:2) dense films, a binary mixture comprised of 20% CO_2 and 80% CH_4 was used. The non-sour (i.e. no H_2S content) mixture was selected in an attempt to better understand the mechanism by which $\text{H}_2\text{S}/\text{CH}_4$ permselectivity increases so drastically under mixed gas feed conditions compared to the ideal $\text{H}_2\text{S}/\text{CH}_4$ selectivity.

The results of permeation experiments conducted at 35°C on a 180°C annealed sample are displayed in Figure 4.11.

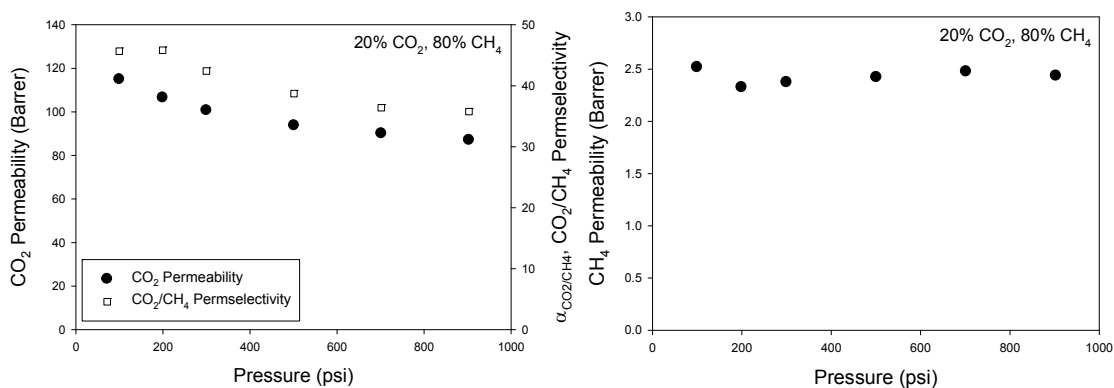


Figure 4.11: 6FDA-DAM:DABA (3:2) dense film permeation results at 35°C for a 20% CO₂, 80% CH₄ mixture.

The CO₂ and CH₄ permeability values shown above are very similar to the values measured during pure gas permeation (Figure 4.4). This finding is in contrast to the results that were obtained for H₂S-containing mixture in the preceding sections. In those cases, the CO₂ and CH₄ permeabilities of the 6FDA-DAM:DABA (3:2) dense films (prior to the onset of plasticization) were significantly depressed compared to the pure gas permeability values. While some decrease in penetrant gas permeability is expected for mixed gas permeation versus pure gas permeation as a result of competitive sorption between the various gases for Langmuir sorption sites, the magnitude of the permeability losses observed for sour gas mixtures is surprising.

Sections 4.5.6 - 4.5.7 will show that competitive sorption arising from the dual-mode sorption model for glassy polymers *does* cause decreased solubility coefficients in 6FDA-DAM:DABA (3:2). However, standard dual-mobility permeation modeling is unable to accurately capture the permeation trends that are observed for sour gas mixtures, even when bulk flow contributions are taken into account. These results indicate that

more complex polymer-penetrant interactions may be present during sour gas permeation.

The CO₂/CH₄ permselectivity values represented in Figure 4.11 are in good alignment with the ideal selectivity value given in Table 4.2. Despite the fairly high partial pressures of CO₂ in the feed gas, the annealed 6FDA-DAM:DABA (3:2) film does not show any significant sign of penetrant-induced plasticization. Competition effects between the CO₂ and CH₄ gases are believed to be the cause of the slightly elevated CO₂/CH₄ permselectivity at low feed pressures.

4.5.6. Mixed Gas Sorption Calculations

Sorption projections for pure CO₂ and CH₄ gases and for a binary mixture consisting of 20% CO₂ and 80% CH₄ are shown in Figure 4.12. Even in the absence of H₂S, the mixed gas feed conditions used for these calculations indicate that a significant drop in CO₂ and CH₄ sorption is expected due to competition for Langmuir sorption sites. The different annealing temperatures used on the 6FDA-DAM:DABA (3:2) dense films does not appear to have a major influence on the relative magnitude of the decrease in sorbed concentration when moving from pure to mixed gas feeds. However, the 180°C annealing temperature has slightly higher sorption capacity for both gases, as was shown by the experimental result in Figure 4.5.

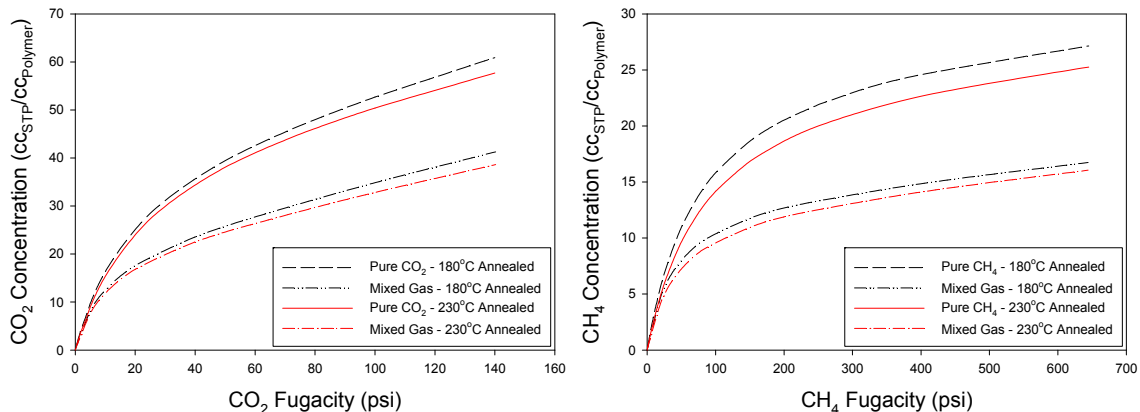


Figure 4.12: Dual-mode sorption model calculations for pure and mixed gas (20% CO₂, 80% CH₄) feeds at 35°C.

Ternary mixtures of H₂S, CO₂, and CH₄ gases were observed to give larger deviations from pure gas permeation properties than binary non-sour gas mixtures. This is at least partially explained by the greater degree of competitive sorption that is present for a ternary mixed gas feed containing high concentrations of the condensable H₂S and CO₂ species. Pure and mixed gas sorption projections are displayed in Figure 4.13 for 6FDA-DAM:DABA (3:2) dense films at 35°C. The sour gas mixture used in these calculations was 10% H₂S, 20% CO₂, and 70% CH₄, which was also used for mixed gas permeation experiments.

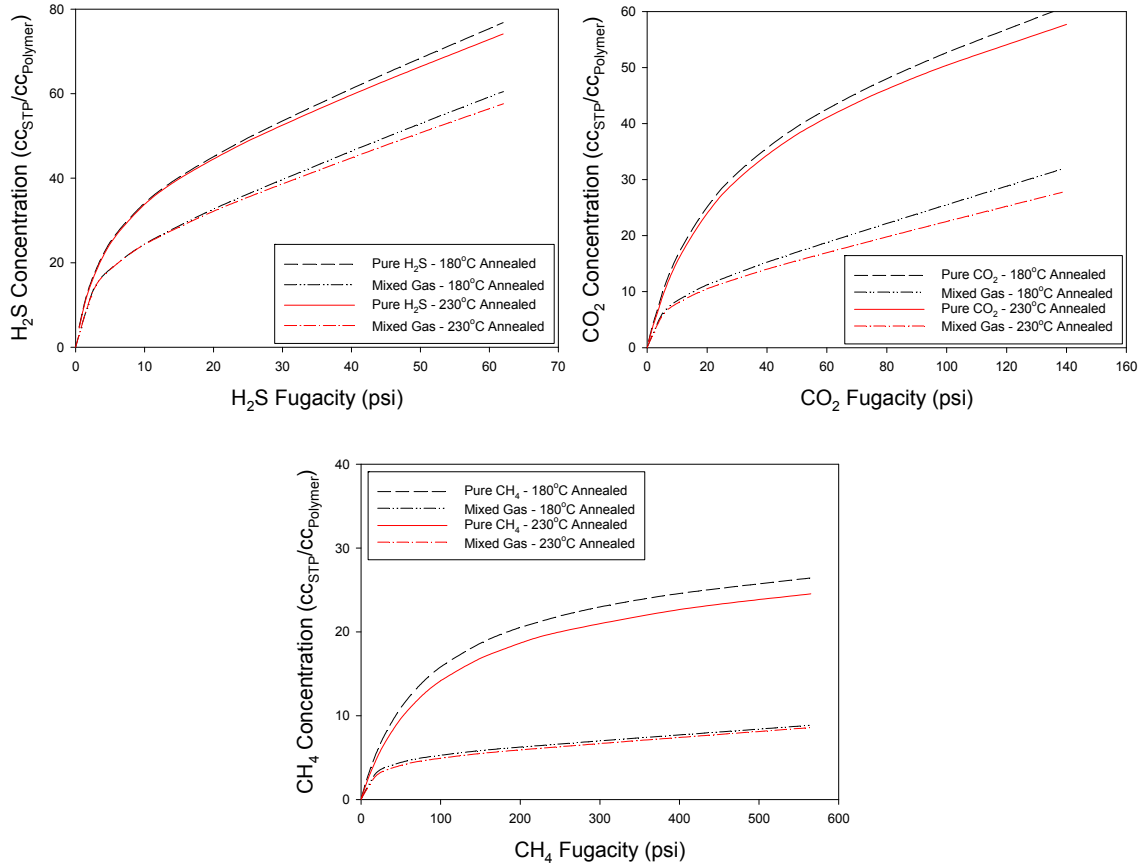


Figure 4.13: Pure and mixed gas (10% H₂S, 20% CO₂, 70% CH₄) sorption predictions based on the dual-mode sorption model at 35°C.

The sorption values shown above indicate that H₂S solubility is affected the least under mixed gas feed conditions compared to pure gas. Very large drops in the CO₂ and CH₄ sorption levels are observed when moving from pure gas to the selected sour gas mixture. In fact, these decreases for the CO₂ and CH₄ gases are noticeably larger than were observed under binary non-sour gas mixture conditions. Therefore, the dual-mode sorption model suggests that major declines in the sorption coefficients for these two gases with sour gas feeds accounts for at least a portion of the permeability losses that were measured.

4.5.7. Pure and Mixed Gas Permeation Modeling

The partial immobilization model was used to determine diffusion coefficients for sour gas components through the Langmuir and Henry's law regimes in Section 4.4.3. Pure gas permeability data and dual-mode sorption model parameters for each gas were used in the calculation of these values. In Figure 4.14, the experimental permeability data is shown alongside the partial immobilization model prediction for pure H₂S, CO₂, and CH₄ permeability through the 6FDA-DAM:DABA (3:2) dense film annealed at 180°C. These plots display excellent agreement between the actual permeation data and the model predictions before the onset of H₂S- and CO₂-induced plasticization and over the entire CH₄ isotherm.

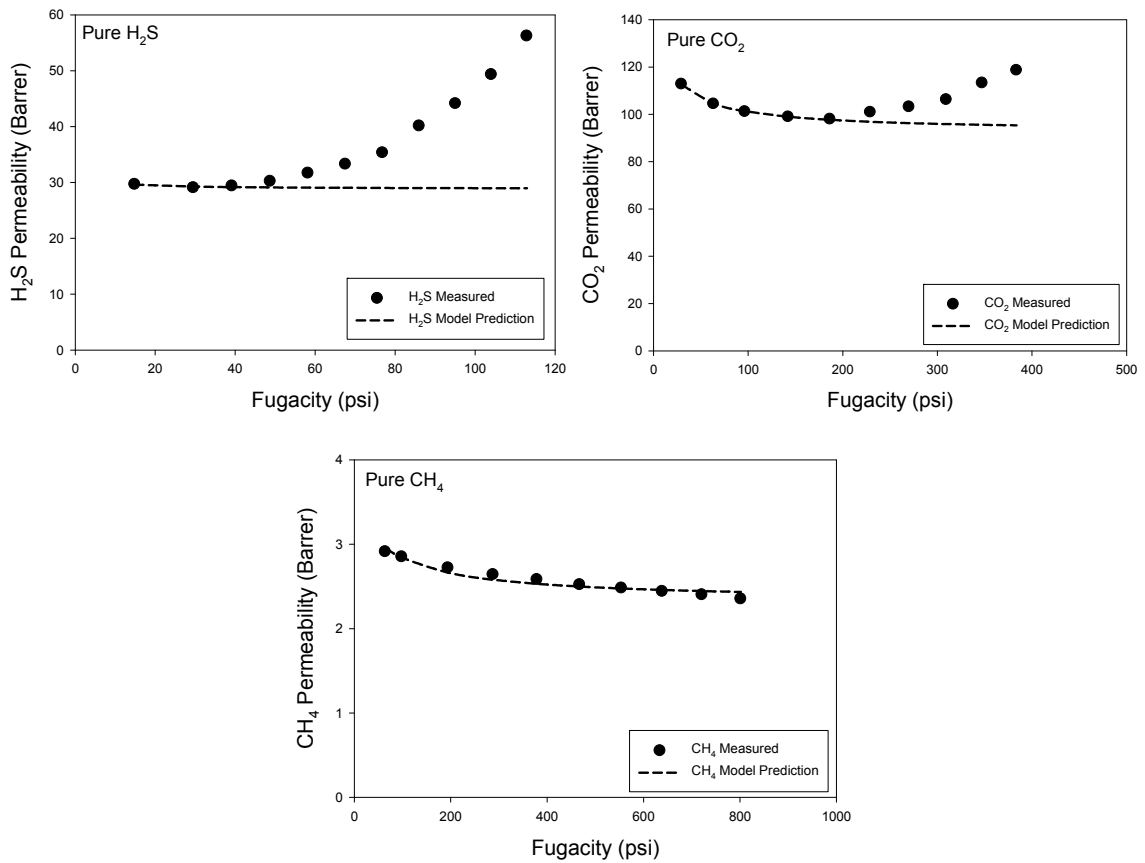


Figure 4.14: Partial immobilization model projections for pure gas permeability at 35°C in the 180°C annealed 6FDA-DAM:DABA (3:2) dense films.

Permeation modeling based on dual-mobility transport through glassy polymers can be extended to mixed gases. Since the model parameters are calculated based on pure gas permeation and sorption data, agreement between mixed gas experimental permeation data and model predictions can be inferior in some cases. This is especially true for mixed gas feeds that lead to significant polymer-penetrant interactions or other effects that are not accounted for in the model. Such effects were noted for H₂S-containing mixtures in the preceding sections. More complex models can be used to counter such inconsistencies between the experimentally determined permeability and the permeation model projections. For instance, the frame of reference permeation model, which was discussed in Section 2.3.2, can be used to take bulk penetrant gas flux through the membrane into consideration. The bulk flux contribution often becomes more important under mixed gas feed conditions, especially when highly condensable species are present.

Figure 4.15 gives the experimental data and permeation model calculations (without and with bulk flux contributions) for a 20% CO₂, 80% CH₄ mixed gas feed with the 180°C annealed 6FDA-DAM:DABA (3:2) dense films. Although the predicted permeability trends do not match the measured values as closely as with pure gas feeds, they are quite accurate. In this case, the more complicated frame of reference model does not lead to significantly improved agreement with experimental results; the two models give permselectivity values that almost perfectly overlap one another. This indicates that bulk flux contributions under these feed conditions are essentially negligible. Based on these results, it appears that either of the two models may be used to predict the performance of 6FDA-DAM:DABA (3:2) dense films for CO₂/CH₄ feed mixtures. This is important, since permeation modeling can be a powerful tool for optimizing separation processes that involve a variety of feed mixtures and it reduces

the need for time consuming, expensive, and often technically challenging permeation experiments.

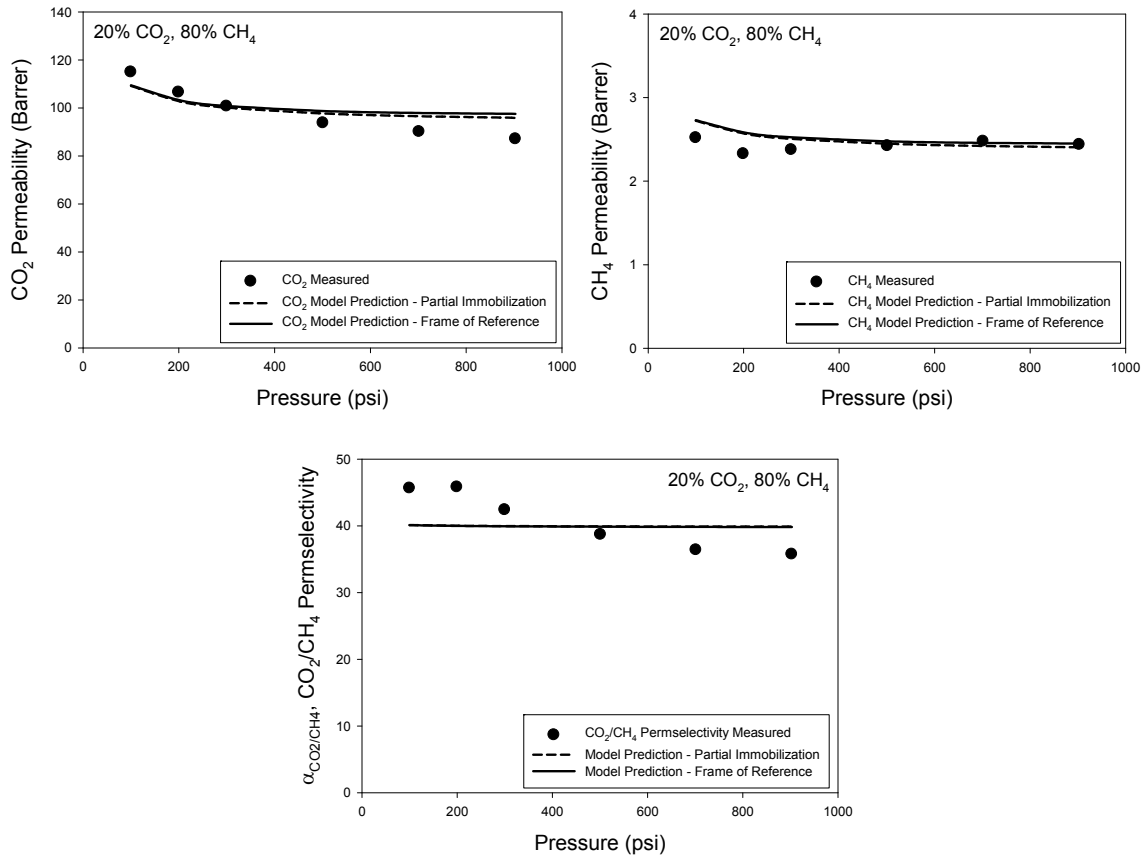


Figure 4.15: Permeation model predictions for 20% CO₂, 80% CH₄ mixed gas feed at 35°C in 6FDA-DAM:DABA (3:2) dense films.

Unlike the CO₂/CH₄ mixture, the results of permeation experiments with H₂S-containing feed mixtures were found to deviate from pure gas permeation behavior and the H₂S/CH₄ ideal selectivity. Permeation model predictions for a 5% H₂S, 95% CH₄ binary sour gas feed are shown in Figure 4.16. Notable differences between the measured permeability values and the predicted values are observed for both H₂S and CH₄. The marked drop in CH₄ permeability at high feed pressures, which corresponds to high H₂S partial pressures, is not captured by either of the models. In addition, the H₂S

permeability is predicted to fall well below the actual experimentally determined level. The inclusion of bulk flux contributions has minimal effect on the predicted permeation and selectivity values, most likely due to the modest overall permeation rate of these two species through the membrane.

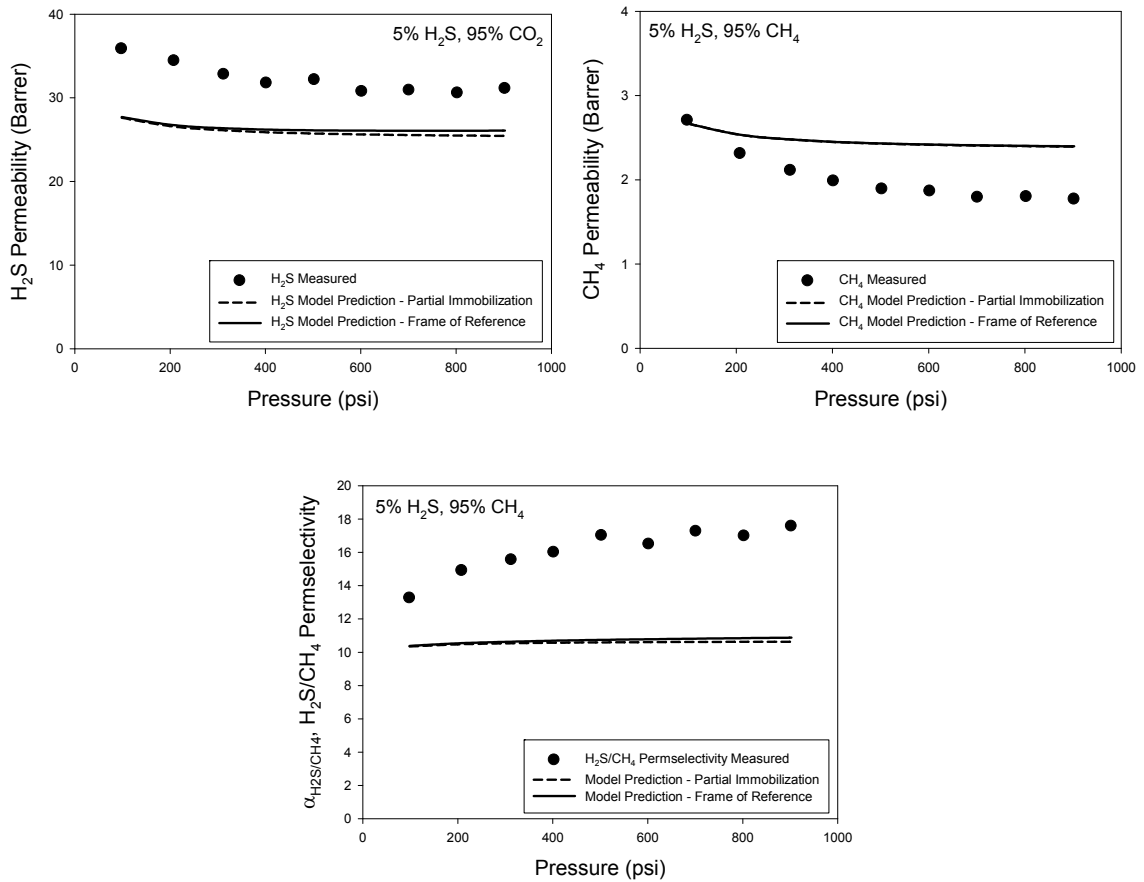


Figure 4.16: Permeation model calculations for 5% H₂S, 95% CH₄ mixed gas feed at 35°C.

The results given above indicate that CH₄ does not compete with H₂S for Langmuir sorption sites nearly as effectively as is predicted; the reduced H₂S permeability that is predicted for the entire isotherm was not measured. Also, the effect of higher partial pressures of H₂S on the CH₄ permeability is underestimated by both models. It is possible that the competitive sorption effect between H₂S and CH₄ is not

fully captured by these models. However, strong H₂S-polymer interaction effects that are not accounted for within the partial immobilization or frame of reference models may also be present. In either case, a more complex permeation model is needed in order to provide reliable predictive capability for permeation with H₂S/CH₄ mixtures.

Ternary mixtures consisting of H₂S, CO₂, and CH₄ present even more complicated systems than the binary mixed gases that were modeled above. Nevertheless, the partial immobilization and frame of reference models were applied for a 10% H₂S, 20% CO₂, 70% CH₄ mixed gas feed, which was used for permeation experiments in Section 4.5.3. The results are provided in Figure 4.17 and Figure 4.18.

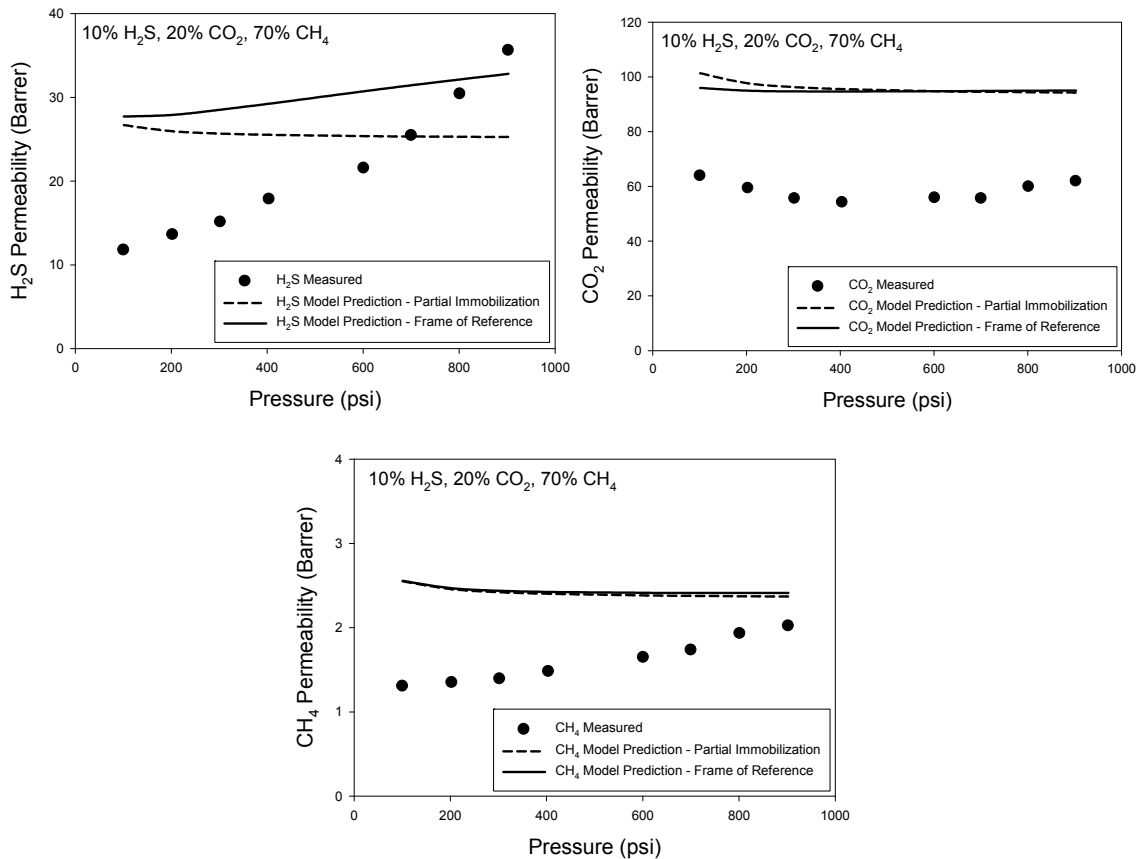


Figure 4.17: Model predictions for H₂S, CO₂, and CH₄ permeability of a 10% H₂S, 20% CO₂, 70% CH₄ mixture at 35°C

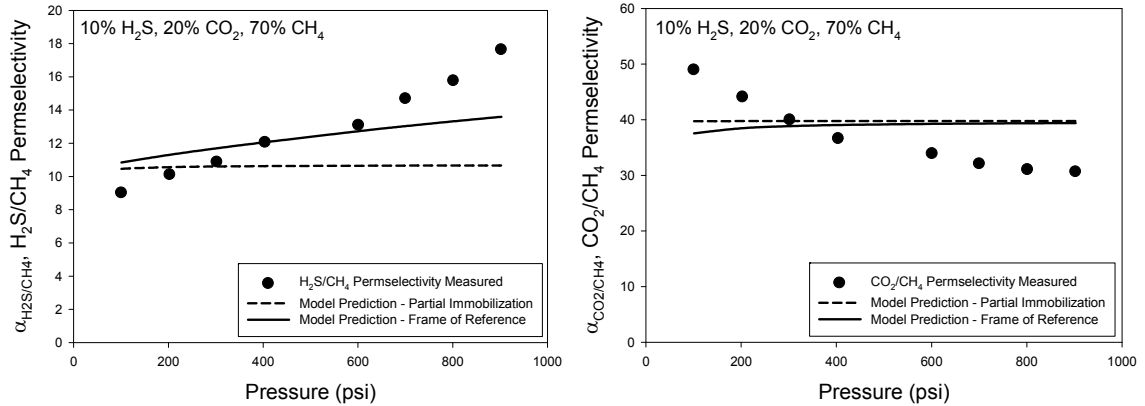


Figure 4.18: Permselectivity projections for 10% H₂S, 20% CO₂, 70% CH₄ mixed gas feed at 35°C.

It is quite clear from the permeability and permselectivity calculations shown above that the presence of H₂S in the feed mixture adds some unaccounted for complexity to the system. The permeability values for all three gases are underestimated for the vast majority of the isotherms, especially prior to the onset of membrane swelling and plasticization. Also, the predicted permselectivity trends are far less complex than the measured values. It is interesting to note that the frame of reference model gives significantly different projections for H₂S permeability and H₂S/CH₄ permselectivity than the simpler partial immobilization model. Surprisingly, the frame of reference model values capture the increasing H₂S permeability, which is *not* entirely due to a membrane plasticization effect, fairly well.

Although at this time it is not possible to identify the exact transport mechanism leading to the poor agreement between experimental permeation results and permeation model projections in the presence of H₂S, it clearly merits further investigation. This will be addressed more completely in CHAPTER 8. Nevertheless, we suggest that mixed gas sorption effects beyond those captured by the dual-mode sorption model are one potential source of this discrepancy; mixed gas sorption experiments may help to

elucidate these hypothetical effects. Also, it is possible that the highly polar H₂S gas influences polymer chain segmental mobility or free volume within the glassy membrane in a manner similar to antiplasticization (Section 2.4.2). In this scenario, the diffusivity of the membrane could be affected, which may account for the currently unexplained permeability depression under sour gas might feed conditions.

4.6. Assessment of Sour Gas Separation Performance

4.6.1. Upper Bound Comparison

The CO₂/CH₄ and H₂S/CH₄ separation properties of 6FDA-DAM:DABA (3:2) are displayed through productivity-efficiency tradeoff plots in Figure 4.19 and Figure 4.20, respectively. The theoretical upper bound levels for CO₂/CH₄ separations using polymeric membranes are also shown in Figure 4.19. In contrast, no theoretical upper bound has yet been documented for H₂S/CH₄ separations due to the scarcity of data in the literature. While it is clear from these figures that the sour gas performance of CA lies significantly below that of 6FDA-DAM:DABA (3:2) and the rubbery polymers, it is more difficult to make an overall assessment regarding the performance of our polyimide compared to the rubbery materials. As expected, CO₂/CH₄ selectivity in the glassy 6FDA-DAM:DABA (3:2) material is higher than the rubbery polymers, which generally have less size-discriminating ability. However, the selectivity and permeability of the rubbery polymers for the H₂S/CH₄ separation is significantly greater than that of 6FDA-DAM:DABA (3:2).

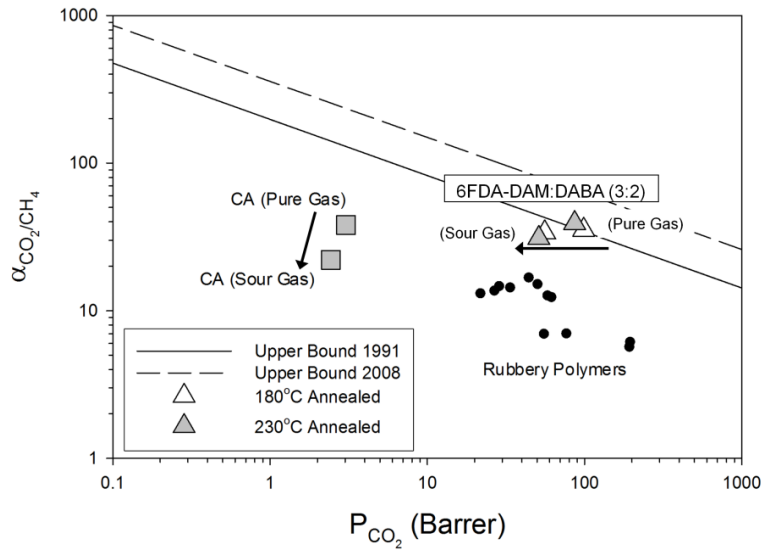


Figure 4.19: Productivity-efficiency tradeoff for CO₂/CH₄ separations [10, 11]. Data are for various candidate materials for aggressive sour gas separations [2, 12-14]. 6FDA-DAM:DABA (3:2) pure gas data measured at 150 psi feed pressure and 35°C, and sour gas data are for the 10% H₂S, 20% CO₂, 70% CH₄ mixture at 35°C and 600 psi.

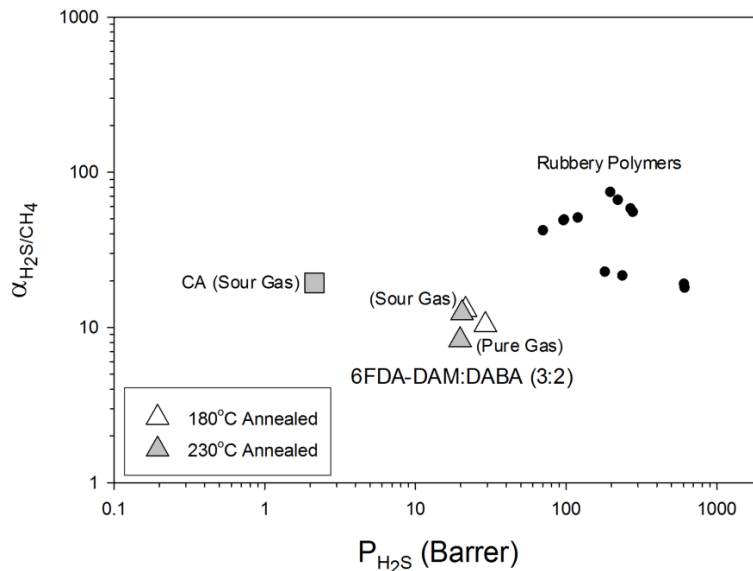


Figure 4.20: Productivity-efficiency tradeoff for H₂S/CH₄ separations. Data are for various candidate materials for aggressive sour gas separations [2, 12-14]. 6FDA-DAM:DABA (3:2) pure gas data measured at 30 psi feed pressure and 35°C, and sour gas data are for the 10% H₂S, 20% CO₂, 70% CH₄ mixture at 35°C and 600 psi.

4.6.2. Combined Acid Gas Analysis

Despite the moderate H₂S/CH₄ ideal selectivity values that were measured, the performance of thermally annealed 6FDA-DAM:DABA (3:2) dense films for aggressive sour gas separations appears quite promising based on the mixed gas permeation results. However, because of the complexity of the separation under investigation and the differing mechanisms by which H₂S and CO₂ removal from natural gas are most easily achieved, it is difficult to make a straightforward comparison of rubbery and glassy polymers. Standard individual efficiency measures for the H₂S/CH₄ and CO₂/CH₄ separations do not capture the full scope of the separation under investigation and inherently favor one type of material over the other. As such, a novel efficiency measure was defined and may be used in conjunction with the typical gas-pair productivity and efficiency metrics. This is the combined acid gas separation factor ($SF_{CAG}^{\#}$), which was introduced in Eq. (2.53).

The current lack of data in the literature on the sour gas separation performance of membrane materials makes material property comparisons especially difficult at present. As discussed in CHAPTER 2, rubbery and glassy polymers tend to possess very different CO₂/CH₄ and H₂S/CH₄ properties from one another. This results in rubbery and glassy polymers being grouped far apart on traditional productivity-efficiency tradeoff plots for single gas pairs, as shown in Figure 4.19 and Figure 4.20. Also, few feed gas compositions have been tested and this has been shown to significantly impact sour gas separation performance. The combined acid gas separation factor attempts to alleviate this issue by accounting for the selectivity of a material for both CO₂ and H₂S, as well as the feed gas composition. While it should not be used as the sole means of assessing membrane performance, the combined acid gas separation factor is useful in

that it enables side-by-side comparison of membranes for the overall sour gas separation.

For the data reported in the literature, we estimate the permeate mole fractions found in Eq. (2.53) by using the definition of permeability Eq. (2.3) to determine the steady state thickness-normalized molar flux of each component. Values for the mole fractions are then determined as simple fractions of the total thickness-normalized molar flux. Using this method, the results of the current study are compared to the literature data in Figure 4.21 through a combined acid gas productivity ($P_{H_2S}+P_{CO_2}$)-efficiency ($SF_{CAG}^\#$) tradeoff plot.

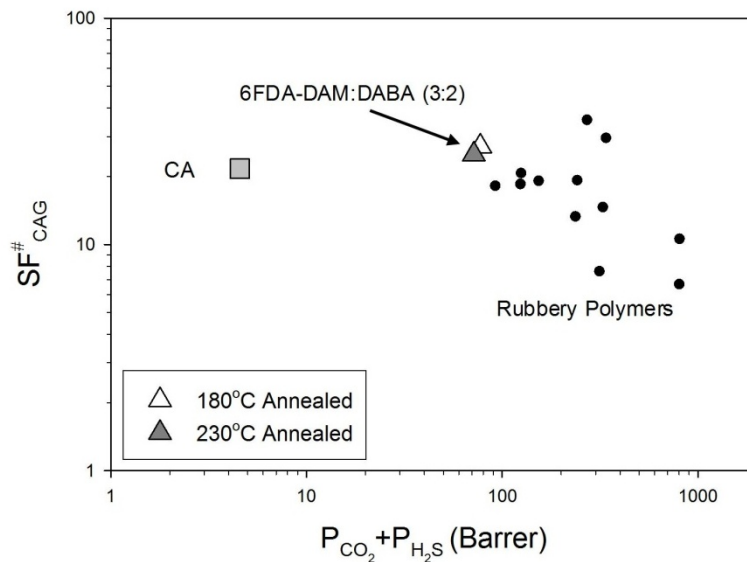


Figure 4.21: Productivity-efficiency tradeoff for combined acid gas separations. Ternary gas data are shown for rubbers (black symbols) as well as the glassy polymers, CA and 6FDA-DAM:DABA (3:2). The data points used for 6FDA-DAM:DABA (3:2) films are for 600 psi feed pressure and 35°C using the 10% H₂S, 20% CO₂, 70% CH₄ mixture.

The location of the 6FDA-DAM:DABA (3:2) samples near the upper right quadrant indicates that this material performs significantly better than CA based on the combined acid gas metric. Also, 6FDA-DAM:DABA (3:2) appears to outperform, or at the

very least is competitive with, the majority of the rubbery polymers if it is assumed that combined acid gas productivity and efficiency follow the same upper-bounded trend as other gas pairs – with efficiency decreasing as productivity rises [10, 11]. Still, further improvements are necessary to render the 6FDA-DAM:DABA polymer backbone a viable membrane material for aggressive sour gas separations. In addition to the productivity and efficiency measures that are captured in Figure 4.21, H₂S- and CO₂-induced plasticization resistance must also be addressed. Modifications to the base 6FDA-DAM:DABA material beyond simple thermal annealing treatments must be explored, and are the subject of the following chapters.

4.7. Path Forward for 6FDA-DAM:DABA Polyimide Backbone

The unusual effects that were observed for the permeation of H₂S-containing mixtures in 6FDA-DAM:DABA (3:2) – namely, large increases in H₂S/CH₄ selectivity and the depression of CH₄, and to a lesser extent CO₂, permeability in the presence of H₂S – are of interest for the development of more advanced materials. In addition to competition between the various species for sorption sites within the polymer matrix, other factors including dynamic fractional free volume changes and restricted polymer chain mobility (i.e. an effect similar to antiplasticization) may account for these effects. Although the ability to accurately model and predict sour gas permeation through glassy polymers could help provide a more complete understanding of the complex interactions taking place, this is not entirely necessary in order to begin the process of improving the material used in this study for the intended separation. Valuable insight for improving the performance of successive generations of membrane materials based on 6FDA-DAM:DABA may be gleaned by examining the current polymer as well as other

materials, both rubbery and glassy, for which sour gas transport data have been reported.

The mixed gas studies on 6FDA-DAM:DABA (3:2) membranes discussed in this chapter did not show large efficiency losses as a result of penetrant-induced plasticization. However, under long-term operation at high pressure, high acid gas concentration natural gas reserves that are the focus of this study, plasticization and performance degradation may be more likely to occur. As a result, it is unlikely that sub- T_g thermal annealing can be relied upon to provide adequate membrane stability moving forward. Moreover, our results from both the pure gas and mixed gas permeation studies indicate that the modest improvements to membrane stability that result from higher temperature thermal annealing are offset by decreased separation efficiency in all cases involving H_2S . An ideal membrane stabilizing technique would be accompanied by substantially improved separation efficiency.

Previous work using the 6FDA-DAM:DABA backbone for CO_2/CH_4 separations has focused on covalent cross-linking for improved plasticization resistance, as discussed in CHAPTER 3. High temperature thermal crosslinking, which is believed to occur spontaneously through a free radical decarboxylation mechanism, has proven effective for feed streams contaminated with very high-concentration CO_2 and higher hydrocarbons (toluene, n-heptane) [6, 15, 16]. Additionally, 6FDA-DAM:DABA has been modified and cross-linked using various diol linker groups through sub- T_g esterification reactions at the carboxylic acid sites. So far, only linear aliphatic, cyclic aliphatic and aromatic diol linker groups have been studied [1]. Both of these covalent cross-linking techniques are expected to impart additional resistance to H_2S -induced plasticization in membranes based on the 6FDA-DAM:DABA backbone. However, the heretofore studied crosslinking modifications are not expected to result in a significant improvement to the

efficiency of the H₂S/CH₄ or CO₂/CH₄ separations under aggressive sour gas feed conditions. These modifications were performed solely with membrane stability improvement in mind.

In their investigation of sour gas separations using supported phosphazene membranes, Orme and Stewart found that the incorporation of ether-containing polar pendant groups improves sour gas separation performance in terms of productivity and efficiency [21]. Chatterjee et al., also report excellent H₂S/CH₄ separation properties in rubbery poly(ether urethane) and poly(ether urethane urea) membranes, which are primarily comprised of polar amide, ester, and ether groups. Similarly, the impressive H₂S/CH₄ separation performance of Pebax® materials may be derived in large part from their highly polar nature. Specifically, an examination of the ether-associated oxygen content in the various Pebax® membranes reported by Baker et al. indicates that a strong correlation with H₂S/CH₄ selectivity exists, as shown in Figure 4.22. As a result, it seems that the incorporation of additional polar groups, particularly flexible ether-containing groups, into the 6FDA-DAM:DABA based materials may give improved the H₂S/CH₄ separation properties. It is likely, however, that the introduction of flexible sorption-enhancing moieties may cause a reduction in the T_g of the glassy 6FDA-DAM:DABA material and a potential loss of CO₂/CH₄ separation efficiency compared to the rigid base polymer. A delicate balance between modification with these polar groups and the maintenance of the unmodified polymer's glassy properties, which have been optimized for CO₂ removal, must be achieved. This complex issue is the focus of CHAPTER 5.

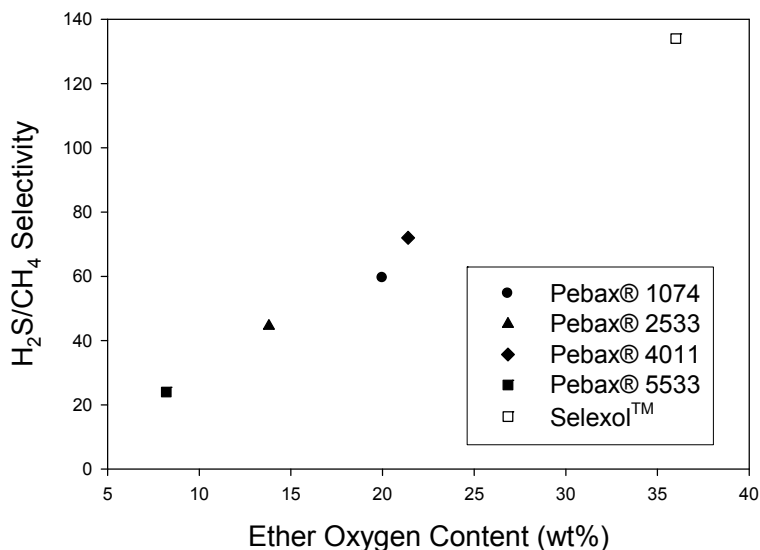


Figure 4.22: H₂S/CH₄ selectivity as a function of ether content in a series of Pebax® rubbers. The value for Selexol™ selectivity is the R_K for H₂S and CH₄ [13, 22].

4.8. Conclusions

Aggressive sour gas separations using 6FDA-DAM:DABA (3:2) dense films were investigated with pure and mixed gas feeds through permeation and sorption testing. The introduction of H₂S at high concentration to the feed streams results in a number of non-ideal transport effects, including plasticization and large deviations between pure and mixed gas separation performance in terms of H₂S/CH₄ selectivity and CH₄ permeability. Sub-T_g thermal annealing was used to increase the plasticization resistance of 6FDA-DAM:DABA (3:2) films up to 35 psi H₂S, thus enabling the collection of meaningful, non-plasticized sour gas transport data. For binary and ternary gas permeation tests using H₂S partial pressures greater than 30 psi, H₂S/CH₄ selectivity improved by 90% over the ideal selectivity in both films, and reached a value of 18 in one film. Additionally, the presence of H₂S did not result in major losses of CO₂/CH₄ separation efficiency compared to the ideal selectivity, as was been reported with CA

(Figure 4.1) [12]. In fact, H₂S partial pressures below approximately 30 psi correspond to significantly enhanced CO₂/CH₄ separation efficiency, in some cases.

The use of the combined acid gas separation factor ($SF_{CAG}^{\#}$) allowed for a more direct comparison of glassy and rubbery polymer membranes. Despite the much higher partial pressures of H₂S and CO₂ that were used in the current study compared to reported data for rubbery materials, the productivity and efficiency performance of 6FDA-DAM:DABA (3:2) is competitive with other high-performing materials. Furthermore, this metric suggests that these copolyimide membranes are superior to the industrial standard glassy polymer, CA, for sour gas separations. While thermal treatment alone did enhance membrane stability against H₂S, it is unlikely to be adequate for the most aggressive sour gas feeds. Potential methods for improving 6FDA-DAM:DABA based membranes in terms of their stability and productivity/efficiency properties for aggressive sour gas separation applications are probably best focused on *crosslinking stabilization* of the matrix. Such approaches can involve a variety of strategies to implement, but all of them provide resistance against swelling induced selectivity losses.

4.9. References

1. Wind, J.D., et al., *Solid-State Covalent Cross-Linking of Polyimide Membranes for Carbon Dioxide Plasticization Reduction*. *Macromolecules*, 2003. **36**(6): p. 1882-1888.
2. Wind, J.D., D.R. Paul, and W.J. Koros, *Natural gas permeation in polyimide membranes*. *Journal of Membrane Science*, 2004. **228**(2): p. 227-236.
3. Staudt-Bickel, C. and W. J. Koros, *Improvement of CO₂/CH₄ separation characteristics of polyimides by chemical crosslinking*. *Journal of Membrane Science*, 1999. **155**(1): p. 145-154.
4. Koros, W.J., et al., *Sub-T(g) Cross-Linking of a Polyimide Membrane for Enhanced CO(2) Plasticization Resistance for Natural Gas Separation*. *Macromolecules*, 2011. **44**(15): p. 6046-6056.

5. Hillock, A.M.W. and W.J. Koros, *Cross-Linkable Polyimide Membrane for Natural Gas Purification and Carbon Dioxide Plasticization Reduction*. *Macromolecules*, 2007. **40**(3): p. 583-587.
6. Kratochvil, A.M. and W.J. Koros, *Decarboxylation-Induced Cross-Linking of a Polyimide for Enhanced CO₂ Plasticization Resistance*. *Macromolecules*, 2008. **41**(21): p. 7920-7927.
7. Koros, W.J.A., GA, US), Wallace, David (Smyrna, GA, US), Wind, John (Berkeley, CA, US), Miller, Stephen J. (San Francisco, CA, US), Staudt-bickel, Claudia (Heidelberg, DE), *Crosslinked and crosslinkable hollow fiber membrane and method of making same utility*, 2007, Chevron U.S.A. Inc. (San Ramon, CA, US): United States.
8. Miller, S.J.S.F., CA, US), Omole, Imona C. (Atlanta, GA, US), Koros, William J. (Atlanta, GA, US), *Method of making a crosslinked fiber membrane from a high molecular weight, monoesterified polyimide polymer*, 2009, Chevron U.S.A. Inc. (San Ramon, CA, US), Georgia Tech Research Corporation (Atlanta, GA, US): United States.
9. Omole, I.C., *Crosslinked Polyimide Hollow Fiber Membranes for Aggressive Natural Gas Feed Streams*, in *School of Chemical and Biomolecular Engineering* 2008, Georgia Institute of Technology: Atlanta, GA. p. 305.
10. Robeson, L.M., *Correlation of separation factor versus permeability for polymeric membranes*. *Journal of Membrane Science*, 1991. **62**(2): p. 165-185.
11. Robeson, L.M., *The upper bound revisited*. *Journal of Membrane Science*, 2008. **320**(1-2): p. 390-400.
12. Chatterjee, G., A.A. Houde, and S.A. Stern, *Poly(ether urethane) and poly(ether urethane urea) membranes with high H₂S/CH₄ selectivity*. *Journal of Membrane Science*, 1997. **135**(1): p. 99-106.
13. Membrane Technology and Research, I., *Low-Quality Natural Gas Sulfur Removal/Recovery*, 1998, The Department of Energy: Morgantown, WV.
14. Houde, A.Y., et al., *Permeability of dense (homogeneous) cellulose acetate membranes to methane, carbon dioxide, and their mixtures at elevated pressures*. *Journal of Applied Polymer Science*, 1996. **62**(13): p. 2181-2192.
15. Qiu, W.L., et al., *Sub-T(g) Cross-Linking of a Polyimide Membrane for Enhanced CO₂ Plasticization Resistance for Natural Gas Separation*. *Macromolecules*, 2011. **44**(15): p. 6046-6056.
16. Chen, C.-C., et al., *Plasticization-resistant hollow fiber membranes for CO₂/CH₄ separation based on a thermally crosslinkable polyimide*. *Journal of Membrane Science*, 2011. **382**(1-2): p. 212-221.

17. Park, J.Y. and D.R. Paul, *Correlation and prediction of gas permeability in glassy polymer membrane materials via a modified free volume based group contribution method*. Journal of Membrane Science, 1997. **125**(1): p. 23-39.
18. Bondi, A., *Physical properties of molecular crystals, liquids, and glasses*. 1968, New York: Wiley.
19. Merkel, T.C. and L.G. Toy, *Comparison of Hydrogen Sulfide Transport Properties in Fluorinated and Nonfluorinated Polymers*. Macromolecules, 2006. **39**(22): p. 7591-7600.
20. Mohammadi, T., et al., *Acid Gas Permeation Behavior Through Poly(Ester Urethane Urea) Membrane*. Industrial & Engineering Chemistry Research, 2008. **47**(19): p. 7361-7367.
21. Orme, C.J. and F.F. Stewart, *Mixed gas hydrogen sulfide permeability and separation using supported polyphosphazene membranes*. Journal of Membrane Science, 2005. **253**(1-2): p. 243-249.
22. Kidnay, A.P., W., *Fundamentals of Natural Gas Processing*. Mechanical Engineering, ed. L.L. Faulkner. 2006, Boca Raton: Taylor & Francis.

CHAPTER 5

CROSSLINKABLE POLYIMIDE MATERIALS FOR AGGRESSIVE SOUR GAS SEPARATIONS

5.1. Overview

This chapter presents the results of synthesis and transport characterization for a series of novel crosslinkable polyimide membrane materials: PEGMC polymers. These materials were engineered specifically to provide improved plasticization resistance under aggressive sour gas feed conditions and augmented H₂S/CH₄ permselectivity as compared to the unmodified 6FDA-DAM:DABA (3:2) polymer investigated in CHAPTER 4. A series of crosslinkable polymers were formed through an esterification crosslinking reaction involving ether-containing diol crosslinking agents – short-chain polyethylene glycols (PEGs) – and the carboxylic acid group of the 6FDA-DABA monomer. Sour gas transport through dense film membranes of three different PEGMC materials were studied using pure and mixed gas permeation and pure gas sorption. The aim of the work described in this chapter was the development of a membrane material based on the 6FDA-DAM:DABA polymer backbone with suitable sour gas transport properties in terms of productivity, efficiency, and stability for subsequent application in the asymmetric hollow fiber membrane morphology.

5.2. Sorption-Selective Materials for H₂S/CH₄ Separations

As discussed in CHAPTER 3, sorption selectivity is the favored membrane selectivity mechanism for H₂S/CH₄ separations as a result of the relative physical

properties of the H₂S and CH₄ gases. As such, a number of researchers have investigated rubbery polymer membranes, which rely primarily upon differences in gas sorption to achieve a separation, for sour gas feeds [1-5].

In general, polyamide-polyether copolymers display the most favorable properties for removing H₂S from natural gas feeds. These membranes have been shown to give excellent H₂S/CH₄ permselectivity and high H₂S permeability under low H₂S partial pressure conditions. For example, Baker et al. report H₂S/CH₄ selectivity as high as 70 in Pebax® 4011 modules for a ternary mixture containing 0.087% H₂S, 4.12% CO₂, and CH₄ balance at 385 psi and 22°C [1]. Also, Chatterjee et al. studied sour gas permeation through several rubbers. They report a H₂S/CH₄ selectivity of 74 in a poly(ether urethane urea) membrane using a ternary mixture (1.3% H₂S/ 27.9% CO₂/70.8% CH₄) at 150 psi and 35°C [2]. Figure 5.1 gives the generic structure of a polyamide-polyether copolymer. It was shown in Figure 4.22 that the polyether content of PEBA^X® membranes correlates with H₂S/CH₄ permselectivity; increasing the fraction of polyether repeats within the polymer is associated with increased H₂S/CH₄ separation efficiency. It is believed that favorable sorption selectivity for H₂S over CH₄ is the mechanism by which these materials achieve such outstanding performance. Additionally, the sorption interactions involving the polyether repeats and H₂S, while favorable, do not appear to be strong enough to hinder H₂S diffusion, as has been hypothesized to occur with polymers containing high concentrations of other more polar functional groups [6].

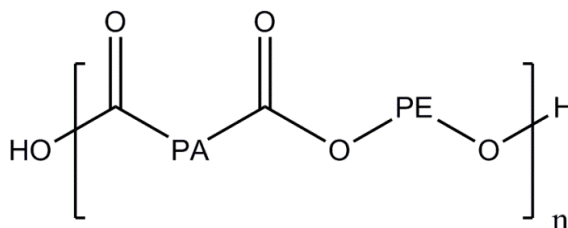


Figure 5.1: Chemical structure of a polyamide-polyether copolymer, where PA is a polyamide block and PE is a polyether block.

The physical solvent SELEXOL™ (Figure 5.2), a commonly used material for absorptive sour gas scrubbing applications, is comprised almost entirely of polyethylene oxide (PEO) repeat units and has very high sorption selectivity for H₂S over CH₄ ($R_K = 134$) [7]. Thus, as the polyether repeat content of PEBAX® materials that use PEO as the polyether block increases towards unity, their structure begins to resemble SELEXOL™, and so does their H₂S/CH₄ selectivity. Unfortunately, polyether repeats such as PEO can crystallize, which is highly detrimental to membrane productivity. For this reason, there is a practical limit towards which the polyether content of PEBAX® materials can be increased before the packing-interrupting effect of the amide repeats in PEBAX® becomes ineffective at inhibiting crystallization. Nevertheless, we hypothesize that the incorporation of polyether repeat units like PEO within polymer membranes may allow for augmented, and possibly tunable, H₂S/CH₄ permselectivity through enhanced H₂S/CH₄ sorption selectivity.

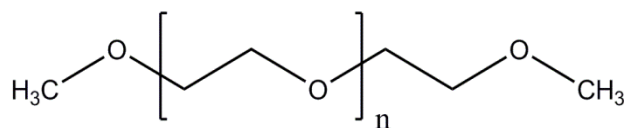


Figure 5.2: Chemical structure of the SELEXOL™ physical solvent used for acid gas separations.

While the H₂S/CH₄ separation properties of PEBAX® and other rubbery materials that mimic SELEXOL™ are impressive, *the CO₂/CH₄ permselectivity of these membranes typically lies well below the Robeson Upper Bound for polymeric membranes*, as shown in Figure 4.1 [8, 9]. Again, this may be related to the sorption selectivity of the materials for CO₂ over CH₄. SELEXOL™ has an R_K value of just 15 for CO₂ and CH₄ [7]. This value for CO₂/CH₄ permselectivity appears to be the approximate maximum for the PEBAX® membranes that have been studied. Since both CO₂ and H₂S must be removed from the sour gas streams that are the focus of the present work, it is believed that rubbery polymers, like PEBAX®, are probably not the ideal membrane material choice. Moreover, these rubbery polymers are not expected to be suitable for high-quality asymmetric hollow fiber membrane fabrication and their mechanical stability is expected to fall below that of advanced glassy materials.

The aforementioned drawbacks of rubbery polymers would be particularly evident in cases where a higher relative content of CO₂ as compared to H₂S makes the CO₂/CH₄ separation the most critical factor in the separation process as a whole. Additionally, it is likely that secondary treatment steps to reduce the H₂S content of sour gas wells down to the stringent pipeline specification (< 4ppm) will be necessary in almost all cases when membranes are employed. This may significantly detract from the actual value of a very highly H₂S/CH₄ selective material [4, 5, 10, 11]. In practice, the economics of natural gas separations favor membranes for bulk acid gas separation to achieve partial contaminant removal with minimal CH₄ loss. Therefore, the focus of the present study is on a membrane material with a proven track record for the CO₂/CH₄ separation and the potential for outstanding H₂S/CH₄ separation performance – namely, the glassy copolyimide 6FDA-DAM:DABA (3:2). At the same time, modifications to the

glassy membrane material that incorporate H₂S-selective rubbery polymer subunits to impart added H₂S/CH₄ sorption selectivity are a major focus of this study.

5.3. PEGMC Polymer Synthesis for Additional Plasticization Resistance and Augmented H₂S/CH₄ Selectivity

5.3.1. Monoesterification of 6FDA-DAM:DABA (3:2)

In the work described within this chapter, a series of crosslinked membrane materials based on the 6FDA-DAM:DABA (3:2) polyimide backbone are synthesized and tested for sour gas separations. A previously reported transesterification crosslinking mechanism is utilized along with a new class of multifunctional crosslinking agents – short-chain PEG molecules – to overcome two drawbacks that were found with unmodified 6FDA-DAM:DABA (3:2) membranes: poor stability against highly aggressive feed conditions and low H₂S/CH₄ selectivity [12-14]. These materials are referred to generically as PEGMC (**P**olyethylene **G**lycol **M**onoesterified **C**rosslinkable) polymers.

Chemical crosslinking of this material was expected to greatly improve plasticization resistance against both H₂S and CO₂ by reducing swelling of the polymer matrix caused by these condensable species. We anticipated that short-chain PEG crosslinkers would contribute to improved H₂S/CH₄ permselectivity, as discussed in the preceding section, since the polyether groups remain after crosslinking and are integrated into the membrane's polymer network. Short-chain PEG crosslinkers were selected because their structure closely resembles that of the highly successful sour gas scrubbing solvent SELEXOL™, except for the terminal hydroxyl groups that enable the esterification reaction, which is central to this crosslinking mechanism.

The structure and properties of these new materials were deduced through solution nuclear magnetic resonance (NMR) spectroscopy, thermogravimetric analysis (TGA), differential scanning calorimetry (DSC), density gradient column analysis, and gel permeation chromatography (GPC). Sour gas separation performance of the synthesized crosslinkable materials was investigated through pure gas permeation and sorption experiments, as well as mixed gas permeation testing. Appropriate crosslinking conditions were determined by testing the solubility of films in hot NMP, an excellent solvent for these materials in their uncrosslinked form, as well as 'gel content' experiments and pure gas permeation.

The protocol for modifying 6FDA-DAM:DABA (3:2) via monoesterification was adapted from the previously reported reaction (see Section 3.1.2) [15]. Figure 5.3 shows the reaction scheme for monoesterification of the 6FDA-DAM:DABA (3:2) backbone with a PEG and the resulting chemical structure of the crosslinkable PEGMC polymer.

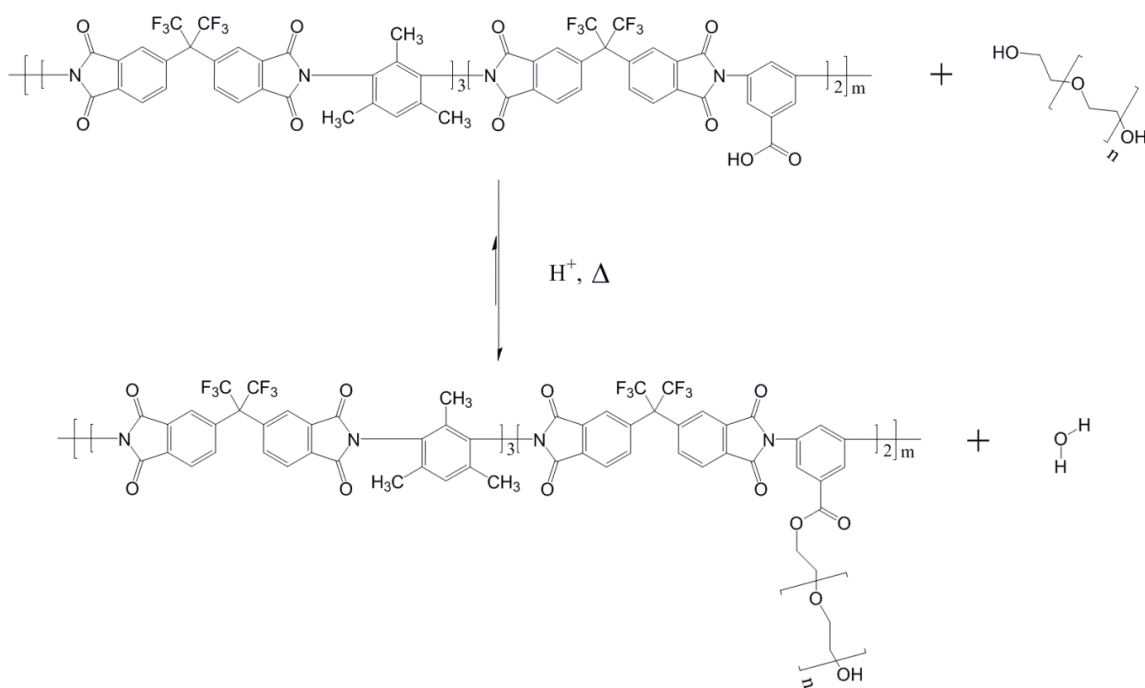


Figure 5.3: PEGMC synthesis reaction via monoesterification of 6FDA-DAM:DABA (3:2) with a short-chain PEG.

Vacuum dried 6FDA-DAM:DABA (3:2) polymer powder from the study described in CHAPTER 4 was dissolved in dry NMP (Sigma-Aldrich, anhydrous 99.5%) to form a 10 wt% solution under N₂ purge (Airgas, UHP grade) at 50°C. After complete dissolution of the polymer, the solution was heated to 130°C and dry toluene (Sigma-Aldrich, anhydrous 99.8%) was added to aid in the removal of H₂O produced during the reaction. Next, 2.5 mg of the acid catalyst para-toluenesulfonic acid (Sigma-Aldrich, 98%) was added per gram of polymer precursor, this was allowed to fully dissolve and mix. A large excess of the short-chain PEG crosslinking agent (40-70 stoichiometric equivalents) was then slowly added to the reactor. Three different crosslinking agents were used in this work: diethylene glycol (DEG, n=1), triethylene glycol (TEG, n=2), and tetraethylene glycol (TetraEG, n=3). Each of the PEGs was obtained from Sigma-Aldrich and had a purity ≥99.0%. The reactor was then maintained at 130°C under N₂ purge for 24 hours while collecting evaporated H₂O and toluene using a Dean-Stark trap to ensure dry reaction conditions throughout the course of the reaction.

After 24 hours, the reactor was cooled to room temperature and then the polymer was precipitated by slowly pouring the solution into a methanol (VWR, ≥99.8%) bath. The precipitate was blended and then washed several times with fresh methanol to remove the NMP solvent and other unused reagents. The PEGMC powder was collected and allowed to dry in a fume hood overnight to remove the majority of the methanol. Any remaining methanol and H₂O were removed by drying the powder under vacuum at 75°C. This low drying temperature was used to ensure that premature crosslinking of the powder did not occur.

GPC experiments were performed on the three PEGMC polymers after the 75°C drying step. The molecular weight and PDI results are shown in Table 5.1.

Table 5.1: GPC results for synthesized PEGMC polymers powders in an uncrosslinked state.

Crosslinking Agent	Mw (kDa)	PDI
DEG	117	3.2
TEG	95	2.6
TetraEG	155	3.8

5.3.2. Crosslinking PEGMC Dense Films

The PEGMC polymers were formed into dense film membranes by knife casting with THF as a volatile solvent. Transesterification crosslinking of the PEGMC materials was achieved by heating the dense films under vacuum conditions. The transesterification reaction and resulting crosslinked PEGMC chemical structure is displayed in Figure 5.4.

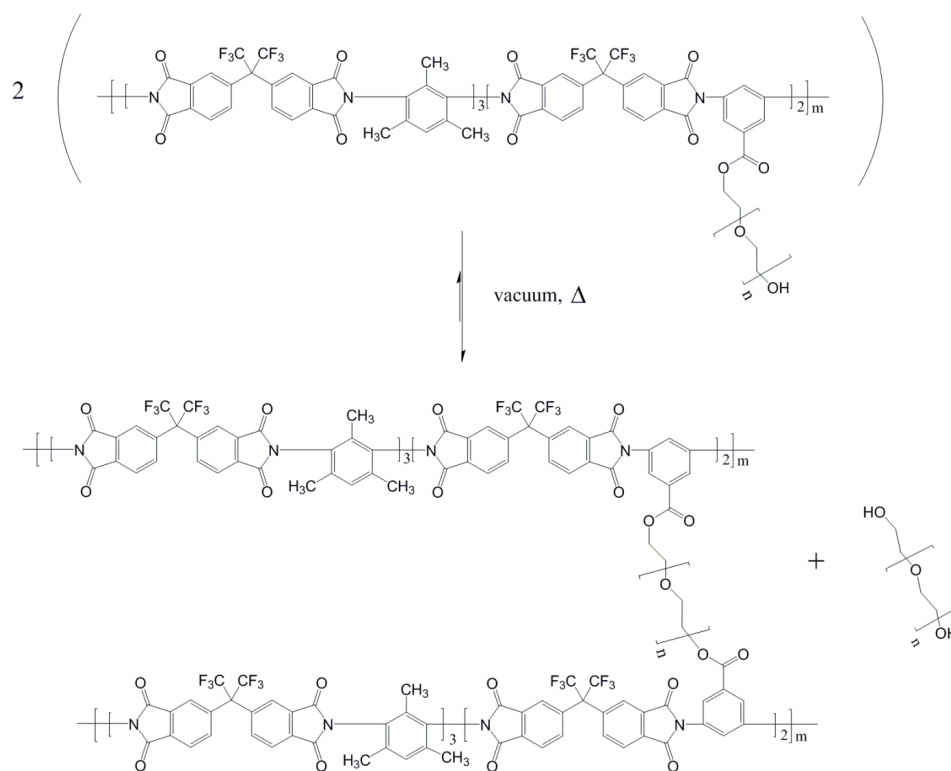


Figure 5.4: Reaction scheme for transesterification crosslinking of PEGMC polymers.

5.4. PEGMC Polymer Properties

5.4.1. PEGMC Synthesis Results

Following synthesis of the PEGMC powders, solution $^1\text{H-NMR}$ was performed in order to probe the chemical structure of the new materials, as well as to determine the extent of monoesterification at the 6FDA-DABA monomer's carboxylic acid site by the various PEG crosslinking agents. Figure 5.5 compares the $^1\text{H-NMR}$ spectra of neat 6FDA-DAM:DABA (3:2) polymer powder with that of the TEG-modified PEGMC powder. The 6FDA-DAM monomer has a single aromatic proton with a peak that does not overlap any other peaks from the polymer or solvents, at a chemical shift of ~ 7.3 ppm, as shown. In the monoesterified PEGMC sample, the methylene proton closest to the ester group is clearly resolved at a chemical shift of $\sim 4.3-4.6$ ppm. It is possible to quantify the conversion of carboxylic acid groups on the 6FDA-DABA monomer to esters by taking the ratio of the area of the methylene peak to the area of the aromatic proton on the 6FDA-DAM monomer and comparing this to the theoretical peak ratio at 100% conversion [12].

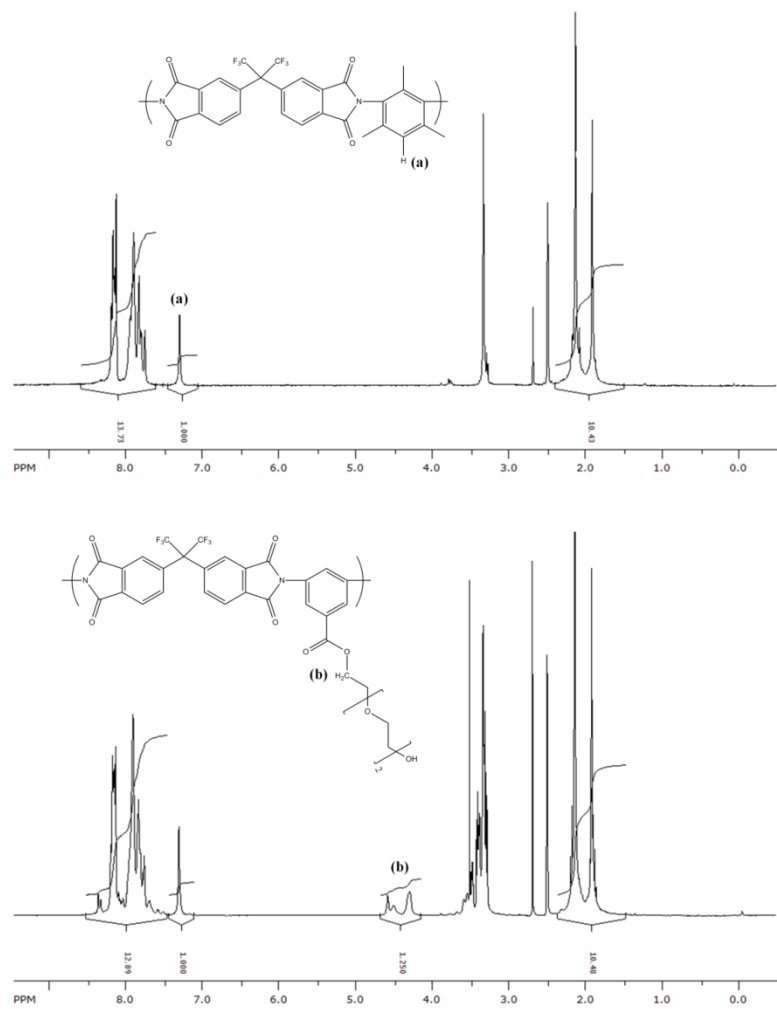


Figure 5.5: ¹H-NMR spectra for neat 6FDA-DAM:DABA (3:2) powder (Top) and monoesterified PEGMC powder using TEG crosslinking agent (Bottom).

$^1\text{H-NMR}$ spectra for the synthesized PEGMC materials with DEG and TetraEG as the crosslinking agents are displayed in Figure 5.6, below.

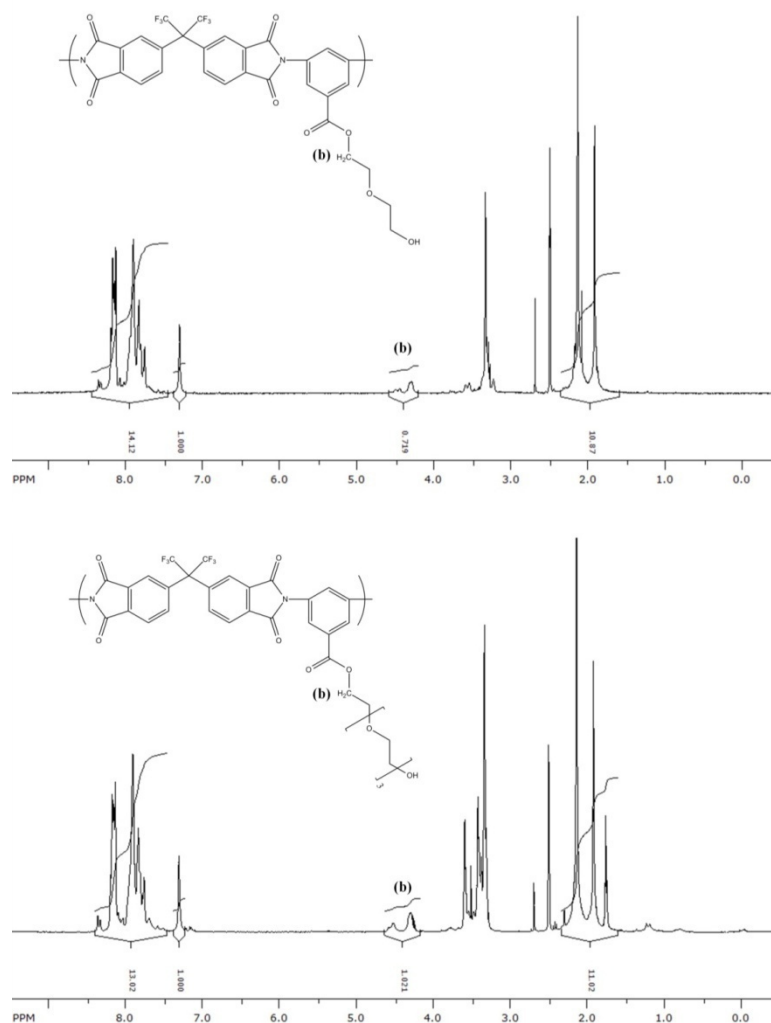


Figure 5.6: $^1\text{H-NMR}$ spectrum of monoesterified (uncrosslinked) PEGMC powers with DEG (Top) and TetraEG (Bottom) crosslinking agents.

Compared to the $^1\text{H-NMR}$ spectrum of unmodified 6FDA-DAM:DABA (3:2), new peaks are visible in the spectra for each of the PEGMC materials in the 3-4 ppm range. These peaks are attributed to the methylene protons of the PEG crosslinker sidechains,

excluding the -CH₂- group nearest the ester bond. The protons associated with the methylene group nearest the ester bond are represented by the peak at ~4.3-4.6 ppm.

The extent of monoesterification of the PEGMC materials can be determined by using Eq. (5.1).

$$\% \text{Monoesterified} = \frac{\left(\frac{A}{B}\right)}{\left(\frac{4}{3}\right)} \times 100 \quad (5.1)$$

In the above equation, *A* represents the area under the peak at ~7.3 ppm, which corresponds to the aromatic proton of the 6FDA-DAM monomer, and *B* represents the area under the peak in the ~4.3-4.6 ppm range, which corresponds to the methylene protons closest to the ester group. The values in the denominator are the theoretical number of protons on a single 6FDA-DAM:DABA (3:2) repeat unit at the same locations described for quantities *A* and *B*, respectively. Figure 5.7 shows the location of these protons on the PEGMC chemical structure.

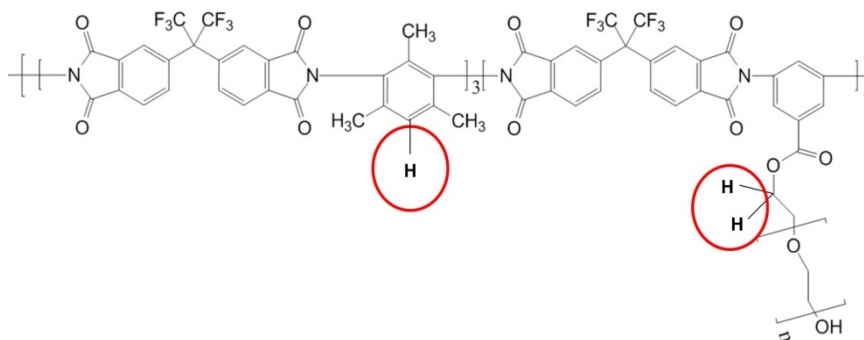


Figure 5.7: The structure of PEGMC is shown and the protons used for calculating monoesterification yield are indicated.

Values for the extent of monoesterification achieved for the PEGMC polymers with DEG, TEG, and TetraEG crosslinking agents are shown in Table 5.2. The greatest

conversion was achieved with the TEG-monoesterified PEGMC material. It has been hypothesized that the NMP solvent may form complexes with the pendant alcohols of the various PEG monoesterification reagents, which might explain the observed incomplete monoesterification despite the large excess of PEG used during synthesis [12]. The measured difference in monoesterification yield with the DEG, TEG, and TetraEG reagents may be due to several factors. These include the length of the linear diol reagent molecule [12], the presence of H₂O in the reactor, and slight fluctuations in reaction conditions.

Table 5.2: Extent of monoesterification of the 6FDA-DAM:DABA (3:2) carboxylic acid sites to form the PEGMC polymers.

Crosslinking Agent	% Monoesterified
DEG	54
TEG	94
TetraEG	77

Despite monoesterification yields below 100% for all the PEGMC samples, the results shown in Table 5.2 indicate that complete crosslinking via the transesterification reaction is possible for all the PEGMC materials that were synthesized. At a minimum, only 50% of the 6FDA-DABA monomers need to undergo monoesterification, since the transesterification reaction may occur either between two monoesterified 6FDA-DABA units or between one monoesterified unit and one unreacted 6FDA-DABA monomer. In the latter case, the pendant crosslinking agent from the monoesterified 6FDA-DABA monomer will form an ester bond with an unreacted carboxylic acid by via condensation of the hydroxyl group.

5.4.2. Crosslinking Efficacy

Several crosslinking temperatures were investigated initially. Films were treated under vacuum at 230°C, 255°C, and 280°C for 18 hours and then cooled gradually down to room temperature. The efficacy of each crosslinking temperature in the different PEGMC films was then probed by placing samples in dry NMP at room temperature and allowing the film to soak for 6 hours. It should be noted that this is a very aggressive test of film stability, since NMP is an excellent solvent for both the base 6FDA-DAM:DABA (3:2) and the uncrosslinked versions of the PEGMC material. The condition of the sample was then evaluated visually, checking for swelling or dissolution. The temperature was progressively increased to 50°C, 75°C, and eventually 100°C over a 24 hour period, with the condition of the sample observed at each temperature. If the film had not dissolved or swollen significantly after soaking at 100°C, crosslinking was deemed to be essentially complete.

The degree of swelling at the beginning and end of these tests is noted in Table 5.3. All of the PEGMC films became at least slightly swollen or were dissolved at room temperature, but this was not viewed as an indication of particularly poor crosslinking or membrane stability due to the aggressive nature of this test.

Table 5.3: Swelling and solubility of PEGMC and unmodified 6FDA-DAM:DABA (3:2) films in NMP solvent.

Crosslinking Agent	Thermal Treatment (°C)	Level of Swelling at Room Temp.	Level of Swelling at 100°C
DEG	230	Moderate	Very High
	255	Moderate	Very High
	280	Low	High
TEG	230	Moderate	Very High
	255	Low	High
	280	Very Low	High
TetraEG	230	Moderate	Very High
	255	Low	High
	280	Low	High
N/A	180	Fully Dissolved	Fully Dissolved
	280	Very High; Mostly Dissolved	Fully Dissolved

Furthermore, the plasticization resistance of PEGMC films that were crosslinked at 230°C, 255°C, and 280°C using TEG as a crosslinking agent were compared by performing pure gas CO₂ and H₂S permeation, as shown in Figure 5.8.

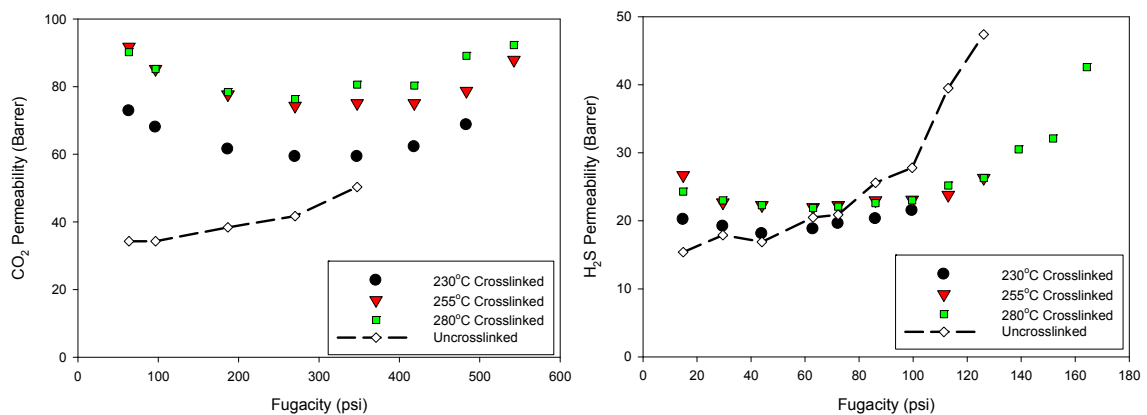


Figure 5.8: Pure gas CO₂ and H₂S permeation at 35°C for PEGMC dense films with a TEG crosslinking agent using several crosslinking temperatures.

Finally, the gel content of crosslinked PEGMC dense films with TEG as the crosslinking agent was measured for the different crosslinking temperatures (Table 5.4). These gel content tests provide a more quantitative measure of the efficacy of a particular crosslinking procedure for the PEGMC films by measuring the fraction of undissolved polymer remaining after an extended solvent soak period. Crosslinked dense film samples were weighed (m_0) before being soaked in anhydrous THF for 48 hrs. The films were then removed from the THF and dried under vacuum at 100°C to remove all residual solvent and moisture. The films were once again weighed (m_1), with the fraction of the sample remaining after the THF soak constituting the sample's gel fraction (GF); Eq. (5.2) shows how gel content was calculated.

$$GF = \frac{m_1}{m_0} \times 100 \quad (5.2)$$

Table 5.4: Gel content of PEGMC films with TEG crosslinking agent.

Thermal Treatment (°C)	Gel Fraction
230	0.96
255	0.97
280	0.99

Ultimately, the 280°C crosslinking temperature was selected for use throughout this dense film study because of the superior membrane stability properties that were obtained in the various tests described above. While minimizing the crosslinking temperature and soak time can be an important consideration for asymmetric membrane morphologies, dense films do not experience the same deleterious changes, such as substructure collapse, that are possible in pore-containing membranes. However, these

effects are considered in CHAPTER 6, which deals with the formation and crosslinking of asymmetric hollow fiber membranes of a PEGMC polymer.

Gel content experiments were also performed on all of the 280°C crosslinked PEGMC films, the results of which are given in Table 5.5.

Table 5.5: Gel content values for 280°C crosslinked PEGMC dense films.

Crosslinking Agent	Gel Fraction
DEG	0.94
TEG	0.99
TetraEG	0.99
N/A (180°C Annealed)	-
N/A (280°C Annealed)	0.36

Despite the range of monoesterification yields shown in Table 5.2, similar gel fraction values were obtained for all the PEGMC samples. This suggests that a very high degree of crosslinking was obtained in all of the PEGMC films, and near-complete monoesterification may not be necessary to achieve significant membrane stability improvement.

Furthermore, the excellent resistance to solvation displayed by the crosslinked PEGMC samples can be specifically attributed to transesterification crosslinking rather than simple high-temperature annealing effects or sub- T_g decarboxylation-induced crosslinking, which has been reported previously for 6FDA-DAM:DABA (3:2) [16-18]. This claim is supported by the fact that the 180°C annealed base polymer samples, which are used throughout the present study, dissolve completely in THF at room temperature, indicating a lack of crosslinking or other strong intermolecular interactions. Additionally, a 6FDA-DAM:DABA (3:2) sample annealed at 280°C was tested to probe the extent of decarboxylation-induced crosslinking at the same treatment temperature

that was used to crosslink the PEGMC films. Although this sample's gel fraction was non-zero, the gel fraction value was much lower than the PEGMC films and the remaining material was very highly gelled, deformed, and non-film-like. On the other hand, it was possible to recover the crosslinked PEGMC samples as intact (although not completely flat) films after the gel content tests. Based on these results, it seems that crosslinking is, in fact, achieved in the PEGMC films via the transesterification scheme given in Figure 5.4, as expected.

5.4.3. Physical Property Analysis

The T_g and density of the PEGMC materials and the base 6FDA-DAM:DABA (3:2) polymer were measured following dense film casting. Values for transesterified (crosslinked) PEGMC samples using the 280°C temperature protocol, are given in Table 5.6. Dense films of the 6FDA-DAM:DABA (3:2) polymer, for which no crosslinking agent was used, are shown for comparison. The change in T_g of crosslinked PEGMC materials compared to 6FDA-DAM:DABA (3:2) is believed to be affected by two main factors: (1) the flexibility of the PEO crosslinks and (2) polymer matrix rigidity due to network formation. These two factors likely exert opposing forces on the resultant T_g of the crosslinked materials. Furthermore, this scenario is complicated by the difference in length of the PEO crosslinks and varying level of monoesterification/crosslinking from one material to the next.

Table 5.6: Properties of the dense films samples used throughout this study.

Crosslinking Agent	Treatment Temperature (°C)	T_g (°C)	ρ (g/cm ³)
DEG	280	374	1.397
TEG	280	384	1.399
TetraEG	280	365	1.398
N/A	180	385	1.402

5.5. PEGMC Pure Gas Transport Properties in Dense Films

5.5.1. Pure Gas Permeation

Pure gas permeation experiments were performed on the three PEGMC films using H_2S , CO_2 , and CH_4 at $35^\circ C$. These results are compared to the pure gas permeation data for 6FDA-DAM:DABA (3:2) films annealed at $180^\circ C$ that was reported in CHAPTER 4. Data are shown for both crosslinked and uncrosslinked PEGMC films for the pure H_2S feed (Figure 5.9 and Figure 5.10) to display the effect of the thermal crosslinking protocol on H_2S permeation.

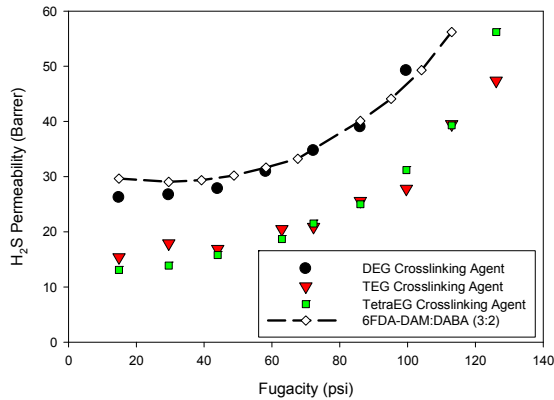


Figure 5.9: Pure H_2S permeation for uncrosslinked PEGMC films and the 6FDA-DAM:DABA (3:2) starting material at $35^\circ C$.

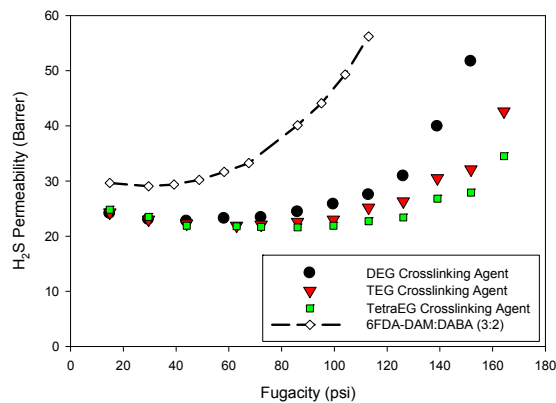


Figure 5.10: Pure H_2S permeation after crosslinking the PEGMC films at $280^\circ C$. Experiments performed at $35^\circ C$.

It is apparent from Figure 5.9 and Figure 5.10 that monoesterification and subsequent transesterification crosslinking of the PEGMC films has several significant effects on H₂S permeation. The uncrosslinked PEGMC films appear to have approximately the same H₂S-induced plasticization resistance and response to plasticization as the unmodified 6FDA-DAM:DABA (3:2) membranes. Essentially, these uncrosslinked materials undergo plasticization upon exposure to even the lowest pure H₂S feed pressures that were tested. There is also a trend towards decreasing H₂S permeability in the uncrosslinked PEGMC films as the crosslinking agent is changed from DEG to TEG and then TetraEG. Furthermore, the PEGMC films have lower H₂S permeability than the 6FDA-DAM:DABA (3:2) base material. This is likely the result of the flexible pendant PEG groups that contain polar ester and hydroxyl moieties, which increase intra- and interchain interactions within the polymer matrix and improve chain packing.

Figure 5.10 demonstrates that crosslinking is an effective means of suppressing undesirable swelling-induced effects for all of the PEG crosslinking agents used. Each of the PEGMC films show a marked improvement in stability against H₂S feeds after crosslinking, and their ability to withstand H₂S-exposure far exceeds that of 6FDA-DAM:DABA (3:2). A significant upswing in H₂S permeability through the crosslinked PEGMC films is not observed until the membranes are exposed to approximately 90 psi of H₂S. Additionally, the plasticization response with pure H₂S feeds in these crosslinked materials seems to be less severe than in the base material, which indicates that performance losses under these conditions are likely to be suppressed. This level of resistance to H₂S-induced performance degradation is expected to be sufficient for most sour gas processing applications.

In addition to improved plasticization resistance upon crosslinking, the H₂S permeability of TEG and TetraEG crosslinked PEGMC films is increased. This effect has been observed by other researchers using alternative transesterification crosslinking agents with 6FDA-based polyimides [13, 19, 20]. These authors postulate that the increased permeability after crosslinking results from the insertion of the crosslinking segments between polymers chains that act to disrupt chain packing – essentially serving as “spacers” between adjacent polymer chains. Additionally, the simultaneous elimination of a fraction of the large, bulky pendant PEG groups that occurs during transesterification crosslinking may create free volume within the polymer matrix. This explains the significant increase in permeability of the films that were crosslinked with TEG and TetraEG, but not DEG, since the degree of monoesterification is much higher in the former two cases (Table 5.2). It is somewhat surprising that the three PEGMC films have such similar H₂S permeability values at low H₂S feed pressures. However, the relative difference in chemical makeup of the three PEGMC materials, assuming complete crosslinking, is minor relative to the polymer structure as a whole, so large deviations in permeation properties are not likely.

The pure gas permeation isotherms for CO₂ and CH₄ feed gases are shown in Figure 5.11. Again, the results for crosslinked PEGMC films are shown alongside those for 6FDA-DAM:DABA (3:2). As with H₂S permeability, the CO₂ and CH₄ permeabilities of the three PEGMC materials fall below that of the unmodified base material. The PEGMC materials appear to have excellent CO₂-induced plasticization resistance, relative to the 6FDA-DAM:DABA (3:2) films. The CO₂ permeability of these films does not experience a significant increase that can be attributed to plasticization until greater than 350 psi feed pressure.

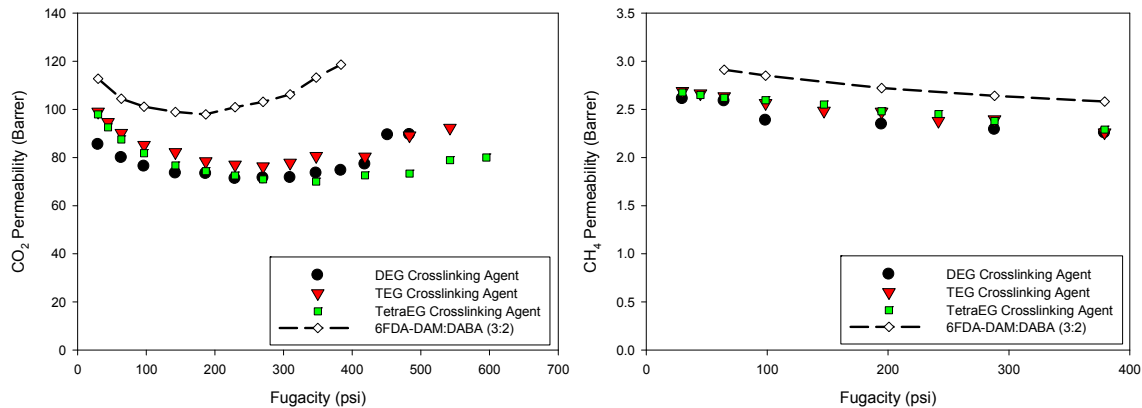


Figure 5.11: Pure CO₂ and CH₄ permeation isotherms at 35°C for PEGMC dense films and 6FDA-DAM:DABA (3:2).

Ideal selectivity values for the H₂S/CH₄ and CO₂/CH₄ separations can be calculated from the pure gas permeation isotherms. These values are tabulated in Table 5.7. It should be noted that the previous investigation of 6FDA-DAM:DABA (3:2) dense films showed significant positive deviations from the ideal H₂S/CH₄ selectivity when mixed gas feeds were used. A similar effect was expected for the PEGMC materials and was, in fact, observed.

Table 5.7: Ideal selectivity values for sour gas separations in crosslinked PEGMC and unmodified 6FDA-DAM:DABA (3:2) films at 65 psi feed pressure and 35°C.

Crosslinking Agent	$\alpha^*_{\text{H}_2\text{S}/\text{CH}_4}$	$\alpha^*_{\text{CO}_2/\text{CH}_4}$
DEG	9.0	30
TEG	8.3	34
TetraEG	8.3	33
N/A	10 ^a	36

^aThe H₂S/CH₄ value for 6FDA-DAM:DABA (3:2) corresponds to 30 psi feed pressure to avoid plasticization effects.

5.5.2. Pure Gas Sorption

Pure gas sorption was performed on PEGMC dense films that had been crosslinked at 280°C with DEG, TEG, and TetraEG crosslinking agents. The results of H₂S and CH₄ pure gas sorption experiments are shown in Figure 5.12.

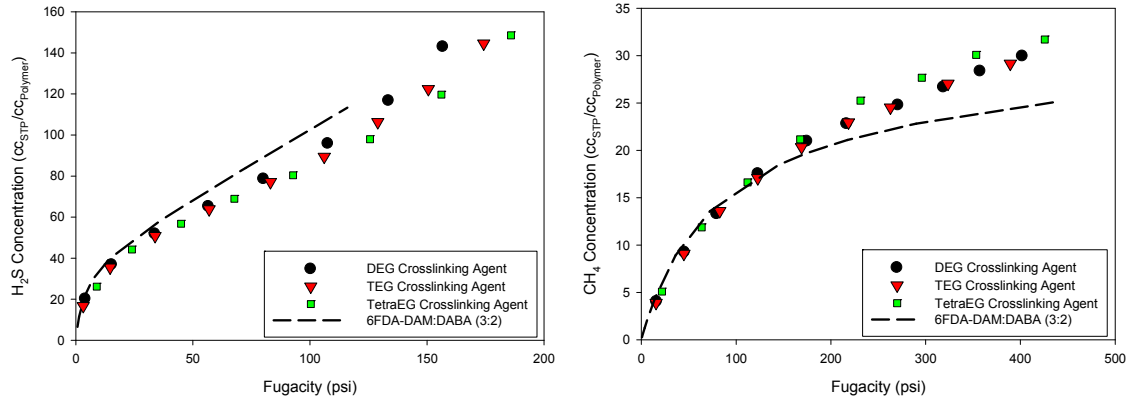


Figure 5.12: Pure gas H₂S and CH₄ sorption isotherms at 35°C for crosslinked PEGMC dense films. The 6FDA-DAM:DABA (3:2) dual-mode model fit is shown for comparison.

The dual-mode sorption model was fit to each of the sorption isotherms using only the data prior to the onset of strong membrane swelling, as indicated by a deviation from linear Henry's Law sorption at high feed pressures Table 5.8 gives the best fit dual-mode parameters for these materials for H₂S and CH₄ sorption.

Table 5.8: Dual-mode sorption model parameters^a for pure H₂S and CH₄ in crosslinked PEGMC and uncrosslinked 6FDA-DAM:DABA (3:2) [N/A] films.

Crosslinking Agent	H ₂ S			CH ₄		
	k_D	C_H	b	k_D	C_H	b
DEG	0.54±0.03	38±2	0.22±0.01	(2.1±0.1)×10 ⁻²	27±1	(9.7±0.5)×10 ⁻³
TEG	0.49±0.02	39±2	0.20±0.01	(1.9±0.1)×10 ⁻²	28±1	(9.0±0.5)×10 ⁻³
TetraEG	0.45±0.02	43±2	0.12±0.01	(1.9±0.1)×10 ⁻²	32±2	(7.6±0.4)×10 ⁻³
N/A	0.66±0.03	38±2	0.26±0.01	(4.4±0.2)×10 ⁻²	27±1	(1.3±0.1)×10 ⁻²

^a k_D [cc_{STP}/(cc_{Polymer}·psi)], C_H [cc_{STP}/cc_{Polymer}], b [1/psi]

As the crosslinking agent is changed to larger PEGs, sorption in the Langmuir mode sorption sites become more heavily favored compared to Henry's Law sorption. This may be explained by the introduction of additional free volume after the transesterification crosslinking reaction due to elimination of a fraction of the pendant PEG groups, as discussed previously.

It is interesting to note that H₂S solubility in the crosslinked materials at high H₂S feed pressures (> 45 psi) lies below the level that was measured in the base 6FDA-DAM:DABA (3:2) material. This is likely due to the reduced level of polymer matrix swelling, even prior to the onset of plasticization in the uncrosslinked material, which is caused by crosslinking. On the other hand, CH₄ solubility at high feed pressures (> 175 psi) in the crosslinked materials appears to be slightly greater in the crosslinked films than in the unmodified material. The crosslinked films have significantly higher Henry's Law constants for CH₄ than the base 6FDA-DAM:DABA (3:2) material, which may result from the incorporation of short alkane segments during the crosslinking reaction. Overall, this means that the ideal sorption selectivity of the modified crosslinked materials at high feed pressures is actually lower than that of the unmodified 6FDA-DAM:DABA (3:2) polymer. Since we hypothesized that the incorporation of PEO segments into the membrane would improve H₂S/CH₄ permselectivity through augmented H₂S/CH₄ sorption selectivity, these effects were unexpected.

However, we have observed large deviations from ideal membrane performance when mixed sour gas feeds are used, and the largest contributor to these deviations is likely to be solubility. As a result, these somewhat surprising pure gas sorption results are not of particular concern to membrane performance as a whole, especially since the mixed gas permeation results for these materials showed excellent H₂S/CH₄ permselectivity. So, while the pure gas sorption data presented here is informative, it

likely does not accurately reflect the levels of individual gas sorption under mixed gas feed conditions.

Figure 5.13 shows the pure CO₂ sorption results for the TEG crosslinked material. The dual-mode sorption model best fit parameters are given in Table 5.9. Similar to H₂S sorption, pure gas CO₂ solubility in the crosslinked material lies slightly below that of the base 6FDA-DAM:DABA (3:2) polymer.

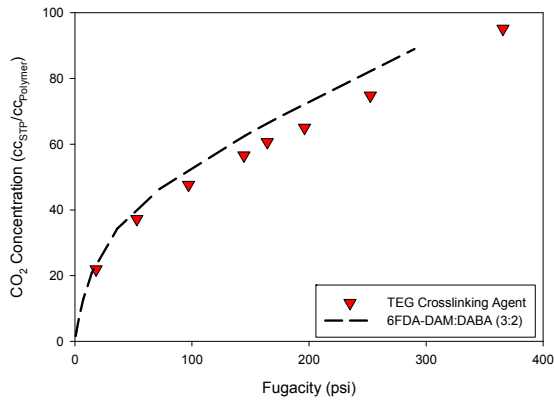


Figure 5.13: Pure CO₂ sorption isotherm for TEG crosslinked PEGMC at 35°C.

Table 5.9: Dual-mode sorption parameters^a for pure CO₂ sorption in TEG crosslinked PEGMC and uncrosslinked 6FDA-DAM:DABA (3:2) [N/A]at 35°C.

Crosslinking Agent	CO ₂		
	k_D	C_H	b
TEG	0.16±0.01	37±2	(6.0±3)×10 ⁻²
N/A	0.16±0.01	44±2	(5.0±3)×10 ⁻²

^a k_D [CC_{STP}/(CC_{Polymer}·psi)], C_H [CC_{STP}/CC_{Polymer}], b [1/psi]

5.5.3. Pure Gas Diffusion Analysis

The pure gas diffusion coefficient isotherms for PEGMC that was crosslinked at 280°C with TEG were calculated from the pure gas permeation and sorption isotherms and through Eq. (2.12). Permeability values below the CO₂ and H₂S plasticization pressures were the only data points that could be used during these calculations.

Because of the improved plasticization resistance of crosslinked PEGMC over the base 6FDA-DAM:DABA (3:2) polymer, this restriction was not as limiting as was the case in Section 4.4.3. The diffusion coefficient isotherms for 280°C crosslinked PEGMC (TEG crosslinker) dense films are given in Figure 5.14.

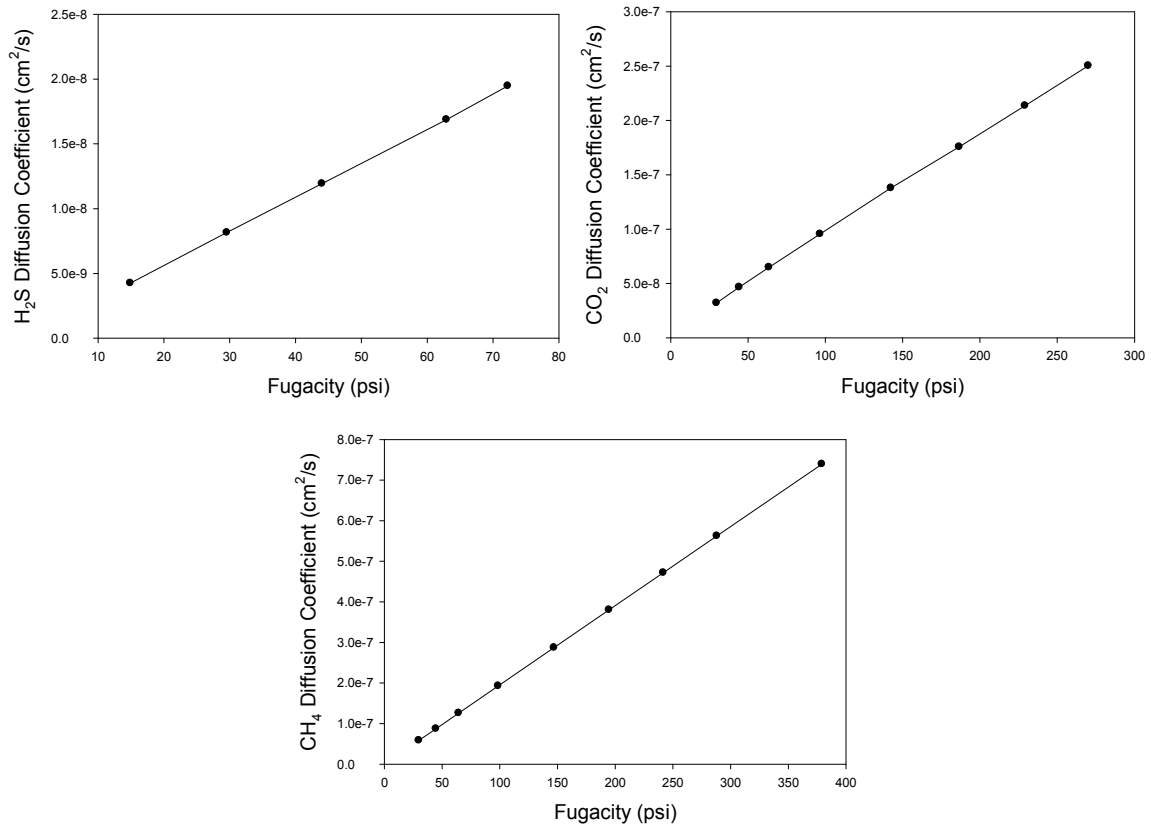


Figure 5.14: Pure gas diffusion coefficients at 35°C for TEG crosslinked PEGMC.

The diffusion coefficients represented in Figure 5.14 are average diffusion coefficient values for the membrane as a whole. In addition, the dual-mobility model can be used in conjunction with the dual-mode sorption model parameters to determine the specific diffusion coefficients of CO₂, H₂S, and CH₄ through the Langmuir and Henry's law regimes, D_H and D_D . The results of these dual-mobility model calculations are shown in Table 5.10.

Table 5.10: Dual-mobility model parameters for 280°C crosslinked PEGMC at 35°C. Values were calculated using pure gas permeation and sorption data.

	TEG Crosslinking Agent		
	H ₂ S	CO ₂	CH ₄
<i>K</i>	16	14	13
<i>F</i>	0.037	0.077	0.024
<i>D_D</i> × 10 ⁻⁸ (cm ² /s)	2.2	24	5.9
<i>D_H</i> × 10 ⁻⁸ (cm ² /s)	0.083	1.8	0.14

It was observed in Section 4.4.3 that the Henry's law regime diffusion coefficient of H₂S was significantly lower than the values for CO₂ and CH₄. While this trend still holds true, it is not as pronounced in the TEG crosslinked PEGMC material as in the base 6FDA-DAM:DABA (3:2) polymer – the H₂S Henry's law diffusivity is greater in the PEGMC material and the CH₄ value is significantly lower. These two effects are attributed to a few changes with the membrane material.

First, the substitution of the very polar carboxylic acid groups for less polar ester linkages and the addition of flexible, slightly polar PEO-containing crosslinkers into the matrix are believed to be responsible for the increase in H₂S diffusivity. The diffusion of the highly polar H₂S gas through these materials is likely to be influenced by dipole-dipole interactions to a much greater extent than the other sour gas components (even the quadrupolar CO₂ gas). Therefore, reducing the polarity of functional groups along the membrane's polymer backbone is likely to reduce so-called 'stickiness' of H₂S within the polymer matrix and increase diffusivity. On the other hand, the diffusivity of CH₄ in the Henry's law regime is believed to have experienced a reduction following the crosslinking reactions as a result of an overall increase in polymer matrix rigidity. Increased membrane rigidity in crosslinked PEGMC compared to the unmodified 6FDA-DAM:DABA (3:2) polymer arises from the high-temperature (280°C) thermal crosslinking reaction, which presumably has the same effects on free volume and polymer chain

interactions as thermal annealing, and the covalent crosslinking reaction, which further restricts polymer chain segmental mobility.

5.6. Mixed Gas Transport

5.6.1. Ternary (20% H₂S / 20% CO₂ / 60% CH₄) Sour Gas Mixture Permeation

Mixed gas permeation was performed on the crosslinked PEGMC and 6FDA-DAM:DABA (3:2) dense films. In this study, a feed mixture representative of highly aggressive sour gas reserves was used. The mixture consisted of 20% H₂S, 20% CO₂, and 60% CH₄. Based on typical US pipeline specification values (Table 1.1), the concentration of both of the acid gas contaminants would have to be drastically reduced prior to pipeline transport if this composition was to be produced in the field. The bulk removal of H₂S and CO₂ using membranes might be considered in such a situation. The results of mixed gas permeation for the tested materials are shown below. As previously mentioned, all the data points presented are an average of at least three measurements and error in permeability is generally less than $\pm 5\%$ of the values shown. Each data point was collected after a minimum of 8 hours at the feed condition of interest and following rigorous checks to confirm that steady-state permeation had been achieved. Permeability creep, which can result from membrane conditioning associated with polymer chain rearrangement, was not found to cause any significant change in permeability over the relatively short time scale of each experiment as a whole. Figure 5.15 gives the H₂S/CH₄ selectivity of these materials for feed pressures up to 900 psi; CO₂/CH₄ selectivity values are shown in Figure 5.16.

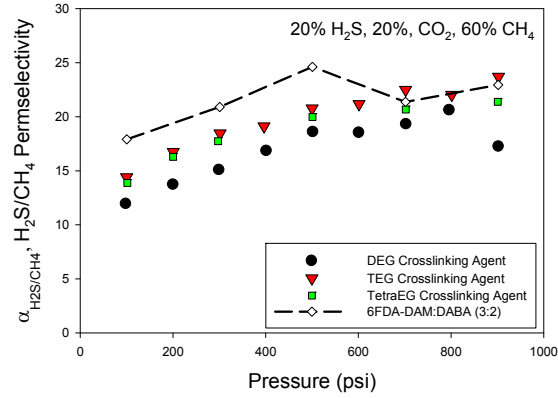


Figure 5.15: Mixed gas H₂S/CH₄ permselectivity of crosslinked PEGMC dense films at 35°C.

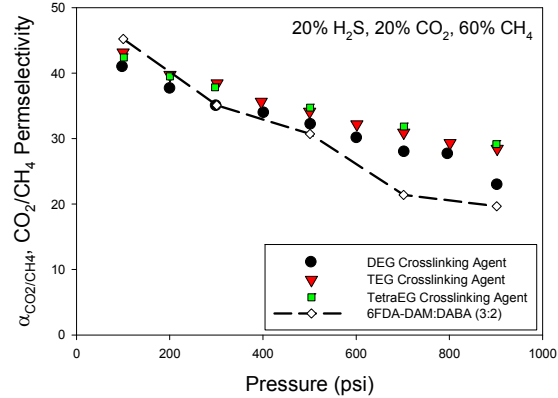


Figure 5.16: Mixed gas CO₂/CH₄ permselectivity of crosslinked PEGMC dense films at 35°C.

Based on the mixed gas H₂S/CH₄ permselectivity data alone, it appears that unmodified 6FDA-DAM:DABA (3:2) may actually be a viable membrane material for this sour gas separation. The H₂S/CH₄ selectivity of 6FDA-DAM:DABA (3:2) is greater than the crosslinked films at low pressure, and is outperformed only by the TEG-crosslinked PEGMC membrane at the top of the pressure range that was tested. However, inspection of the CO₂/CH₄ selectivity results gives a more complete picture of the separation. Again, 6FDA-DAM:DABA (3:2) appears to have a slight advantage at the very low end of the pressure range, where swelling and plasticization are less of a

concern. As the feed pressure is increased, though, the CO₂/CH₄ selectivity of the base material falls off much more quickly than the crosslinked PEGMC films, ultimately reaching a modest level of approximately 20 at the high end of the pressure range that was tested.

It is clear from the CO₂/CH₄ results that a significant degree of plasticization occurs in the 6FDA-DAM:DABA (3:2) film over the course of the experiment. Although a moderate level of swelling actually benefits the H₂S/CH₄ separation, making the 6FDA-DAM:DABA (3:2) film look superior to the PEGMC films, it is highly undesirable from a long-term membrane stability standpoint and for maintaining acceptable CO₂/CH₄ separation performance. In light of these considerations, it is likely that the crosslinked PEGMC materials are indeed better suited for aggressive sour gas feeds such as the mixture used in this work. In particular, the film with the TEG crosslinking agent is promising due to its high H₂S/CH₄ permselectivity at the top end of the pressure range and its excellent CO₂/CH₄ permselectivity over the course of the test. Even with a feed pressure of 900 psi – which corresponds to values of 120 psi H₂S and 140 psi CO₂, in terms of fugacity on the upstream face of the membranes – the TEG-crosslinked PEGMC film has outstanding selectivity for both of the acid gases.

Mixed gas permeability isotherms for H₂S, CO₂, and CH₄ are given in Figure 5.17. These graphs shed more light on the degree of swelling and plasticization within the various films that were tested. The CH₄ permeability data, especially, indicates that the uncrosslinked 6FDA-DAM:DABA (3:2) film lacks the level of stability in the presence of H₂S and CO₂ that is offered by the crosslinked PEGMC films. The fact that CH₄ permeability in the base material more than triples over the course of the experiment suggests that the uncrosslinked polymer chains become highly swollen and lose much of their capacity to perform separations based on size discrimination, which is the normal

separation mode for the CO₂/CH₄ separation in these materials. These trends would result in large losses of valuable CH₄ into the permeate, which would be potentially reinjected as a waste stream in the reservoir.

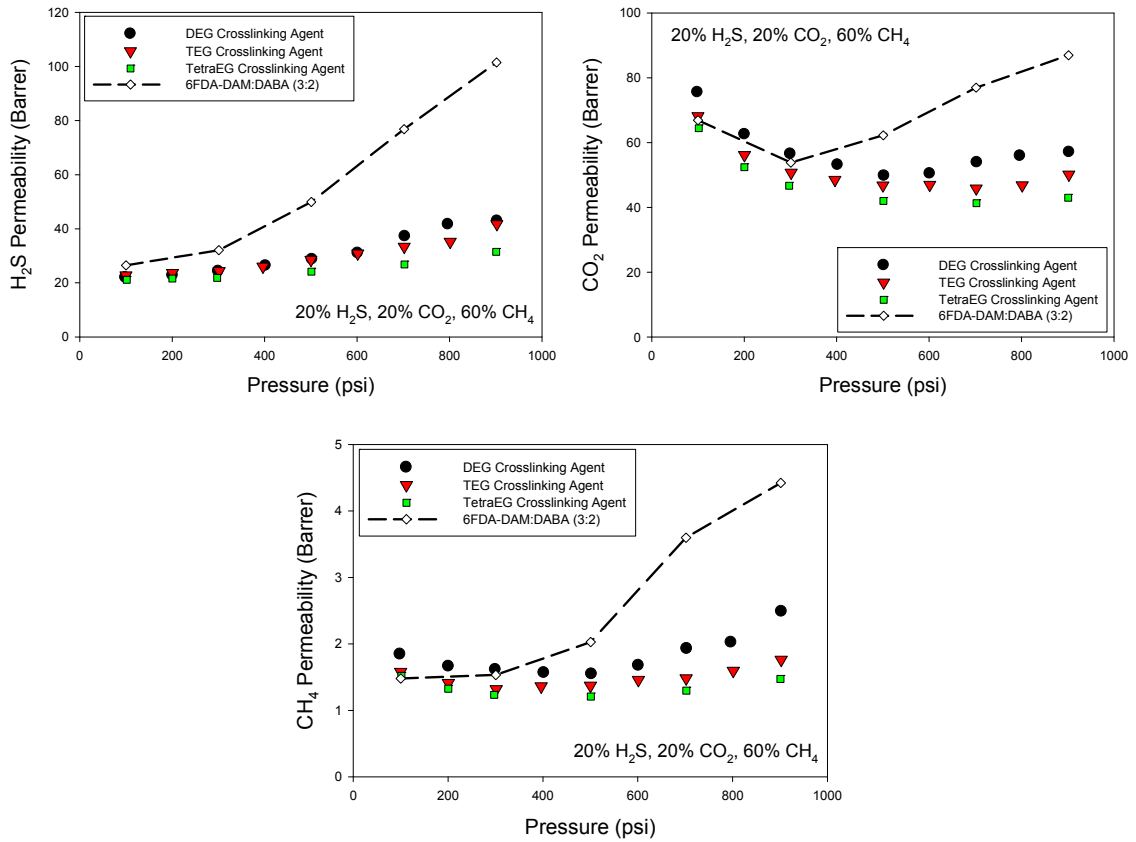


Figure 5.17: Crosslinked PEGMC sour gas permeability at 35°C for a 20% H₂S, 20% CO₂, 60% CH₄ mixed gas feed.

It is also interesting to note that the H₂S permeability of all the films, including the crosslinked PEGMC films, increases with increasing feed pressure. This is expected due to the very high condensability of H₂S and its capacity to form polymer-penetrant interactions with the polymer backbone that is used in all of these materials. However, whereas the unmodified 6FDA-DAM:DABA (3:2) film experiences uncontrolled swelling and, ultimately, plasticization, the swelling levels within the crosslinked PEGMC films are

restricted by the intra- and inter-chain covalent crosslinks. This allows the PEGMC films to accept additional H₂S sorption as the feed pressure is increased without sacrificing much of the size sieving character that imparts high CO₂/CH₄ permselectivity. The inclusion of PEO units within the crosslinks means that when controlled swelling takes place, H₂S molecules gain better access to the favorable H₂S sorption sites. We postulate that this leads to greater overall H₂S/CH₄ permselectivity due to the additional H₂S/CH₄ sorption selectivity imparted by the PEO subunits.

5.6.2. Non-Zero Downstream Pressure Ternary Sour Gas Mixture Permeation

The 20% H₂S, 20% CO₂, 60% CH₄ mixed gas was used to test the effect of non-vacuum downstream pressure on the separation performance of the 280°C crosslinked PEGMC material with TEG as the crosslinking agent. The permeations system used for these tests was a slightly modified isochoric dense film system, as described in Section 4.5.3.

The results of non-vacuum dense film permeation with this sour gas mixture are shown in Figure 5.18. Only a limited number of data points were collected due to the extended experimentation time required to reach 760 Torr downstream pressure.

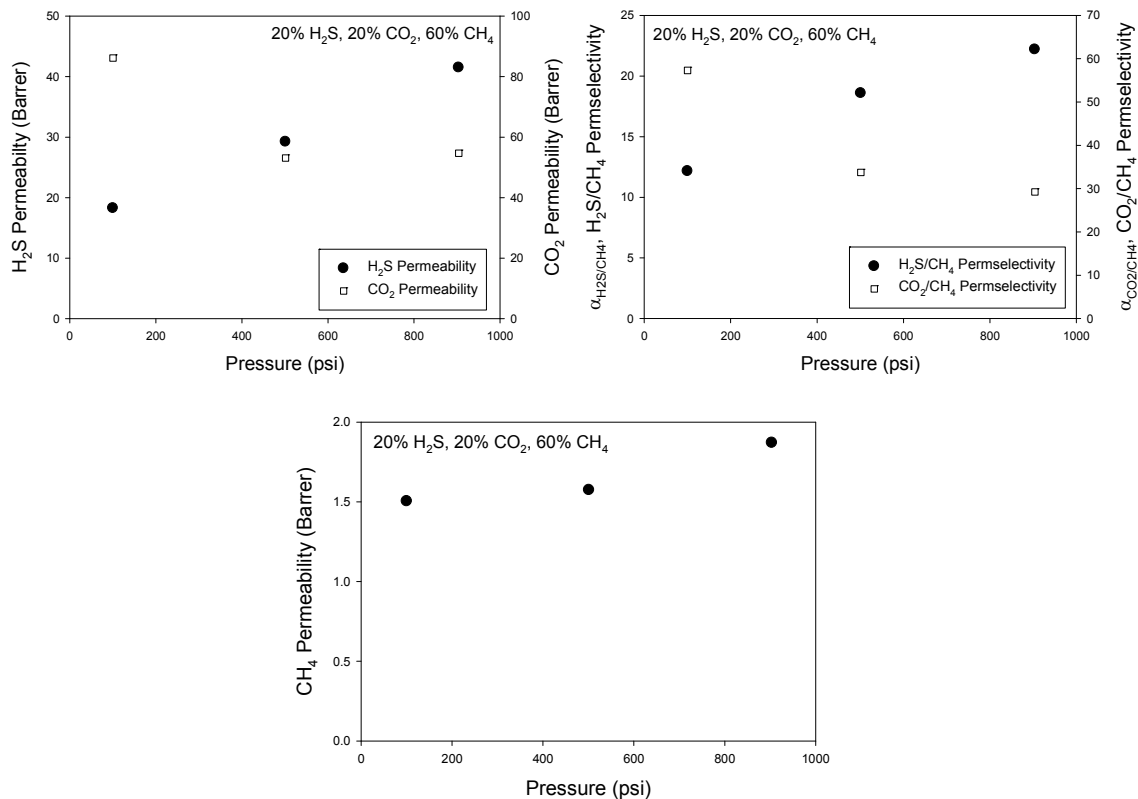


Figure 5.18: Non-vacuum-downstream pressure permeation results for TEG crosslinked PEGMC with a 20% H₂S, 20% CO₂, 60% CH₄ feed.

As discussed in Section 4.5.4, non-vacuum-downstream permeation conditions are expected to favor plasticization. This is due to higher average sorbed concentrations of penetrant gases, particularly the fast gases CO₂ and H₂S for sour gas separations, throughout the membrane.

In Figure 5.18, it appears that the CH₄ permeability of the crosslinked PEGMC material increases slightly more rapidly than was observed under vacuum downstream permeations conditions (Figure 5.17). However, the CO₂/CH₄ and H₂S/CH₄ permselectivity values obtained for the non-vacuum-downstream case are in close agreement with the values collected previously with vacuum-downstream conditions. Therefore, it appears that the transesterification crosslinking reaction used with the

PEGMC membrane imparts sufficient stability into the polymer matrix to prevent plasticization under these more challenging feed conditions. Based on this, it seems the crosslinked PEGMC membrane material is well-suited for the more realistic non-vacuum operating conditions that are likely to be encountered in the field. This an important result to obtain for membranes in the dense film morphology and indicates that the PEGMC material will likely be able to stand up to isobaric permeation experimentation once it is formed into asymmetric hollow fibers. This hypothesis is tested in CHAPTER 7.

5.6.3. Binary (20% CO₂ / 80% CH₄) Acid Gas Mixture (A) Permeation

A binary acid gas mixture consisting of 20% CO₂ and 80% CH₄ was used for permeation experiments with the TEG crosslinking agent PEGMC material that had been crosslinked at 280°C. These permeation results are shown in Figure 5.19.

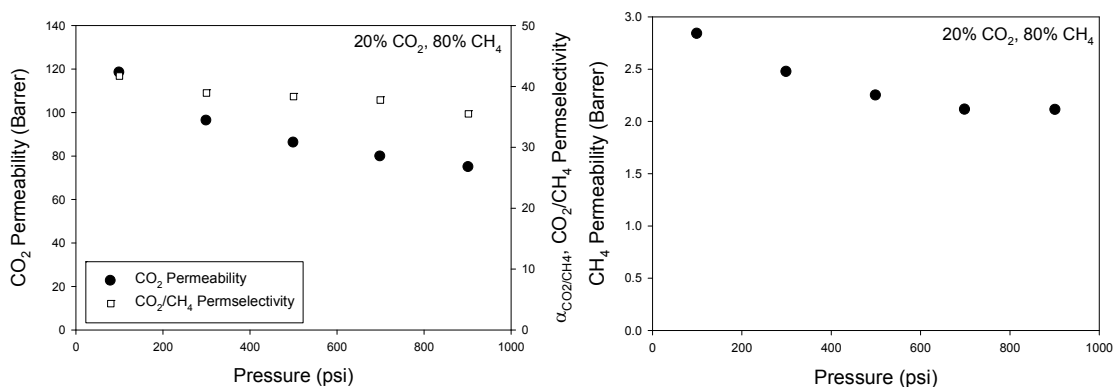


Figure 5.19: Permeation results for 20% CO₂, 80% CH₄ mixture with TEG crosslinked PEGMC, crosslinked at 280°C.

The crosslinked PEGMC dense film does not show any indication of penetrant-induced plasticization under the feed conditions used in these tests. CO₂/CH₄ permselectivity is very stable at approximately the ideal selectivity value that was measured using pure gas feeds.

Similar to the effect described in Section 4.5.5, the CO₂ and CH₄ permeability values that were measured for this binary non-sour mixture are in good agreement with the pure gas CO₂ and CH₄ permeability values. This result is in sharp contrast to the measured CO₂ and CH₄ permeability values for H₂S-containing mixed gas feeds, when the permeation rates are significantly depressed compared to the pure gas levels.

5.6.4. Binary (50% CO₂ / 50% CH₄) Acid Gas Mixture (B) Permeation

A second binary non-sour gas mixture comprised of 50% CO₂, 50% CH₄ was used to test TEG crosslinked PEGMC dense films. This more aggressive acid gas mixture corresponds to a CO₂ fugacity of 335 psi in the feed at the highest pressure that was tested. Results of these permeation experiments are shown in Figure 5.20.

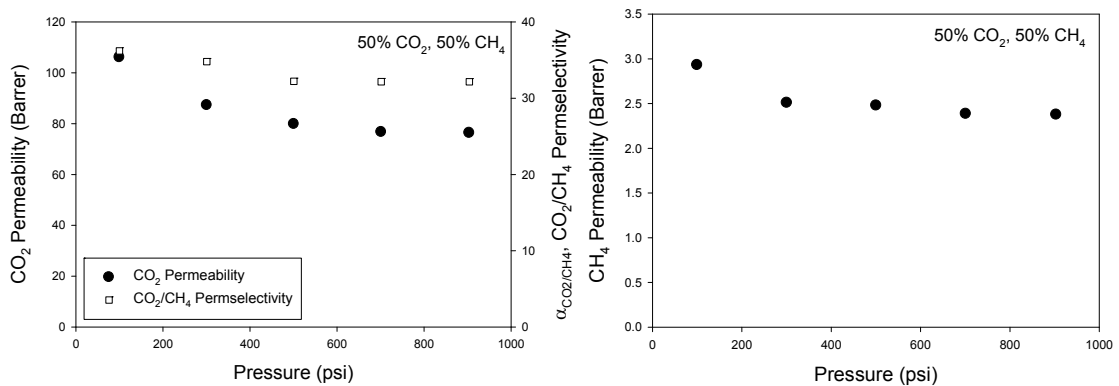


Figure 5.20: Mixed gas (50% CO₂, 50% CH₄) permeation at 35°C for PEGMC with TEG crosslinking agent.

Despite the higher CO₂ partial pressure in the feed compared to the 20% CO₂, 80% CH₄ mixture, there is still no sign of CO₂-induced plasticization in the 280°C crosslinked PEGMC material. The permselectivity and permeability values for both components are, again, in good agreement with the pure gas results. The CO₂ and CH₄

permeability depression phenomenon that has been observed for sour gas mixtures is not present with this 50% CO₂, 50% CH₄ feed.

5.6.5. Mixed Gas Sorption Calculations

The dual-mode sorption model for mixed gas feeds can be used to gain insight into gas sorption levels under realistic, mixed gas feed conditions that correspond to a few of the mixed gas permeation tests performed in this work. Figure 5.21 and Figure 5.22 shows the predicted H₂S, CO₂, and CH₄ sorption isotherms for pure mixed gas feeds in the base 6FDA-DAM:DABA (3:2) material and the crosslinked TEG-modified PEGMC material. These predictions are calculated from the best-fit dual-mode model parameters listed in Table 5.8 and Table 5.9. A binary non-sour gas mixture consisting of 20% CO₂ and 80% CH₄ is assumed in the first figure and a ternary sour gas mixture with 20% H₂S, 20% CO₂ and 60% CH₄ is used for the second set of calculations.

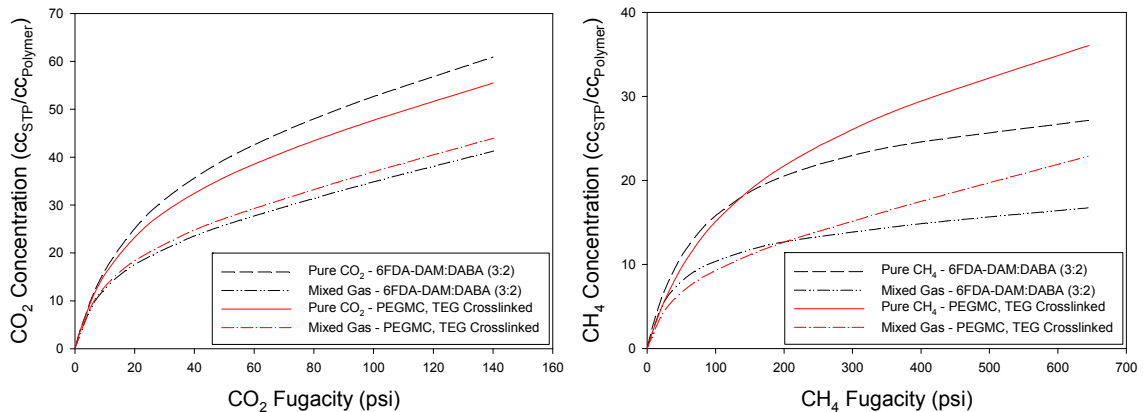


Figure 5.21: Dual-mode sorption model calculations for pure and mixed gas (20% CO₂, 80% CH₄) feeds at 35°C.

The sorption calculations associated with the binary mixture are not particularly surprising. CO₂ and CH₄ experience a decrease in sorbed concentration when going from pure to mixed gas feeds, and this is associated with competition for Langmuir

sorption sites. The CH_4 sorption decrease in the PEGMC material appears to be somewhat greater than the CO_2 sorption decrease. This suggests that mixed gas permeation may result in greater CO_2/CH_4 permselectivity values than pure gas permeation because of these sorption effects. Such an effect was, in fact, observed for a 20% CO_2 , 80% CH_4 mixture compared to the ideal CO_2/CH_4 selectivity.

The ternary sour gas mixture results in more complex sorption projections compared to the binary mixture discussed above. These results are given in Figure 5.22. As a result of the high Langmuir affinity constant values associated with H_2S , the difference between the pure and mixed gas sorption isotherms is relatively minor. CO_2 sorption experiences a more pronounced depression under mixed gas feed conditions, but CH_4 sorption is reduced to an even greater extent. Again, this is a result of the very low Langmuir affinity constant of CH_4 compared to the other two species with which it competes for Langmuir sorption sites. These results imply that $\text{H}_2\text{S}/\text{CH}_4$ and CO_2/CH_4 permselectivity under mixed gas feed conditions should exceed the ideal selectivity values, provided swelling or plasticization is not a major factor.

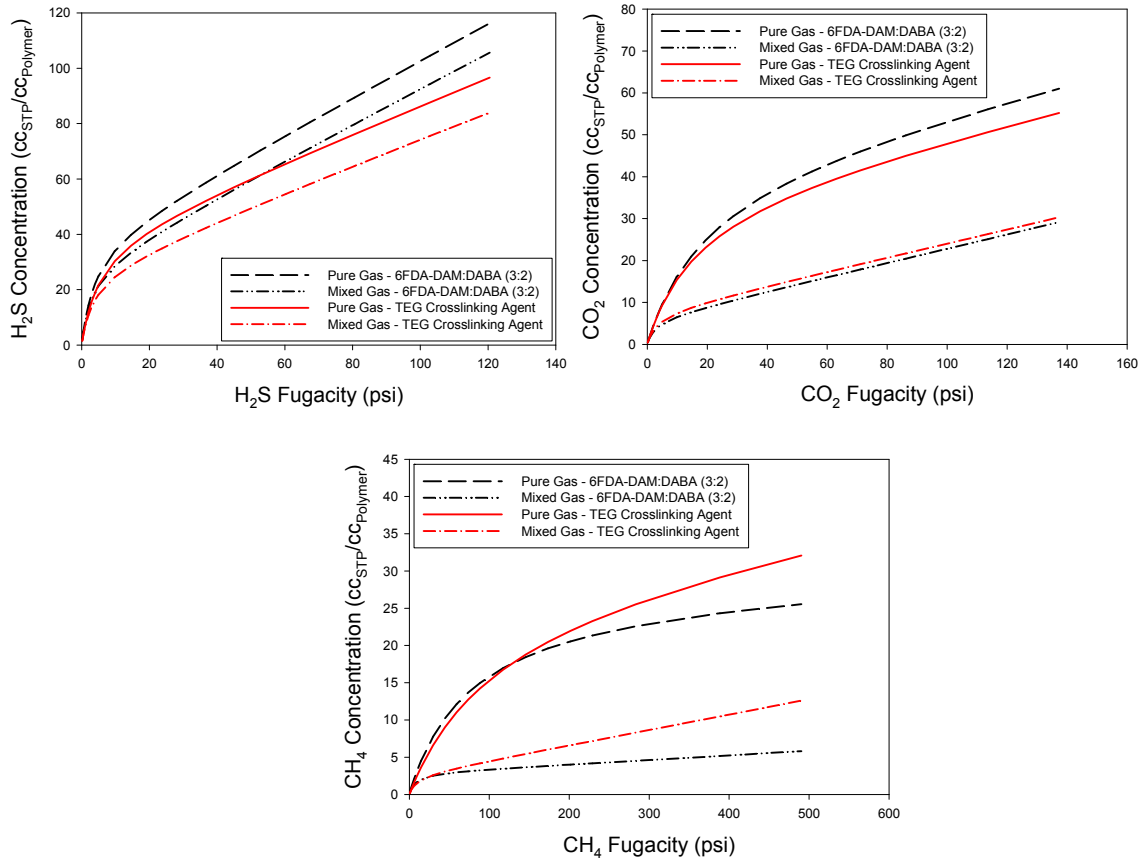


Figure 5.22: Pure and mixed gas (20% H₂S, 20% CO₂, 60% CH₄) sorption isotherms at 35°C for 6FDA-DAM:DABA (3:2) and TEG crosslinked PEGMC at 35°C.

Based on the mixed gas sorption calculations, it is clear that strong competitive sorption effects exist in these sour gas separation systems. This reinforces the finding that pure gas permeation and sorption results alone are not likely to reflect the selectivity of these membranes under more realistic feed conditions consisting of multiple feed species. Although the mixed gas sorption predictions are a good starting point, mixed gas sorption experiments would be a more powerful tool for evaluating membrane performance for sour gas separations. This would allow for calculation of the actual sorption selectivity contribution to overall membrane permselectivity, and would provide valuable insight regarding the competitive sorption effects that obviously play a major

role in sour gas transport through these materials. Unfortunately, these tests were beyond the scope of the current study and equipment available.

5.6.6. Mixed Gas Permeation Modeling

Figure 5.23 presents experimental permeability data from Section 5.5.1 alongside the partial immobilization model predictions for pure H₂S, CO₂, and CH₄ permeability through the TEG crosslinked PEGMC dense films crosslinked at 280°C. There is close agreement between the experimental permeation data and the model predictions before the onset of H₂S- and CO₂-induced plasticization and for the entire CH₄ isotherm.

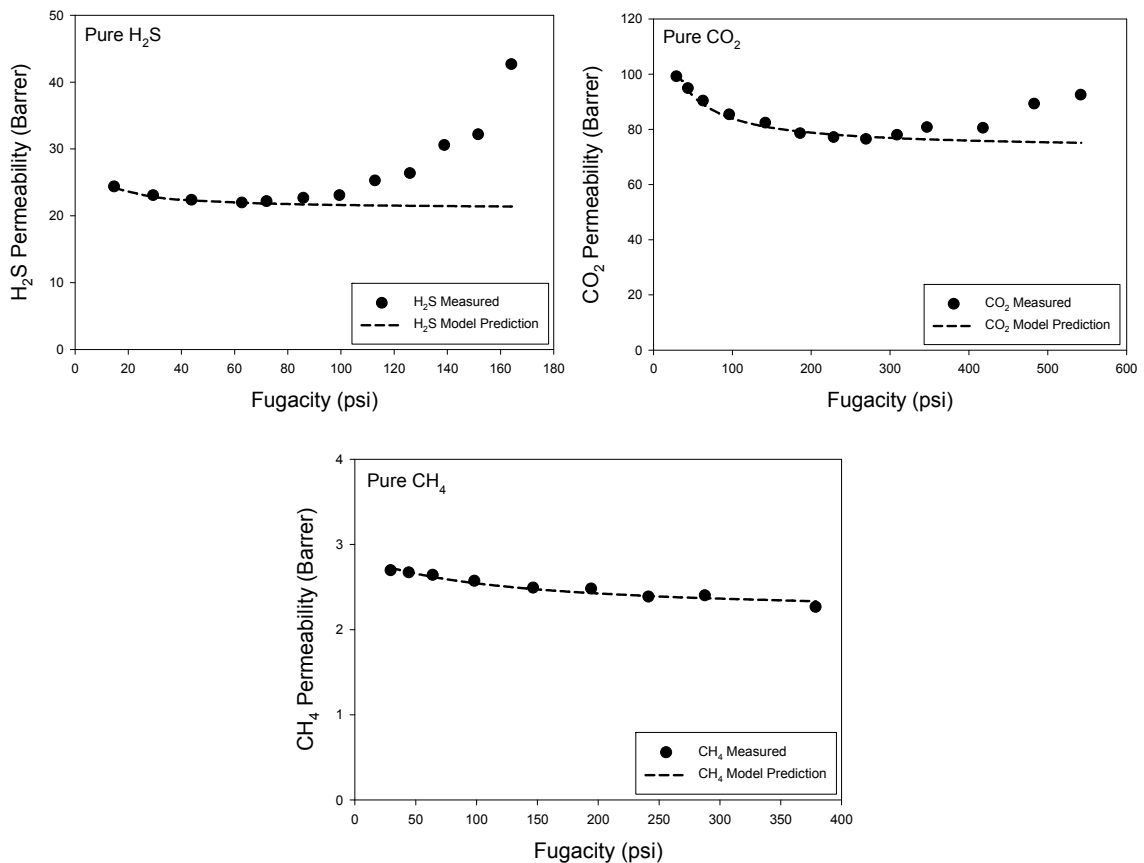


Figure 5.23: Pure gas permeation showing agreement between experimental data and partial immobilization model predictions at 35°C.

Permeation calculations based on the partial immobilization and frame of reference models are shown for TEG crosslinked PEGMC dense films with 20% CO₂, 80% CH₄ and 50% CO₂, 50% CH₄ mixed gas feeds in Figure 5.24 and Figure 5.25, respectively. In both cases, the projected permeability and permselectivity values given by both models are in close agreement with the experimental values. Based on these results, it appears that competitive sorption (and possibly the bulk flux contribution) is the primary effect of using a mixed gas feed rather than pure gases when H₂S is not present in the mixture.

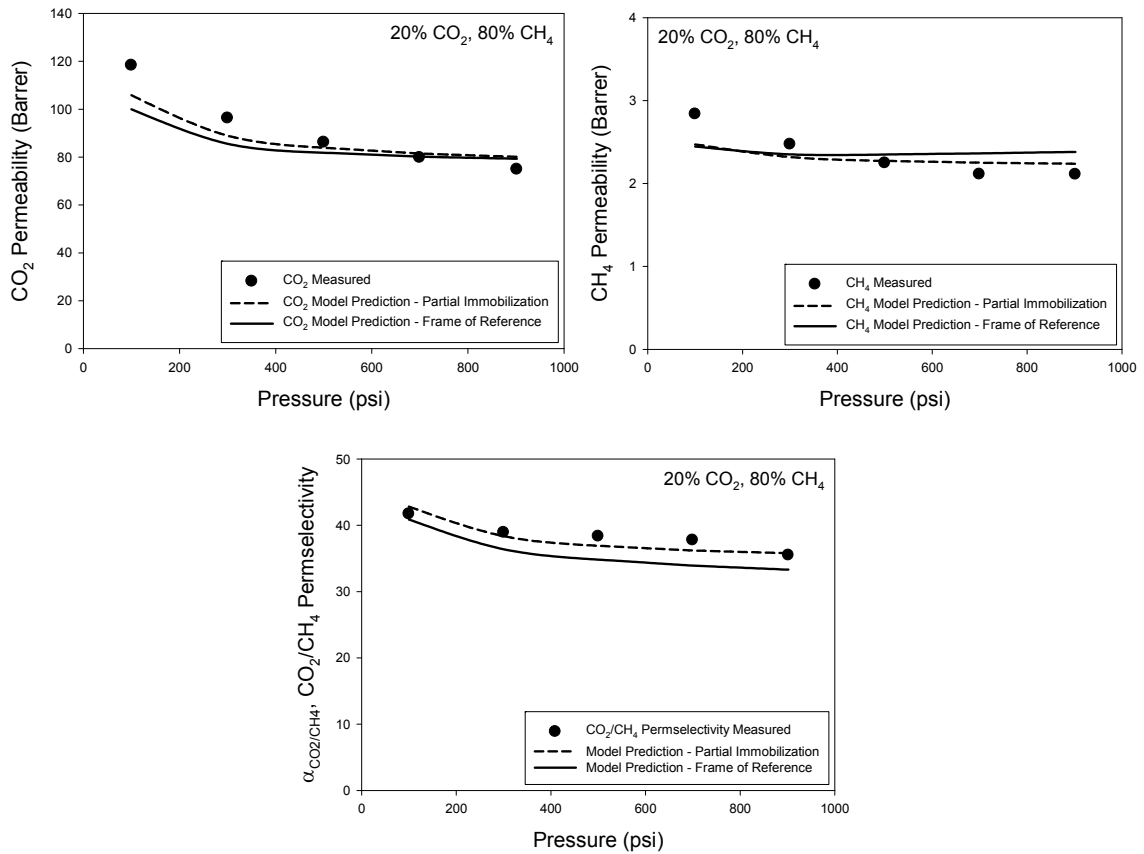


Figure 5.24: Permeation model predictions for 20% CO₂, 80% CH₄ mixed gas feed in TEG crosslinked PEGMC crosslinked at 280°C.

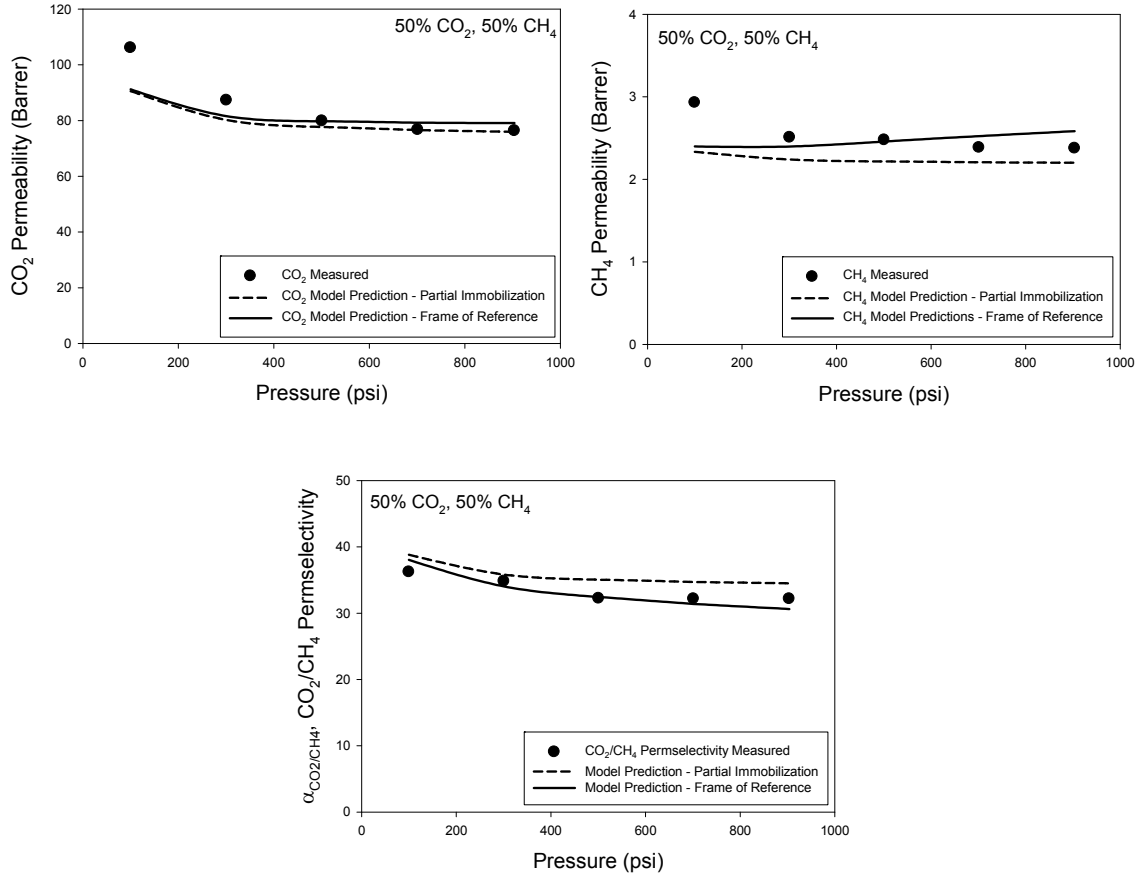


Figure 5.25: Partial immobilization and frame of reference model predictions for 50% CO₂, 50% CH₄ mixed gas feed permeation at 35°C.

A ternary mixture (20% H₂S, 20% CO₂, 60% CH₄) corresponding to the mixed gas used in Section 5.6.1 is assumed for the permeation model projections shown in Figure 5.26 and Figure 5.27. Unfortunately, the permeation and permselectivity values given by both the partial immobilization and frame of reference models are generally quite poor at capturing the experimentally measured trends. Again, the actual CO₂ and CH₄ permeabilities lie well below the modeled values. Also, the H₂S/CH₄ permselectivity calculation does not reflect the marked increase that was observed over the course of the permeation isotherm. These deviations are presumably the result of the same

phenomena that were present in the base 6FDA-DAM:DABA (3:2) dense films and are attributed to the H₂S penetrant, although the exact mechanism is undetermined.

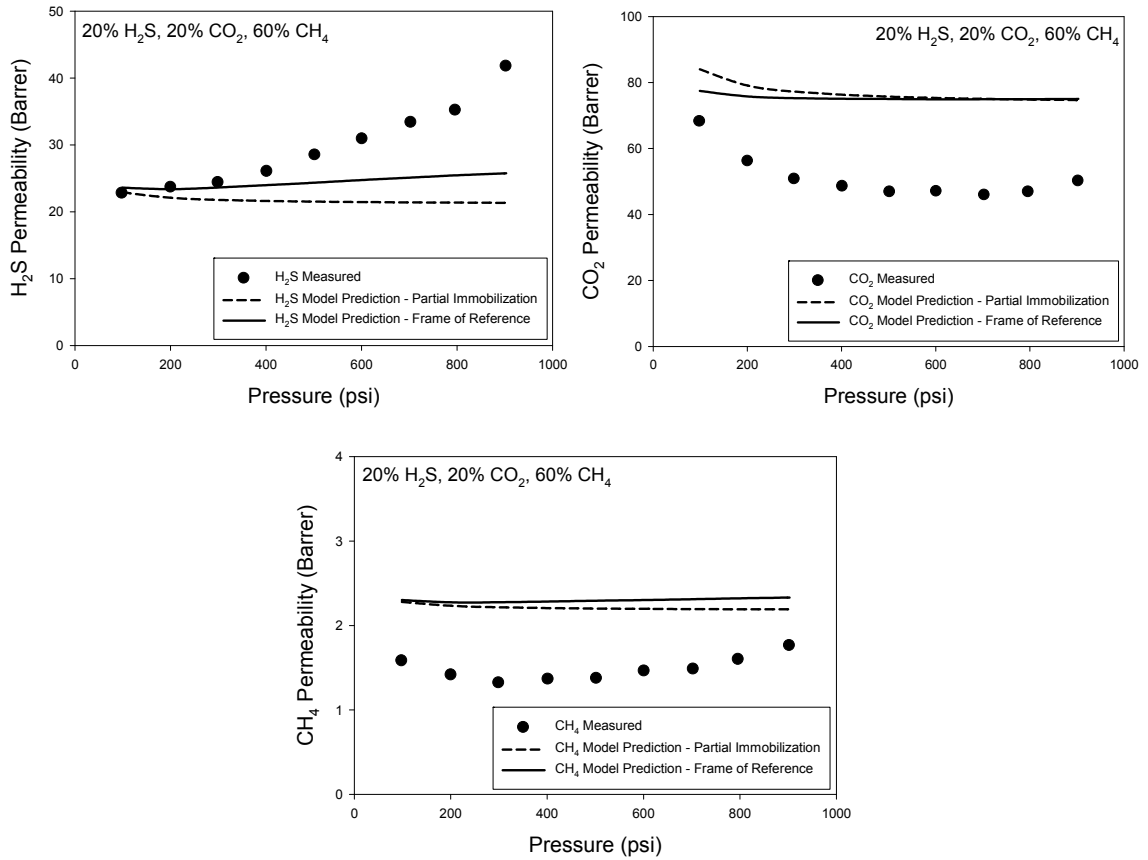


Figure 5.26: Permeability calculations for 20% H₂S, 20% CO₂, 60% CH₄ mixed gas feed with TEG crosslinked PEGMC treated at 280°C.

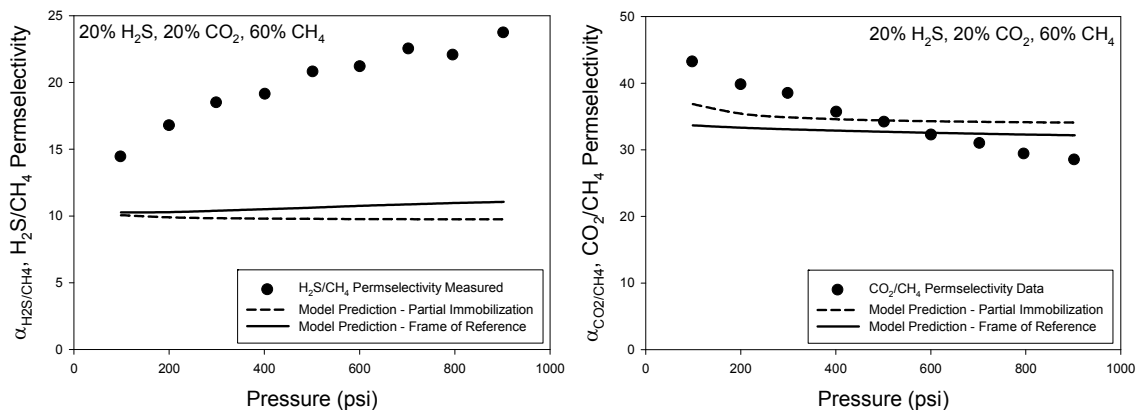


Figure 5.27: H₂S/CH₄ and CO₂/CH₄ permselectivity projections for 20% H₂S, 20% CO₂, 60% CH₄ mixed gas feed at 35°C.

As mentioned in CHAPTER 4, the unique permeation effects observed under sour gas feed conditions warrant further investigation. Possible diffusion-limitations, such as those caused by H₂S-induced *antiplasticization*, may be able to better explain the observations made in this chapter. Future work in this area should include development of more complex models to account for these effects. The insufficiency of the partial immobilization and frame of reference models at predicting sour gas permeation values for the glassy polyimides used in this work represents a significant hurdle to their application in an industrial setting. Extensive permeation testing to determine membrane performance under all possible feed conditions is not realistic, so more accurate permeation models are required. Furthermore, the development of such a model may help in the continuing optimization of membrane materials for sour gas separation applications by revealing the physical mechanism behind these atypical effects.

5.7. Conclusions

Previous work, including that presented in CHAPTER 4, has shown that the 6FDA-DAM:DABA polymer backbone is attractive for membrane-based gas separations, including CO₂ and H₂S removal from sour gas. However, several potential pitfalls still needed to be addressed in order to ensure suitable performance of 6FDA-DAM:DABA (3:2) membranes under aggressive sour gas feed conditions. Specifically, improved CO₂- and H₂S-induced plasticization resistance and enhanced H₂S/CH₄ selectivity were identified as material requirements for 6FDA-DAM:DABA (3:2).

Modification of the base polyimide backbone with short-chain PEG crosslinking agent is an attractive option to achieve these goals for several reasons. As with other covalently crosslinked polymers that have been studied for use in gas separation membranes, plasticization resistance is expected to be greatly improved by crosslinking. Also, we hypothesized that it is possible to augment H₂S/CH₄ permselectivity through the incorporation of H₂S-sorption-favoring PEO subunits into the polyimide membrane. In order to add the PEG crosslinking agents to the polymer, we were able to use a well-studied esterification crosslinking reaction scheme on the 6FDA-DAM:DABA backbone. This particular crosslinking mechanism allows for solution processing of the polymer into a desired membrane morphology and subsequent solid-state crosslinking via a sub-T_g thermal treatment. Furthermore, the concentration of PEO repeats within the membrane can be controlled in two ways. First, the length of the PEG crosslinking agent can be changed to increase or decrease the number of PEO repeats per crosslink. Second, the ratio of 6FDA-DAM to 6FDA-DABA monomers that constitute the polymer backbone can be altered to give a higher or lower frequency of crosslinks within the polymer matrix. This potential for control over the concentration of PEO within the membrane means that

we may be able to tune the crosslinked material towards higher or lower H₂S/CH₄ permselectivity, depending on the feed stream for which it will be used.

A series of crosslinkable polyimides, collectively called PEGMC polymers, was synthesized using DEG, TEG, and TetraEG as crosslinking agents for 6FDA-DAM:DABA (3:2). These polymers were shown to have high monoester yield, meaning that complete crosslinking was possible. In fact, after dense film casting and a sub-T_g thermal crosslinking treatment, all of the films were found to be insoluble in NMP solvent. This, along with pure gas permeation that showed greatly improved CO₂ and H₂S plasticization resistance compared to the base polymer and uncrosslinked PEGMC films, indicated that the crosslinking reaction was effective. Several crosslinking temperatures were investigated, and a 280°C soak temperature was eventually chosen for use throughout the study.

Pure gas permeation on the crosslinked PEGMC films showed that H₂S-induced swelling did not occur until approximately 90-120 psi feed pressure and CO₂-induced swelling was not apparent until greater than 350 psi. The ideal selectivity of the PEGMC materials for H₂S/CH₄ and CO₂/CH₄ was slightly below that of the unmodified base polymer. However, significant deviations from ideal selectivity were observed in the original sour gas study with 6FDA-DAM:DABA (3:2) dense films. Similar effects were anticipated and, ultimately, observed with the PEGMC materials, so the depressed ideal selectivity values were not taken as a particularly important indicator of poor membrane performance, per se.

Mixed gas permeation was performed with a 20% H₂S, 20% CO₂, 60% CH₄ mixture at feed pressures up to 900 psi. These conditions are representative of some of the most aggressive sour gas feed streams that are likely to be encountered in the field.

Despite these extremely challenging testing conditions, the performance of the crosslinked PEGMC materials was generally very impressive. Apparent plasticization due to the acid gases was significantly reduced compared to the base 6FDA-DAM:DABA (3:2) material. Also, the TEG and TetraEG crosslinked PEGMC films, in particular, maintained excellent CO₂/CH₄ permselectivity – greater than 27 – while also giving much improved H₂S/CH₄ permselectivity at the highest pressures that were tested. The H₂S/CH₄ selectivity of the TEG crosslinked material reached a value as high as 24. The individual gas permeabilities for the crosslinked PEGMC was much more stable than those of the unmodified polymer, which again indicates greater swelling and plasticization resistance in the PEGMC films.

Pure gas sorption experiments were performed on the crosslinked materials. These results show that the ideal sorption selectivity for both H₂S/CH₄ and CO₂/CH₄ of the PEGMC films may actually fall below that of 6FDA-DAM:DABA (3:2) at high feed pressures. This is somewhat surprising for the H₂S/CH₄ separation, since the inclusion of PEO repeats in the PEGMC materials was hypothesized to augment H₂S/CH₄ sorption selectivity. One possible explanation for the reduction in CO₂ and H₂S solubility in the PEGMC films is that the crosslinking reaction moderates chain mobility and low-level swelling of the polymer matrix prior to the onset of plasticization, thus decreasing sorption of the condensable species. In any case, the pure gas sorption values that were measured in this study are not likely to directly reflect the actual gas solubility or solubility selectivities under mixed gas feed conditions. Despite this fact, mixed gas modeling based on the pure gas measurements and dual mode sorption model coefficients provide insight into binary and even ternary feeds.

Strong competitive sorption and polymer-penetrant effects are believed to have a significant impact on the effective mixed gas sorption levels, particularly at high feed

pressures. Sorption calculations were performed in order to gain an understanding of the competitive sorption effects under realistic, mixed gas feed conditions. These calculations showed that for a 20% H₂S, 20% CO₂ and 60% CH₄ mixture H₂S sorption is only slightly reduced compared to the pure gas level, while CH₄ sorption is most susceptible to the sorption-reducing competition effects. Mixed gas sorption experimentation is recommended for future sour gas transport studies to corroborate the predictions made here. This would give more accurate measurements of effective sorption and sorption selectivity values; however, it is difficult to perform.

Based on the pure and mixed gas transport results of this study, the novel PEGMC materials appear to provide excellent CO₂/CH₄ selectivity, H₂S/CH₄ selectivity, acid gas permeability, and penetrant-induced plasticization. Unlike the 6FDA-DAM:DABA (3:2) polyimide that they are based on, these crosslinked membranes are expected to be robust enough for application in the aggressive sour gas separation applications that are projected to grow in importance as high-quality natural gas reserves become depleted over the next several decades. In particular, the PEGMC material synthesized with TEG as a crosslinking agent shows excellent sour gas separation performance in dense film form. The formation and characterization of asymmetric hollow fiber membranes of the crosslinkable TEG-modified PEGMC material are the subject of CHAPTER 6 and CHAPTER 7.

5.8. References

1. Membrane Technology and Research, I., *Low-Quality Natural Gas Sulfur Removal/Recovery*, 1998, The Department of Energy: Morgantown, WV.
2. Chatterjee, G., A.A. Houde, and S.A. Stern, *Poly(ether urethane) and poly(ether urethane urea) membranes with high H₂S/CH₄ selectivity*. Journal of Membrane Science, 1997. **135**(1): p. 99-106.

3. Mohammadi, T., et al., *Acid Gas Permeation Behavior Through Poly(Ester Urethane Urea) Membrane*. Industrial & Engineering Chemistry Research, 2008. **47**(19): p. 7361-7367.
4. Hao, J., P.A. Rice, and S.A. Stern, *Upgrading low-quality natural gas with H₂S- and CO₂-selective polymer membranes: Part I. Process design and economics of membrane stages without recycle streams*. Journal of Membrane Science, 2002. **209**(1): p. 177-206.
5. Hao, J., P.A. Rice, and S.A. Stern, *Upgrading low-quality natural gas with H₂S- and CO₂-selective polymer membranes: Part II. Process design, economics, and sensitivity study of membrane stages with recycle streams*. Journal of Membrane Science, 2008. **320**(1-2): p. 108-122.
6. Vaughn, J. and W.J. Koros, *Effect of the Amide Bond Diamine Structure on the CO₂, H₂S, and CH₄ Transport Properties of a Series of Novel 6FDA-Based Polyamide-Imides for Natural Gas Purification*. Macromolecules, 2012. **45**(17): p. 7036-7049.
7. Kidnay, A. and W. Parrish, *Fundamentals of Natural Gas Processing*. Mechanical Engineering, ed. L.L. Faulkner. 2006, Boca Raton: Taylor & Francis.
8. Robeson, L.M., *Correlation of separation factor versus permeability for polymeric membranes*. Journal of Membrane Science, 1991. **62**(2): p. 165-185.
9. Robeson, L.M., *The upper bound revisited*. Journal of Membrane Science, 2008. **320**(1-2): p. 390-400.
10. Bhide, B.D., A. Voskericyan, and S.A. Stern, *Hybrid processes for the removal of acid gases from natural gas*. Journal of Membrane Science, 1998. **140**(1): p. 27-49.
11. Vaughn, J., *Development and Evaluation of Aromatic Polyamide-imide Membranes for H₂S and CO₂ Separations from Natural Gas*, in *School of Chemical and Biomolecular Engineering 2013*, Georgia Institute of Technology: Atlanta, GA.
12. Wind, J.D., et al., *Solid-State Covalent Cross-Linking of Polyimide Membranes for Carbon Dioxide Plasticization Reduction*. Macromolecules, 2003. **36**(6): p. 1882-1888.
13. Hillock, A.M.W. and W.J. Koros, *Cross-Linkable Polyimide Membrane for Natural Gas Purification and Carbon Dioxide Plasticization Reduction*. Macromolecules, 2007. **40**(3): p. 583-587.
14. Wind, J.D., D.R. Paul, and W.J. Koros, *Natural gas permeation in polyimide membranes*. Journal of Membrane Science, 2004. **228**(2): p. 227-236.
15. Omole, I.C., S.J. Miller, and W.J. Koros, *Increased Molecular Weight of a Cross-Linkable Polyimide for Spinning Plasticization Resistant Hollow Fiber Membranes*. Macromolecules, 2008. **41**(17): p. 6367-6375.

16. Kratochvil, A.M. and W.J. Koros, *Decarboxylation-Induced Cross-Linking of a Polyimide for Enhanced CO₂ Plasticization Resistance*. *Macromolecules*, 2008. **41**(21): p. 7920-7927.
17. Qiu, W.L., et al., *Sub-T(g) Cross-Linking of a Polyimide Membrane for Enhanced CO₂ Plasticization Resistance for Natural Gas Separation*. *Macromolecules*, 2011. **44**(15): p. 6046-6056.
18. Chen, C.-C., et al., *Plasticization-resistant hollow fiber membranes for CO₂/CH₄ separation based on a thermally crosslinkable polyimide*. *Journal of Membrane Science*, 2011. **382**(1–2): p. 212-221.
19. Wind, J.D., et al., *The Effects of Crosslinking Chemistry on CO₂ Plasticization of Polyimide Gas Separation Membranes*. *Industrial & Engineering Chemistry Research*, 2002. **41**(24): p. 6139-6148.
20. Wind, J.D., et al., *Carbon Dioxide-Induced Plasticization of Polyimide Membranes: Pseudo-Equilibrium Relationships of Diffusion, Sorption, and Swelling*. *Macromolecules*, 2003. **36**(17): p. 6433-6441.

CHAPTER 6

FORMATION AND CROSSLINKING OF DEFECT-FREE ASYMMETRIC HOLLOW FIBER MEMBRANES FROM PEGMC POLYIMIDE

6.1. Overview

In CHAPTER 1, several challenges that must be overcome prior to widespread commercial adoption of gas separation membranes were discussed. To summarize, these key elements are: (1) the development of high-efficiency membrane modules with excellent separation surface area-to-volume ratios for large-scale commercial processes, (2) the creation of advanced materials capable of high-efficiency separations, (3) the development of a capability to alter morphologies at multiple levels within the cross-section of a membrane, and (4) the development of production methods that rapidly, economically, and efficiently combine the first three elements into “defect-free” modules [1]. CHAPTER 4 and CHAPTER 5 dealt extensively with the development of a novel advanced membrane material, PEGMC, for aggressive sour gas feed applications. In this chapter, the other three points are addressed. The aim of the work described in this chapter is the formation of high quality, defect-free asymmetric hollow fiber membranes from the PEGMC polyimide. Specifically, the PEGMC polymer synthesized with TEG as crosslinking agent was selected for continued development into asymmetric hollow fibers because of its excellent productivity, efficiency, and plasticization resistance for H₂S/CH₄ and CO₂/CH₄ separations.

6.2. Spinning PEGMC Hollow Fibers

The morphology of asymmetric hollow fiber membranes is largely determined during the spinning process. As discussed in CHAPTER 2, commercially attractive asymmetric hollow fiber membrane morphologies are characterized by an ultra-thin integral selective skin layer and a highly interconnected porous substructure. Also, the fiber should have adequately sized outside and inside diameters (OD: ~200-250 μm and ID: ~100-125 μm [2]), be circular, concentric, and have no macrovoids in the fiber wall. Dry-jet/wet-quench spinning is used in this work to form fibers with the aforementioned characteristics. This nuanced manufacturing technique involves numerous spinning variables, and this section presents our initial attempt at spinning PEGMC hollow fibers by intelligently controlling these parameters.

6.2.1. Polymer Properties

For simplicity, the PEGMC polymer with TEG crosslinking agent is referred to by the more specific acronym TEGMC (**T**riethylene **G**lycol **M**onoesterified **C**rosslinkable) for the remainder of this dissertation. Three batches of TEGMC were synthesized for the various spinning attempts described in this chapter. Previous work has shown that high molecular weight polymer – yet, not so high as to reduce processability – is essential to the spinning of high quality fiber membranes based on the 6FDA-DAM:DABA backbone [3-6]. Increased polymer molecular weight is believed to improve spinnability (i.e. the capacity to draw a continuous, stable fiber) [4] and the ability to produce defect-free fibers [7]. The molecular weight and polydispersity measurements of the TEGMC polymer and 6FDA-DAM:DABA (3:2) precursor polymer used for each of the three spinning attempts reported in this chapter are shown in Table 6.1. Molecular weight

values greater than approximately 80 kDa are most desirable [3, 6], and all of the polymer batches used in the current work surpassed that standard.

Table 6.1: Molecular weight and PDI properties of the polymer batches used for each spinning attempt described in this chapter as measured by GPC.

	Polymer			
	6FDA-DAM:DABA (3:2)		TEGMC	
	M_w (kDa)	PDI	M_w	PDI
Spin #1	200	4.7	95	2.6
Spin #2	240	2.3	120	3.2
Spin #3	240	2.3	110	2.9

Although there large molecular weight loss occurs after monoesterification of the base 6FDA-DAM:DABA (3:2) polymer, there is evidence of a similar degree of molecular weight loss in monoesterified PDMC [6, 8]. Very high performance PDMC asymmetric hollow fibers were formed via the dry-jet/wet-quench spinning process from a monoesterified polymer batch with $M_w = 120$ kDa; the 6FDA-DAM:DABA (3:2) polymer precursor for this batch of PDMC was approximately 360 kDa. Therefore, the M_w values shown in the table above were deemed to be acceptable for spinning TEGMC hollow fibers.

6.2.2. Dope Formulation

6.2.2.1. Dope Composition Selection Theory

Apart from the quality of the starting material itself, the dope composition used in the dry-jet/wet-quench spinning process is perhaps the most critical variable controlling spinnability and fiber morphology. The typical starting point for attempting to spin a new polymer is to map out the miscibility behavior of the polymer in the solvent(s) and non-solvent(s) that comprise the majority of a spinning dope. The dope must be an

essentially homogenous solution to enable drawing, so the solvents used and their concentrations should be sufficient to fully dissolve the polymer at the spinning conditions of interest. As mentioned in CHAPTER 2, this is complicated by the non-solvents and other additive species that are often also included in a dope formulation to assist in skin formation. These components make rapid spinning of defect-free fiber membranes possible, but also make the selection of an appropriate dope formula more difficult.

While it is theoretically possible to calculate polymer miscibility for a polymer/solvent/non-solvent system using Gibbs free energy of mixing calculations [3], the requisite experimentally-determined input parameters for such calculations are most often not available, nor are they easily obtained. Moreover, most dopes consist of multiple solvents and/or non-solvents, as well as additives. This significantly adds to the complexity of the mathematical methods. Nevertheless, a hypothetical ternary phase diagram derived from Gibbs free energy of mixing calculations is shown in Figure 6.1. The binodal line, which separates the miscible one-phase region (on the left) from the immiscible two-phase region (on the right), is the most useful system property for dope formulation purposes.

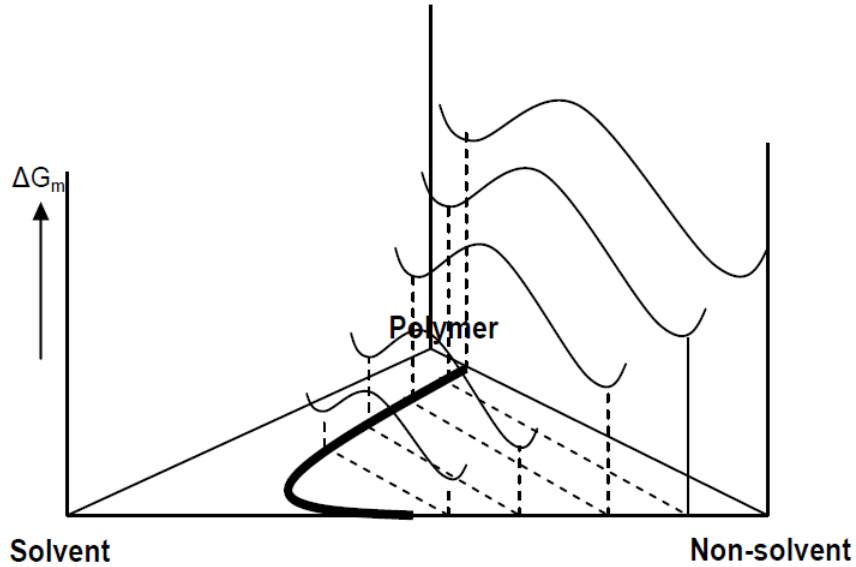


Figure 6.1: Ternary phase diagram from a Gibbs free energy of mixing calculation for a spinning dope (polymer/solvent/non-solvent) system, with the binodal line in bold [3, 9].

Despite the difficulty in calculating these ternary phase diagrams, estimations of the polymer miscibility line (the binodal) are usually adequate. Cloud point determination is a relatively fast and accurate way to locate the binodal line location for a new dope system. Described in CHAPTER 3, these experiments consist of making numerous small dopes with various compositions of the system components and looking for the point at which the sample dope appearance changes from homogeneous and transparent to cloudy. Two-phase solutions – those which fall toward the non-solvent corner of the ternary phase diagram and inside the binodal – are either cloudy or will simply not fully dissolve the polymer. Figure 6.2 depicts a ternary phase diagram for a spinning dope and shows how the cloud point technique can be used to map the binodal.

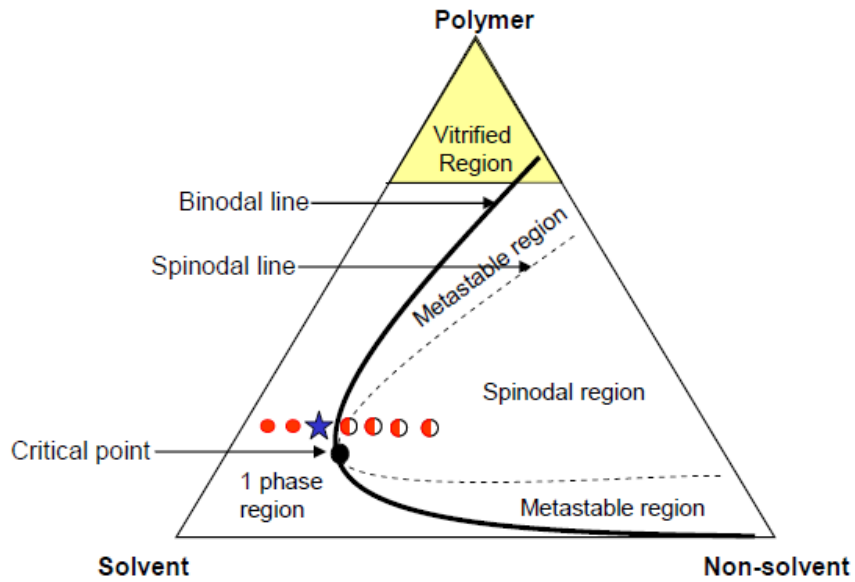


Figure 6.2: Ternary phase diagram showing the cloud point technique. Red circles and red semi-circles represent experimental dope compositions in the one- and two-phase regions, respectively, with the binodal located at the composition where the transition occurs [3].

A first iteration spinning dope formulation is selected such that it lies within the one-phase region and close to the apparent binodal. This increases the probability that the dope will be spinnable and that rapid phase separation of the fiber walls will occur once the nascent fiber is submerged in a non-solvent quench bath. A good potential dope composition is indicated in Figure 6.2 by the blue star-shaped marker.

6.2.2.2. Initial Dope Formula for TEGMC Spinning

The non-polymer components of the dope used in this work and their approximate concentrations for cloud point experiments were selected based on previous studies into the formation of 6FDA-DAM:DABA (3:2) and PDMC asymmetric hollow fiber membranes [3, 5, 6, 10]. Binodal lines were determined for these polymers through the cloud point experimental technique, and the results of these tests can be found in the references [5, 6, 8]. NMP was selected as the non-volatile solvent and THF was chosen for use as the volatile solvent component. The non-solvent used in the dope was EtOH, which is relatively volatile based on its boiling point temperature and vapor pressure at 50°C (Table 6.2). The non-solvent quench bath was comprised of water, due largely to its being benign, environmentally friendly, and a strong non-solvent for polyimides such as 6FDA-DAM:DABA.

Table 6.2: Boiling point temperature and vapor pressure values for volatile and non-volatile dope components.

Component	Boiling Point Temp. (°C)	Vapor Pressure at 50°C (kPa)
H ₂ O	100	120
NMP	202	2.8
THF	66	440
EtOH	78	290

In addition to the polymer and liquid components of the dope, lithium nitrate (LiNO₃) was added in low concentration as a viscosity enhancer and to help increase the rate of phase separation during the non-solvent quench step.

Cloud point experiments were performed on the dope system with polymer concentrations of 25, 30, and 35 wt%. The LiNO₃ concentration was held constant at 6.5 wt% for all cloud point samples, and the THF concentration was maintained at 10 wt%.

In order to map the approximate binodal line location at each polymer concentration, the NMP:EtOH ratio was altered. The results of cloud point experiments with TEGMC-containing dopes are shown in Figure 6.3.

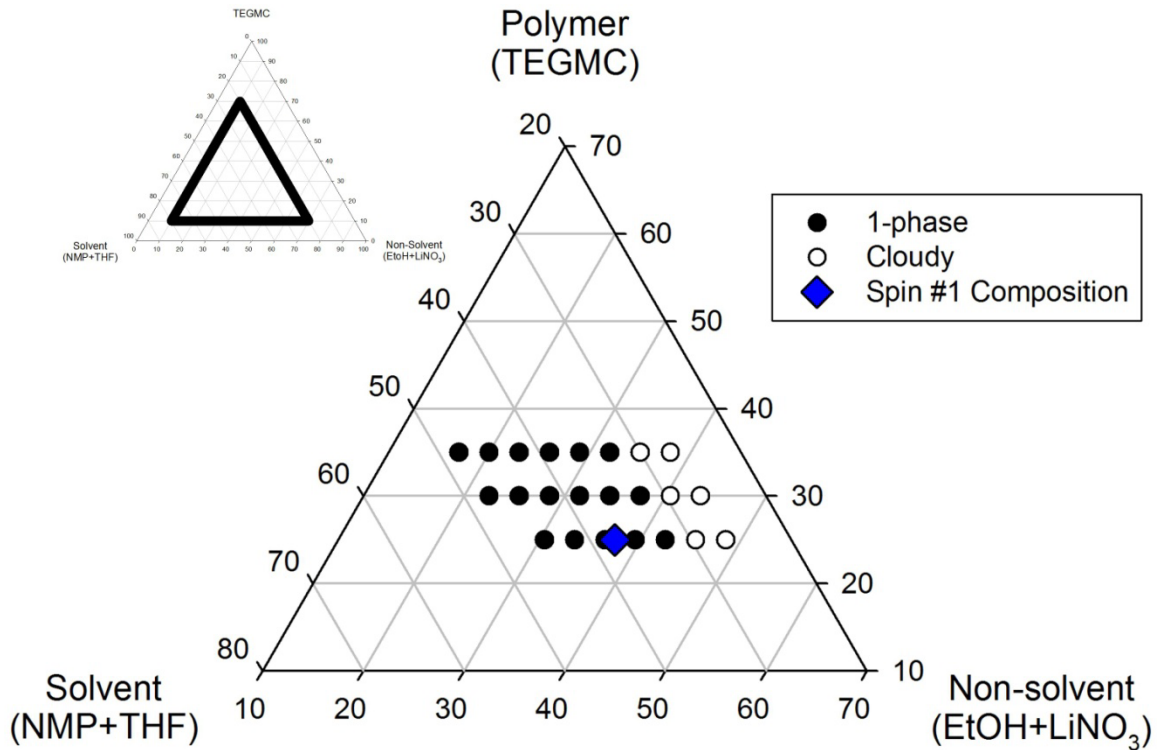


Figure 6.3: Ternary phase diagram constructed based on cloud point experiments using TEGMC polymer at approximately 50°C. The binodal is located where experimental dopes transition from one to two-phase (cloudy).

Based on the results of the cloud point experiments and the estimated binodal line location shown in Figure 6.3, a preliminary dope composition was selected. The 25 wt% polymer dope compositions were more attractive because of the excessive viscosity of the 30 and 35 wt% dopes. Table 6.3 lists the concentrations of the various dope components used in this initial dope formulation.

Table 6.3: Potential dope composition for first TEGMC fiber spinning attempt based on results of cloud point experiments.

Component	wt% in Dope
TEGMC Polymer	25.0
NMP	27.5
THF	10.0
EtOH	31.0
LiNO ₃	6.5

Prior to moving forward with the preparation of a full-sized spinning dope, a small experimental dope with this composition was formed. This smaller dope was used to perform syringe tests, which were described in CHAPTER 3. As mentioned, these syringe tests are useful in that they can reveal some of the potential drawbacks of the selected dope composition, like slow phase separation rate, macrovoids, or low capacity for drawing, without the need to conduct an entire spin. The process of spinning, even on the lab scale, is heavily time-consuming and can be very expensive when specialty polymers are involved, so syringe tests are valuable.

Figure 6.4 provides a few SEM images of the fibers that were collected from the syringe tests. Overall, the preliminary TEGMC dope composition was promising based on these tests: no macrovoids were observed, the phase separation rate of the dope was acceptable, and the viscosity of the dope was qualitatively determined to be appropriate for spinning.

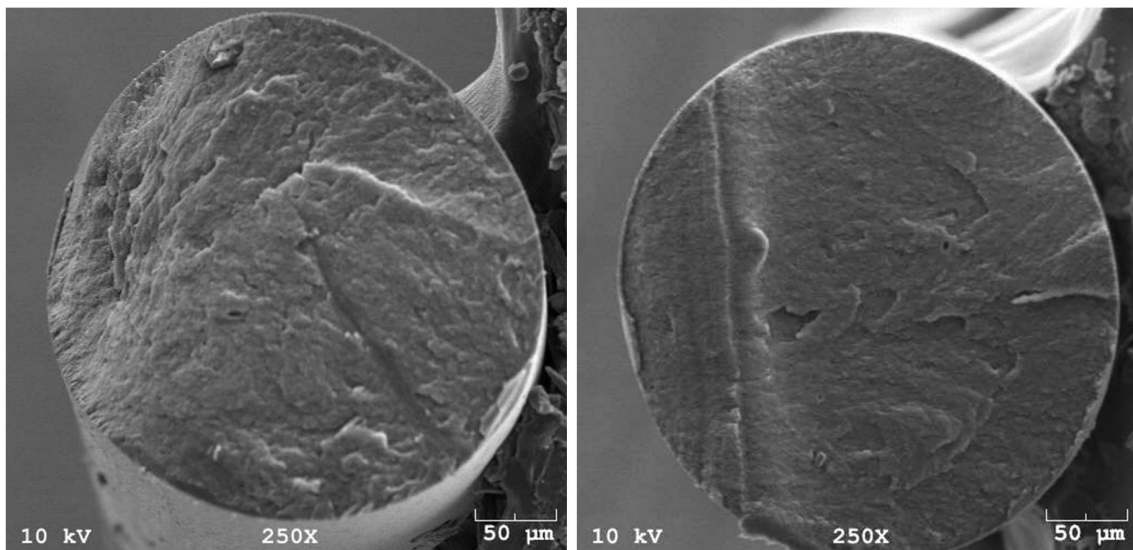


Figure 6.4: SEM images of fiber cross sections from syringe tests using the initial dope formulation.

6.2.3. TEGMC Spinning: Initial Study

Following the promising results of syringe testing, hollow fibers of the crosslinkable TEGMC polymer were spun using the dope composition shown in Table 6.3. The bore fluid composition chosen for this spin was 80 wt% NMP and 20 wt% H₂O. This composition was based on the bore fluids used in previous spinning studies [3, 5, 6] and submersion testing of a small dope sample to ensure solvent neutrality – the bore fluid neither dissolved the dope nor caused it to phase-separate.

The initial spinning conditions used in this study were selected to meet several morphological and practical requirements. First, skin formation on the outermost layer of the fibers, through evaporation of the volatile dope components, was promoted by heating the spinneret to 70°C and using fairly large air gap heights of up to 10 cm. Also, the rate of phase separation during the quench step was accelerated by heating the quench bath water to 50°C. Finally, the dope and bore fluid extrusion rates (180 mL/hr

and 60 mL/hr, respectively) and fiber take-up rate (up to 50 m/min) were selected so that appropriate fiber dimensions and commercially viable production rates could be maintained. Table 6.4 presents the range of values that were investigated for the various spinning conditions that may be controlled. In addition to these, the room temperature was noted to be 23°C and the relative humidity within the spinning area was 59% during the spin.

Table 6.4: Spinning conditions used during the first attempt at spinning TEGMC hollow fibers.

Spinning Parameter	Values Used
Dope Extrusion Rate	180 mL/hr
Bore Fluid Extrusion Rate	60 mL/hr
Spinneret Temperature	70°C
Air Gap	2.5-10 cm
Quench Bath Temp.	50°C
Quench Bath Height	1 m
Take-up Rate	25-50 m/min

The exact spinning conditions used for the various fiber states that were collected during this spin are given in Table 6.5. This spin was performed with the Extended II spinneret.

Table 6.5: Spinning conditions used for select fiber states from Spin # 1.

Fiber ID (Spin # - State #)	Dope Flow Rate (mL/hr)	Bore Fluid Flow Rate (mL/hr)	Air Gap (cm)	Take-up Rate (m/min)
1 - 2	180	60	5	37.5
1 - 3	180	60	3.5	50
1 - 5	180	60	10	37.5
1 - 6	180	60	5	25
1 - 7	180	60	5	50
1 - 9	180	60	10	25

6.2.4. Characterization of Fibers from Initial Spinning Study

After completing the spinning and solvent exchange processes, SEM was performed on the uncrosslinked (75°C dried) TEGMC fibers to investigate their morphological properties. Several SEM images of the uncrosslinked fibers are shown in Figure 6.5. These fibers were found to be circular and concentric. Furthermore, State #6 was found to contain macrovoids in the fiber wall, as shown in image (C) of Figure 6.5. Although macrovoids were not detected in any of the other states during SEM imaging, it is possible that this was a result of the particular cross sections that were used. Ideally, all evidence of macrovoids should be eliminated in future iterations of TEGMC fibers.

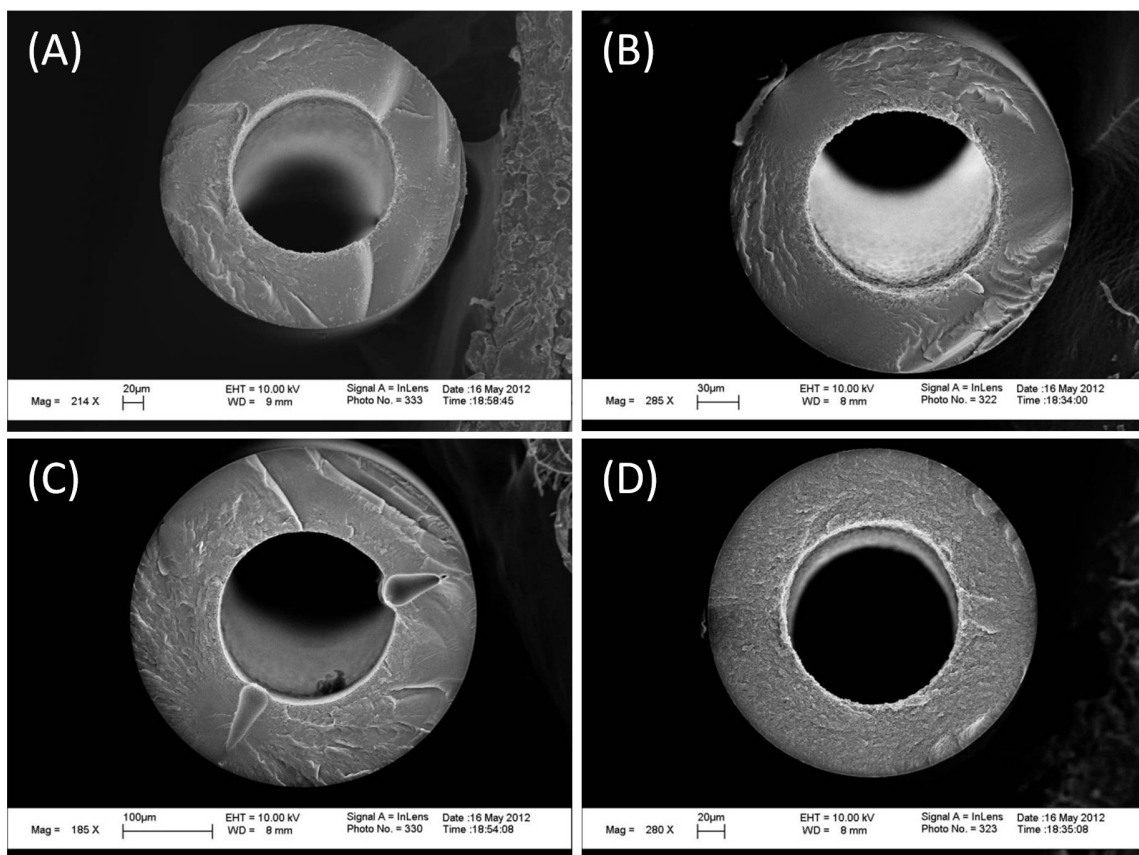


Figure 6.5: Cross section SEM images of several TEGMC fibers from Spin #1. (A) is State #2, (B) is State #3, (C) is State #6, and (D) is State #7. All fibers samples are uncrosslinked.

The dimensions of the fibers from Spin #1 fall within the 200-250 μm OD/100-125 μm ID range that are often said to be optimal. With the exception of State #6, which was collected at a low take-up rate of just 25 m/min, all the fibers shown above have outside diameters of 230-270 μm and inside diameters between 110-140 μm .

Pure gas permeation experiments were performed on the uncrosslinked TEGMC fibers at 35°C using a bore-side feed configuration and 100 psig feed pressure. A constant pressure permeation system was utilized; pure gas N₂, O₂, and He permeation results are used more heavily than CO₂, H₂S, or CH₄ permeation properties for the purposes of initial hollow fiber characterization. These less condensable gases are chosen in order to avoid any possible swelling or plasticization effects, which would complicate skin layer integrity and thickness characterization.

Pure gas permeation experiments can be used to assess the skin integrity, skin thickness, and substructure resistance of the fibers. The skin integrity (whether or not the fibers are defect-free) is measured by comparing the permselectivity of the hollow fibers for a given gas pair to that of dense films of the same polymer. Fibers are deemed to be defect-free if the permselectivity of the hollow fibers for a gas pair is $\geq 90\%$ of the dense film value [7, 11]. Additionally, the effective skin layer thickness of a defect-free asymmetric hollow fiber membrane, l_{skin} (μm), can be calculated [Eq. (6.1)] from the dense film permeability and hollow fiber permeance for a given gas under the same feed conditions.

$$l_{skin} = \frac{P_i}{\left(\frac{P}{l}\right)_i} \quad (6.1)$$

Furthermore, the substructure resistance of asymmetric hollow fibers can be characterized to some degree by comparing their permselectivity for a high

permeance/low permeance gas pair, such as He/N₂, to that of a lower permeance gas pair, such as O₂/N₂. Significant substructure resistance may be present when, for example, the He/N₂ permselectivity is a lower percentage of the intrinsic dense film value than the O₂/N₂ permselectivity [12].

The results of pure gas permeation characterization on selected uncrosslinked TEGMC fiber states using N₂, O₂, and He are presented in Table 6.6 through Table 6.8. Pure gas N₂, O₂, and He measurements of permeability and ideal selectivity values for uncrosslinked TEGMC dense films are also shown in Table 6.7 and were used in the effective skin layer thickness calculations. It should be noted that '5-minute' epoxy (ScotchWeld™ DP-100, 3M Company) was used to make these fiber modules.

Table 6.6: Pure gas permeation characterization of uncrosslinked Spin #1 TEGMC fibers at 35°C.

Fiber ID (Spin # - State #)	(P/l) _{N₂} (GPU)	(P/l) _{O₂} (GPU)	(P/l) _{He} (GPU)	$\alpha^*_{O_2/N_2}$	α^*_{He/N_2}
1 - 2	11	41	270	3.7	25
1 - 3	12	45	310	3.7	26
1 - 5	6.9	28	190	4.1	27
1 - 6	8.6	35	240	4.0	27
1 - 7	8.4	36	260	4.3	31
1 - 9	7.0	30	190	4.2	27

Table 6.7: Dense film permeability and permselectivity values for uncrosslinked TEGMC at 35°C and 100 psi.

TEGMC Dense Film Value	
P _{N₂} (Barrer)	2.0
P _{O₂} (Barrer)	8.7
P _{He} (Barrer)	65
P _{CH₄} (Barrer)	1.1
P _{CO₂} (Barrer)	34
$\alpha^*_{O_2/N_2}$	4.4
α^*_{He/N_2}	33
$\alpha^*_{CO_2/CH_4}$	32

Table 6.8: Effective skin layer thickness and skin integrity values (ideal selectivity as a percentage of the intrinsic value) for uncrosslinked TEGMC fibers from Spin #1.

Fiber ID (Spin # - State #)	l_{skin} (nm)[#]	% of Dense Film $\alpha^*_{O_2/N_2}$	% of Dense Film α^*_{He/N_2}
1 - 2	210	84	77
1 - 3	190	84	80
1 - 5	310	93	83
1 - 6	250	91	83
1 - 7	240	98	95
1 - 9	310	95	83

[#]Skin thickness calculation based on the average of N₂, O₂, and He permeation

Based on the pure gas permeation results presented above, several of the uncrosslinked TEGMC fibers formed during Spin #1 appear to be defect-free or nearly defect-free. In particular, State #7 has promising properties in terms of productivity (effective skin layer thickness) and ideal selectivity (skin integrity). Furthermore, the fibers from State #7 appear to have fairly low substructure resistance. The substructure resistance contribution for most of the other states is significant enough to cause a large drop between the “% of Dense Film” ideal selectivity for O₂/N₂ and He/N₂ separations.

Pure gas permeation properties for CO₂ and CH₄ feeds at 35°C and 100 psig are given in Table 6.9. H₂S pure gas values were not measured during this chapter due to module-making considerations that are discussed later in Section 6.6. The State #3 fiber module failed during CH₄ permeation. Although it is difficult to say with certainty, it is most likely that a major ‘blow out’ occurred in the skin layer of one or more of the fibers. Though not observed in the SEM images of State #3 fibers, macrovoids may have contributed to this module failure.

Table 6.9: Pure CO₂ and CH₄ permeation properties for Spin #1 uncrosslinked TEGMC fibers.

Fiber ID (Spin # - State #)	(P/l)_{CH₄} (GPU)	(P/l)_{CO₂} (GPU)	α^*_{CO₂/CH₄}
1 - 2	14	360	26
1 - 3	N/A	N/A	N/A
1 - 5	8.8	290	33
1 - 6	11	360	33
1 - 7	11	350	32
1 - 9	8.5	270	32

Again, based on the values for the CO₂/CH₄ separation in the uncrosslinked TEGMC fibers, it seems that the first spinning attempt was quite successful. Defect-free fibers with fairly good morphological properties were obtained using several different spinning conditions. The primary area of improvement that was targeted for next generation TEGMC fibers was a reduction in the skin layer thickness of the fibers. Additionally, it was hoped that all macrovoids could be eliminated from the TEGMC fibers by modifying the dope composition.

6.3. Spinning Defect-free PEGMC Fibers

6.3.1. Reformulation of PEGMC Dope

The original dope formulation that was used in the first spinning study was slightly altered in an attempt to obtain better quality fibers. As mentioned, the specific goal of this dope reformulation was the elimination of all macrovoids and the formation of defect-free skin layers with thinner effective thickness. Overall, the dope used in Spin #1 successfully showcased the excellent spinnability of the TEGMC polymer and the

viability of the dope system (solvents, non-solvents, additive), but small improvements were still necessary.

The reformulation for our second spinning attempt was chosen such that the dope composition would more closely approach the apparent binodal of the system to allow for more rapid phase separation in the water quench bath. This was accomplished by decreasing the NMP: EtOH ratio. Table 6.10 gives the composition of this second iteration dope and Figure 6.6 shows the Spin #2 dope location on the system ternary phase diagram.

Table 6.10: Second generation dope composition for TEGMC asymmetric hollow fiber spinning.

Component	wt% in Dope
TEGMC Polymer	25.0
NMP	23.5
THF	10.0
EtOH	35.0
LiNO ₃	6.5

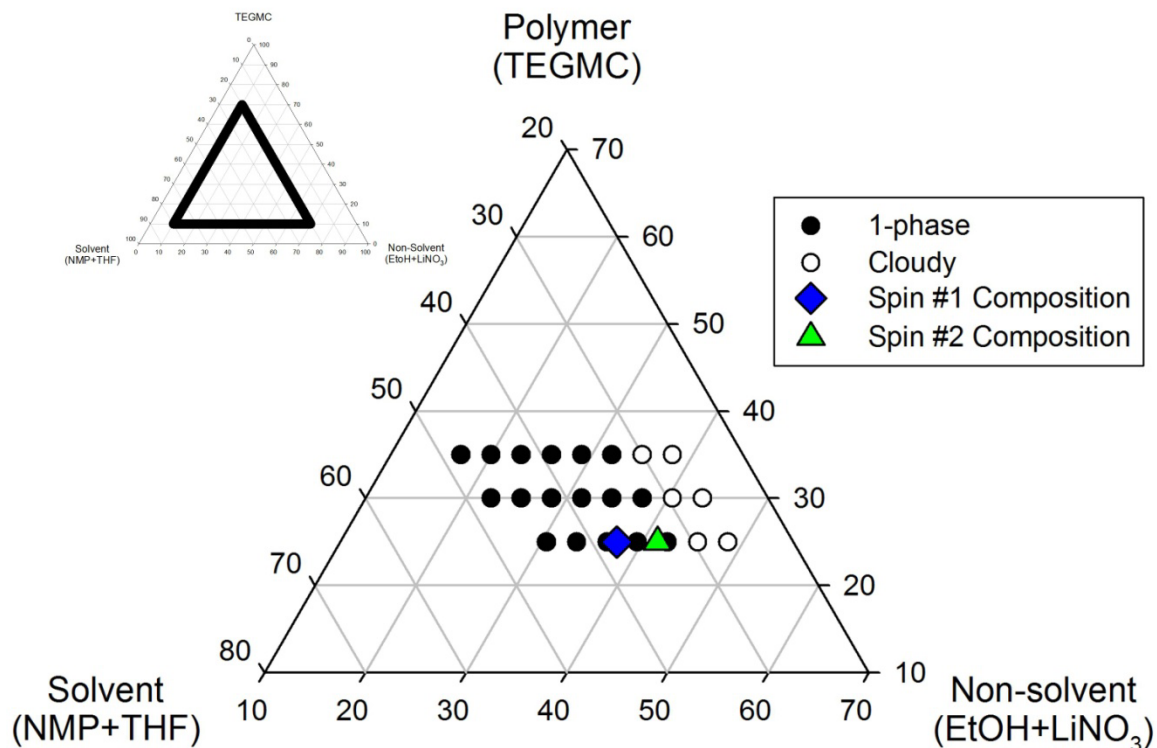


Figure 6.6: Ternary phase diagram for TEGMC-containing dope showing the location of the Spin #2 dope. The apparent binodal location for the system is located where the dopes transition from one to two-phase (cloudy). Experimental dopes were evaluated at 50°C.

6.3.2. Results of Second Spinning Study

The spinning conditions used during Spin #2 were essentially identical to those used initially (Table 6.4). A greater emphasis was placed on spinning states with air gaps in the middle of the range, since those air gaps were found to give superior results during Spin #1. Also, undesirable fiber instability, manifested as so-called ‘pulsing’ and even line breakage, was observed for the highest air gaps during Spin #1.

Detailed spinning conditions for the best states collected during this second spinning study are shown in Table 6.11, below. For Spin #2, the spinneret temperature was 70°C, the water quench bath was maintained at 50°C, the room temperature was

23°C, and the relative humidity was 49%. Again, the Extended II spinneret was used to form the asymmetric hollow fiber TEGMC membranes during this study.

Table 6.11: Spinning conditions used for select fiber states during Spin #2.

Fiber ID (Spin # - State #)	Dope Flow Rate (mL/hr)	Bore Fluid Flow Rate (mL/hr)	Air Gap (cm)	Take-up Rate (m/min)
2 - 3	180	60	5	50
2 - 4	180	60	7.5	25
2 - 5	180	60	10	25
2 - 6	180	60	5	50
2 - 9	180	60	7.5	50

Despite the identical spinning parameters for State #3 and State #6, they are listed separately in the Table 6.11. This separate treatment is used because previous researchers have found that fiber quality can slightly vary for identical states collected at different times over the course of a spin. Presumably, this is due to slight compositional differences within the dope volume, an effect that may arise during the degassing stage of spin preparation when a small evacuated volume is established above the dope inside the sealed syringe pump. It is possible that the volatile dope components vaporize from the top of the dope and enter this volume, causing a slight compositional variation between the top and bottom of the dope.

6.3.3. Characterization of PEGMC Fibers

The second-generation uncrosslinked TEGMC asymmetric hollow fibers were inspected with SEM imaging to make sure that no significant morphological defects were present. Figure 6.7 shows SEM images for the cross sections of several fiber states. The fibers are generally highly circular, meaning that the phase separation rate of the dope in the water quench bath is sufficient. However, some non-concentricity is apparent in all of the fiber cross sections shown. This is attributed to slight misalignment of the bore fluid

extrusion needle in the spinneret assembly. Although it is possible that these non-concentric fibers will have lower mechanical stability than a perfectly concentric version would, this effect was not expected to be substantial. No macrovoids were observed after changing the dope composition for this spinning attempt.

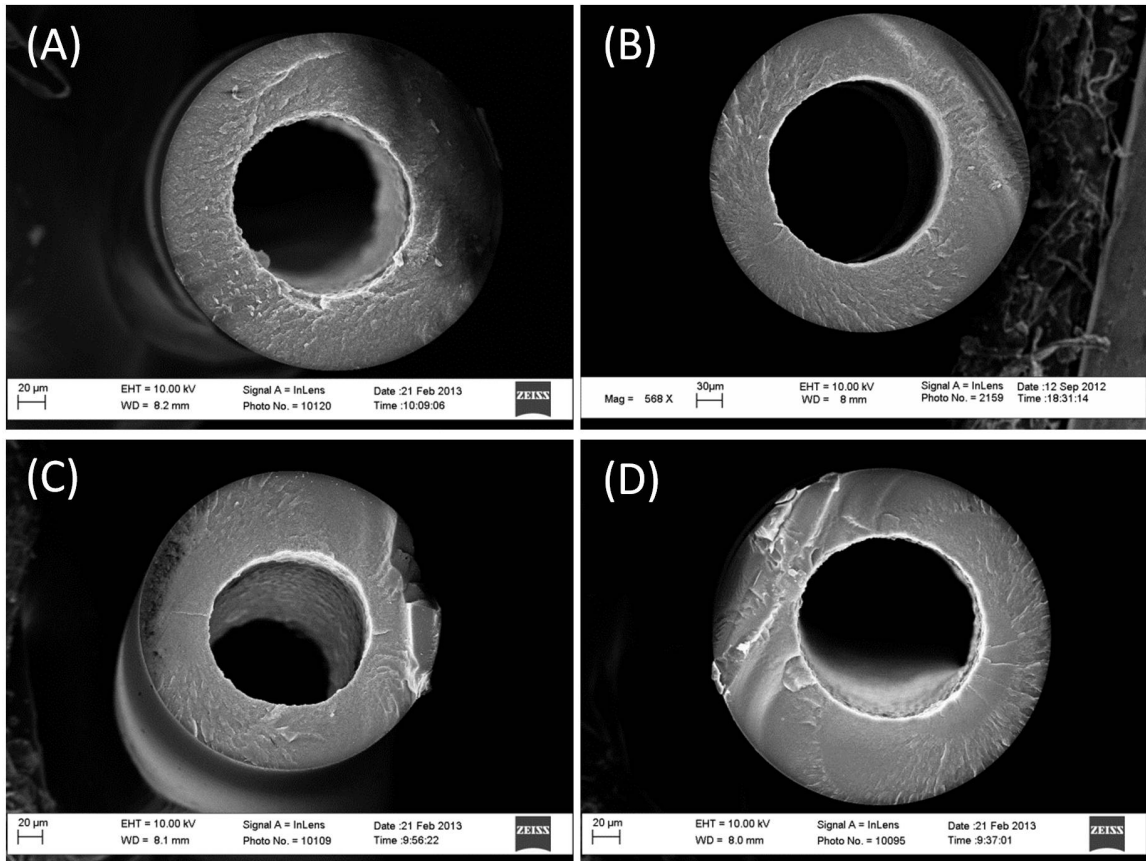


Figure 6.7: SEM images of TEGMC Spin #2 cross sections. (A) is State 3, (B) is State 4, (C) is State 6, (D) is State 9. All samples shown are uncrosslinked.

Pure gas permeation experiments were performed on the uncrosslinked TEGMC fibers using N_2 , O_2 , and He gases at 35°C with 100 psig feed pressure in a constant pressure permeation apparatus. The results for the best states from this spin are shown in Table 6.12 and Table 6.13. Fiber modules tested in this section were again made with 5-minute epoxy.

Table 6.12: Spin #2 pure gas permeation results at 35°C and 100 psig feed pressure.

Fiber ID (Spin # - State #)	(P/I) _{N₂} (GPU)	(P/I) _{O₂} (GPU)	(P/I) _{He} (GPU)	$\alpha^*_{O_2/N_2}$	α^*_{He/N_2}
2 - 3	6.0	28	180	4.6	31
2 - 4	5.2	23	150	4.5	30
2 - 5	7.0	33	220	4.5	31
2 - 6	4.0	19	150	4.6	38
2 - 9	6.8	33	270	4.9	39

Table 6.13: Skin thickness and skin integrity measurements for uncrosslinked Spin #2 TEGMC fibers.

Fiber ID (Spin # - State #)	l_{skin} (nm) [#]	% of Dense Film $\alpha^*_{O_2/N_2}$	% of Dense Film α^*_{He/N_2}
2 - 3	330	104	94
2 - 4	390	102	91
2 - 5	290	106	95
2 - 6	460	105	118
2 - 9	270	110	120

[#]Skin thickness calculation based on the average of N₂, O₂, and He permeation

Several of the uncrosslinked TEGMC fiber states from Spin #2 have outstanding permeation properties. State #9 has especially good productivity and efficiency characteristics. Both the O₂/N₂ and He/N₂ ideal selectivity values of the State #9 fibers exceed the dense film selectivity values. This effect has been observed previously, and the enhanced separation efficiency of asymmetric hollow fiber membranes is attributed to alignment of the polymer chains in the axial direction due to the high shear forces that are present at the outermost portion of the fiber (where the spinneret is in contact with the extruded dope) [3, 13-15]. The effective skin layer thickness of the State #9 fibers is also quite impressive and results in the highest permeance values that were measured out of all the Spin #2 states. Also, the substructure resistance of all the Spin #2 states appears to be minimal.

Table 6.14 presents the CO₂ and CH₄ permeation values for uncrosslinked TEGMC fibers. The CO₂/CH₄ permselectivity of almost all the states listed below is greater than the dense film selectivity value.

Table 6.14: Pure CO₂ and CH₄ permeation values for uncrosslinked TEGMC fibers from Spin #2 at 35°C and 100 psig feed pressure.

Fiber ID (Spin # - State #)	(P/l)_{CH₄} (GPU)	(P/l)_{CO₂} (GPU)	α*_{CO₂/CH₄}
2 - 3	4.8	220	45
2 - 4	4.2	190	45
2 - 5	5.3	250	47
2 - 6	5.1	180	36
2 - 9	8.1	320	39

Although the effective skin layer thickness values of the Spin #2 fibers actually seem to be slightly higher than those for the Spin #1 fibers, the second spinning study is still viewed as largely successful. The problem of macrovoids in the fiber walls was completely eliminated. Also, the substructure resistance was generally reduced compared to the initial fiber batch. In particular, the fibers from State #9 (Fiber ID: 2 - 9) appear to be of outstanding quality and certainly merit further investigation for crosslinking and, if successful, under the realistic aggressive sour gas feed conditions that are the focus of this work.

Despite these excellent results, a third and final TEGMC fiber spin attempt was planned. The main goals of Spin #3 were further optimization of the spinning parameters to reduce skin layer thickness and the correction of the bore fluid needle misalignment issue that led to some non-concentricity in this fiber batch. Additionally, we hoped to collect more fibers using the same spinning conditions that were used for the '2 - 9' fibers.

6.4. Optimizing PEGMC Spinning for High Performance Fibers

6.4.1. Spin Optimization

No changes were made to the dope composition for this third TEGMC spinning attempt. Based on the results of Spin #2, there is little reason to believe an alteration to the dope composition was necessary. Hence, the dope composition for Spin #3 is also given by Table 6.10.

The primary improvement that was identified based on the Spin #2 fiber characterization results was better concentricity of the fibers. As such, careful spinneret needle adjustment was attempted during the spinning setup. Unfortunately, the bore fluid needle alignment is largely determined by the construction of the spinneret assembly itself. So, only a small degree of control over this alignment and, therefore, fiber concentricity is afforded to the user. Spinneret needles tend to slowly become misaligned over time. This may be due to the high viscosity of spin dopes and the presumably strong forces exerted on the side of the bore fluid needle where the dope enters the spinneret assembly, particularly during the first stages of spinning when the spinneret volume is being filled with dope. As a result, spinneret needles require periodic realignment. However, it is often very difficult to determine when this more involved and costly realignment procedure is needed. In this case, it was believed that simpler adjustment of the spinneret assembly would be sufficient.

The targeted spinning parameters were essentially identical to those used in Spin #1 and Spin #2, as will be shown.

6.4.2. Results of Third Spinning Study

The spinning conditions associated with some of the most promising fiber states from Spin #3 are shown in Table 6.15. These spinning parameters were modeled on the conditions used for the most successful fibers from Spin #1 and Spin #2. In particular, we attempted to replicate Fiber IDs '1 - 7' and '2 - 9' with State #1 and State #2 from this spin. The room temperature during spinning was noted to be 21°C and the relative humidity in the spinning area was 49%. The same Extended II spinneret used for Spin #1 and Spin #2 was used during this study.

Table 6.15: Spinning parameters for select states from Spin #3 with the TEGMC polymer.

Fiber ID (Spin # - State #)	Dope Flow Rate (mL/hr)	Bore Fluid Flow Rate (mL/hr)	Air Gap (cm)	Take-up Rate (m/min)
3 - 1	180	60	7.5	50
3 - 2	180	60	5	50
3 - 4	180	60	10	37.5
3 - 5	180	60	2.5	50

Unfortunately, there were some complications with spinnability during this study. Pulsing of the dope was noted, as well as frequent line breakage. These issues prevented the collection of fibers for some of the states that were most highly anticipated. Also, many of the states there were successfully collected were much shorter (fewer fibers) than would normally be desired. While complications such as these are sometimes encountered, they were prevalent during Spin #3. It is possible that the spinneret needle alignment issue, discussed above, was a contributing factor. Nevertheless, we were able to collect enough fibers to perform SEM and permeation characterization for several states.

6.4.3. PEGMC Fiber Characterization

The uncrosslinked TEGMC fibers from Spin #3 were again inspected using SEM imaging of the cross sections to check for morphological defects. The cross section images for several of the most promising fiber states are shown in Figure 6.8, below. Unfortunately, the fibers still appear to be non-concentric, even after attempting to adjust the alignment of the bore fluid needle. Aside from this flaw, the fibers obtained from this third spinning study possess excellent morphology. They are circular, free of macrovoids, and the fiber dimensions are acceptable.

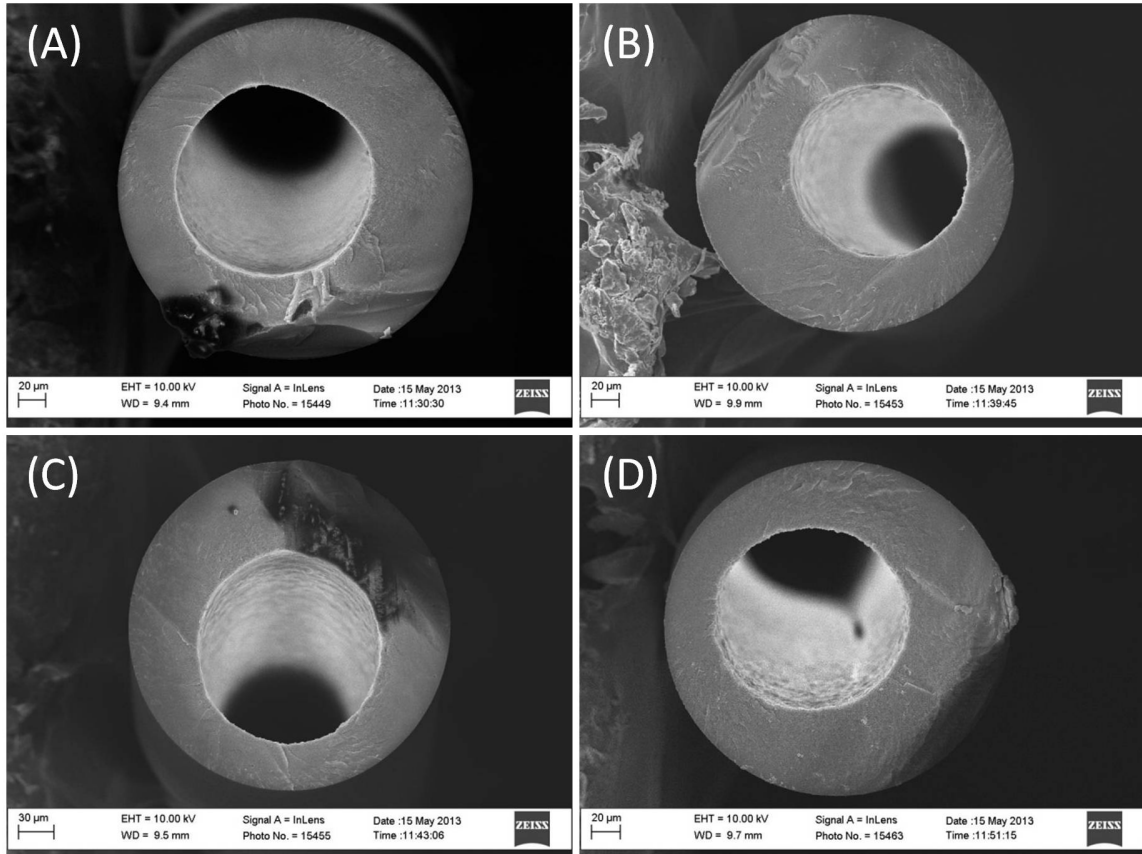


Figure 6.8: Uncrosslinked TEGMC fiber cross sections from Spin #3. (A) is State 1, (B) is State 2, (C) is State 4, (D) is State 5.

The uncrosslinked TEGMC fibers from this spin were characterized with pure N₂, O₂, and He at 35°C and 100 psig feed pressure. A constant pressure permeation system was used for these measurements. As with the first two fiber batches, the skin integrity, skin thickness, and substructure resistance of the fibers was assessed. These pure gas permeation results are shown in Table 6.16 and Table 6.17.

Table 6.16: Pure O₂, N₂, and He permeation results for Spin #3 fibers at 35°C and 100 psig feed pressure.

Fiber ID (Spin # - State #)	(P/l) _{N₂} (GPU)	(P/l) _{O₂} (GPU)	(P/l) _{He} (GPU)	$\alpha^*_{O_2/N_2}$	α^*_{He/N_2}
3 - 1	14	60	420	4.3	30
3 - 2	12	55	400	4.5	33
3 - 4	7.8	39	270	4.9	35
3 - 5	17	75	550	4.5	33

Table 6.17: Skin thickness and substructure resistance characteristics of uncrosslinked Spin #3 TEGMC fibers.

Fiber ID (Spin # - State #)	l_{skin} (nm) [#]	% of Dense Film $\alpha^*_{O_2/N_2}$	% of Dense Film α^*_{He/N_2}
3 - 1	150	98	91
3 - 2	160	102	100
3 - 4	240	111	106
3 - 5	120	102	100

[#]Skin thickness calculation based on the average of N₂, O₂, and He permeation

Based on the results given in the tables above, defect-free states were obtained during Spin #3, despite the difficulties that were encountered. Furthermore, the calculated skin layer thicknesses were smaller on average than either of the first two fiber batches, which was one of the goals of this spin. Substructure resistance also seems to be fairly low for the Spin #3 fiber states shown above. Overall, State #4 (Fiber ID '3 - 4') was considered to be the most promising for application in sour gas applications moving forward. Although the skin layer thickness of the State #4 fibers is

quite a bit greater than that of the other states, it is not prohibitively large and its O₂/N₂ selectivity is superior. The selectivity value of 4.9 is the highest that was measured for any of the uncrosslinked TEGMC fibers for all three of the spin attempts – it is equal to the O₂/N₂ selectivity of the outstanding ‘2 - 9’ fibers.

The pure CO₂ and CH₄ permeation properties of these Spin #3 fibers are tabulated below. Again, the values in Table 6.18 indicate that the Spin #3 fibers are generally of a good quality. The State #4 fibers have lower permeance values than the other states, but their excellent CO₂/CH₄ separation efficiency is attractive.

Table 6.18: Uncrosslinked Spin #3 TEGMC fiber permeation properties for CO₂ and CH₄ at 35°C and 100 psig.

Fiber ID (Spin # - State #)	(P/l) _{CH₄} (GPU)	(P/l) _{CO₂} (GPU)	α* _{CO₂/CH₄}
3 - 1	15	670	45
3 - 2	13	640	51
3 - 4	7.7	460	60
3 - 5	15	710	47

Taking into consideration the results of fiber characterization from all three of the spinning attempts, it is clear that a large number of defect-free states were obtained overall and that a marked improvement over the Spin #1 fibers was displayed in the Spin #2 and #3 fibers. Apart from the slight non-concentricity of the second and third fiber batches, they seemed to contain several nearly ideal states based on the characterization performed in this chapter. Fibers ‘2 - 9’ and ‘3 - 4’ are especially promising and were the obvious top candidates for sour gas permeation testing in CHAPTER 7.

However, the crosslinking protocol and efficacy of crosslinking hollow fiber TEGMC membranes had to be established before their sour gas permeation properties

could be investigated. It was mentioned previously that asymmetric membrane morphologies require significantly more optimization of the thermal crosslinking treatment than dense films, and this subject is addressed in the following section. In addition, Section 6.6 presents another important practical consideration for testing these TEGMC hollow fiber membranes: the selection of an appropriate epoxy for sour gas module-making. The standard module-making procedure for non-aggressive feeds calls for the use of '5-minute' epoxy (ScotchWeld™ DP-100), but this potting adhesive was found to be ineffective for sour gas feeds early on in the dense film portion of this work.

6.5. Crosslinking PEGMC Fibers

6.5.1. Optimization of Thermal Treatment Conditions

Unlike crosslinkable membranes in the dense film morphology, the conditions used for effecting crosslinking in asymmetric hollow fibers have the potential to drastically impact the membrane's productivity and efficiency properties. The susceptibility of asymmetric hollow fibers is related to the highly porous substructure that constitutes the overwhelming majority of the fiber wall. The pores can collapse under overly aggressive thermal treatment conditions. In particular, the very small pores in the fiber's transition layer, which lies between the outer dense skin layer and the inner highly porous supporting layer, are prone to collapse.

Even at treatment temperatures well below the T_g of a particular material, polymer chain segmental mobility is increased. Given sufficient time and in the absence of forces that can 'prop open' the pores of an asymmetric hollow fiber, a process of densification can begin to seriously impact fiber permeation properties. The morphological changes that are associated with fiber densification are two-fold: (1)

collapse of pores directly underneath the skin layer can result in a larger effective skin layer thickness while maintaining solution-diffusion transport and the near-intrinsic permselectivity of defect-free fibers, alternatively (2) partial compaction of pores in the fiber wall can result in the addition of significant mass transfer resistance resembling Knudsen-diffusion. In the second case, the added substructure resistance is either non-selective or much less selective than the dense skin layer, and this leads to decreased separation efficiency as well as decreased productivity.

While it is important to keep the productivity and efficiency consequences of a particular crosslinking protocol in mind, the success of a crosslinking reaction for gas separation membranes ultimately hinges upon its capacity to improve the stability of the membrane against penetrant-induced plasticization. Optimization of the crosslinking conditions for TEGMC fibers is, therefore, critical to the production of viable crosslinked membranes. The crosslinking conditions include treatment temperature, soak time, crosslinking atmosphere, and the presence of crosslinking promoters. A number of potential crosslinking protocols were investigated by comparing the pure gas permeance, ideal selectivity, and CO₂-induced plasticization resistance of defect-free fibers treated under differing conditions. Additionally, the solubility of these crosslinked fibers in NMP was used as a more qualitative measure of fiber crosslinking efficacy.

The crosslinking protocol used for PDMC asymmetric hollow fiber membranes by previous researchers consisted of a 200°C thermal soak for 2 hrs under vacuum conditions. Unfortunately, the crosslinking study of TEGMC dense films in CHAPTER 5 indicated that temperatures greater than about 230°C were required to drive the transesterification crosslinking reaction for these materials. As such, 230°C was the minimum crosslinking temperature investigated for TEGMC hollow fibers. A range of soak times were considered, since longer reaction times were expected to yield a

tradeoff between more complete crosslinking and greater membrane densification. A two hour soak was the minimum used in this work, and this was based on the PDMC crosslinking protocol mentioned above. Furthermore, vacuum and non-vacuum crosslinking atmospheres were tested with the hypothesis that inert gas non-vacuum conditions may reduce the densification effect by keeping the pores ‘propped open’ with low pressure gas.

Table 6.19 lists the various crosslinking protocols for TEGMC fibers investigated in this study. The use of catalysts for the crosslinking reaction was not considered in this work. Following crosslinking, the fibers were allowed to gradually cool down to room temperature (20-25°C/hr) in all cases.

Table 6.19: Various crosslinking conditions for the TEGMC fibers.

Crosslinking Protocol	Soak Temp. (°C)	Soak Time (hrs)	Atmosphere
A	230	6	Vacuum
B	255	2	Vacuum
C	255	6	Vacuum
D	255	6	UHP Ar
E	280	2	Vacuum

SEM images showing the skin layer portion of uncrosslinked TEGMC fibers and those that were crosslinked at 255°C and 280°C are shown in Figure 6.9. It is difficult to distinguish any significant differences in the morphology of the dense skin and transition layers in the three fibers. Even with this highest crosslinking temperature used in this work, the porosity of the fiber substructure is maintained. Furthermore, the skin layer thicknesses of the uncrosslinked and crosslinked fibers appear to be approximately the same. However, assessments of skin layer thickness based on SEM imaging are not very reliable. Pure gas permeation measurements tend to be much more informative.

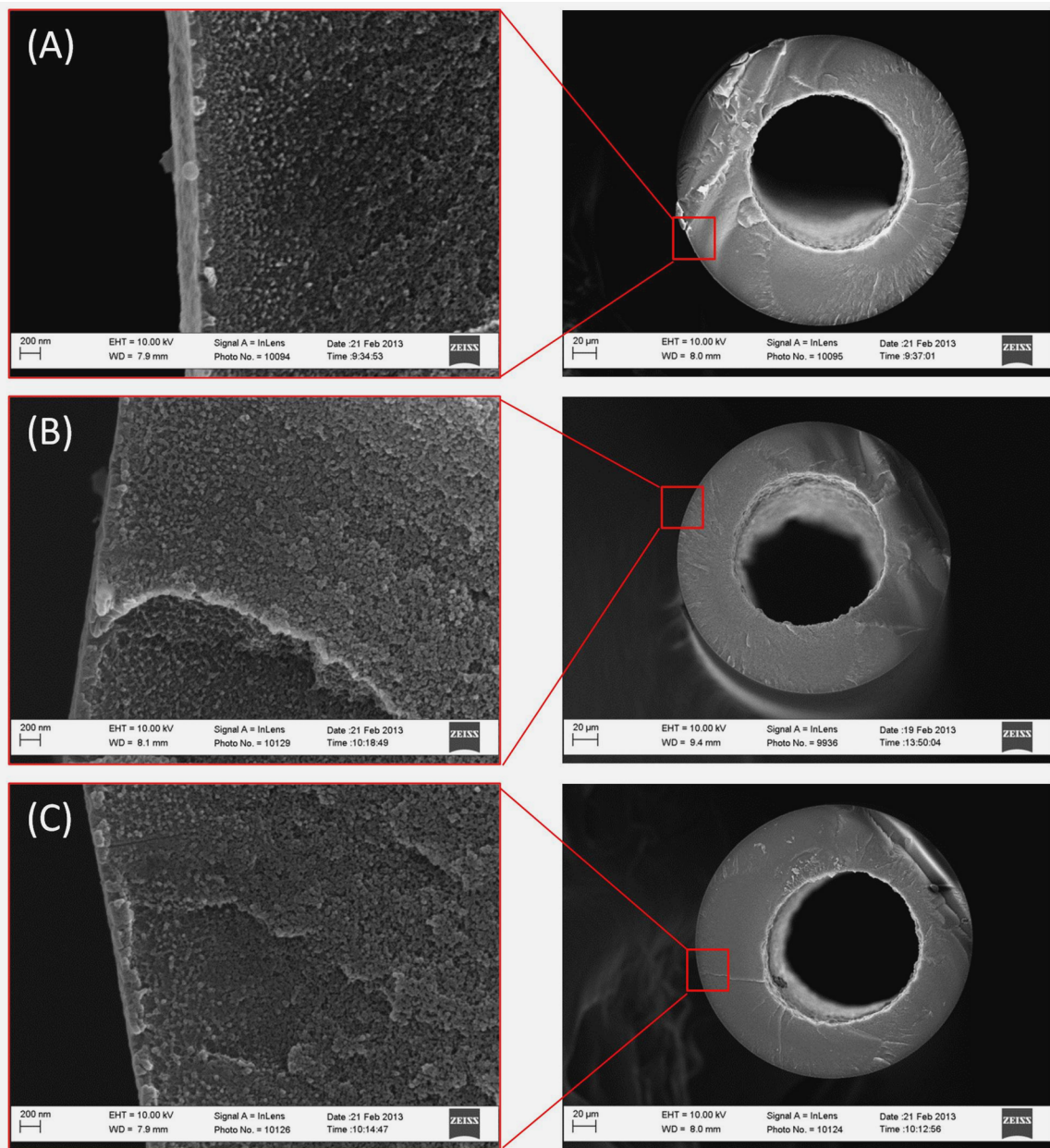


Figure 6.9: SEM images showing the skin and transition layer morphology of TEGMC fibers (ID '2 - 9'). (A) is uncrosslinked, (B) is crosslinked at 255°C with protocol C and (C) is crosslinked at 280°C with protocol E.

6.5.2. Effect of Crosslinking and Crosslinking Conditions on Fiber Performance

The efficacy of the three different crosslinking temperatures was previously assessed in the dense film morphology in CHAPTER 5; the CO₂- and H₂S-induced

plasticization responses were measured, the solubility of films in dry NMP was tested, and gel content experiments were performed. These results are given in Table 5.3, Figure 5.8, and Table 5.4, respectively. Although the 280°C crosslinking temperature was eventually chosen, the 255°C treatment temperature also expressed good stability under these aggressive testing conditions for dense films.

A similar set of experiments was conducted on the TEGMC fibers that were crosslinked with the procedures listed in Table 6.19. To start, crosslinked fiber samples were placed in NMP at room temperature and allowed to soak for several hours. The temperature was then incrementally increased to 50°C, 75°C, and 100°C, and the state of the fibers was noted after several hours at each point. In all cases, swelling of the fibers was apparent even at the lowest temperature. The fibers that were treated with protocols A and B were essentially dissolved at the 50°C temperature, but all the other fiber samples were still visible in the NMP solvent after the 100°C soak. Based on these results, crosslinking Protocols A and B were not believed to be strong candidates.

Pure gas CO₂ and CH₄ permeation results for uncrosslinked and crosslinked TEGMC fibers (Fiber ID '2 - 9') are shown in Table 6.20. These results primarily give an indication of the effects of the various thermal treatments on hollow fiber permeance loss. Since bore-side feeds were used instead of the shell-side feed tests used for high pressure mixed gas studies, the absolute magnitude of the permeance and selectivities are less meaningful than their relative values in this preliminary screening study. The 280°C crosslinking temperature results in the most significant permeance depression compared to the uncrosslinked fibers, and the 255°C crosslinking temperature yields fibers with the highest permeance. Also, it is somewhat surprising that the 230°C crosslinked fibers have such low permeance relative to the fibers that were crosslinked

at higher temperatures. All of the fibers used in these tests were potted with 5-minute epoxy and were allowed to age for at least six months prior to permeation measurement.

Table 6.20: Pure gas CO₂ and CH₄ permeation results for '2 - 9' TEGMC fibers with different crosslinking procedures at 35°C and 100 psig feed pressure using bore-side feeds.

Crosslinking Protocol	(P/l) _{CH₄} (GPU)	(P/l) _{CO₂} (GPU)	$\alpha^*_{CO_2/CH_4}$
Uncrosslinked	2.5	180	72
A	1.3	73	56
B	1.4	85	61
C	1.5	90	60
D	3.2	100	31
E	0.9	68	78

Two main effects are believed to take place during the thermal treatment of TEGMC fibers: (1) transesterification crosslinking via the reaction shown in Figure 5.4, which was actually found in dense films to *increase the intrinsic permeability* of the TEGMC material (Figure 5.9 and Figure 5.10), and (2) densification of the porous fiber substructure, which is expected to decrease fiber productivity. The optimal combination of these two effects for fiber productivity appears to occur with the 255°C crosslinking temperature. The 280°C crosslinking temperature, used in Protocol E, that was employed throughout the dense film study seems to be too aggressive for use in the asymmetric hollow fiber membrane morphology and was eliminated from consideration as a potential standard crosslinking protocol.

It appears that the vacuum crosslinking atmosphere is more promising than the non-vacuum (UHP Ar) atmosphere that was tested in this work. While similar CO₂ permeance is obtained for fibers crosslinked under these two different conditions, the separation efficiency of the vacuum-crosslinked fibers is much better. Furthermore, the

non-vacuum protocol was ineffective, since improved productivity – through propping open the pores in the fiber substructure – was the main goal of this procedure.

The CO₂-induced plasticization response of uncrosslinked TEGMC fibers and those that were crosslinked using Protocols A, B, and C are shown in Figure 6.10. Aside from the initial screening studies discussed so far in this chapter, shell-side feed configuration was used for permeation measurements; the high feed pressures involved in the mixed gas permeation (discussed in CHAPTER 7) and pure gas isotherm measurements (shown below) were found to cause blow outs of the fibers under bore-side feed. In general, we have observed higher permeance under the bore-side configuration than with shell-side feeds, and, presumably, this is caused by slight expansion or compaction differences of the fiber walls due to the transmembrane pressure differential in the two feed models. In any case, the lower permeance values that appear in Figure 6.10, and elsewhere in the remaining pages of this document when shell-side feeds are used, are believed to be the result of this process configuration change.

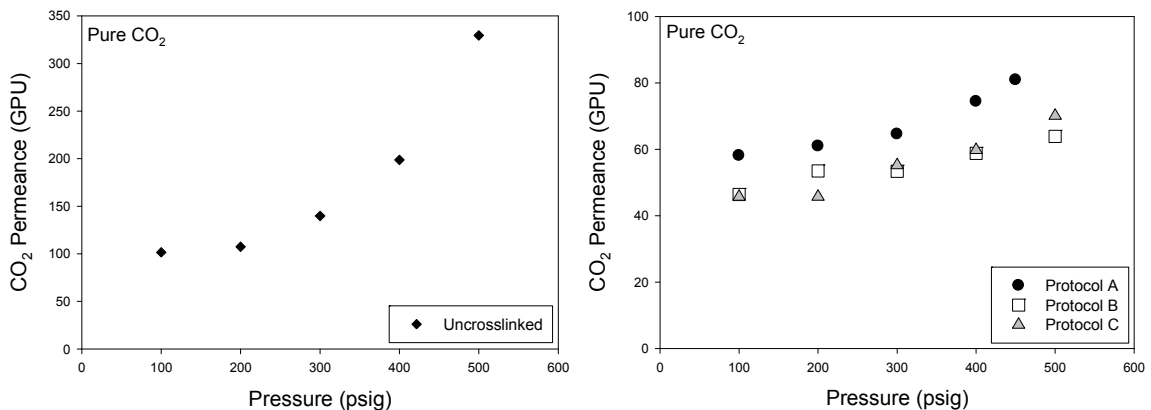


Figure 6.10: Pure CO₂ permeance in uncrosslinked (left) and crosslinked (right) TEGMC fibers (Fiber ID '2 - 9') at 35°C with *shell-side feed*.

Unlike typical dense film permeation for curves, the CO₂ permeance trends for the crosslinked fibers in Figure 6.10 do not pass through a clearly defined minimum. This trend of gradually increasing condensable gas (CO₂ or, later, H₂S) permeance without clear dual-mobility permeation behavior is a fairly normal permeation response for asymmetric hollow fiber membranes due to their more rapid swelling than thicker dense films membranes. It does not necessarily indicate poor crosslinking or resistance against penetrant-induced plasticization. The observed permeance increase for the crosslinked fiber modules is much smaller than the CO₂ permeance upswing observed in the uncrosslinked fiber module. However, there only appears to be minor differences in the plasticization pressure and permeation response after plasticization of the crosslinked fibers using Protocols A, B, or C. The Protocol C fibers had the only measureable plasticization pressure, at around 200 psig.

A more complete investigation of CO₂- and H₂S-induced plasticization using pure and mixed gas feeds is included in CHAPTER 7. The findings of the NMP solubility tests and pure gas permeation measurements presented in this section, as well as the results of the dense film TEGMC crosslinking investigation (Section 5.4.2), indicate that crosslinking Protocol C has the potential to give high performance for aggressive feeds. As such, the crosslinked TEGMC fibers used in the remainder of this work are treated with Protocol C: 255°C, 6 hr soak, vacuum atmosphere.

6.6. Module-Making Considerations for Sour Gas Experimentation

6.6.1. Epoxy Selection for Potting Fibers

The hollow fiber module-making procedure used in this work calls for potting fibers with epoxy to form a hermetic seal between the outer portion of the fibers and the

module components. The standard epoxy that is used for almost all gases and feed conditions is '5-minute' Scotch-Weld™ DP-100 (3M Company). However, several alternative types of epoxy have been used under particularly aggressive feed conditions, such as high temperatures, highly condensable gas feeds, or toxic feeds.

Based on experience gained during dense film permeation experimentation with sour gas feeds, it was determined that the standard 5-minute epoxy was unlikely be acceptable for use in hollow fiber membrane modules intended for sour gas permeation testing. Delamination of the dense film samples was observed during sour gas permeation when 5-minute epoxy was used to seal the film-aluminum tape interface. So, although the preliminary hollow fiber characterization performed in this chapter involved modules that were fabricated with the 5-minute epoxy, it was necessary to find an acceptable alternative epoxy protocol for the more aggressive sour gas permeation tests that are the focus of CHAPTER 7.

A high-temperature epoxy, Duralco™ 4525 (Cotronics, Corp.), was previously used during the dense film portion of this work and was found to provide a very reliable seal under the extremely demanding sour gas feed conditions that were used. Therefore, Duralco™ 4525 was expected to be a good choice in hollow fiber permeation testing, too. Unfortunately, there are several drawbacks to this particular epoxy, which complicate its application to hollow fiber membranes. Firstly, the curing time for Duralco™ 4525 at room temperature is approximately 24 hrs. Also, the resin and hardener that comprise this two-part epoxy must be hand-mixed in a weighing boat or similar container and then poured into the module. This is in contrast to the 5-minute epoxy, which comes in a cartridge and can easily be simultaneously mixed and then injected into a module with a mixing nozzle. Both of these properties of Duralco™ 4525 significantly complicate the module-making process.

While the issues mentioned above are inconvenient, they ultimately do not impact the permeation properties of the asymmetric hollow fiber membranes being tested. However, previous researchers have in some cases noted a significant drop in the permeance of fibers potted with high-temperature epoxy, such as Duralco™ 4525. This has been attributed to outgassing from the epoxy mixture during the extended curing time and essentially irreversible sorption of these by-product gases into the fiber membranes. Carbon molecular sieve fiber membranes appear to be the most prone to such an effect, but it is nevertheless undesirable for all fiber membrane types.

In order to avoid this adverse effect, an extra step was added into the module-making process. Rather than potting the modules almost immediately after mixing the Duralco™ 4525 epoxy, the mixture was placed in a vacuum oven at room temperature (~25°C) for 1 hr prior to potting. Most of the outgassing is believed to take place during this vacuum step, and this is evidenced by bubbling of the epoxy mixture when it is placed in the vacuum oven and a marked decrease in the unpleasant odor of the epoxy mixture after vacuum treatment. It should be noted that the viscosity of the epoxy mixture increases significantly after the 1 hr vacuum degassing treatment, however the mixture remains workable and module potting was not seriously complicated. This epoxy procedure was used for all crosslinked fiber modules in CHAPTER 7.

The results of pure gas permeation on TEGMC hollow fiber membranes that were fabricated using various epoxies and preparation methods are given in Table 6.21. In addition to the 5-minute and Duralco™ 4525 epoxies mentioned so far, another high-temperature epoxy, Duralco™ 4461-IP, was tested. It has been previously shown to obtain similar thermal and chemical stability to 4525, without as large of a permeance reduction. However, because of our experience using Duralco™ 4525 with the dense film membranes and sour gas feeds, in the end it was preferred over the less well-

studied 4461-IP adhesive. The effect of non-degassed Duralco™ 4525 epoxy on fiber permeance is not as pronounced as some researchers have found. Nevertheless, the degassing procedure is used with Duralco™ 4525 throughout our studies as a precautionary measure.

Table 6.21: Comparison of '2 - 9' TEGMC fiber permeation properties for modules made with various epoxies. Measured at 100 psig and 35°C using bore-side feed.

Epoxy Protocol	Crosslinking Protocol	(P/I) _{N₂} (GPU)	(P/I) _{O₂} (GPU)	(P/I) _{He} (GPU)	$\alpha^*_{O_2/N_2}$	α^*_{He/N_2}
5-Minute	Uncrosslinked	6.8	33	270	4.9	40
5-Minute	Protocol C	2.6	15	160	5.8	62
Duralco™ 4525, No Degas	Protocol C	2.0	14	170	7.0	85
Duralco™ 4525, with Degas	Protocol C	2.5	16	190	6.4	76
Duralco™ 4461-IP, No Degas	Protocol C	2.9	18	180	6.2	62

6.6.2. Fiber Post-treatment

As shown in Section 6.5, defect-free crosslinked TEGMC fibers were obtained as a result of the spinning studies described in this chapter. Ideally, these fibers could be used under aggressive feed conditions without further post-treatment. However, asymmetric hollow fiber membranes are often more susceptible to swelling and plasticization than their dense film counterparts. This can lead to losses in permselectivity under mixed gas feed conditions that are not observed for dense film measurements. One explanation for this effect is the ultra-thin skin layers of asymmetric hollow fibers, which lead to steeper sorbed gas concentrations profiles across the membrane.

Post-treatments have been used in past studies to “caulk” pinhole defects in fibers with intermediate skin integrity. One such post-treatment procedure involves the

application of a thin polydimethylsiloxane (PDMS) layer to the outside of the fibers after they have been potted in a module. This process is described in greater detail in APPENDIX D. PDMS is a highly permeable rubbery polymer that, when applied to these slightly defective fibers, is able to drastically reduce the rate of transport through pinhole defects without significantly reducing permeation across the fibers as a whole. In this way, the permselectivity can be enhanced to near the intrinsic dense film value without imparting a major productivity penalty.

For the purposes of the present study, the pinhole caulking effect of the PDMS fiber post-treatment was not thought to be necessary – the measured fiber permselectivity values that approach or exceed the dense film value seem to indicate that major defects are not present in the TEGMC fiber membranes. Yet, as a result of the highly aggressive feed streams that are used in CHAPTER 7 and the propensity of asymmetric hollow fibers, in general, to experience penetrant-induced swelling, PDMS post-treatments were used with some of the TEGMC asymmetric hollow fiber modules. Primarily, this was done as a control to show that the effect of the PDMS coating would be minimal (i.e. limited to small permeance reduction for all gases due to the added mass transfer resistance). However, it will be shown in CHAPTER 7 that the effect of PDMS was more significant under aggressive mixed gas feed conditions.

The pure gas permeation properties of state '2 - 9' TEGMC fibers before and after crosslinking and PDMS post-treatment are given in Table 6.22 and Table 6.23. The permeance values are lowest in the samples that were both crosslinked and PDMS post-treated, but these fibers also have the highest O_2/N_2 and He/N_2 permselectivity. Even though the TEGMC membranes appear to be defect-free, this result suggests that the PDMS post-treatment somehow mitigates undesirable elongation- (due to transmembrane pressure acting on the fiber's bore-side) or swelling-induced changes to the skin morphology, which can cause permeability increases. Again, since the fibers

already show effectively defect-free selectivities without post-treatment, this result was truly unexpected. Nevertheless, it indicates that the PDMS post-treatment may actually be more beneficial than previously anticipated, especially under aggressive feeds that can induce changes to the skin layer morphology.

Table 6.22: Pure gas N₂, O₂, and He permeation results for '2 - 9' TEGMC fibers before and after PDMS post-treatment. Measured at 35°C with 100 psig feed pressure and bore-side feed.

Fiber Treatments	(P/I) _{N₂} (GPU)	(P/I) _{O₂} (GPU)	(P/I) _{He} (GPU)	α [*] _{O₂/N₂}	α [*] _{He/N₂}
Uncrosslinked, Non-PT	6.8	33	270	4.9	39
Protocol C, Non-PT	1.9	9.7	100	5.1	59
Protocol C, PDMS PT	1.6	8.7	99	5.4	62

Table 6.23: Pure gas CO₂ and CH₄ permeation results for '2 - 9' TEGMC fibers before and after PDMS post-treating. Bore-side feeds of 100 psig used at 35°C.

Fiber Treatments	(P/I) _{CH₄} (GPU)	(P/I) _{CO₂} (GPU)	α [*] _{CO₂/CH₄}
Uncrosslinked, Non-PT	2.5	180	72
Protocol C, Non-PT	1.6	81	51
Protocol C, PDMS PT	0.78	50	64

6.7. Conclusions

Asymmetric hollow fiber membranes of the crosslinkable TEGMC polymer were formed using a dry-jet/wet-quench spinning process. Viable dope compositions and spinning parameters were determined through cloud-point experimentation, syringe tests, and from previous spins involving similar materials. Ultimately, three spinning studies were performed and defect-free or nearly defect-free asymmetric hollow fibers were obtained during each attempt.

The Spin #1 fibers, however, showed signs of morphological defects – namely, macrovoids. As a result, the dope composition was slightly altered for Spins #2 and #3 to more closely approach the apparent binodal line. These later two spins yielded a greater

number of defect-free states and no macrovoids were detected. However, some fiber non-concentricity was observed for Spin #2 and Spin #3. The fibers states '2 - 9' and '3 - 4' were found to be particularly promising for eventual sour gas permeation experimentation due to their excellent permselectivity, low substructure resistance, and fairly high productivity.

Crosslinking of the TEGMC fibers was investigated through an extension of the work performed in CHAPTER 5. A number of potential crosslinking protocols were tested using SEM imaging, NMP solubility experiments, and pure gas permeation. Ultimately, a crosslinking protocol consisting of a 6 hr soak at 255°C under vacuum conditions was selected for use in CHAPTER 7.

Finally, a few practical considerations related to module-making were addressed. Duralco™ 4525 was identified as the preferred module-making epoxy for sour gas permeation tests with crosslinked TEGMC fibers, as opposed to the 5-minute epoxy that is normally used for module making. Also, a PDMS post-treatment was identified for use under aggressive feed conditions in order to achieve unusually large increases in selectivity. This is thought to result from the combined effects of added diffusion selectivity, due to polymer chain alignment in the skin layer, and the preservation of amore ideal skin morphology under aggressive feed conditions by the PDMS coating.

6.8. References

1. Koros, W.J., *Evolving beyond the thermal age of separation processes: Membranes can lead the way*. AIChE Journal, 2004. **50**(10): p. 2326-2334.
2. McKelvey, S.A., D.T. Clausi, and W.J. Koros, *A guide to establishing hollow fiber macroscopic properties for membrane applications*. Journal of Membrane Science, 1997. **124**(2): p. 223-232.

3. Omole, I.C., *Crosslinked Polyimide Hollow Fiber Membranes for Aggressive Natural Gas Feed Streams*, in *School of Chemical and Biomolecular Engineering*2008, Georgia Institute of Technology: Atlanta, GA. p. 305.
4. Omole, I.C., S.J. Miller, and W.J. Koros, *Increased Molecular Weight of a Cross-Linkable Polyimide for Spinning Plasticization Resistant Hollow Fiber Membranes*. *Macromolecules*, 2008. **41**(17): p. 6367-6375.
5. Chen, C.C., *Thermally Crosslinked Polyimide Hollow Fiber Membranes for Natural Gas Purification*, in *School of Chemical and Biomolecular Engineering*2011, Georgia Institute of Technology: Atlanta, GA.
6. Ma, C., *Highly Productive Ester Crosslinkable Composite Hollow Fiber Membranes for Aggressive Natural Gas Separations*, in *School of Chemical and Biomolecular Engineering*2012, Georgia Institute of Technology: Atlanta, GA.
7. Carruthers, S., *Integral-skin Formation in Hollow Fiber Membranes for Gas Separations*, in *Department of Chemical Engineering*2001, University of Texas at Austin: Austin, TX.
8. Ma, C., *Optimization of Asymmetric Hollow Fiber Membranes for Natural Gas Separation*, in *School of Chemical and Biomolecular Engineering*2011, Georgia Institute of Technology: Atlanta, GA.
9. Mulder, M., *Basic Principles of Membrane Technology Second Edition*. 1996: Kluwer.
10. Wallace, D.W., *Crosslinked Hollow Fiber Membranes for Natural Gas Purification and Their Manufacture from Novel Polymers*, in *Department of Chemical Engineering*2004, University of Texas at Austin: Austin, TX.
11. Pesek, S.C. and W.J. Koros, *Aqueous quenched asymmetric polysulfone membranes prepared by dry/wet phase separation*. *Journal of Membrane Science*, 1993. **81**(1-2): p. 71-88.
12. Clausi, D.T., S.A. McKelvey, and W.J. Koros, *Characterization of substructure resistance in asymmetric gas separation membranes*. *Journal of Membrane Science*, 1999. **160**(1): p. 51-64.
13. Ismail, A.F., et al., *Direct measurement of rheologically induced molecular orientation in gas separation hollow fibre membranes and effects on selectivity*. *Journal of Membrane Science*, 1997. **126**(1): p. 133-137.
14. Ismail, A.F., et al., *Production of super selective polysulfone hollow fiber membranes for gas separation*. *Polymer*, 1999. **40**(23): p. 6499-6506.
15. Sharpe, I.D., A.F. Ismail, and S.J. Shilton, *A study of extrusion shear and forced convection residence time in the spinning of polysulfone hollow fiber membranes for gas separation*. *Separation and Purification Technology*, 1999. **17**(2): p. 101-109.

CHAPTER 7

SOUR GAS SEPARATIONS WITH CROSSLINKABLE PEGMC ASYMMETRIC HOLLOW FIBER MEMBRANES

7.1. Overview

In this chapter, the highest-quality TEGMC asymmetric hollow fiber membranes that were fabricated in CHAPTER 6 are further investigated. Their effectiveness at performing simultaneous CO₂ and H₂S removal from aggressive sour gas feeds is assessed using pure and mixed gas permeation experiments. Pure gases are used primarily to determine the plasticization resistance properties of crosslinked TEGMC fibers. Also, mixed gas feeds enable the characterization of these fibers under conditions that mimic aggressive sour gas separation applications. Furthermore, physical aging of the TEGMC fibers is addressed through a long-term permeation study. The work described in this chapter is unique within the gas separation membranes literature in terms of the H₂S concentrations and partial pressures in the feed that are used with asymmetric hollow fiber membranes and non-vacuum downstream conditions. These distinct experimental conditions were enabled by a novel constant-pressure hollow fiber permeation system that was used; this system was described in CHAPTER 3. The primary goal of this chapter was to demonstrate that crosslinked TEGMC hollow fiber membranes possess adequate permeation properties under realistic conditions to make them an attractive alternative to traditional absorption-based sour gas separation technologies.

7.2. Pure Gas Permeation

Permeation characterization is ultimately the most critical factor in determining whether or not asymmetric hollow fibers membranes have adequate separation performance for potential application in an industrial setting. While mixed gas permeation experiments are expected to give permeance property measurements that more accurately reflect the performance of hollow fiber membranes under realistic conditions, pure gas permeation is also valuable. As with permeation characterization of dense films, pure gas feeds can be used to determine the ideal selectivity properties and individual gas plasticization response of hollow fiber membranes. Also, a greater understanding of competitive sorption and other polymer-penetrant interaction effects that take place in mixed gas permeation can be obtained by comparing these results to pure gas permeation results, when such effects are absent.

The TEGMC fibers that are used in this chapter are mostly from the '2 - 9' spinning state discussed in CHAPTER 6. However, fibers from the '3 - 4' spinning state are also used for the long-term physical aging study that is the subject of Section 7.2.3. These two states were found to give the most promising characteristics based on the preliminary evaluation that was performed in CHAPTER 6, and their productivity and efficiency properties were found to be very similar. All of the crosslinked fibers tested in this chapter were treated using 'Protocol C,' which consists of a 255°C treatment temperature, a 6 hr soak under vacuum, and gradual cooling back down to room temperature. With the exception of some modules used in the physical aging study, all modules were formed using Duralco™ 4525 epoxy with the degassing procedure described in the previous chapter.

Furthermore, all '2 - 9' TEGMC fiber modules used in this work were allowed to age for at least 6 months prior to testing. It will be shown in Section 7.2.3 that physical aging plays a major role in the productivity and efficiency of these fibers, especially during the first few months following spinning. Therefore, the '2 - 9' fibers were purposely allowed to age in an attempt to eliminate the majority of this transient permeation behavior from our measurements. Ideally, fiber treatments or the careful selection of storage conditions would enable a significant reduction or, even more preferably, elimination of these large time-dependent physical aging effects. While this is considered in the following sections, such a storage protocol was not used on the '2 - 9' TEGMC fibers that are tested in this work.

7.2.1. Pure CH₄ Permeance Measurements

Pure CH₄ permeation was conducted on the crosslinked TEGMC fibers from state '2 - 9' with and the without PDMS post-treatment (referred to as Non-PT and PDMS PT, respectively). A shell-side feed configuration was used to prevent module 'blow out' failures, which can sometimes occur at high feed pressures with bore-side feed due to excessive skin layer elongation. Permeation isotherms for feed pressures up to 500 psig are shown in Figure 7.1.

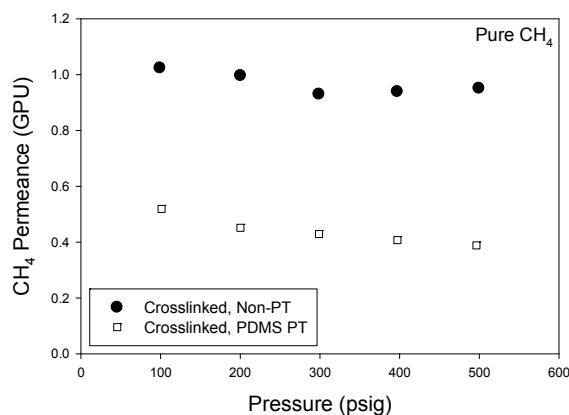


Figure 7.1: Pure CH₄ permeation in crosslinked TEGMC hollow fibers at 35°C using a shell-side feed.

Both of the modules give excellent resistance to CH₄-induced swelling and plasticization, as was expected. The PDMS post-treated module has lower permeance for CH₄ and a slightly more pronounced dual-mobility permeation response – that is, decreasing permeance with increasing feed pressure – as compared to the non-post-treated module. This is likely due to the added mass transfer resistance of the PDMS coating and the slightly more defect-free skin layer for the post-treated TEGMC fibers.

A more apt term to describe the skin layer quality of crosslinked ‘2 - 9’ TEGMC fibers after PDMS post-treatments might be “*defect-resistant*” or “*self healing*”. It is clear from the initial fiber characterization given in CHAPTER 6 and the general shape of the CH₄ permeance isotherm above that the non-post-treated fibers do not possess the major pin-hole type defects that we typically think of for asymmetric hollow fiber membranes. However, it is believed that the PDMS coating on the already defect-free fibers makes them less prone to the expansion of morphological imperfections under high pressure or condensable gas feed conditions by ‘filling in’ any nascent defects. It is hypothesized that the shell-side feed configuration is critical to this effect of PDMS.

Ideally, the productivity of the crosslinked fibers should be higher than was measured in Figure 7.1. The effective skin layer thickness of these fibers, based on the material's dense film CH₄ permeability of 2.8 Barrer under approximately the same feed conditions, is between 2.5 μm and 5 μm. A number of factors lead to the permeability depression that is observed between these fibers and the untreated '2 - 9' fibers that were characterized in Section 6.3 ($I_{skin} = 270$ nm). These include the crosslinking treatment, physical aging time, shell-side feed configuration, and PDMS post-treatment. Nevertheless, their outstanding permselectivity and other properties that have been measured to this point justify their continued investigation in the current study.

At the same time, further optimization of the spinning dope, crosslinking treatment protocol, and post-treatment/module-making process are needed before these fibers can be considered to be commercially viable. These are some of the recommendations for future work included in CHAPTER 8.

7.2.2. Plasticization Resistance Measurement of Crosslinked and Uncrosslinked Fibers

The pure gas CO₂ and H₂S plasticization response of TEGMC fibers was measured using shell-side feeds at 35°C. The measured pure CO₂ permeance isotherms for TEGMC fibers before and after crosslinking and PDMS post-treatment are displayed in Figure 7.2. As mentioned in CHAPTER 6, it is not abnormal for asymmetric hollow fiber membranes to give permeation isotherms for condensable species, like CO₂ and H₂S, which do not pass through a minimum. Permeation trends of this sort do not necessarily indicate poor membrane stability or especially high susceptibility to plasticization. Instead, mixed gas permselectivity is the most reliable measure of these properties.

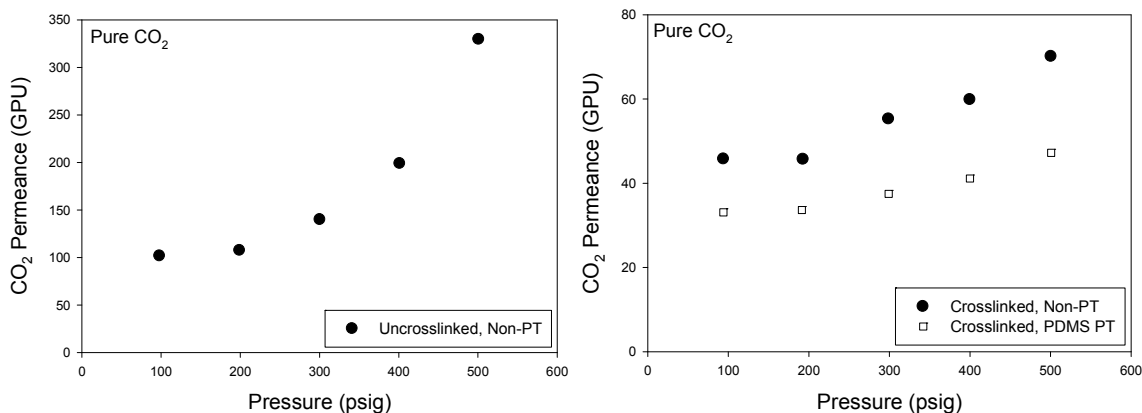


Figure 7.2: CO₂ permeance of '2 - 9' TEGMC fibers with various treatments. Measured using shell-side feed at 35°C.

The crosslinked TEGMC fibers, with and without PDMS post-treatment, have similar CO₂ permeance trends in terms of their swelling-induced plasticization pressure. In both cases, a moderate degree of plasticization is apparent at CO₂ feed pressures greater than 200 psig. However, the post-treated fibers seem to give a slightly more gradual permeance upswing. Also, compared to the radical CO₂ permeance upswing for the uncrosslinked TEGMC fibers, the swelling-induced plasticization response of the crosslinked fibers is well-controlled.

The CO₂ permeance of the PDMS post-treated TEGMC fibers is about 25% lower than the non-post-treated fibers. This is ascribed to the added transport resistance of the PDMS layer, *not* to the “caulking” of any pre-existing pin-holes. As mentioned previously, the permeation trends for the non-post-treated fibers do not indicate that pin-hole defects are present in the crosslinked TEGMC skin. The CO₂ permeance in crosslinked TEGMC fibers is relatively less impacted by the PDMS post-treatment compared to the CH₄ permeance. This is likely due to the intrinsic permeability of PDMS for CO₂ and CH₄. Since PDMS is a rubbery polymer and it is expected to be more permeable to condensable species, like CO₂.

The CO₂/CH₄ ideal selectivity for crosslinked TEGMC asymmetric hollow fiber membranes with a shell-side feed configuration can be calculated from the results of the pure gas CO₂ and CH₄ permeation. These values are shown in Table 7.1. Compared to the crosslinked TEGMC dense film value of 34, these ideal selectivity values in the asymmetric hollow fibers indicate improved separation efficiency. Presumably, this is due to added diffusion selectivity from polymer chain alignment in the skin layer. It appears that the PDMS post-treatment allows this effect to be fully realized through the previously described effects.

Table 7.1: Ideal selectivity values for crosslinked TEGMC fibers under shell-side feed at 35°C.

Crosslinked Fibers	(P/l)_{CH4} (GPU)	(P/l)_{CO2} (GPU)	α*_{CO2/CH4}
Protocol C, Non-PT	1.0	46	46
Protocol C, PDMS PT	0.52	33	63

Finally, the capacity of TEGMC fibers to resist H₂S-induced plasticization was evaluated using pure H₂S feeds at 35°C. A specially developed constant-pressure permeation system, described in CHAPTER 3, had to be used for all hollow fiber permeation measurements involving H₂S. A unique feature of this system is the use of digital mass flowmeters for the measurement of the permeate and retentate flow rates. Typically, a bubble flowmeter is used for the permeate volumetric flow rate measurement. In the case of H₂S-containing feeds, however, it was necessary to prevent operator exposure to the test gases by designing a fully sealed system. All gases used in these experiments, including the permeate, retentate, and gas used for GC sampling, were routed to the roof-mounted acid gas scrubbing unit to ensure safe disposal.

Figure 7.3 presents the pure H₂S permeation isotherms for TEGMC fibers. As expected, the crosslinked TEGMC fibers have significantly lower H₂S permeance than the uncrosslinked fibers. Again, this is presumed to be due to accelerated physical aging under the high temperature conditions associated with crosslinking (annealing). The uncrosslinked fibers have a H₂S plasticization pressure of about 45 psig, above which the H₂S permeance increases dramatically. At the 90 psig feed pressure, H₂S permeance in the uncrosslinked membranes is 197% of the 15 psig value.

Somewhat surprisingly, the crosslinked fibers without post-treatment also appear to have a H₂S plasticization pressure around 45 psig. This is quite a bit lower than the dense film plasticization pressure measured in CHAPTER 5 (~90 psia). However, as was mentioned previously, asymmetric hollow fiber membranes often display permeance upswings at lower pressures, and this is not necessarily viewed as a sign of poor membrane stability. The highly condensable nature of the H₂S gas makes swelling-induced permeance increases even more likely under these feed conditions than with other species.

The application of a PDMS post-treatment to the crosslinked fibers seems to be highly effective at suppressing these non-ideal effects in the crosslinked fibers. After post-treating, there is an apparent H₂S plasticization pressure of about 65 psig, and the H₂S permeance increases gradually after passing through the minimum value. The exact mechanism behind this improved resistance to plasticization after PDMS-coating is not fully understood at this time, but may be related to the added 'defect-resistance' afforded by the PDMS coating that was mentioned previously. This hypothesis suggests that in addition to typical swelling-induced plasticization effect, which is not expected to be healed with the PDMS coating, a second effect related to changing skin layer morphology under swelling-induced stresses may be present.

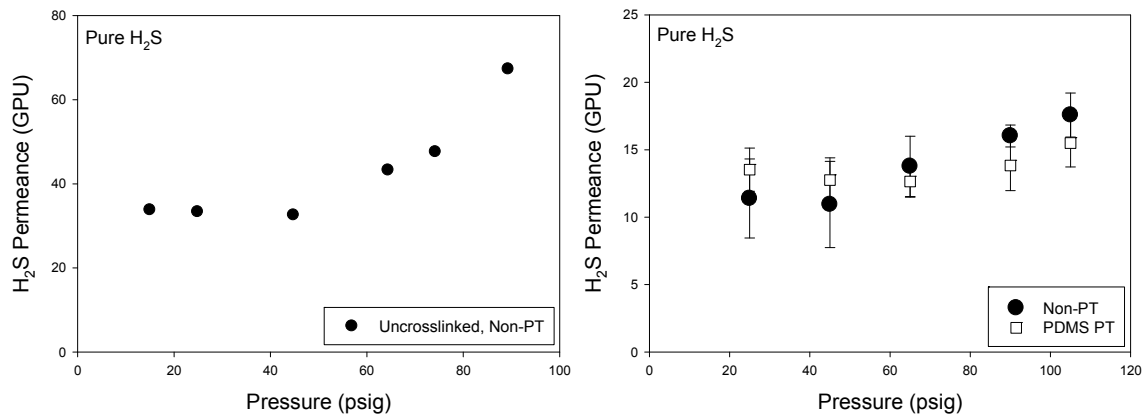


Figure 7.3: H₂S permeation in '2 - 9' TEGMC fibers with various treatments. Measured using shell-side feed at 35°C.

The slightly higher permeance of the PDMS post-treated fibers compared to the crosslinked fibers without post-treatment was unexpected. The mass transfer resistance of the PDMS layer to H₂S was expected to be essentially negligible, since H₂S is so highly favored for permeation through rubbery polymers. Nevertheless, there does not appear to be a physical explanation in support of higher H₂S permeance through the post-treated fibers. As such, this is simply believed to be the result of experimental error during the measurement of H₂S permeance at low feed pressures. We believe this error arises from limitations of the hollow fiber sour gas permeation system.

Regrettably, the digital mass flowmeters used with this system have poor sensitivity compared to the standard bubble flowmeters used to measure non-toxic gases. This is especially problematic for membrane-feed combinations that give low permeate flow rates, since less gas flowing to the mass flowmeter results in fairly low signal-to-noise ratios. Unfortunately, the crosslinked TEGMC fibers with low pressure H₂S in the feed are intrinsically a low permeance combination.

Long permeation times were used in an attempt to average out the poor signal-to-noise ratio through the collection of large data sets. This was mostly successful, based on moving average calculations of the permeation rate over experiments that were typically at least 2 hours in length. Yet, despite these methodical data collection procedures, low flow rate sour gas measurements are undoubtedly subject to somewhat higher experimental error than the other permeation measurements performed in this work. As mentioned earlier, a typical dense film or hollow fiber permeation measurement is expected to have error of $\pm 5\%$ at most. However, the error bars included in Figure 7.3 for the crosslinked fibers indicate that a higher level of uncertainty is present for these tests, especially at low feed pressures.

It should be noted that this effect is largely limited to the experiments involving low feed pressure, pure H₂S, and crosslinked TEGMC fibers shown in the figures above. This combination of experimental variables makes for exceedingly low permeate flow rates. The mixed gas experiments presented later in this chapter have high CO₂ content, which is a faster gas than H₂S, and involve much greater feed pressures (up to 700 psig). As such, the signal-to-noise ratios from the digital mass flowmeters are much better for these experiments and the experimental error is expected to be typical ($\pm 5\%$, or less).

Obviously, improvements to this experimental setup should be made. At the same time, it must be pointed out that because of H₂S gas handling concerns these sour gas permeation measurements are not straightforward by any stretch of the imagination. In fact, these barriers to sour gas experimentation are so significant that, to the best of our knowledge, these are the first pure H₂S asymmetric hollow fiber permeance measurements reported in the literature. As such, further optimization of the permeation system and process of making these sour gas measurements is still ongoing.

The above discussion notwithstanding, it appears that the PDMS post-treatment is essential to the maintenance the TEGMC skin morphology when the H₂S partial pressure in the feed is greater than about 45 psig.

7.2.3. Physical Aging Study on TEGMC Fibers

The phenomenon of physical aging in glassy polymer membranes has been studied in a number of materials previously [1-6]. Physical aging is a time-dependent process that takes place after membrane formation, and it involves the diffusion of free volume out of the membrane and the simultaneous contraction of the polymer matrix. In general, physical aging causes a reduction in membrane productivity and an increase in permselectivity due to the free volume effects that were described in CHAPTER 2. Membrane thickness has been found to significantly impact the rate of physical aging. Ultra-thin membranes, like often found in the asymmetric hollow fiber membrane morphology, age much more quickly than thicker membranes, such as dense films.

In a recent study, PDMC asymmetric hollow fiber membranes were investigated over several months in order to determine the extent of physical aging after membrane formation by dry-jet/wet-quench spinning [7]. The CO₂ permeance of these fibers was observed to fall to approximately 40% of the original measured value. This large productivity reduction is obviously undesirable, and represents another potential hurdle to the application of asymmetric hollow fibers to industrial gas separations.

In order to elucidate the impact of physical aging on TEGMC fiber productivity, a long-term permeation study was conducted using the '3 - 4' TEGMC fibers developed during Spin #3 in CHAPTER 6. These fibers were rapidly potted in modules following spinning and solvent exchange in an attempt to measure their permeation properties

before significant aging effects had set in. Pure CO₂ and CH₄ feeds were used in this work.

7.2.3.1. Physical Aging Under Ambient Storage Conditions

Crosslinked and uncrosslinked TEGMC hollow fibers were allowed to age under ambient conditions. The permeation properties of these fibers over a ~25 week aging period are shown in Figure 7.4 and Figure 7.5. Modules used in this study were fabricated with 5-minute epoxy and bore-side feeds were used.

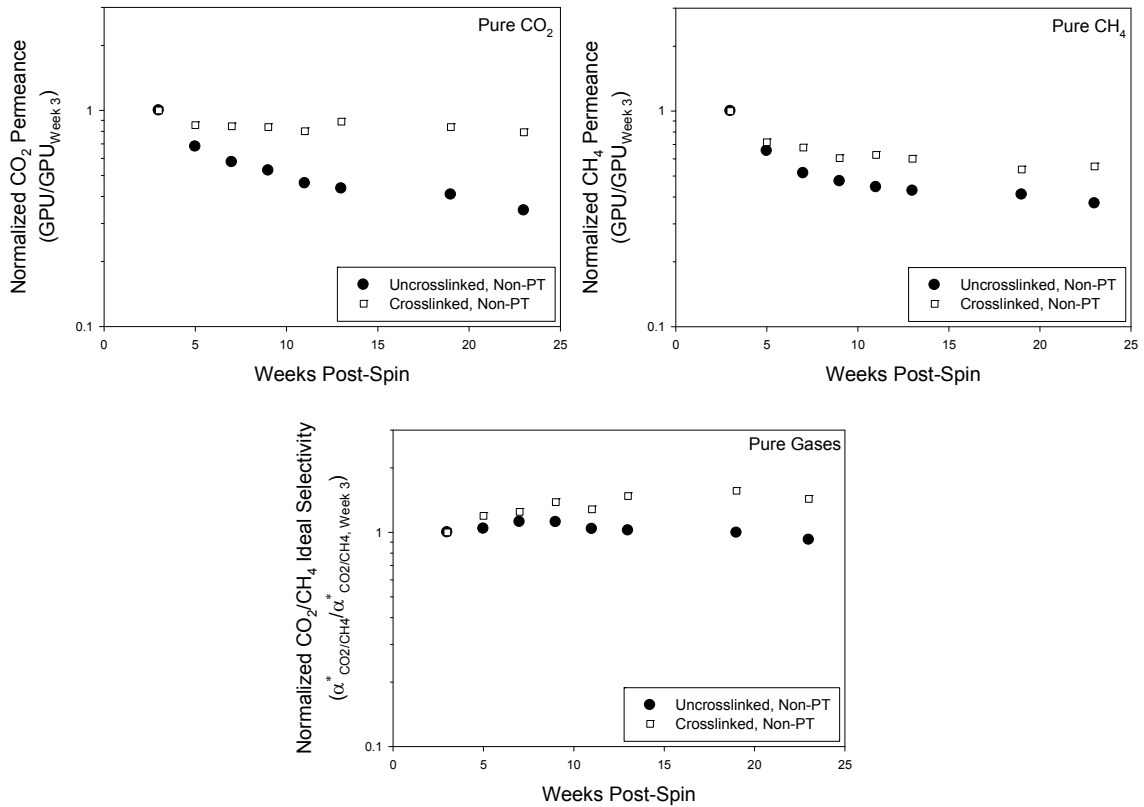


Figure 7.4: Normalized pure gas CO₂ and CO₄ permeation at 35°C in TEGMC fibers stored under ambient conditions for several months.

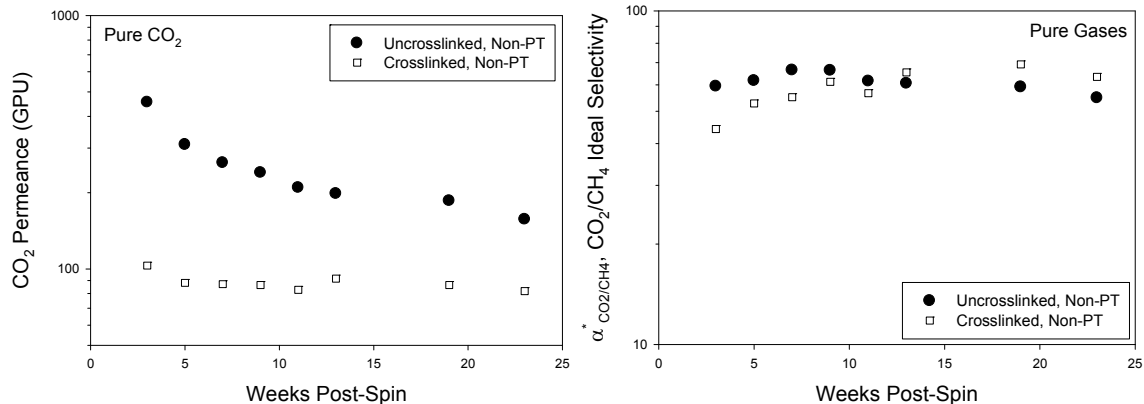


Figure 7.5: Permeation properties at 35°C of TEGMC fibers stored under ambient conditions for several months.

Both the crosslinked and uncrosslinked TEGMC fibers stored under these conditions experience significant permeance reductions during the course of the study. The crosslinked fibers are less affected by physical aging than the uncrosslinked fibers. This is almost certainly due to the fact that the crosslinking process (annealing) itself essentially causes rapid physical aging and [effective] skin layer thickening due to the high temperatures and increased polymer chain mobility involved. This means that the crosslinked fiber membranes are much closer to their fully “relaxed” state than the uncrosslinked fibers at the start of this experiment.

The CO₂ permeance of the crosslinked TEGMC fibers drops by about 20% and the CH₄ permeance is reduced by approximately 40% between the first and last measurements. As a result, there is a fairly large increase in CO₂/CH₄ ideal selectivity for the crosslinked fibers. The original permeation measurements indicated a CO₂/CH₄ ideal selectivity of just over 40, but this number increased to over 60 after 23 weeks of aging.

Despite the large gain in CO₂/CH₄ separation efficiency for the crosslinked fibers, the huge permeance drops that are observed are undesirable. Additionally, the transient permselectivity behavior is not ideal, since it would complicate any attempts at process

modeling of these fibers. Therefore, alternative storage conditions were investigated as a method for slowing down or, ideally, freezing the physical aging process.

7.2.3.2. Suppression of Aging Effects with Active CO₂ Feed Storage

In the same study of PDMC hollow fibers mentioned above, active CO₂ feed storage conditions were used to mitigate the effect of physical aging [7]. It was found that a continuous CO₂ feed to the modules at relatively low pressure (~15 psig) effectively reduced the rate of physical aging. Presumably, the condensable CO₂ feed gas sorbs into the free volume microvoids within the fiber membrane and limits their rate of diffusion out of the polymer matrix.

A similar active CO₂ feed study was performed on the TEGMC fibers in parallel with the ambient storage physical aging study. The crosslinked and uncrosslinked fiber modules were kept under ~15 psig CO₂ at all times, except when being tested. Permeation results using CO₂ and CH₄ feed gases are shown in Figure 7.6 and Figure 7.7. These modules were fabricated using Duralco™ 4525 epoxy because of the potential for failure under the long term CO₂-exposure conditions, and this resulted in somewhat lower permeance values than those measured in Figure 7.5.

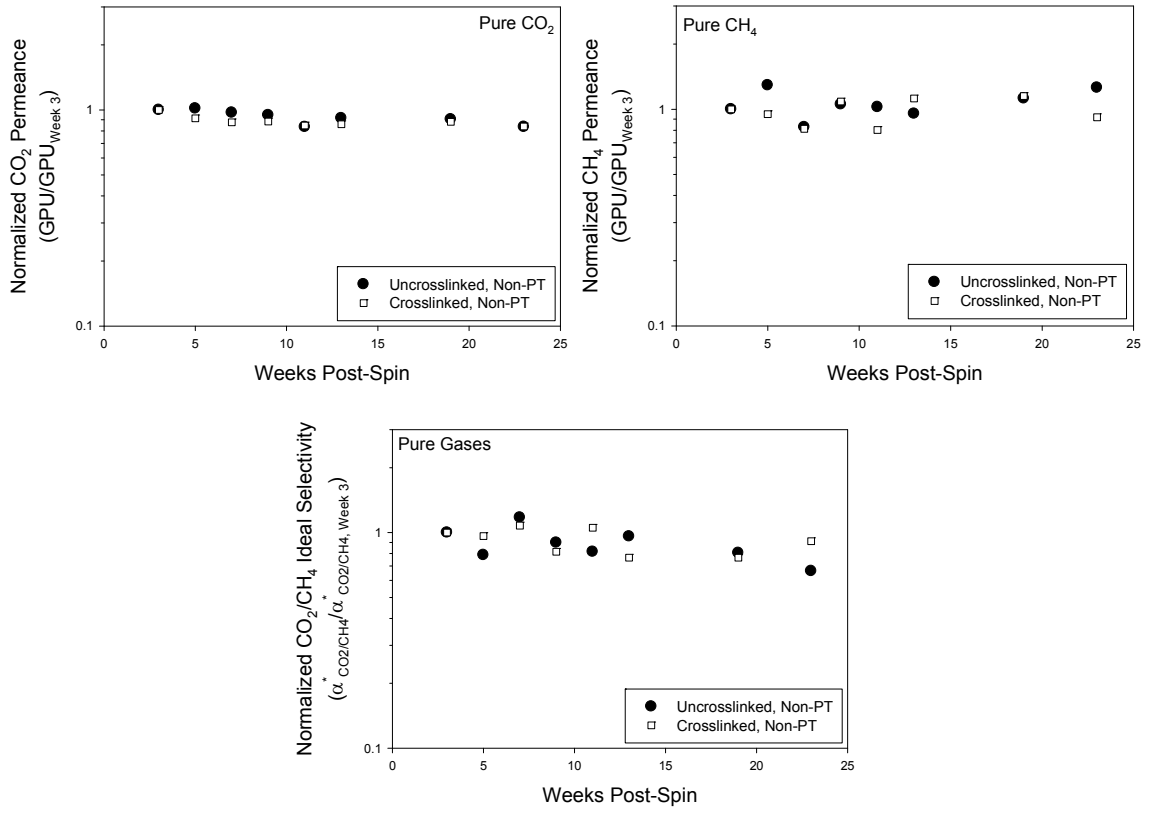


Figure 7.6: Normalized pure gas CO₂ and CH₄ permeation in TEGMC fibers stored under active CO₂ feed for several months.

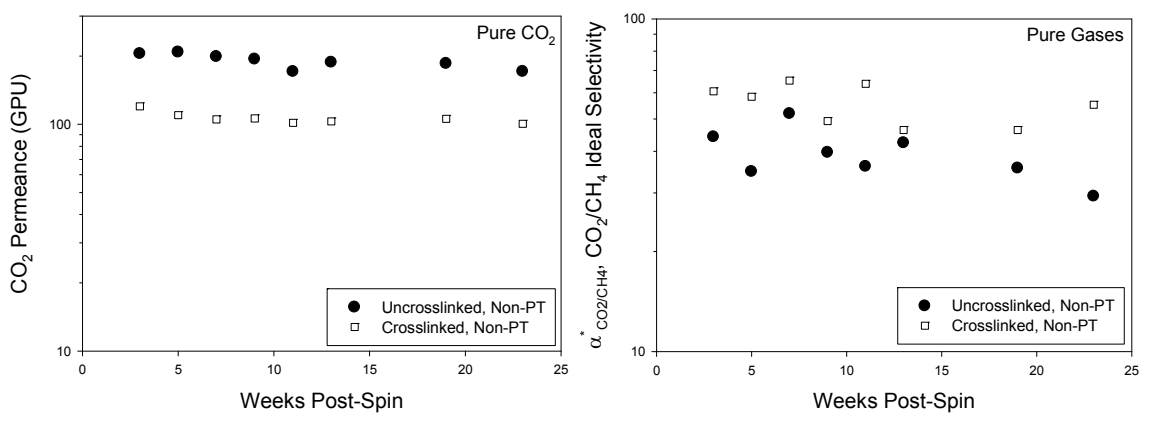


Figure 7.7: Permeation properties of TEGMC fibers stored under active CO₂ feed for several months.

It is clear from the results given above that aging under active CO₂ feed is effective at preventing the large permeance reductions that were observed under ambient storage conditions. The CO₂ and CH₄ permeance of the crosslinked TEGMC fibers decrease by around 10% each. In particular, the physical aging trends of the uncrosslinked TEGMC fibers under these conditions are surprising. In contrast to the > 65% CO₂ permeance loss under ambient storage, the uncrosslinked fibers under active CO₂ feed only experience a CO₂ permeance loss of about 15%.t.

It appears that the active CO₂ feed storage procedure allows the TEGMC fibers to maintain a chain packing status that is very similar to the non-aged fibers. Relaxation of the polymer matrix and loss of free volume is reduced. Also, it should be noted that the active feed conditions used here (pure CO₂ at 15 psig) are quite mild. More aggressive active feed conditions consisting of higher CO₂ partial pressure may allow for the indefinite arrest of the physical aging phenomenon. In any case, the current results demonstrate that this simple method is effective for maintaining excellent TEGMC hollow fiber productivity for long-term natural gas separation applications.

7.3. Mixed Gas Permeation

Several sour and non-sour gas mixtures were used in order to characterize the performance of crosslinked TEGMC hollow fiber membranes under realistic aggressive natural gas feed conditions. The crosslinked fiber modules used in this section were fabricated with degassed Duralco™ 4525 epoxy and fiber from the '2 - 9' spinning state of Spin #2. These fibers were selected because of their excellent pure gas permeation properties and good morphological properties, but also because a large enough quantity of fiber from this state had been collected during spinning to enable the completion of

this work without having to switch between states. The '2 - 9' fibers used here had aged for approximately 6 months before this study was started. This was detrimental to the productivity of the modules, but was actually considered to be more appropriate for membrane characterization; no significant additional time-dependent aging was expected to take place in the fibers as this mixed gas study proceeded. PDMS post-treated and non-post-treated modules were investigated.

7.3.1. Binary (50% CO₂ / 50% CH₄) Acid Gas Mixture Permeation

The mixed gas permeation properties of crosslinked TEGMC hollow fiber membranes were initially evaluated using a non-sour natural gas mixture comprised of 50% CO₂ and 50% CH₄. We first wanted to evaluate the mixed gas feed asymmetric hollow fiber membrane performance without the potential H₂S-polymer interactions that were observed in CHAPTER 4 and CHAPTER 5 for dense films.

Permeation results for non-post-treated and PDMS post-treated modules are given in Figure 7.8. At the highest pressure tested, 700 psig, the CO₂ fugacity in the feed is 277 psi. These conditions are fairly challenging, so some amount of membrane swelling is likely. Despite this, the CO₂ and CH₄ permeance values that were measured in both of the fibers are in good agreement with the pure gas values measured earlier in this chapter. More importantly, the performance of both crosslinked TEGMC modules with this binary CO₂/CH₄ feed are very impressive in terms of their permselectivity. The non-post-treated fibers give CO₂/CH₄ permselectivity values that closely resemble the dense film efficiency with this feed mixture (see Figure 5.20) over the entire isotherm; these values range between 41 and 28 at the low and high pressure ends, respectively. Although there is a decrease in permselectivity as the feed pressure is increased, this

was believed to be at least partially the result of standard dual-mobility transport effects – as was the case for crosslinked TEGMC dense films.

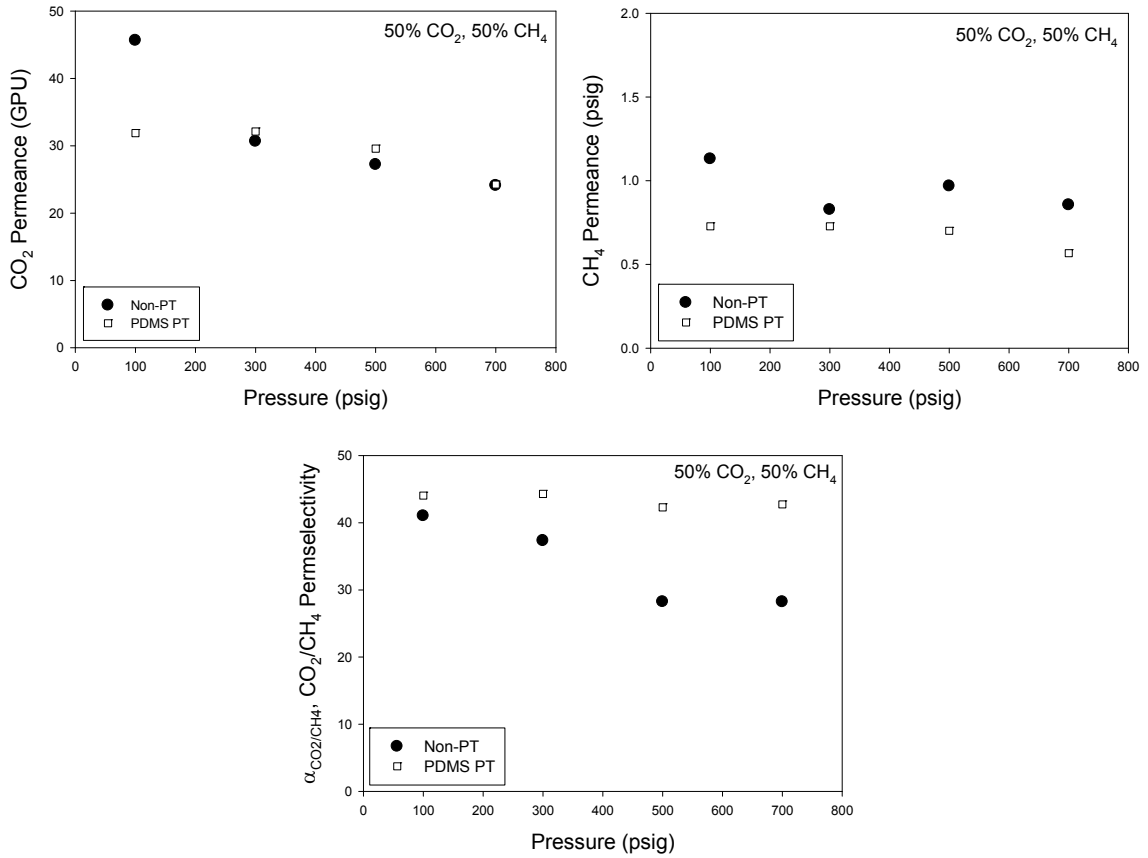


Figure 7.8: Mixed gas (50% CO₂, 50% CH₄) permeation results for crosslinked TEGMC fibers. Measured using shell-side feed at 35°C.

However, the PDMS post-treated modules have even greater permselectivity, and this is attributed to the “self healing” enhancement that the PDMS coating provides. Again, this hypothesis suggests that the PDMS coating may function as a active sealant for sites in the fiber’s skin that behave normally under low pressure feeds, but experience an expansion of morphological imperfections under aggressive feed conditions due to swelling-induced stresses. The CO₂/CH₄ permselectivity of the post-

treated module is greater than 42 for all feed pressures tested, which is well above the dense film ideal selectivity of crosslinked TEGMC.

It is believed that high shear forces during the spinning process lead to polymer chain orientation in the skin layer. In turn, this imparts greater diffusion selectivity into the TEGMC fibers than was measured for crosslinked TEGMC dense films and higher overall permselectivity for TEGMC fibers than analogous dense films, *as long as defects caused by elongation under high transmembrane pressures or swelling are suppressed*. Whereas the PDMS post-treatment allows this condition to be met over the entire pressure range, the non-post-treated fibers succumb to minor swelling-induced morphological defects in their skin layer. As a result, the PDMS post-treated fibers maintain their ultra-high CO₂/CH₄ permselectivity for all pressures tested.

7.3.2. Mixed Gas Permeation with Higher Hydrocarbon Contaminant

As an extension of the 50% CO₂, 50% CH₄ permeation experiments discussed above, a similar feed gas containing a representative higher hydrocarbon contaminant (toluene) was used. This “dirty” feed mixture was comprised of 50% CO₂, 500 ppm toluene, and 49.95% CH₄.

Toluene is a highly condensable species ($T_c = 521.8$ K) that is used as a proxy for the higher hydrocarbon contaminants of natural gas, particularly aromatics, which asymmetric hollow fiber membranes are likely to encounter in the field. As such, it is important that the crosslinked TEGMC membranes are capable of withstanding exposure to reasonably high concentrations of this contaminant without severe performance degradation. Previous investigations of PDMC hollow fiber have shown that the presence of toluene in a feed mixture may cause a reduction in membrane permeance due to *antiplasticization* [7, 8]. However, the threat of toluene-induced

plasticization is also a reasonable concern and is potentially much more deleterious to membrane separation performance.

The permeation properties of crosslinked TEGMC hollow fibers *without* post-treatment are shown in Figure 7.9 for mixed gas feeds with and without toluene.

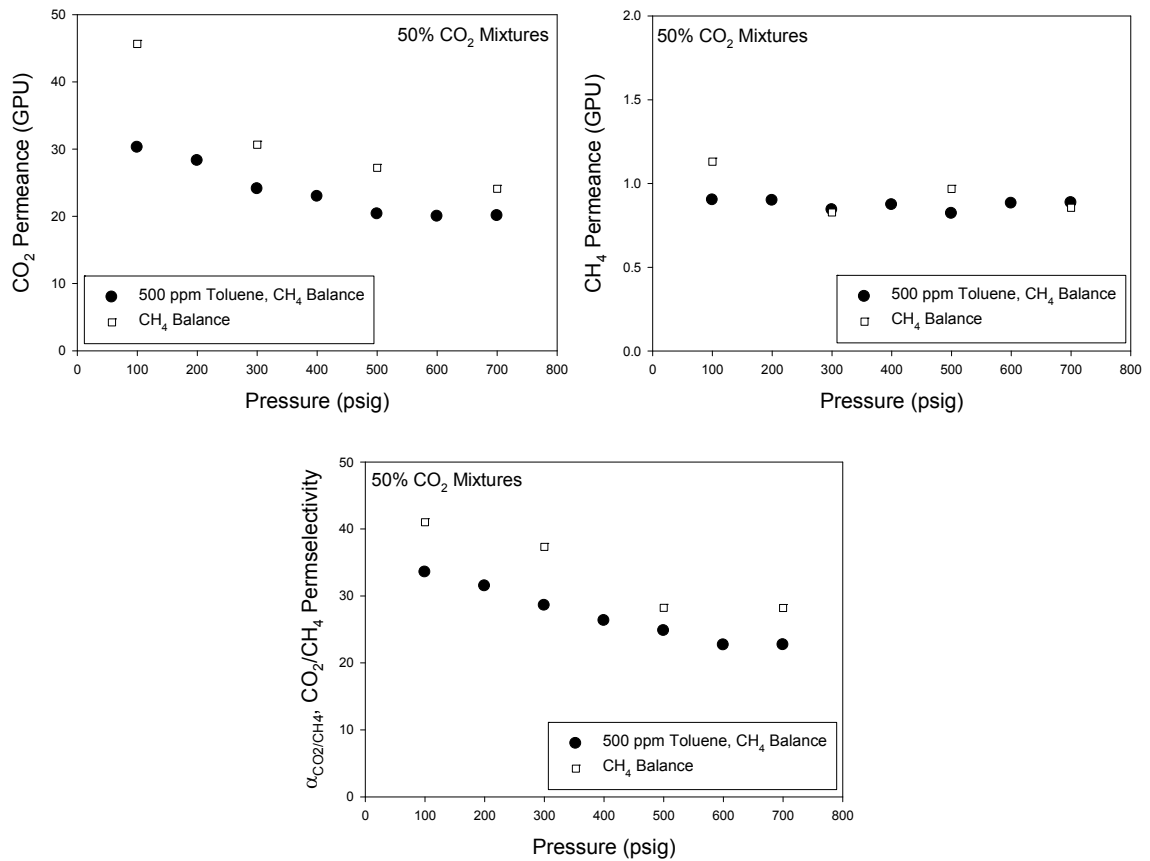


Figure 7.9: Mixed gas permeation of 50% CO₂ mixtures with and without 500 ppm toluene contaminant through crosslinked TEGMC fibers using shell-side feed at 35°C.

The permeance trend that is observed for these crosslinked TEGMC hollow fibers is similar to the trend for crosslinked PDMC hollow fibers [7]; the presence of toluene in the feed mixture causes a reduction in overall permeance, mainly through a decrease in the transport of CO₂ across the membrane. It is believed that this effect is a manifestation of membrane antiplasticization caused by sorption of the bulky toluene

molecules into the polymer matrix. Polymer chain mobility and free volume reductions are associated with toluene-induced antiplasticization. However, compared to the crosslinked PDMC fibers, the magnitude of the CO₂ permeance depression in these crosslinked TEGMC fibers is smaller. In the ultra-thin PDMC membranes, CO₂ permeance without toluene is just over 100 GPU. However, the 500 ppm toluene feed causes a reduction in CO₂ permeance of nearly 50%, with values ranging between 50 and 60 GPU. This is compared to an observed permeance loss of about 20-30% in the crosslinked TEGMC membranes.

In any case, while the permeance losses associated with antiplasticization are undesirable, they are unlikely to be easily avoided. On the other hand, the possibility of plasticization is a much more serious and, fortunately, treatable concern for the performance of natural gas separation membranes. In our crosslinked TEGMC fibers, CO₂/CH₄ permselectivity losses on the order of 20% were observed for the 500 ppm toluene-containing feed compared to the “clean” natural gas mixture. The permselectivity depression associated with toluene-induced antiplasticization in the PDMC material was only about 10%, or so. In general, the lower CO₂/CH₄ permselectivity in “dirty” feeds is attributed to the greater effect of antiplasticization on the fast CO₂ gas than CH₄.

While it is obvious that this toluene-induced antiplasticization effect detracts from the separation efficiency of the crosslinked TEGMC fibers, these membranes do not appear to be plasticized when exposed to the challenging levels of both CO₂ and toluene in this study. The CO₂ permeance decreases as the feed pressure is increased to 700 psig, and the CH₄ permeance is essentially constant for all feed pressures.

The finding that toluene-contaminated feeds *do not* induce TEGMC membrane plasticization is important to the viability of these asymmetric hollow fibers from a

practical standpoint. Despite rigorous development and testing of a membrane material like TEGMC for specific feed applications, it is likely that any natural gas separation membrane will at some point be exposed to higher hydrocarbons and other contaminants for which it was not originally intended. Usually, membranes that can withstand these acute harsh conditions without experiencing severe failures, like plasticization, can be rapidly reconditioned to their pre-exposure state [9]. This has been accomplished by purging the fiber modules with clean feed gas (i.e. 50% CO₂, 50% CH₄, no toluene) after exposure to and antiplasticization by toluene-contaminated feeds.

7.3.3. Ternary (5% H₂S / 45% CO₂ / 50% CH₄) Sour Gas Mixture (A) Permeation

TEGMC fiber performance with sour gas feed mixtures is the most important metric to this work as a whole. A 5% H₂S, 45% CO₂, 50% CH₄ mixture was used to evaluate the permeation properties of TEGMC asymmetric hollow fibers under realistic, aggressive feed conditions that replicate the sour gas feeds for which they have been developed. The permeation results for crosslinked TEGMC membranes with and without post-treatment are presented in Figure 7.10 and Figure 7.11, below.

The permeance measurements for H₂S and CO₂ are almost identical for the non-post-treated and PDMS post-treated fibers. In both cases, there does not appear to be any significant evidence of membrane plasticization. The CH₄ gas in the non-post-treated fibers, however, does experience a swelling-induced permeance upswing. An increase of about 45% in the CH₄ permeance is observed at 700 psig compared to the 100 psig value. In contrast, the CH₄ permeance in the PDMS post-treated membrane actually decreases as the feed pressure is increased. As discussed previously, it is possible that the increasing CH₄ permeance of the non-post-treated fibers is caused by the exacerbation or development of morphological imperfections in the skin layer. The

PDMS coating on the post-treated membranes may prevent this increase in CH₄ permeance as previously described.

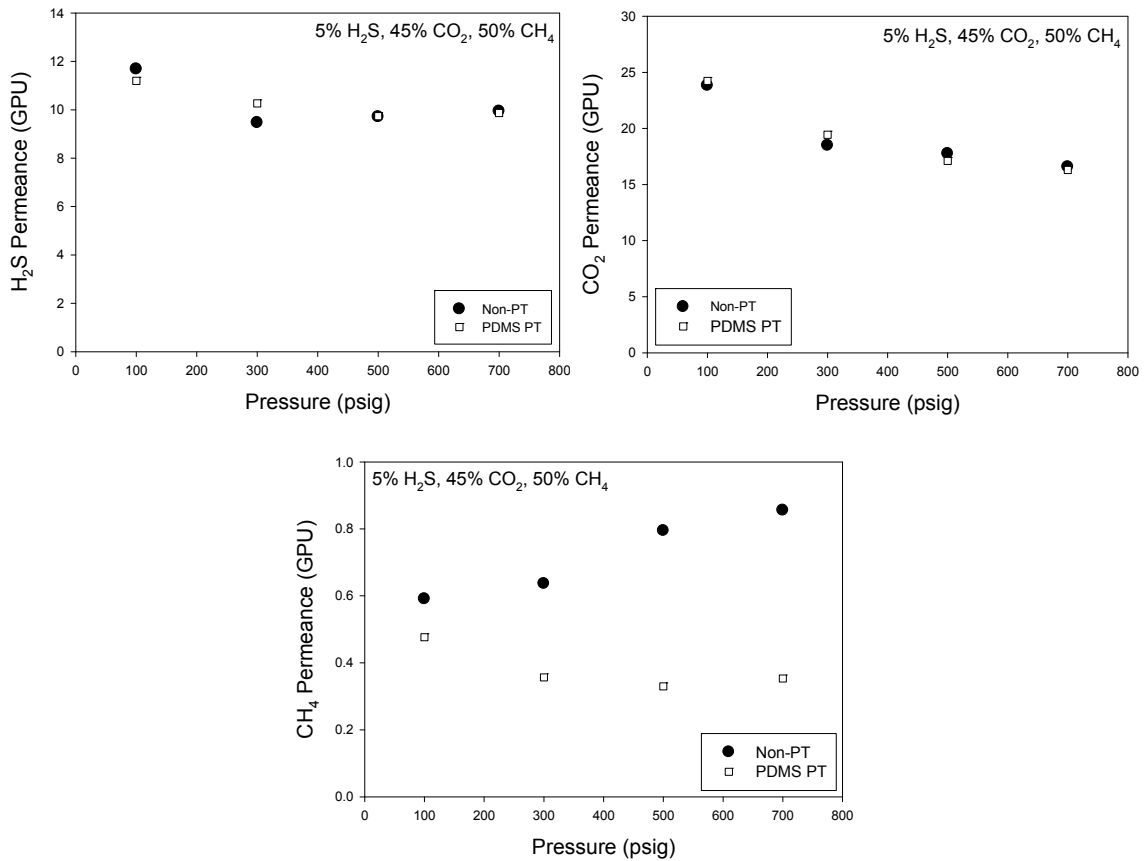


Figure 7.10: Sour gas (5% H₂S, 45% CO₂, 50% CH₄) permeance measurements in crosslinked TEGMC fibers at 35°C.

It would be interesting to study the permeation properties of these PDMS post-treated TEGMC fibers under bore-side feed conditions with a sour gas mixture such as the one used here. In such a scenario, it is possible that the preventive PDMS sealing of minor skin layer imperfections would *not* be nearly as effective as with the shell-side feed. Instead of being forced into any nucleating skin layer defects at high pressure, the PDMS coating on the outside of the fibers might simply delaminate from the TEGMC skin at these locations, resulting in much lower permselectivity, if not total fiber failure.

Unfortunately, such an investigation was beyond the scope of the current work. It is, however, included as a recommendation for continuing research in this area.

In any case, the performance of these crosslinked fibers is quite impressive. At the highest pressure tested, these feed conditions correspond to effective H₂S and CO₂ pressures (in terms of fugacity) of greater than 25 psig and 250 psig, respectively. Few, if any, studies in the literature using asymmetric hollow fiber membranes for sour gas separations have reported non-defective permeation measurements under such harsh conditions.

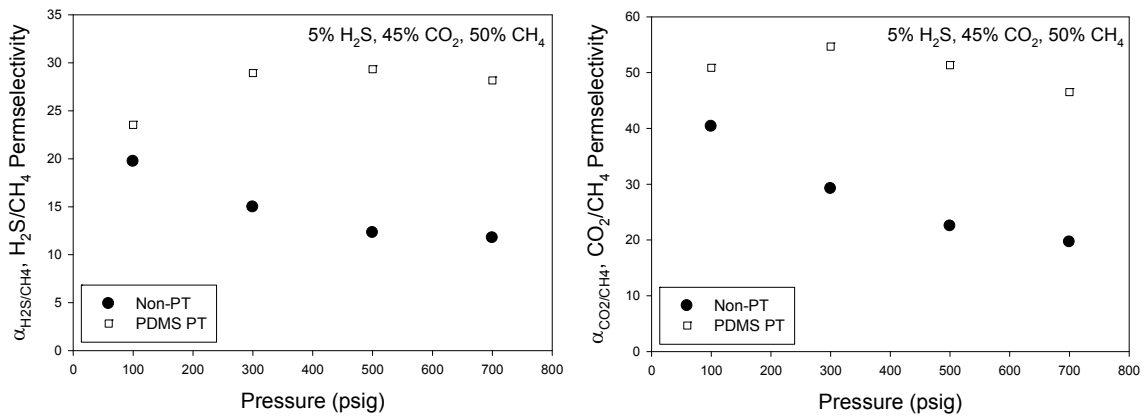


Figure 7.11: Permselectivity of crosslinked TEGMC fibers using a 5% H₂S, 45% CO₂, 50% CH₄ sour gas mixture.

The H₂S/CH₄ and CO₂/CH₄ permselectivity results for crosslinked TEGMC asymmetric hollow fibers indicate that the PDMS post-treatment results in significantly improved separation efficiency. H₂S/CH₄ permselectivity in the non-post-treated fibers is fairly high at the 100 psig feed pressure. However, the increased CH₄ permeance that was noted in Figure 7.10 causes the permselectivity to decay to a value of just 12 at 700 psig. Similarly, the CO₂/CH₄ permselectivity of the non-post-treated fibers is 40 at

the low end of the isotherm – a value that closely matches the dense film separation efficiency – but decreases to just 20 at the highest feed pressure.

On the other hand, the PDMS post-treated fibers give exceptionally high permselectivity values. $\text{H}_2\text{S}/\text{CH}_4$ permselectivity starts at around 24 and rapidly increases to greater than 28 for the remainder of the isotherm. These values even outperform the highest dense film $\text{H}_2\text{S}/\text{CH}_4$ permselectivity that was measured (24) for crosslinked TEGMC. Furthermore, the CO_2/CH_4 permselectivity of the PDMS post-treated fibers is greater than 46 for all of the feed pressures tested. Once again, these values are significantly greater than the CO_2/CH_4 ideal selectivity in analogous dense films. While somewhat surprising, hollow fiber permselectivity values that exceed the dense film ideal selectivity are not unheard of. As mentioned previously, it is believed that polymer chain alignment in the membrane skin layer due to high shear during the spinning process is responsible for this effect.

7.3.4. Ternary (20% H_2S / 20% CO_2 / 50% CH_4) Sour Gas Mixture (B) Permeation

A second, more aggressive sour gas mixture comprised of 20% H_2S , 20% CO_2 , and 60% CH_4 was used to further evaluate the permeation properties of crosslinked TEGMC hollow fibers under even more challenging conditions. Although the total acid gas content of this feed is less than that of the first sour gas mixture, the greater H_2S concentration means that plasticization of the membranes is likely to occur at lower feed pressures. The highest feed pressure used in this set of experiments was 500 psig; this corresponds to effective H_2S and CO_2 pressures (in terms of fugacity) of 81 psig and 86 psig, respectively.

The H_2S , CO_2 , and CH_4 permeance of crosslinked TEGMC fibers with and without PDMS post-treatment are shown in Figure 7.12 and Figure 7.13. As was the

case with permeation through the first sour gas mixture, the H₂S and CO₂ permeance isotherms for the non-post-treated and PDMS post-treated modules are essentially identical. Based on the permeance trends of these gases, plasticization does not appear to play a significant role under the conditions studied here. The H₂S permeance of the non-post-treated fibers does pass through a minimum value at around 300 psig, but the permeance does not increase radically after that point, so it is more likely that an intermediate degree of swelling is present.

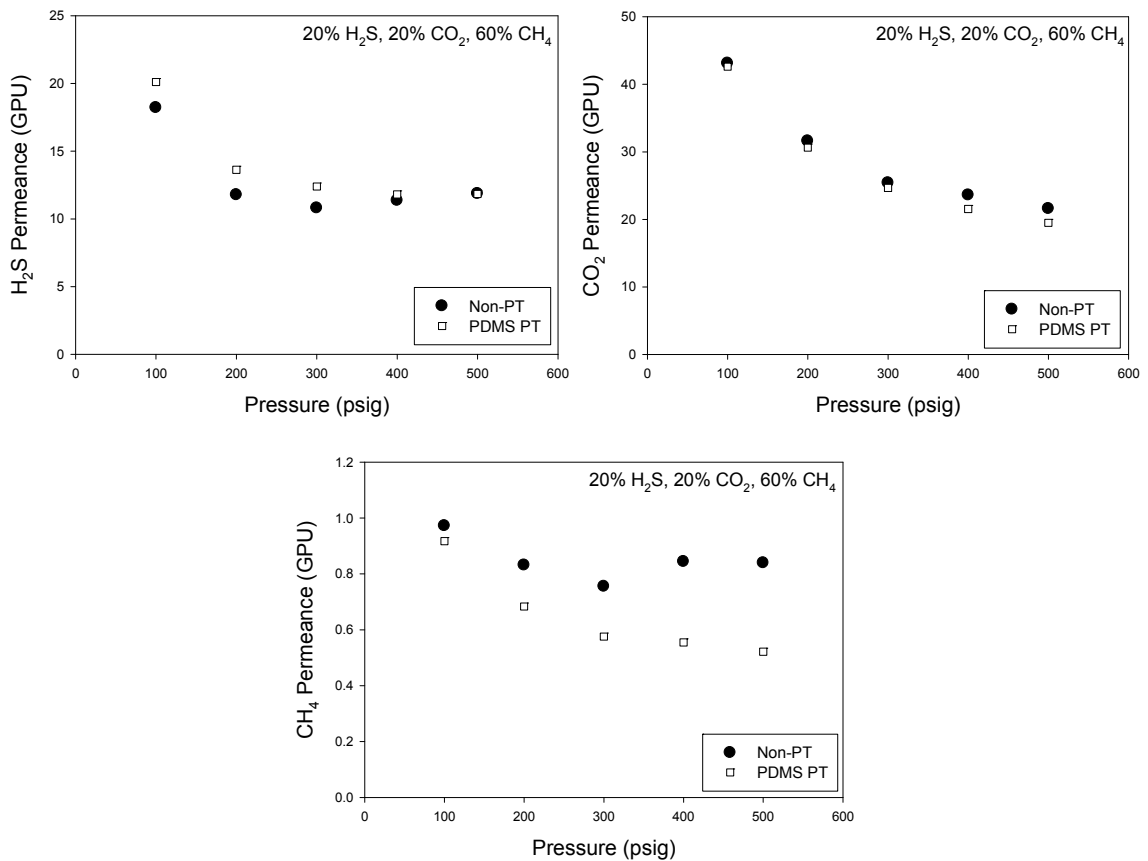


Figure 7.12: Permeance measurements for a sour gas mixture (20% H₂S, 20% CO₂, 60% CH₄) in crosslinked TEGMC fibers at 35°C.

The CH₄ permeance of the non-post-treated fibers indicates that some defects may be introduced at high feed pressures. However, the PDMS post-treatment again

seems to be effective at suppressing these non-ideal effects. The CH₄ permeance in post-treated fibers decreases over the whole pressure range that was tested, suggesting that a high-quality, defect-free, and non-plasticized skin layer is maintained.

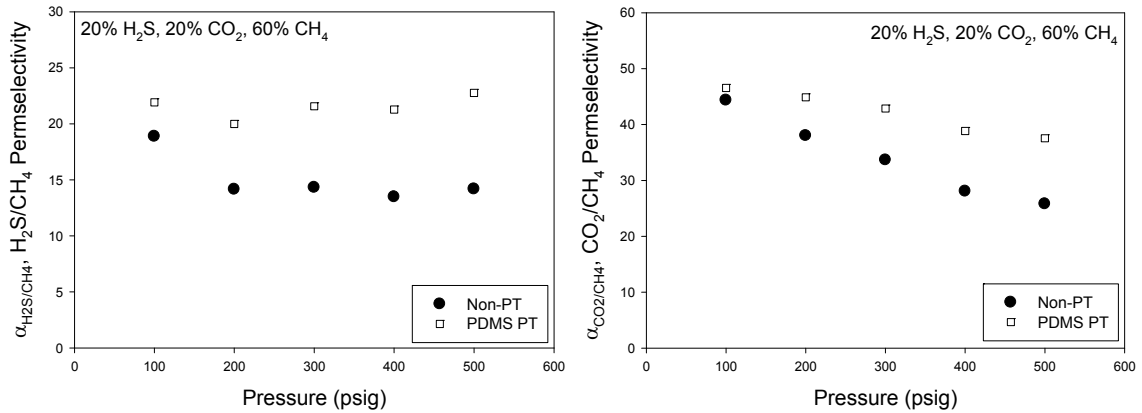


Figure 7.13: Sour gas permselectivity of crosslinked TEGMC fibers at 35°C.

The H₂S/CH₄ separation efficiency in the crosslinked TEGMC fibers follows a similar trend for this feed mixture as was observed in the 5% H₂S, 45% CO₂, 50% CH₄ mixture. The non-post-treated fibers give reduced selectivity at high feed pressures. This is believed to result from the evolution of minor skin layer imperfections, which in their early stages only significantly impact the CH₄ permeance. Although the PDMS post-treated H₂S/CH₄ permselectivity is not quite as high as was measured with the first sour gas mixture, it is still greater than 20 over the entire pressure range tested. It is believed that this reduced separation efficiency is caused by a higher degree of membrane swelling under these more challenging conditions. Nevertheless, the fact that TEGMC fibers are able to maintain H₂S/CH₄ permselectivity values in excess of 20 for these extreme feed conditions is very notable. This level of separation performance approaches that of the crosslinked TEGMC dense films using the same feed mixture (see Figure 5.15 and Figure 5.16); for the dense films, H₂S/CH₄ permselectivity was as

high as 24 and CO_2/CH_4 permselectivity ranged from 43 to 29 at the low and high pressure ends of the isotherm, respectively.

In terms of CO_2/CH_4 permselectivity in the crosslinked TEGMC fibers, the PDMS post-treatment again appears to give a significant improvement. At low feed pressures, the non-post-treated fiber value is similar to that of the post-treated fibers. However, this value drops from around 44 to 26 as the feed pressure is increased to 500 psig. In contrast, the PDMS post-treated fibers have a starting CO_2/CH_4 permselectivity of 47, and this only decreases to 38 at the 500 psig feed pressure. Based on these numbers, the CO_2/CH_4 permselectivity of these crosslinked fibers is greater than that of the crosslinked dense films. Again, this is ascribed to polymer chain alignment in the skin layer. Similar to the $\text{H}_2\text{S}/\text{CH}_4$ permselectivity, the CO_2/CH_4 separation efficiency with this feed mixture is slightly lower than for the 5% H_2S , 45% CO_2 , 50% CH_4 mixture. This is believed to result from a higher degree of swelling of the polymer matrix, which the PDMS layer cannot fully negate, under these very aggressive feed conditions.

7.4. Conclusions

The permeation results presented in this chapter are encouraging for the application of crosslinked TEGMC asymmetric hollow fiber membranes to realistic aggressive sour gas separation applications. Despite the pure gas H_2S and CO_2 permeation isotherms, which seem to indicate that these membranes are susceptible to swelling and plasticization, their performance under mixed gas feeds is exceptional.

For a 50% CO_2 , 50% CH_4 binary feed mixture, the permselectivity of the non-post-treated fibers closely resembles the separation efficiency that was measured using dense film membranes. Furthermore, the application of a PDMS post-treatment to the

crosslinked TEGMC fibers reveals that efficiency values even greater than those measured with dense films can be obtained. Polymer chain alignment in the fiber skin layer is believed to be responsible for this effect.

The addition of a highly condensable contaminant species (toluene), which is representative of the higher hydrocarbons contaminants found in natural gas feeds, had a moderately negative effect on the separation performance of these materials. A loss of productivity was observed and this was believed to be due to the antiplasticization phenomenon. Also, CO_2/CH_4 permselectivity was found to decrease under these antiplasticized conditions. However, there was no indication of the much more harmful plasticization effect. Therefore, it is likely that the fibers could be fairly easily returned to their pre-toluene-exposure performance by sweeping the membranes with “clean” feed.

Two sour gas mixtures were used to assess the performance of these membranes under relevant sour gas feed conditions. While the non-post-treated fibers performed well at low feed pressures, there were some signs of swelling and, possibly, plasticization. The PDMS post-treated fibers, however, gave outstanding results in terms of both permselectivity and stability. For the 5% H_2S , 45% CO_2 , 50% CH_4 feed, these fibers gave $\text{H}_2\text{S}/\text{CH}_4$ permselectivity values as high as 29 and a CO_2/CH_4 selectivity that reached 55 – both of these numbers are significantly higher than the separation efficiency values measured in analogous dense films. Under even more challenging feed conditions (20% H_2S , 20% CO_2 , 60% CH_4) the crosslinked TEGMC membranes also gave noteworthy permselectivity and stability. The PDMS post-treated fibers gave $\text{H}_2\text{S}/\text{CH}_4$ permselectivity greater than 20 for all feed pressures tested and CO_2/CH_4 selectivity as high as 47. Again, polymer chain alignment in the skin layer due to high shear membrane formation is believed to impart extra diffusion selectivity and give superior overall permselectivity compared to dense films.

Physical aging of the TEGMC asymmetric hollow fiber membranes was also considered in this chapter. This is a potentially important practical consideration for membrane units that will be deployed to the field and are expected to perform with high productivity over long time periods. It was found that storage of these membranes under ambient conditions led to very significant permeance drops over the course of a 23 week study. Although crosslinked membranes were less affected by physical aging, their transient separation performance was still undesirable. These physical aging effects were significantly reduced by storing the fibers under a low pressure active CO₂ feed. This simple and effective method is important for the commercial attractiveness of these asymmetric hollow fiber membranes, since it allows for their transport and potential long-term storage without the risk of major productivity losses or other unexpected permeation property changes.

The findings related to TEGMC hollow fibers that are discussed in this chapter certainly seem to indicate that they may be well-suited for application in industrial sour gas separations in the future. The sour gas feed conditions used in this chapter are, to our knowledge, by far the most aggressive conditions used on asymmetric hollow fiber membranes in the literature. The fact that the PDMS post-treated, crosslinked TEGMC membranes were able to resist H₂S- and CO₂-induced plasticization under the 5% H₂S, 45% CO₂, 50% CH₄ and 20% H₂S, 20% CO₂, 60% CH₄ sour gas feed conditions is impressive in and of itself, but the high H₂S/CH₄ and CO₂/CH₄ permselectivity results that were obtained are remarkable. Of course, further improvement of these membranes is still required. In particular, the productivity of these membranes must be improved in order to make them a feasible alternative to the absorption processes that they are intended to replace.

7.5. References

1. Kratochvil, A.M., *Thickness Dependent Physical Aging and Supercritical Carbon Dioxide Conditioning Effects on Crosslinkable Polyimide Membranes for Natural Gas Purification*, in *School of Chemical and Biomolecular Engineering*2008, Georgia Institute of Technology: Atlanta, ga.
2. Paul, D.R., J.H. Kim, and W.J. Koros, *Physical aging of thin 6FDA-based polyimide membranes containing carboxyl acid groups. Part I. Transport properties*. *Polymer*, 2006. **47**(9): p. 3094-3103.
3. Kim, J.H., W.J. Koros, and D.R. Paul, *Physical aging of thin 6FDA-based polyimide membranes containing carboxyl acid groups. Part I. Transport properties*. *Polymer*, 2006. **47**(9): p. 3094-3103.
4. Kim, J.H., W.J. Koros, and D.R. Paul, *Physical aging of thin 6FDA-based polyimide membranes containing carboxyl acid groups. Part II. Optical properties*. *Polymer*, 2006. **47**(9): p. 3104-3111.
5. Kim, J.H., W.J. Koros, and D.R. Paul, *Effects of CO₂ exposure and physical aging on the gas permeability of thin 6FDA-based polyimide membranes: Part 2. with crosslinking*. *Journal of Membrane Science*, 2006. **282**(1–2): p. 32-43.
6. Kim, J.H., W.J. Koros, and D.R. Paul, *Effects of CO₂ exposure and physical aging on the gas permeability of thin 6FDA-based polyimide membranes: Part 1. Without crosslinking*. *Journal of Membrane Science*, 2006. **282**(1–2): p. 21-31.
7. Ma, C., *Highly Productive Ester Crosslinkable Composite Hollow Fiber Membranes for Aggressive Natural Gas Separations*, in *School of Chemical and Biomolecular Engineering*2012, Georgia Institute of Technology: Atlanta, GA.
8. Omole, I.C., *Crosslinked Polyimide Hollow Fiber Membranes for Aggressive Natural Gas Feed Streams*, in *School of Chemical and Biomolecular Engineering*2008, Georgia Institute of Technology: Atlanta, GA. p. 305.
9. Chen, C.C., *Thermally Crosslinked Polyimide Hollow Fiber Membranes for Natural Gas Purification*, in *School of Chemical and Biomolecular Engineering*2011, Georgia Institute of Technology: Atlanta, GA.

CHAPTER 8

SUMMARY AND RECOMMENDATIONS

8.1. Conclusions

8.1.1. Benchmarking an Advanced Polyimide for Sour Gas Separations

A high-performing glassy polyimide, 6FDA-DAM:DABA (3:2), was investigated in the dense film morphology for possible membrane-based separation applications involving sour gases. In the past, membranes of this polymer have demonstrated excellent CO₂/CH₄ separation performance under aggressive feed conditions. Also, it has been successfully formed into asymmetric hollow fiber membranes. As a result, it was the most attractive candidate material for aggressive (high pressure, high H₂S and CO₂ concentration) sour gas separations.

Using mixed gas feeds with between 5% and 20% H₂S, the 6FDA-DAM:DABA (3:2) dense films were shown to give moderate H₂S/CH₄ permselectivity. This level of separation efficiency for H₂S/CH₄ was, however, an improvement over the poor H₂S/CH₄ ideal selectivity that was measured using pure gas feeds. Although the transport mechanism behind this enhanced permselectivity under mixed gas feed conditions is still not fully understood, it is believed to be related to H₂S-induced diffusion limitations of the more bulky CH₄ molecule, as well as competitive dual-mode sorption effects.

Nevertheless, H₂S/CH₄ permselectivity values as high as 18 were obtained at a feed pressure of 900 psi for 5% H₂S, 95% CH₄ and 10% H₂S, 20% CO₂, 70% CH₄ mixtures. While these values were an improvement over the ideal selectivity, they still were not overly attractive compared to alternative membrane materials, especially rubbery polymers, and do not surpass the reported selectivity of CA (19).

CO₂/CH₄ permselectivity values well in excess of the intrinsic ideal selectivity were observed at low feed pressures using sour gas mixtures. However, it was found that swelling-induced plasticization of the 6FDA-DAM:DABA (3:2) polymer matrix occurred at fairly low H₂S and CO₂ partial pressures. The CO₂/CH₄ permselectivity of plasticized films was found to decay to as low as 20 for a 20% H₂S, 20% CO₂, 60% CH₄ mixture. These observations led to the conclusion that the base 6FDA-DAM:DABA (3:2) polyimide would not be adequate for the aggressive sour gas feeds in question.

Crosslinking was identified as a potentially useful tool for the improvement of membrane stability. It was also determined that greater H₂S/CH₄ permselectivity might be achieved through modifications to the base 6FDA-DAM:DABA (3:2) polymer that incorporated PEO repeats; a strong correlation between PEO content in rubbery polymers and H₂S/CH₄ permselectivity was established.

8.1.2. Development of a Novel Crosslinkable Polyimide for Sour Gas

Feeds

A series of novel crosslinkable polymers, referred to generically as PEGMC materials, were synthesized. These are based on the 6FDA-DAM:DABA polymer backbone and an esterification crosslinking reaction scheme that has been used in the past to form PDMC. The crosslinking agents used to synthesize PEGMC were short-chain PEGs. These PEO-containing crosslinkers were selected based on the hypothesis that they would provide improved membrane stability, through the crosslinking reaction, and augmented H₂S/CH₄ permselectivity, through added H₂S/CH₄ sorption selectivity.

After demonstrating the efficacy of PEGMC synthesis and crosslinking in dense films, permeation and sorption experiments were performed. Using a 20% H₂S, 20% CO₂, 60% CH₄ mixture at 900 psi, permselectivity values for H₂S/CH₄ and CO₂/CH₄ of 24

and 29, respectively, were measured in the TEG crosslinked material. Moreover, the plasticization resistance of the PEGMC films with TEG crosslinking agent was much higher than the base 6FDA-DAM:DABA (3:2) dense films. The H₂S and CO₂ plasticization pressures, in terms of fugacity, were found to be approximately 100 psi and 400 psi, respectively.

Based on these outstanding sour gas separation properties under highly aggressive feed conditions, the TEG crosslinked PEGMC material – referred to specifically as TEGMC – was selected for further development into asymmetric hollow fiber membranes through a dry-jet/wet-quench spinning process.

8.1.3. Formation of Defect-free Crosslinkable Asymmetric Hollow Fiber Membranes

Established principles of dry-jet/wet-quench spinning and experience gained from the formation of asymmetric hollow fiber membranes of similar polymers (6FDA-DAM:DABA and PDMC) were used to form TEGMC hollow fibers. Three spinning studies were performed using different TEGMC polymer batches, dope compositions, and spinning parameters. Defect-free fibers were formed in all studies, but the macroscopic and permeation properties of the Spin #2 and Spin #3 fibers were found to be superior.

In particular, two states – ‘2 - 9’ and ‘3 - 4’ – proved to have the most attractive combination of permselectivity, productivity, and morphology. The O₂/N₂ ideal selectivity of these uncrosslinked TEGMC hollow fiber states was 4.9, compared to a dense film ideal selectivity of 4.4, and the effective skin layer thickness was calculated to be between 240-270 nm.

Several crosslinking protocols were considered. Ultimately, a crosslinking temperature of 255°C, soak time of 6 hours, and vacuum crosslinking environment were chosen. Also, these fiber states were post-treated with a highly permeable PDMS coating mainly as a control to show that pin-hole defects were not present in the fiber skin layers. However, indications of a complex permselectivity-enhancing effect with the PDMS post-treatment were observed; the unique morphology of the TEGMC skin layer and PDMS coating appear to work together to give ultra-high permselectivity relative to dense film ideal selectivity values, especially under more aggressive feed conditions.

Despite lower than desired permeance in the crosslinked fibers (particularly under shell-side feed and after significant physical aging effects), the crosslinked TEGMC fiber states mentioned above were shown to be of sufficient quality to move forward with sour gas permeation characterization.

8.1.4. Permeation Characterization of Asymmetric Hollow Fibers Under Realistic, Aggressive Sour Gas Feed Conditions

The crosslinked TEGMC fibers were evaluated using binary non-sour natural gas feed mixtures and two sour natural gas mixtures – 5% H₂S, 45% CO₂, 50% CH₄ and 20% H₂S, 20% CO₂, 60% CH₄ – at pressures as high as 700 psig. Although the non-post-treated TEGMC fibers showed reasonably high H₂S/CH₄ and CO₂/CH₄ permselectivity at low to moderate feed pressures and under non-sour feeds, these attractive properties were found to degrade under more aggressive conditions presumably due to a combination of swelling and the introduction of morphological imperfections, which are believed to be distinct from fiber ‘blow out’-type failures or plasticization.

The PDMS post-treated fibers, however, gave truly outstanding permselectivity and membrane stability under these aggressive feeds. For the 5% H₂S-containing mixture, H₂S/CH₄ permselectivity as high as 29 was found, with a corresponding CO₂/CH₄ permselectivity of greater than 50. No signs of plasticization were observed at the highest feed pressure (700 psig). Furthermore, permselectivity values for H₂S/CH₄ and CO₂/CH₄ with the 20% H₂S-containing feed were greater than 20 and 38, respectively, for all feed pressures tested (up to 500 psig). Again, there was no sign of membrane plasticization.

The permselectivity values for PDMS post-treated TEGMC fibers under sour gas feed conditions were found to exceed the dense film permselectivity values in some cases. This is attributed to a few simultaneous effects, which combine to give truly unique transport properties. First, polymer chain alignment is believed to be present in the skin due to high shear forces at the dope-spinneret interface during the spinning process. Such an effect has been found in the past to impart added diffusion selectivity and, therefore, greater overall permselectivity. Also, the PDMS coating is believed to be critical to realizing the full benefit of polymer chain alignment on permselectivity. Under shell-side feed conditions, the highly permeable PDMS coating is thought to 'actively heal' nascent morphological imperfections in the fiber's skin layer – presumably caused by excessive elongation or "stretch" of the dense polymer matrix due to swelling stresses. Because of the exciting results that arise from these phenomena, this hypothesis requires further investigation.

Based on the extraordinary permeation results of the post-treated and crosslinked TEGMC fibers, it seems that the materials and membranes developed in the course of this study have the potential to be an attractive alternative to the incumbent sour gas separation technologies. Moreover, their tunable properties and the inherent

benefits of membrane gas separation processes mean that these materials may enable the production of previously uneconomical or technologically unfeasible sour gas reserves.

8.1.5. Comparison of PEGMC to Alternative Sour Gas Separation Membrane Materials

The overarching goal of the work described in this dissertation was the development of high performance polymeric membranes for aggressive sour gas feed applications. Critical metrics for such a material include sour gas permeability, CO₂/CH₄ permselectivity, H₂S/CH₄ permselectivity, resistance against penetrant-induced plasticization or other performance losses associated with aggressive feed conditions, spinnability in order to form high-quality asymmetric hollow fiber membrane modules, and the potential for manufacturing scale-up. It is our belief that the PEGMC materials, specifically crosslinked TEGMC, provide the most attractive performance out of all the polymeric membranes that have been investigated in the literature for sour gas separations when these factors are taken into consideration.

The combined acid gas separation factor, $SF_{CAG}^{\#}$, that was developed in this work gives an indication of the overall sour gas separation efficiency of a membrane material. Figure 8.1 presents a typical productivity-efficiency tradeoff plot using $SF_{CAG}^{\#}$ for the various membrane materials that have been studied with sour gas feeds [1-3]. Values for crosslinked TEGMC from the dense film study and from the asymmetric hollow fiber membrane study (using the calculated effective skin thickness of 5 μ m) are shown. It should be noted that the sour gas mixtures used with TEGMC are significantly more aggressive than those used for the rubbery polymers and neat CA. Therefore, it is

expected that the performance of these materials may be overestimated compared to TEGMC.

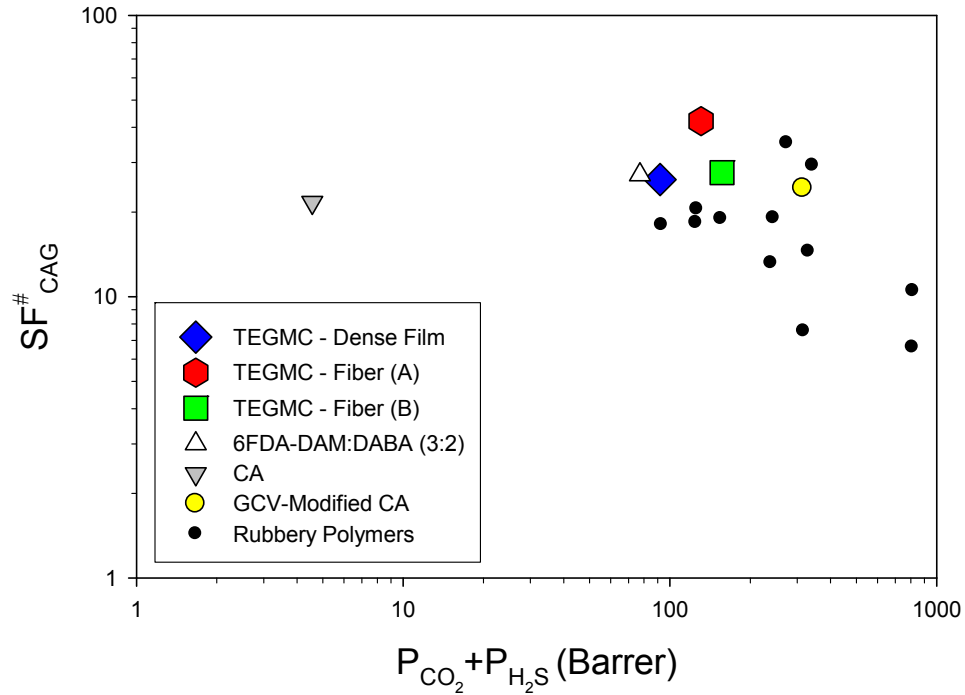


Figure 8.1: Productivity-efficiency tradeoff for combined acid gas separations. Ternary gas data are shown for rubbers (black symbols) as well as for several glassy polymers. The data points for crosslinked TEGMC, 6FDA-DAM:DABA (3:2), and GCV-Modified CA correspond to ternary sour gas mixtures with total feed pressure greater than 500 psi (5% H₂S, 45% CO₂, 50% CH₄ for TEGMC – Fiber (A); 10% H₂S, 20% CO₂, 70% CH₄ for 6FDA-DAM:DABA (3:2); and 20% H₂S, 20% CO₂, 60% CH₄ for the others)

The combined acid gas performance of the crosslinked TEGMC membranes is very competitive with the most attractive alternatives – locations near the top right quadrant are most desirable. Furthermore, the fact that these materials were tested under much more aggressive feed conditions than the rubbery polymers and neat CA indicates that they are more likely to be capable of withstanding realistic aggressive sour gas feed conditions without major performance losses. Another problem with many rubbery polymers is the formation of high-quality defect-free asymmetric hollow fibers.

Unless high performance membrane modules of a particular material can be fabricated, industrial application is unlikely.

The GCV-Modified CA material that also gives very attractive productivity-efficiency tradeoff properties is a recently developed plasticization-resistant polymer based on CA. While its efficiency and productivity properties for the sour gas separation are clearly very competitive with the other materials shown, it is unlikely that this material can be economically manufactured into high-quality membrane modules given its current synthesis procedure. So far, GCV-Modified CA membranes have been only formed into the dense film morphology. The conversion of CA to GCV-Modified CA is an intensive reaction that involves long reaction times, aggressive temperatures, and wet conditions, as described in the reference [3]. Based on the synthesis reaction and the inherent difficulty of spinning defect-free CA asymmetric hollow fibers, it is considered unlikely that GCV-Modified CA membranes can be formed into commercially attractive membrane modules.

The current cost of the 6FDA-DAM:DABA (3:2) precursor material for PEGMC is on the order of \$10,000/kg. Therefore, the capital cost of TEGMC membranes is likely to be one of their most unattractive qualities at present. However, the price listed above is for small batch synthesis of the specialty 6FDA-DAM:DABA (3:2) polymer on an as-needed basis. It is very likely that the economics of the polyimide synthesis would improve dramatically if TEGMC membranes were produced for industrial application due to superior economies of scale. It has been estimated that the unit price for 6FDA-DAM:DABA could easily decrease to below \$1,000/kg in such a scenario.

For comparison, the cost of CA is much lower (\$20-100/kg) due to its widespread use and less complex monomers. However, it is expected that the GCV-Modification

would greatly increase the processing cost of membrane formation because of the difficult post-treatment reaction that must be performed on CA membranes to obtain the GCV-Modified form of the material.

The above discussion lends credence to the position that the crosslinked TEGMC membranes are the most attractive currently available material for aggressive sour gas separations. Despite this, several areas of improvement must be addressed in the future. These are discussed in the following section.

8.2. Recommendations for Future Work

8.2.1. Investigation of PEGMC Materials with Alternative Monomer Ratios and Longer PEG Crosslinking Agents

The PEGMC materials studied in the present work were synthesized with 6FDA-DAM:DABA (3:2) as the backbone polymer and using the three shortest PEG molecules – DEG, TEG, and TetraEG – as crosslinking agents. However, one of the most attractive properties of this novel crosslinkable polymer is the large amount of separation property tunability that is expected to be possible through adjustments to the composition of PEGMC during synthesis.

The 6FDA-DAM to 6FDA-DABA monomer ratio can be altered during the initial polyimide formation reactions. In doing so, the frequency of crosslinking sites along the polymer backbone can be controlled; a higher relative 6FDA-DABA content means that there will be more carboxylic acid sites where the PEG crosslinkers can be attached through esterification. Additionally, the length of the PEG crosslinkers can be changed during monoesterification to give more or less PEO repeat units per crosslink. Since these PEO groups are believed to favor H₂S sorption and, as a result, H₂S/CH₄

permselectivity, longer PEG crosslinking agents may allow for the development of materials that are skewed towards H₂S/CH₄ permselectivity rather than CO₂/CH₄.

Based on the above discussion, it is clear that only a very limited range of the possible PEGMC polymer compositions were investigated in this study. It would be interesting to measure the sour gas permeation properties of TEGMC materials with lower or even inverted 6FDA-DAM to 6FDA-DABA ratios, such as 1:1, 2:3, or 1:2. After crosslinking, these materials would be expected to give even greater membrane stability and resistance to penetrant-induced plasticization than was measured in our membranes.

Perhaps an even more interesting material would result from the use of greater 6FDA-DABA content *and* longer PEG crosslinking agents, with $n = 5-10$. Although it is expected that a practical limit for PEG crosslinker length exists because of the T_g depression and crystallinity effects that it introduces into the material, longer PEGs coupled with a very high crosslinking density might enable superior H₂S/CH₄ permselectivity while simultaneously maintaining the high intrinsic rigidity of the 6FDA-DAM:DABA backbone.

8.2.2. Study of the Possible Diffusion-Limiting Effect of H₂S

The sour gas permeation studies on 6FDA-DAM:DABA (3:2) and crosslinked PEGMC dense films (CHAPTER 4 and CHAPTER 5) indicate that some currently unexplained transport phenomenon is present for H₂S-containing feeds. It was found that the introduction of H₂S into a feed mixture causes much lower CH₄ permeability than under pure gas feed conditions. While competitive sorption accounts for part of this permeability loss, this factor alone is not large enough to explain the low CH₄ permeation rate and resulting high H₂S/CH₄ permselectivity that was observed for mixed gas feeds.

It was suggested that the polar H₂S molecule, which is capable of hydrogen bonding with polar moieties on the 6FDA-DAM:DABA polymer backbone (such as carboxylic acids, esters, and even carbonyls), may actually influence the diffusivity of other penetrants through the polymer membrane. Antiplasticization is a phenomenon involving the sorption of a highly condensable low molecular weight diluent species into a polymer matrix and a corresponding loss of fractional free volume and polymer chain mobility. Typically, antiplasticization is accompanied by decreased permeability through the membrane. It is possible that the highly interacting H₂S molecule has an effect similar to antiplasticization as it passes through the polymer matrix – effectively reducing the diffusion coefficient of CH₄ through the polymer without being negatively impacted itself.

A careful investigation of sour gas permeation in glassy polymer membranes, such as 6FDA-DAM:DABA or PEGMC, should be conducted using a combination of pure and mixed gas permeation and pure and mixed gas sorption. In particular, mixed gas sorption involving sour gases will be helpful in revealing the actual solubility and diffusion coefficients of the various sour gas species through these materials during mixed gas permeation. Calculations of the mixed gas diffusion coefficient (from Eq. [2.12]) can then be compared against the effective diffusion coefficient predictions from the partial immobilization model or the frame of reference model.

8.2.3. Development of Improved Model for H₂S Permeation

As an extension of the above recommendation, a more accurate model for the prediction of sour gas permeation through glassy polymer membranes should be developed. Two permeation models, the partial immobilization model and the frame of reference model, were employed in CHAPTER 4 and CHAPTER 5 of this work in an

attempt to demonstrate a predictive capability for sour gas permeation. Although these models gave fairly accurate predictions of pure gas and binary non-sour mixed gas permeation, their performance for H₂S-containing sour gas mixtures was unacceptable.

Therefore, after further elucidation of the potential diffusion-limiting transport effects caused by H₂S, an appropriate permeation model should be identified or developed to give improved modeling accuracy for sour gas permeation in glassy polymers. One such model has previously been developed for natural gas permeation through toluene-antiplasticized Matrimid® 5218 asymmetric hollow fibers [4]. This permeation model focuses on fractional free volume changes within the glassy polymer matrix under the changing feed conditions, and is largely based on work by Maeda and Paul [5-8].

In addition to capturing H₂S-associated diffusion effects, a newly developed sour gas permeation model may be further improved by incorporating extensions to the partial immobilization model that are directed at non-ideal sorption effects. Two such models are proposed by Esekhile, et al. for butane isomer permeation applications [9].

8.2.4. Optimization of Dry-Jet/Wet-Quench PEGMC Spinning For Reduced Skin Thickness

The highest-quality uncrosslinked TEGMC asymmetric hollow fiber membranes that were spun in this work were found to have skin layers of effective thickness between 240 nm and 270 nm. While these values approach the desired minimum practical skin thickness of approximately 100 nm, there is room for improvement. Furthermore, the formation of a skin layer with minimal thickness during the spinning process appears to be especially important to this work because of the productivity losses that were observed after crosslinking, PDMS post-treatment, and changing the feed configuration

from bore-side to shell-side. Physical aging was also found to be major factor influencing the productivity of TEGMC hollow fibers, so post-spinning fiber storage should be considered just as important to the ultimate fiber performance as the variables involved in the actual dry-jet/wet-quench spinning process.

Continued development of the TEGMC dope, spinning conditions, and post-spin storage procedure are recommended. Recent work on PDMC asymmetric hollow fiber membranes has shown that meticulous optimization of these variables can yield fibers with ultra-thin skin layers that are free of defects [10]. Fibers with these qualities are more attractive for commercial application and are more likely to maintain sufficiently high productivity even after crosslinking.

8.2.5. Dual-layer Asymmetric Hollow Fiber Spinning With PEGMC as a Sheath

Along with the optimization of TEGMC spinning variables for monolithic hollow fiber membrane formation, it is recommended that the fabrication of dual-layer fibers with TEGMC as the selective sheath layer polymer be included in future studies of this material.

Dual-layer fibers are very attractive for commercial applications because they allow the formation of fiber membranes with outstanding permeation properties based on expensive specialty polymers, which comprise the fiber sheath layer. However, instead of using the costly high-performance polymer throughout the fiber cross section, less expensive commercially available polymers can be spun into the fiber core, which simply acts as a highly porous support for the selective sheath layer on the outside portion of the fiber.

Dual-layer PDMC asymmetric hollow fiber membranes have been formed using the polyamide-imide Torlon® as a core polymer. It is likely that Torlon® will have similar

compatibility with TEGMC to that of PDMC. As such, dual-layer hollow fibers consisting of a Torlon® core and a TEGMC sheath are an obvious starting point for this investigation.

8.2.6. Optimization of Crosslinking Protocol for Higher Fiber Permeance

The thermal crosslinking step performed on the TEGMC asymmetric hollow fiber membranes was observed to be the most deleterious factor for their productivity. The relatively high temperatures (> 230°C, or so) that appear to be necessary to drive the transesterification crosslinking reaction under vacuum conditions result in a significant permeation loss due, presumably, to accelerated physical aging of the skin layer. It is also possible that partial collapse of the membrane's porous substructure was caused by increased polymer chain mobility at these aggressive temperatures.

Several potential crosslinking temperatures, soak times, and atmospheres were considered in this work. However, large permeance drops were noted in all cases. As such, a wider range of crosslinking protocols should be studied in future work on the TEGMC hollow fiber membranes in order to better optimize their separation performance. Esterification promoters have been briefly considered by previous researchers focused on PDMC crosslinking, but without much success. Nevertheless, the crosslinking catalyst used in those studies (p-TSA) and other esterification-promoting catalysts should also be included in such a study on TEGMC.

Ideally, the combined effects of optimized dry-jet/wet-quench spinning parameters – leading to lower effective skin layer thickness – and less harmful crosslinking conditions should yield TEGMC asymmetric hollow fibers with permeance levels that make them more competitive with alternative sour gas separation technologies.

8.2.7. Study of PDMS Post-treatment Effect on TEGMC Hollow Fiber Membrane Skin Layer

Through the course of our CHAPTER 7 discussion, the apparent ‘active healing’ effect of PDMS post-treatment was alluded to. As mentioned in that discussion, crosslinked TEGMC hollow fibers *with* a PDMS coating seem to be more ‘defect-resistant’ at high pressures than non-post-treated fibers.

Using PDMS post-treated fibers, H₂S/CH₄ and CO₂/CH₄ permselectivity values were obtained for sour gas feed mixtures that, in several cases, exceeded the dense film separation efficiency values. At the same time, the H₂S and CO₂ permeance of the PDMS post-treated hollow fibers was almost identical to the non-post-treated fibers. This indicates that the improved permselectivity results with a PDMS coating are not due to “caulking” of pin-hole defects in the skin layer. Rather, we believe that the PDMS post-treatment actively “heals” minor elongation- or swelling-induced morphological imperfections in the skin layer as they arise under more aggressive feed conditions. It seems that the measured hollow fiber separation efficiency values that exceed dense film values are a result of spinning-related polymer chain alignment in the skin layer. However, the full effect of this favorable polymer chain morphology is only realized under aggressive feed conditions when the PDMS post-treatment is present. To our knowledge, these results are unprecedented for asymmetric hollow fiber membranes.

Although a hypothesis regarding the mechanism behind these transport properties was proposed, there was insufficient time to fully investigate this exciting phenomenon; these unique permeation properties only became apparent at the very end of the work described in this dissertation. It is recommended that further exploration into

these effects be performed, as they seem to represent a truly unique and possibly very impactful finding in the area of asymmetric hollow fiber gas separation membranes.

In particular, it would be interesting to measure the mixed gas permeation properties of crosslinked TEGMC hollow fiber membranes with and without the PDMS post-treatment using a bore-side feed configuration. It is hypothesized that the shell-side feeds used for mixed gases in this work are crucial to the active healing effect that the PDMS coating appears to have on nascent skin layer defects. Under a high pressure or swelling-inducing environment with a bore-side feed configuration, it is believed that the PDMS layer would be incapable of imparting the same degree of “defect resistance;” essentially, delamination of the TEGMC-PDMS interface would occur at locations where the skin layer experiences excessive elongation or swelling. This failure of the PDMS to prevent defect nucleation is expected to result in permselectivity losses under bore-side mixed gas feeds that resemble or fall below to permselectivity trends of the non-post-treated TEGMC fibers.

In addition, other post-treatment protocols should be investigated to see if similar effects occur. One of the frequently used post-treatments for polyimide asymmetric hollow fibers is a so-called ‘reactive post-treatment,’ which essentially involves performing a polyamidation reaction on the outer surface of the fibers after they are potted into a module [11, 12].

8.2.8. Pyrolysis of PEGMC and PDMS Post-treated PEGMC to Form Carbon Molecular Sieve (CMS) Membranes

The final recommendation for future investigations of PEGMC membranes involves the formation of CMS membranes with PEGMC and PDMS post-treated PEGMC membrane precursors. CMS materials have been shown to give excellent

permselectivity for a number of gas separations, including CO₂/CH₄. Recent work using sour gas feeds indicates that these materials may also be very attractive for H₂S/CH₄ separations because of the ultra-high diffusion selectivity that they can attain and their greater stability compared to polymeric membranes.

Appropriate pyrolysis conditions should be determined for the formation of high-quality CMS membranes of this type. The permeation properties of the membranes can then be evaluated using mixed gas permeation with a variety of aggressive sour gas feed mixtures.

8.3. References

1. Membrane Technology and Research, I., *Low-Quality Natural Gas Sulfur Removal/Recovery*, 1998, The Department of Energy: Morgantown, WV.
2. Chatterjee, G., A.A. Houde, and S.A. Stern, *Poly(ether urethane) and poly(ether urethane urea) membranes with high H₂S/CH₄ selectivity*. *Journal of Membrane Science*, 1997. **135**(1): p. 99-106.
3. Achoundong, C.S.K., *Engineering Economical Membrane Materials for Aggressive Sour Gas Separations*, in *School of Chemical and Biomolecular Engineering* 2013, Georgia Institute of Technology: Atlanta, GA.
4. Lee, J.S., W. Madden, and W.J. Koros, *Antiplasticization and plasticization of Matrimid® asymmetric hollow fiber membranes. Part B. Modeling*. *Journal of Membrane Science*, 2010. **350**(1-2): p. 242-251.
5. Maeda, Y. and D.R. Paul, *Effect of antiplasticization on gas sorption and transport. I. Polysulfone*. *Journal of Polymer Science Part B: Polymer Physics*, 1987. **25**(5): p. 957-980.
6. Maeda, Y. and D.R. Paul, *Effect of antiplasticization on gas sorption and transport. II. Poly(phenylene oxide)*. *Journal of Polymer Science Part B: Polymer Physics*, 1987. **25**(5): p. 981-1003.
7. Maeda, Y. and D.R. Paul, *Effect of antiplasticization on gas sorption and transport. III. Free volume interpretation*. *Journal of Polymer Science Part B: Polymer Physics*, 1987. **25**(5): p. 1005-1016.

8. Maeda, Y. and D.R. Paul, *Effect of antiplasticization on selectivity and productivity of gas separation membranes*. Journal of Membrane Science, 1987. **30**(1): p. 1-9.
9. Esekhile, O., W. Qiu, and W.J. Koros, *Permeation of butane isomers through 6FDA-DAM dense films*. Journal of Polymer Science Part B: Polymer Physics, 2011. **49**(22): p. 1605-1620.
10. Ma, C., *Highly Productive Ester Crosslinkable Composite Hollow Fiber Membranes for Aggressive Natural Gas Separations*, in *School of Chemical and Biomolecular Engineering*2012, Georgia Institute of Technology: Atlanta, GA.
11. Wallace, D.W., *Crosslinked Hollow Fiber Membranes for Natural Gas Purification and Their Manufacture from Novel Polymers*, in *Department of Chemical Engineering*2004, University of Texas at Austin: Austin, TX.
12. Husain, S., *Formation of Non-crosslinked Asymmetric Hollow Fiber Mixed Matrix Polymer/Molecular Sieve Membranes*, in *School of Chemical and Biomolecular Engineering*2006, Georgia Institute of Technology: Atlanta, GA.

APPENDIX A

NON-IDEAL GAS PROPERTY CALCULATIONS

Compressibility factor and fugacity coefficient corrections are used extensively throughout this work. These corrections for non-ideal gas behavior are necessary for accurate mass balances and effective driving force values, which directly affect membrane transport property calculations like permeability and sorption coefficient. The compressibility factor (Z) is a measure of the deviation of the molar volume of a real gas from that of an ideal gas. The fugacity coefficient (Φ_i), which is used to calculate the fugacity of a component (f_i), is a measure of the deviation of the chemical potential of a real gas from that of an ideal gas.

The Peng-Robinson equation of state is often used to calculate compressibility factor and fugacity coefficients for natural gas mixtures and gas/condensate mixtures [1]. The Peng-Robinson equation of state is given in the following equations:

$$P = \frac{R \cdot T}{\tilde{v} - b} - \frac{a(T)}{\tilde{v}^2 + 2(\tilde{v} \cdot b) - b^2} \quad (\text{A.1})$$

$$a(T) = a(T_c) \cdot \alpha(T_r, \omega) \quad (\text{A.2})$$

$$a(T_c) = 0.45724 \frac{R^2 \cdot T_c^2}{p_c} \quad (\text{A.3})$$

$$\alpha(T_r, \omega) = \left[1 + \kappa (1 - T_r^{0.5}) \right]^2 \quad (\text{A.4})$$

$$\kappa = 0.37464 + 1.54226 \cdot \omega - 0.26992 \cdot \omega^2 \quad (\text{A.5})$$

$$T_r = \frac{T}{T_c} \quad (\text{A.6})$$

$$b = 0.07780 \frac{R \cdot T_c}{p_c} \quad (\text{A.7})$$

In the above equations, R is the universal gas constant, \tilde{v} is the molar volume, T_r is the reduced temperature, T_c is the critical temperature, p_c is the critical pressure, and ω is the acentric factor. The acentric factor is a measure of the non-sphericity of a molecule, and values for many compounds are tabulated in the literature.

The Peng-Robinson equation of state can be expressed as a cubic for Z :

$$Z^3 - (1 - B)Z^2 + (A - 3B^2 - 2B)Z - (AB - B^2 - B^3) = 0 \quad (\text{A.8})$$

$$A = \frac{a \cdot p}{R^2 \cdot T^2} \quad (\text{A.9})$$

$$B = \frac{b \cdot p}{R \cdot T} \quad (\text{A.10})$$

$$Z = \frac{p \cdot \tilde{v}}{R \cdot T} \quad (\text{A.11})$$

Eqs. (A.1-A.11) can be used to calculate the compressibility factor of a pure gas if certain properties of the gas are known. Namely, the critical point properties and acentric factor. However, the Peng-Robinson equation of state is most useful for mixed gas feed cases, when the various components within a gaseous mixture can interact with one another. In such a situation, mixing rules are needed in order to determine the effective mixture values for the various parameters define above in terms of critical properties and the acentric factor.

$$a_{mix} = \sum_i^n \sum_j^n y_i \cdot y_j \cdot a_{ij} \quad (\text{A.12})$$

$$a_{ij} = \sqrt{a_i \cdot a_j} (1 - k_{ij}) \quad (\text{A.13})$$

$$b_{mix} = \sum_i^n y_i \cdot b_i \quad (\text{A.14})$$

The binary interaction parameter, k_{ij} , in Eq. A.13 is determined empirically and values for many gas pairs can be found in the literature. Values for the critical properties, acentric factor, and binary interaction parameters of CO₂, H₂S, CH₄, and N₂ are given in Table A. and Table A.2.

Table A.1: Critical properties and acentric factors for common sour gas components [2, 3].

Species	T_c (K)	p_c (bar)	ρ_c (mol/L)	ω
CO ₂	304.1282	73.773	10.6249	0.22394
H ₂ S	373.15	89.997	10.19	0.1
CH ₄	190.564	45.992	10.139	0.01142
N ₂	126.192	36.958	11.1839	0.0372

Table A.2: Binary interaction parameters for sour gas [3, 4].

Gas Pair	Temperature Range (K)	k_{ij}
CO ₂ -CH ₄	199-283	0.144
H ₂ S-CH ₄	227-344	0.081
CO ₂ -H ₂ S	221-353	0.106
CO ₂ -N ₂	218-303	-0.016
H ₂ S-N ₂	256-344	0.152
CH ₄ -N ₂	90-183	0.044

The compressibility factor of a mixed or pure gas can be solved for any temperature and pressure by solving Eq. (A.*) iteratively. However, other sources should be used in conjunction with these calculations to ensure that the mixed or pure gas is, in fact, a gas under the conditions of interest. One such source is the thermodynamic property calculator, Supertrapp, developed by NIST, which enables vapor-liquid equilibrium calculations. In addition to the compressibility factor, the Peng-Robinson equation of state can be reformulated to allow for the calculation of the fugacity coefficient of pure or mixed gases.

$$\ln \Phi_i = \ln \left(\frac{f_i}{p_i} \right) = Z - 1 - \ln(Z - B) - \frac{A}{2\sqrt{2}B} \ln \left(\frac{Z + (1 + \sqrt{2}B)}{Z + (1 - \sqrt{2}B)} \right) \quad (\text{A.15})$$

$$\ln \Phi_i = \ln \left(\frac{f_i}{y_i \cdot p_i} \right) = \frac{b_i}{b_{mix}} (Z - 1) - \ln(Z - B) - \frac{A}{2\sqrt{2}B} \left(\frac{2 \sum_j^n y_j \cdot a_{ij}}{a_{mix}} - \frac{b_i}{b_{mix}} \right) \ln \left(\frac{Z + 2.414B}{Z - 0.414B} \right) \quad (\text{A.16})$$

Eq. (A.15) gives the pure gas fugacity coefficient for component i and Eq. (A.16) allows for calculation of the fugacity coefficient of component i in a mixture of n components.

References

1. Peng, D.-Y. and D.B. Robinson, *A New Two-Constant Equation of State*. Industrial & Engineering Chemistry Fundamentals, 1976. **15**(1): p. 59-64.
2. Prausnitz, J.M., R.N. Lichtenthaler, and E.G. Azevedo, *Molecular Thermodynamics of Fluid-Phase Equilibria*. 3 ed. Prentice Hall International Series in the Physical and Chemical Engineering Sciences, ed. N.R. Amundson. 1999, Upper Saddle River, NJ: Prentice Hall.

3. Linstrom, P.J.M., W.G., ed. *NIST Chemistry WebBook*. NIST Standard Reference Database Number 69. National Institute of Standards and Technology: Gaithersburg, MD, 20899.
4. Nishiumi, H., T. Arai, and K. Takeuchi, *Generalization of the binary interaction parameter of the Peng-Robinson equation of state by component family*. *Fluid Phase Equilibria*, 1988. **42**: p. 43-62.

APPENDIX B

SYNTHESIS OF 6FDA-DAM:DABA COPOLYIMIDE

The 6FDA-DAM:DABA polymer backbone was synthesized by a two-step polycondensation reaction scheme. The synthesis procedure was performed as follows:

1. Monomer Purification

- a. Dry the dianhydride (6FDA) (>99%, Alfa Aesar, Inc.) and diamine [DAM (>96%, Sigma-Aldrich) and DABA (>98%, Sigma-Aldrich)] reagents under vacuum at approximately 20°C below their sublimation temperature for 18hrs.
- b. Assemble a cleaned sublimation apparatus with one of the monomer reagents inside.
- c. Sublimate the monomer by submerging the apparatus in an oil bath at an appropriate temperature for the monomer being purified. Maintain liquid N₂ in the cold finger and pull vacuum on the sublimator.
- d. Store the purified monomer in air tight container and use as soon as possible.
- e. Repeat steps b-d for the remaining reagents.

2. Solvent Drying

- a. Dry molecular sieve beads (4Å) in vacuum oven at 150-175°C for ~24 hrs.
- b. Remove the dried molecular sieve, transfer to clean glass flasks, and seal the flasks with rubbery septa.
- c. Needle transfer NMP (anhydrous, >99.5%, Sigma-Aldrich) solvent and acetic anhydride (AcAn) (>99.5%, Sigma-Aldrich) to the flasks and allow

at least 24 hrs for the molecular sieve beads to extract H₂O from the liquids.

3. Polyamic Acid Formation

- a. Assemble cleaned and dried synthesis reactor (shown in Figure B.1), including reaction flask, stirrer, thermometer, liquids dispenser, Dean-Stark trap, condenser, and other connectors.
- b. Purge the assembly with dry N₂ gas for at least 1 hr.
- c. Using a propane torch, heat all of the glassware of the reaction assembly to remove all traces of H₂O inside the reactor.
- d. Needle transfer ~60% of the required NMP volume to the reactor (an 18-20 wt% solids solution should be eventually be formed)
- e. Carefully weigh the amount of diamines required to form the 6FDA-DAM:DABA polymer backbone with the desired monomer ratio.
- f. While stirring the reactor and purging with N₂, add the diamines into the reactor and wash any stuck diamine into the reactor with some of the remaining NMP. Quickly reseal the reactor.
- g. The reactor should be kept cool (~ 0°C) by submerging it in an ice bath.
- h. After the diamines are completely dissolved, and the temperature is stable at ~0°C, carefully weigh ~1/4 the total amount of dianhydride and add it to the reactor. Again, rinse the walls of the reactor with NMP.
- i. Repeat the above step until all the required dianhydride is added.
- j. Still maintaining a temperature of ~0°C, wait until all the dianhydride has been dissolved.
- k. The reaction solution viscosity should rise significantly after a few hours. Once the viscosity rise is apparent, remove the reactor from the ice bath and allow the solution temperature to rise to room temperature.

- I. After 24 hrs of reacting the dianhydride and diamines, the polyamic acid reaction should be essentially complete.

4. Chemical Imidization

- a. Needle transfer the calculated amount of β -picoline (>99.5%, Sigma-Aldrich) catalyst to the reactor.
- b. Allow the β -picoline to dissolve completely, then slowly needle transfer the appropriate amount of the AcAn dehydrating agent.
- c. Allow the reaction to continue for 24 hrs at room temperature while under N_2 purge.

5. Precipitation

- a. Disconnect the reactor flask from the assembly and slowly pour the reaction solution into a MeOH (>99.8%, VWR) bath. The polymer should phase separate upon contacting the MeOH, which acts as a non-solvent.
- b. Blend the polymer, then filter the product to remove most of the liquids.
- c. Soak the powder in fresh MeOH overnight.
- d. Filter and wash the powder with fresh MeOH at least 3-4 times.
- e. Dry the polymer powder in a fume hood at room temperature until it is mostly dry.
- f. Finish drying the product by placing it in a vacuum oven at 200-210°C for 24 hrs. This high-temperature drying process also serves to bring imidization of the polyamic acid precursor to completion (i.e. thermal imidization of remaining non-imidized precursor polymer).

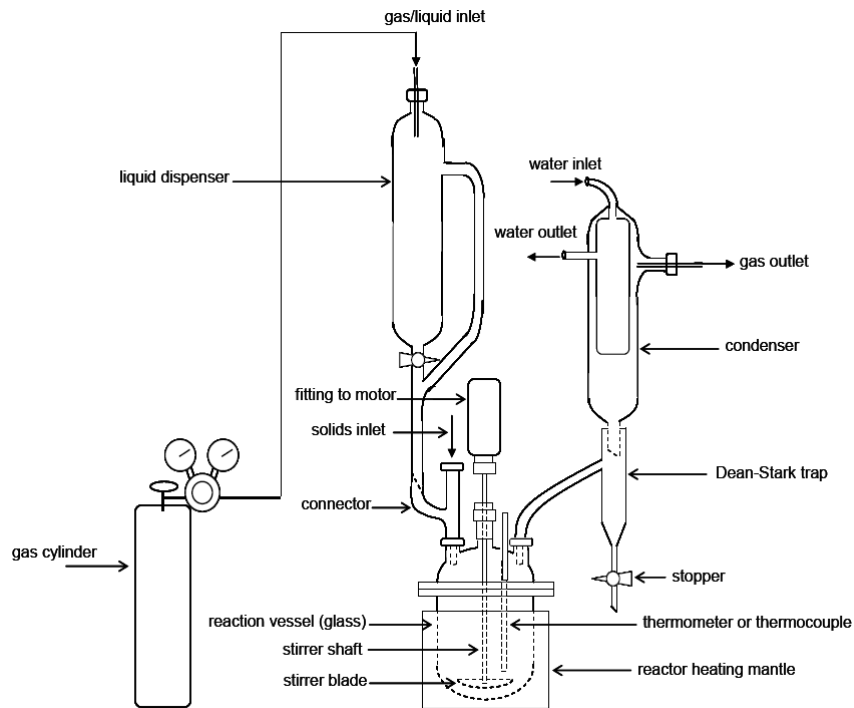


Figure B.1: A schematic of the assembled reaction setup for the 6FDA-DAM:DABA synthesis and monoesterification reactions [1, 2].

References

1. Omole, I.C., *Crosslinked Polyimide Hollow Fiber Membranes for Aggressive Natural Gas Feed Streams*, in *School of Chemical and Biomolecular Engineering 2008*, Georgia Institute of Technology: Atlanta, GA. p. 305.
2. Ma, C., *Highly Productive Ester Crosslinkable Composite Hollow Fiber Membranes for Aggressive Natural Gas Separations*, in *School of Chemical and Biomolecular Engineering 2012*, Georgia Institute of Technology: Atlanta, GA.

APPENDIX C

MONOESTERIFICATION OF DABA-CONTAINING POLYIMIDES

The 6FDA-DAM:DABA precursor is monoesterified through the reaction mechanism shown in Figure C.1. In this case, a polyethylene glycol (PEG) crosslinking agent is used.

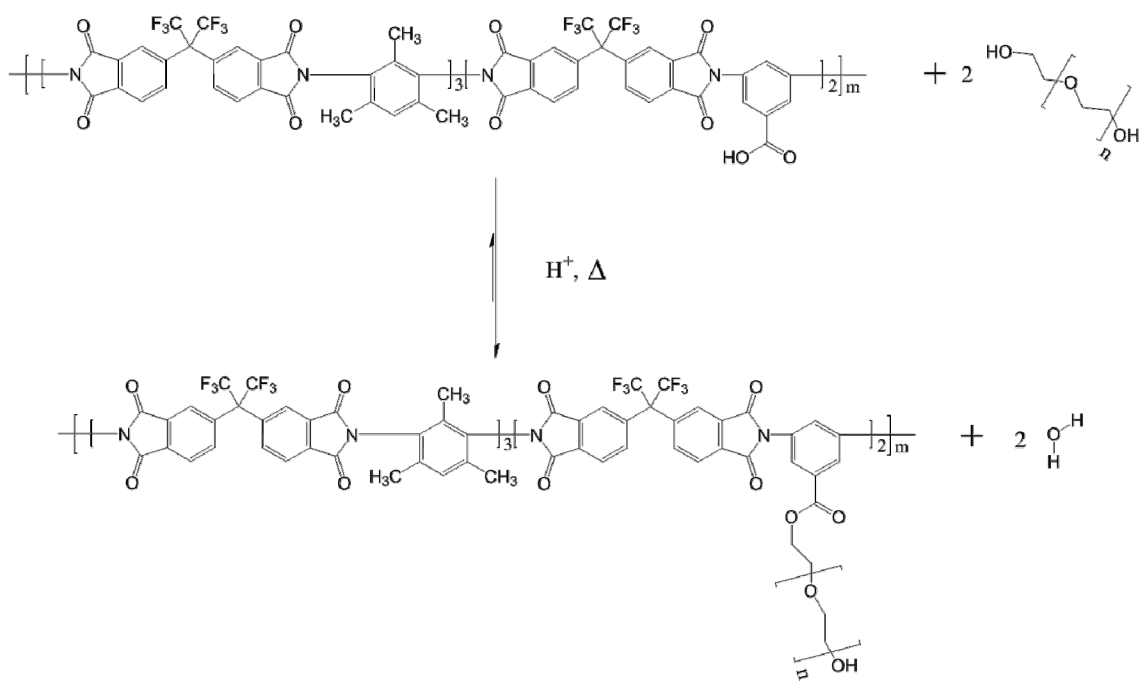


Figure C.1: Monoesterification of 6FDA-DAM:DABA (3:2) with a PEG crosslinking agent.

Regardless of the diol crosslinking agent used, the monoesterification reaction is performed as follows:

- 1) Dry polyimide powder and molecular sieve (4Å) beads at 175°C under vacuum overnight.

- 2) Clean and dry glassware for reaction setup and solvent/reagent dehydration flasks.
- 3) Needle-transfer NMP solvent, diol crosslinking agent, and toluene or ODCB to round bottom flasks with molecular sieve beads.
- 4) Assemble glassware in fume hood as shown in Figure B.1 of APPENDIX B.
- 5) With N₂ purging the reactor, heat the glassware with propane torch to remove any trace moisture.
- 6) Weigh the dried polyimide powder precisely and add quickly to the reactor.
- 7) Add dry NMP to reactor to form a homogeneous solution with 18 wt% polymer; stir and heat solution to 50°C while maintaining N₂ purge.
- 8) Needle transfer 2.5 mL toluene or ODCB (drying agent) per gram polymer to the reaction solution.
- 9) Add 2.5 mg *p*-toluenesulfonic acid (*p*-TSA) catalyst per gram polymer to the reaction solution.
- 10) Increase reaction solution temperature to 130°C.
- 11) Slowly add 40-70 stoichiometric equivalents of the diol crosslinking agent to the reaction solution.
- 12) React for 24 hrs at 130°C while continually stirring reaction solution, purging with N₂, and collecting H₂O / drying agent in Dean-Stark trap; empty Dean-Stark trap periodically to avoid backflow into reactor.
- 13) Turn off heat and allow reaction solution to cool to below 50°C.
- 14) Precipitate monoesterified polymer by very slowly pouring reaction solution into MeOH.
- 15) Blend polymer then filter and wash several times with fresh MeOH.
- 16) Allow the polymer powder to air-dry overnight in a fume hood.

- 17) Transfer powder to appropriate container and dry at 75°C in vacuum oven for 24 hrs. This low temperature is selected to prevent crosslinking.
- 18) The monoesterified polymer powder is now ready for characterization or processing into the desired membrane type.

APPENDIX D

HOLLOW FIBER MEMBRANE POST-TREATMENT [1, 2]

Asymmetric hollow fiber membranes are often treated with a secondary high-permeability polymer coating to “plug” minor defects, often referred to as pin-hole defects, in the skin of the fiber membrane. This technique essentially involves the prevention of Knudsen diffusion through the defects in the hollow fiber skin, and has been described in more detail elsewhere [3].

In the present work, a crosslinkable polydimethylsiloxane (PDMS), Sylgard® 184 (Dow Corning Corp.), was used to perform the membrane post-treatment. The procedure followed is given below:

1. A 3 wt% Sylgard® 184 solution (using a 10:1 ratio of the base and curing agent) was formed with heptane (anhydrous, >99%, Sigma-Aldrich) as the solvent.
2. After mixing, the solution was heated at 75°C for 1 hr to obtain chain extension and branching of the PDMS polymer.
3. The shell-side of the fiber-containing module was filled with the PDMS-heptane solution (i.e. the outer face of the hollow fibers were exposed to the solution) and gently agitated to ensure contact with the entire fiber membrane area. The fibers were allowed to soak in the solution for 5 min, and then the solution was drained from the module.
4. Step 3 was repeated.
5. The module was then placed in a vacuum oven at 75°C for 2 hrs to complete the PDMS polymerization process and fully dry the heptane solvent from the fibers.

References

1. Wallace, D.W., *Crosslinked Hollow Fiber Membranes for Natural Gas Purification and Their Manufacture from Novel Polymers*, in *Department of Chemical Engineering*2004, University of Texas at Austin: Austin, TX.
2. Omole, I.C., *Crosslinked Polyimide Hollow Fiber Membranes for Aggressive Natural Gas Feed Streams*, in *School of Chemical and Biomolecular Engineering*2008, Georgia Institute of Technology: Atlanta, GA. p. 305.
3. Henis, J.M.S. and M.K. Tripodi, *Composite hollow fiber membranes for gas separation: the resistance model approach*. *Journal of Membrane Science*, 1981. **8**(3): p. 233-246.

VITA

Brian Edward Kraftschik was born in January, 1987 in Ravenna, OH. After attending Irondequoit High School in Rochester, NY, Brian enrolled at the University of Rochester in 2005. He graduated from UofR in 2009 with a Bachelors of Science in Biomedical Engineering. During this time, Brian developed a keen interest in Chemical Engineering and became especially intrigued with the field of membrane science through the course of his senior design project. Ultimately, Brian chose to pursue this field of study and joined the School of Chemical and Biomolecular Engineering at Georgia Institute of Technology in Atlanta, GA as a PhD student. He was fortunate enough to be accepted into the research group of Dr. William J. Koros, where he would spend the next four years working on his dissertation. Upon completion his doctorate, Brian accepted an industrial research position with Praxair, Inc. in Buffalo, NY.

Permanent Address: 50 Hearthstone Ln.
Rochester, NY 14617